

Photo-Activatable Oligonucleotides for Protein Modification and Surface Immobilization

Zur Erlangung des akademischen Grades eines

DOKTORS DER NATURWISSENSCHAFTEN

(Dr. rer. nat.)

von der KIT-Fakultät für Chemie und Biowissenschaften

des Karlsruher Instituts für Technologie (KIT)

genehmigte

DISSERTATION

von

Dipl.-Chem. Antonina Francevna Kerbs

aus

Almaty, Kasachstan

KIT-Dekan: Prof. Dr. Willem Klopper

Referent: Priv. Doz. Dr. Ljiljana Fruk

Korreferent: Prof. Dr. Christopher Barner-Kowollik

Tag der mündlichen Prüfung: 21.10.2016



This document is licensed under the Creative Commons Attribution – Share Alike 3.0 DE License (CC BY-SA 3.0 DE): <http://creativecommons.org/licenses/by-sa/3.0/de/>

Ich erkläre hiermit wahrheitsgemäß, dass die vorliegende Doktorarbeit im Rahmen der Betreuung durch Priv. Doz. Dr. Ljiljana Fruk selbständig verfasst und keine anderen als die angegebenen Quellen und Hilfsmittel verwendet sowie alle wörtlich oder inhaltlich übernommenen Stellen als solche kenntlich gemacht wurden. Des Weiteren erkläre ich, dass ich mich derzeit in keinem laufenden Promotionsverfahren befinde, keine vorausgegangenen Promotionsversuche unternommen habe sowie die Satzung zur Sicherung guter wissenschaftlicher Praxis beachtet habe. Zusätzlich erkläre ich, dass die elektronische Version der Arbeit mit der schriftlichen übereinstimmt und dass die Primärdaten gemäß Abs. A (6) der Regeln zur Sicherung guter wissenschaftlicher Praxis des KIT beim Institut für Biologische Grenzflächen 1 zur Archivierung abgegeben wurden.

Karlsruhe, den 03.11.2016

Antonina Kerbs

Die vorliegende Arbeit wurde von Oktober 2012 bis Juni 2016 unter der Anleitung von Priv. Doz. Dr. Ljiljana Fruk am Karlsruher Institut für Technologie – Universitäts- und Großforschungsbereich angefertigt.

Für meine Familie

Abstract

The ability to synthesize and modify short DNA sequences has helped to advance numerous research fields such as genomics, molecular biology, molecular engineering and nanobiotechnology. DNA has ceased to be used only as a genetic code carrier, but became also an important structural and functional element for the assembly of nanostructures, in design of the antisense therapeutics and for development of the microarray and biosensors technology. Various strategies with different extent of success have been used to introduce number of functional groups to DNA and in such way, enable both the further biomolecular studies and the surface immobilization.

Within this thesis, covalent coupling strategies, namely light-induced Diels-Alder cycloaddition and nitrile imine-mediated tetrazole-ene cycloaddition (NITEC) were employed for attachment of DNA to different molecules and surfaces in a temporally and spatially controlled manner. The functionalization of DNA with photo-activatable groups; 2,5-dimethylbenzophenone derivative (PE1), 2-methoxy-6-methylbenzaldehyde derivative (PE2) for Diels-Alder cycloaddition, and tetrazole derivative (Tz) for NITEC was achieved utilizing phosphoramidite, H-phosphonate and amide coupling methodologies. In order to determine the suitability of the light-induced reactions for further DNA modification, detailed kinetic studies using functionalized DNAs were performed, indicating that photoenol containing DNA (PE2-DNA) is the most efficient reacting agent for further applications in protein conjugation and surface structuring. This was additionally confirmed by successful light-induced conjugation of PE2-DNA to horseradish peroxidase (HRP), which resulted in HRP-DNA conjugate with preserved inherent functions of both the DNA and protein.

Finally, light-induced immobilization of DNA onto glass surface was performed in order to establish mild, simple and easily controllable route to DNA surface structuring. To achieve that, two different strategies, which differ in the level of resolution and versatility of the achieved pattern, were employed for DNA patterning: one based on the use of the shadow mask and the other on Direct Laser Writing (DLW). DLW enabled design of the DNA line pattern with resolution of 600 nm, surpassing other commercially available strategies and also allowing for fast and simple structuring of multiple DNA sequences and subsequent immobilization of complementary DNA and DNA-protein conjugates for future protein array applications.

This was the first demonstration of the use of light-induced chemistry and direct laser writing for precise patterning of DNA sequences on the surface, paving the way for advanced applications in design of biomolecular arrays and new functional materials.

Zusammenfassung

Die Fähigkeit kurze DNA Sequenzen zu synthetisieren und zu modifizieren, hat entscheidende Weiterentwicklungen in Forschungsbereichen wie der Genomik, Molekularbiologie, Molekulartechnik und Nanobiotechnologie ermöglicht. Die DNA ist nicht mehr nur ein Träger der Erbinformation, sondern ist zu einem wichtigen struktur- und funktionsgebenden Element für die Nanostrukturierung, die Entwicklung der Antisense-Therapeutika und DNA Chip-Technologie sowie der Biosensorik geworden. Diverse Strategien wurden mit unterschiedlichem Erfolg zur Einführung zahlreicher funktioneller Gruppen verwendet, um weitere biomolekulare Studien und Oberflächenimmobilisierung zu ermöglichen.

Im Rahmen dieser Arbeit wurden kovalente Kupplungsstrategien wie die lichtinduzierte Diels-Alder Cycloaddition und die lichtinduzierte Nitrilimin-vermittelte Tetrazol-En Cycloaddition (NITEC) verwendet, um DNA zeitlich und räumlich kontrolliert an verschiedene Moleküle und Oberflächen anzubinden. Die DNA-Funktionalisierung mit lichtaktivierbaren Molekülen wie den 2,5-Dimethylbenzophenon- (PE1) und 2-Methoxy-6-methylbenzaldehyd- (PE2) Derivaten für die Diels-Alder-Reaktion und dem Tetrazol-Derivat (Tz) für die NITEC wurde mittels Phosphoramidit- und H-Phosphonat-Methoden sowie der Amidkupplung realisiert. Um die Eignung der lichtinduzierten Reaktionen für die weitere DNA-Modifikation zu überprüfen, wurden detaillierte kinetische Untersuchungen von Reaktionen funktionalisierter DNA durchgeführt und es konnte festgestellt werden, dass PE2-modifizierte DNA den effizientesten Reaktionspartner für weitere Anwendungen wie die Proteinkonjugation oder die Oberflächenstrukturierung darstellt. Dies wurde zusätzlich durch erfolgreiche lichtinduzierte Konjugation von PE2-DNA mit der Meerrettichperoxidase (HRP) bestätigt. Die natürlichen Funktionen der DNA und des Enzyms blieben in dem gebildeten HRP-DNA-Konjugat erhalten.

Im letzten Teil der Arbeit wurde die lichtinduzierte Immobilisierung von DNA auf Silizium- und Glasoberflächen durchgeführt, um somit eine milde, einfache und leicht-kontrollierbare Route zur DNA-Oberflächenstrukturierung zu etablieren. Hierzu wurden zwei verschiedene Strategien verfolgt, die zum einen auf dem Einsatz einer Schattenmaske, zum anderen auf dem Direkten Laserschreiben (DLW) basieren. Die beiden Methoden unterscheiden sich hinsichtlich des Auflösungsvermögens und der Vielseitigkeit der erreichbaren Muster. Mittels DLW konnte ein Linienmuster mit einer Auflösung von 600 nm

geschrieben werden, was andere kommerziell erhältliche Strategien übertrifft. Somit konnte eine schnelle und einfache Strukturierung der Oberfläche mit mehreren DNA-Sequenzen sowie die anschließende Immobilisierung der komplementären DNA und von Protein-DNA Konjugaten erreicht werden, was in der Zukunft in der Protein-Chip-Technologie Anwendung finden könnte.

Zum ersten Mal wurde die Anwendung der lichtinduzierten Diels-Alder Reaktion in Verbindung mit direktem Laserschreiben für eine präzise Strukturierung von DNA-Sequenzen auf der Oberfläche demonstriert und somit der Weg für weitere Anwendungen im Bereich der Entwicklung biomolekularer Chips und neuer funktionaler Materialien geebnet.

Publications Arising from this Thesis

- **Clickable Tyrosine Binding Bifunctional Linkers for Preparation of DNA-Protein Conjugates**
D. Bauer, I. Ahmed, A. Vigovskaya, Lj. Fruk, *Bioconjugate Chem.* **2013**, 1094-1101.
- **A Self-Reporting Tetrazole-Based Linker for the Biofunctionalization of Gold Nanorods**
L. Stolzer, A. Vigovskaya, C. Barner-Kowollik, L. Fruk, *Chem. Eur. J.* **2015**, *21*, 14309-14313.
- **Photo-Induced Chemistry for the Design of Oligonucleotide Conjugates and Surfaces**
A. Vigovskaya, D. Abt, I. Ahmed, C. M. Niemeyer, C. Barner-Kowollik, L. Fruk, *J. Mater. Chem. B* **2016**, *4*, 442-449.
- **DNA Surface Structuring using Direct Laser Writing and Light-Induced Cycloadditions**
A. Kerbs, P. Mueller, M. Kaupp, I. Ahmed, A. S. Quick, D. Abt, M. Wegener, C. M. Niemeyer, C. Barner-Kowollik, L. Fruk, in preparation.

Contents

1	Introduction	1
1.1	DNA Synthesis and Modification.....	1
1.2	Oligonucleotide Synthesis	4
1.2.1	Phosphoramidite (phosphite triester) Method	4
1.2.2	H-phosphonate Method for Oligonucleotide Synthesis	7
1.2.3	Phosphate Triester Method for Oligonucleotide Synthesis.....	9
1.3	Modification of Oligonucleotides with Various Functional Moieties.....	10
1.3.1	Oligonucleotide Modification on the Solid Support	10
1.3.2	In-solution Modification of Oligonucleotides.....	11
1.4	DNA Coated Surfaces	15
1.4.1	Physisorption of DNA onto Charged Surfaces	15
1.4.2	Chemisorption of Modified DNA	16
1.4.3	Covalent Attachment of DNA onto Various Surfaces	17
1.4.4	Photochemical Reactions for the DNA Immobilization	20
1.4.4.1	Light-induced Diels-Alder Cycloaddition	23
1.4.4.2	Nitrile Imine-Mediated Tetrazole-Ene Cycloaddition (NITEC).....	25
1.5	Methods for DNA Surface Structuring.....	27
2	Research Objectives	31
3	Results and Discussion.....	33
3.1	Synthesis of the Photo-Activatable Oligonucleotides	33
3.1.1	Phosphoramidite Method	34
3.1.2	H-Phosphonate Strategy for PE-DNA Preparation	39
3.1.3	Amide Coupling Strategy for the Preparation of PE- and Tz-DNA.	41
3.2	Kinetic Study of Light-Induced Cycloaddition Reactions	45
3.2.1	Light-Induced Cycloaddition of PE-DNA with the Model Maleimide.....	46
3.2.2	Photoenol- vs. Tetrazole-DNA Photoreaction with Model Maleimide.....	51
3.3	Photoenol Modified Oligonucleotides in DNA Bioconjugation and Structuring.....	65
3.3.1	Light-Induced Conjugation of PE ₂ -DNA ₂₅₄ to Horseradish Peroxidase (HRP) 65	
3.3.2	Light-Induced Biofunctionalization of Maleimide Coated Copper Nanoparticles 72	
3.3.3	Light-Induced Reactions for Spatially Controlled Immobilization of DNA.....	79
3.3.4	Photo-Encoding of Maleimide Surfaces with DNA by Direct Laser Writing ...	84

3.3.4.1	DNA Array Prepared by DLW Using Single DNA Sequence.....	86
3.3.4.2	Optimization of the DLW Procedure: Dose and Resolution Tests	89
3.3.4.3	DLW for Multi-DNA Array Preparation	92
4	Summary and Outlook	99
5	Experimental Part.....	101
5.1	Materials and Methods	101
5.1.1	Chemicals	101
5.1.2	Instruments and Methods	103
5.2	Syntheses	110
5.3	DNA Modification.....	125
5.4	Photoreactions	130
5.4.1	Kinetic Study of the Photo-Induced Cycloaddition Reaction.	132
5.4.2	Spatially Controlled Immobilization of PE2-DNA2 54 on Maleimide Functionalized Silicon Wafers.	134
5.4.3	Direct Laser Writing (DLW).....	135
5.4.4	Synthesis of Do-TEG-Mal 71 Coated Copper Nanoparticles.	138
6	Bibliography.....	141
7	List of Figures	151
8	List of Tables.....	155
9	Abbreviations	157
10	Danksagung.....	159

1 Introduction

1.1 DNA Synthesis and Modification

Deoxyribonucleic acid (DNA) is a biopolymer of crucial importance for the genetic information transfer, and the discovery of its structure and mode of action^[1] has initiated remarkable developments in molecular biology and genetics,^[2] but also opened the route for DNA to become an important element in nanostructuring,^[3] biosensing and optoelectronic device design.^[4] DNA is a polymeric species with remarkable self-assembling ability, which leads to the formation of the double helix structure (Figure 1.1). The structure consists of four different monomers, the deoxyribonucleotides, composed of a *deoxyribose sugar*, one of four nitrogen-containing *nucleobases*; adenine (A), guanine (G), cytosine (C) and thymine (T) bound to the sugar at the 1'-position through 1-N- β -glycosidic bond, and a *phosphate group* at the 5'-position of the sugar. The binding of nucleotides within the single strand is enabled by a covalent phosphodiester bond between the sugar of one nucleotide and the phosphate of the next one, resulting in an alternating 5'-3'-phosphate-sugar backbone (Figure 1.1).

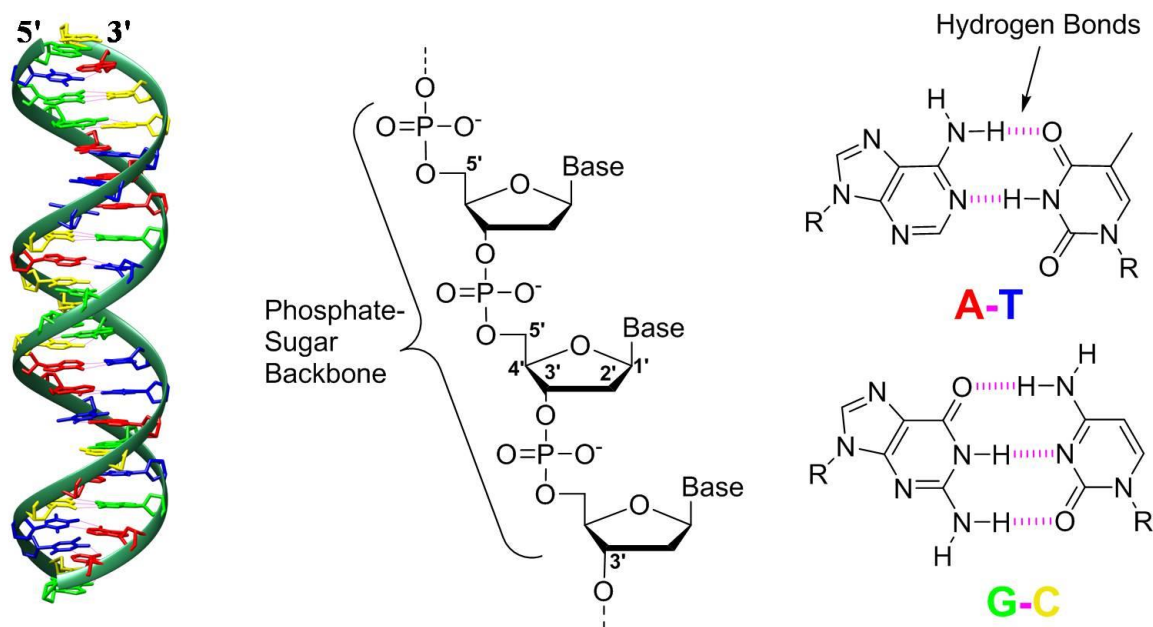


Figure 1.1: Space model of the DNA double helix (left), structure of the single DNA strand (middle) and the principle of the base pairing (right), R = phosphate-sugar backbone.

As first described by Watson and Crick,^[1f] two anti-parallel polynucleotide strands pair to each other as a result of the hydrogen bond formation between nucleobases, and form a right-

handed double helix (B-DNA), the most common form found within most living organisms. Several other forms of DNA are known, which differ in the level of stacking and hydration of the double helix backbone (A-DNA and Z-DNA). However, the pairing within all forms is highly specific and it results in formation of the base pairs between adenine and thymine (A-T) and guanine and cytosine (G-C). The double helix is additionally stabilized by hydration of the phosphate groups and hydrophobic interactions between the aromatic ring systems that results in stacking of the bases (π - π interaction). Double helix structure has exceptional stability and flexibility, which is crucial for both the packing and the transfer of genetic material, and there is a complex machinery composed of numerous proteins involved in DNA repair, unwinding and copying.

Interestingly, due to the high specificity of the base pairing and the robust structure, DNA is also an advantageous building block for applications in bionanotechnology. In early 1980s, Ned Seeman demonstrated the use of the DNA as a structural element for the construction of three-dimensional networks.^[5] The concept of DNA self-organization was elaborated and expanded to the scaffold-strand technique known as DNA origami, first described by Yan *et al.*^[6] and Shih *et al.*^[7] and further developed by Rothemund.^[8] The most important feature used in DNA assembly and structuring is the ability of the single stranded DNA to bind to its complementary strand with high specificity. This ability has particularly been useful in enabling the immobilization of various species onto different surfaces, in the process referred to as DNA directed immobilization (DDI).^[9] Advantages of the DDI compared to other methods of immobilization are its biocompatibility (it proceeds in aqueous solutions) and binding reversibility. Namely, double stranded DNA can be unfolded (dehybridized) using either heat or various chemical agents allowing for a control of immobilization and the release of immobilized species.^[10] In such way, platforms for biosensing^[11] and drug delivery systems^[12] could be designed. Short chemically synthesized DNA strands (10-25 bp) are commonly used for such applications as they are readily available and reversibility of the binding processes can be easily estimated and controlled.

DNA origami technology also employs DDI as a mean of immobilization and structuring, but uses longer DNA (usually around 7 000 bp) from natural sources such as viruses, to build the platform, which can vary in shape and size, and to which different DNA modified species can be immobilized.^[13] In such way the distances between immobilized species can be precisely controlled aiding the design of new materials for biosensing.

Recently, natural nucleic acids, those extracted directly from the cells of various organisms, have also been used in material science.^[4a, 14] In one such application, DNA was employed as a template for growth of nanoparticles. Hung *et al.* used a salmon sperm DNA–surfactant complex and light-induced reduction of gold salt precursor to prepare a complex anisotropic gold crystalline structure.^[15] Moreover, natural DNA has been shown to be remarkably interesting material for preparation of optoelectronic devices^[16] and organic catalysts.^[17] An overview of the different applications of natural DNA is given in the extensive review by Hung and co-workers.^[14c]

As mentioned earlier, short DNA strands, usually employed in DNA structuring and immobilization, are prepared by automated chemical synthesis. A range of the possible nucleic acid applications can additionally be extended by introduction of various chemical modifications to basic DNA structure. Synthetic oligonucleotides became particularly interesting after 1977 when Paterson *et al.* showed that gene expression can be modified by addition of exogenous, short nucleic acids.^[18] A year later, Zamecnik and Stephenson demonstrated that a short oligodeoxyribonucleotide (13-mer) could inhibit the translation of proteins specified by Rous sarcoma virus 35S RNA in the wheat embryo cell-free system.^[19] These discoveries led to the development of technologies, which enabled the gene expression manipulation within the living cells by employing synthetic oligonucleotides. Such oligonucleotide therapeutics have already shown promise in the treatment of viral diseases and cancer.^[20] Best investigated route is the antisense mechanism, in which the complementary oligonucleotide is hybridized to mRNA of the targeted gene and in such way that it selectively inhibits the gene expression.^{[21],[22]} However, years of research resulted in only a small number of nucleic acid therapeutics being used for the human disease treatment. For example, *Pegaptanib*, a pegylated anti-vascular endothelial growth factor (VEGF) aptamer, was approved for the treatment of age-related macular degeneration, a disease, which causes damage to the macula, a small spot near the center of a retina and is crucial for sharp, central vision, allowing people to see objects that are straight ahead.^[23] The major issues with the therapeutic use of oligonucleotides are their instability in biological fluids (degradation by nucleases), poor cell penetration and inefficient tissue-specific delivery. However, in recent years some of these issues were addressed by introduction of DNA backbone modifications,^[24] conjugation to biomolecules^[25] or the use of viral and synthetic vectors for systemic delivery.^[26] In general, oligonucleotide applications in both the biomedicine (either as diagnostic or therapeutic agents) or nanotechnology (i. e. surface modification and structuring) require use

of oligonucleotides, which contain a variety of functional groups to enable their further modification and conjugation.^[27] Most of the modifications are introduced during the oligonucleotide synthesis and the following section will give an overview of the chemical strategies used for preparation of synthetic oligonucleotides.

1.2 Oligonucleotide Synthesis

Oligonucleotides can be prepared by chemical synthesis using three main methods: phosphate triester, phosphoramidite (phosphite triester) and H-phosphonate method with phosphoramidite being the most common one.

1.2.1 Phosphoramidite (phosphite triester) Method

The ground for the chemical synthesis of oligonucleotides was laid in 1955 when A. M. Michelson and A. R. Todd prepared a di-thymidine dinucleotide for the first time.^[28] Further significant contribution was given by Har Gobind Khorana and his team, who introduced a phosphodiester method for the preparation of dinucleotide segments in 1956. Following such success, but almost two decades later, the segments were combined to afford 77 units of double stranded DNA corresponding to the gene for alanine transfer ribonucleic acid (tRNA) from yeast.^[29] It should be noted that Korana and colleagues have also developed the orthogonal protection/deprotection scheme, which is still used today (Figure 1. 2).^[30]

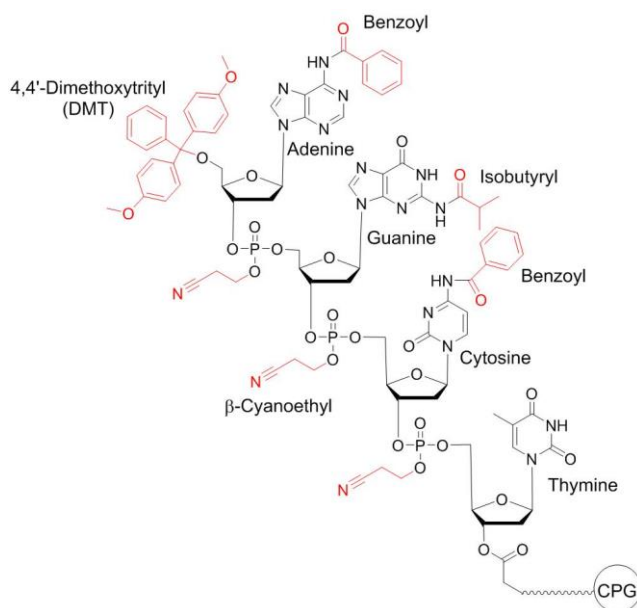
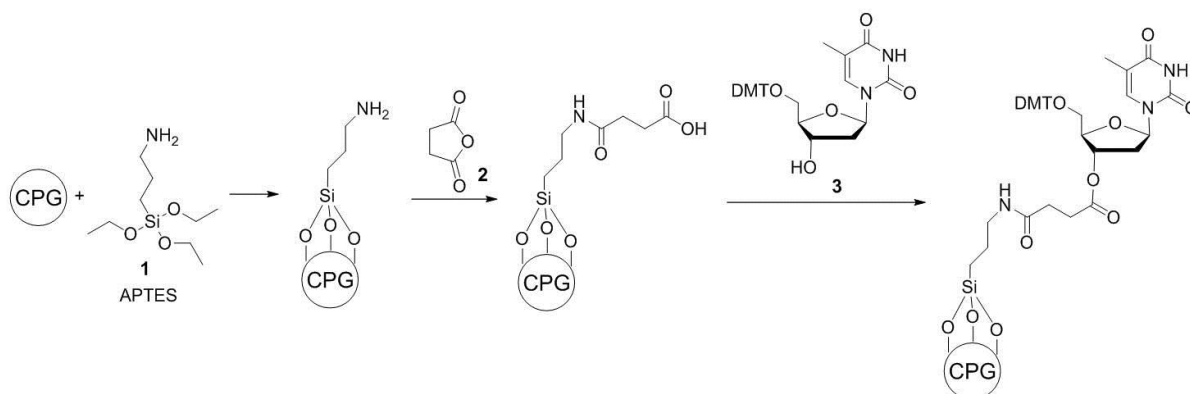


Figure 1.2: Common protecting groups (red) used in the oligonucleotide synthesis developed by Korana *et al.*^[30-31]

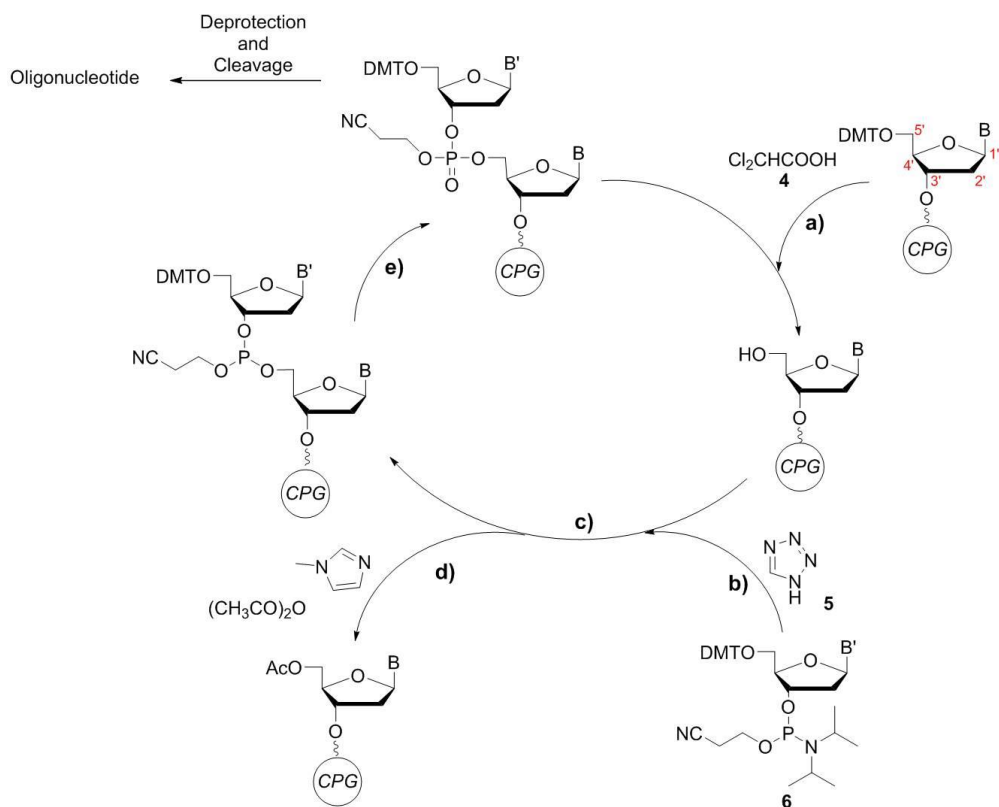
For the protection of 5'-OH group of sugar 4,4'-dimethoxytrityl, (DMT) protecting group was used.^[32] The exocyclic amino groups of nucleobases were protected by isobutyryl (iBu) for guanine and benzoyl (Bz) for adenine and cytosine.^[30, 33] The next important step in oligonucleotide synthesis was made by Letsinger *et al.*^[34] They, at the same time as Merrifield,^[35] applied solid phase synthesis, developed for peptide preparation, to the preparation of oligonucleotides. Styrene-divinylbenzene polymer was employed as a solid support, but this posed a significant synthetic challenge as the polymer swelled in some commonly used solvents and also absorbed the reagents limiting the efficiency of the synthesis.^[36] The method was further optimized in the 1980s by Caruthers and colleagues,^[37] who improved upon the Letsinger method and introduced the phosphoramidite monomer building blocks,^[38] which are still used today in an automated standard oligonucleotide synthesis. For the protection of reactive P(III) phosphite group they used β -cyanoethyl group, and employed dialkylamino group as a leaving group, providing an ideal balance between the stability during phosphoramidite preparation and the ease of activation during oligonucleotide synthesis.^[39] This resulted in a stable phosphitylating reagents, phosphoramidite nucleosides, which could be stored until they were needed making this method commercially viable. In the coupling reaction, phosphoramidite monomer is first activated by addition of a weak acid tetrazole and the resulting phosphite triester is oxidized to a phosphate in an additional step. Polymeric solid support was replaced by HPLC-grade silica, known as a controlled pore glass (CPG), due to its excellent properties such as ease of derivatization, straightforward removal of solvents and reagents, chemical inertness to reagents used for the synthesis, robustness and non-swelling in common organic solvents. Depending on the scale of the synthesis, CPG can also be packed in columns of different dimensions, which can range from 0.05 mL to several liters and by varying the glass pore size from 500 to 3000 Å, different lengths of oligonucleotides (50-200 bases) can be prepared. For the automated synthesis, CPG is usually functionalized with 40 nmol to 1 μ mol of the starting base. To achieve this, CPG is first activated with (3-aminopropyl)triethoxysilane (APTES) **1** and then treated with succinic anhydride **2** in order to generate the carboxylic groups, which are subsequently condensed with 3'-hydroxy groups of the starting nucleoside **3** in the presence of *N,N'*-dicyclohexylcarbodiimide (DCC) (Scheme 1.1).^[40] In the course of optimization of the synthetic protocols, it has been shown that a spacer length and the nature of the bond between the CPG matrix and the lead nucleoside were important for the overall yield and the product purity.^[41] In order to avoid the folded

conformation of the spacer due to the hydrogen bonding, dipole-dipole or π - π -interactions, spacers with more than 25 atoms were recommended and are still used today.^[42]



Scheme 1.1: Functionalization of CPG with APTES **1** and succinic anhydride **2** and a subsequent condensation with the lead nucleoside **3** (thymidine).

The preparation of nucleoside phosphoramidite building blocks is performed in three steps: protection of exocyclic amino groups, tritylation and phosphitylation^[31, 43] and typical oligonucleotide synthesis cycle within the automated systems is depicted in Scheme 1.2.



Scheme 1.2: Oligonucleotide synthesis cycle based on the phosphoramidite method; B, B' = nucleobases, DMT = 4,4'-dimethoxytrityl protecting group.^[30-31]

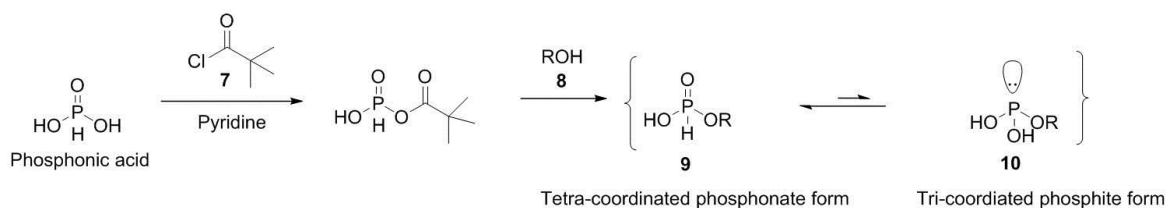
The reaction cycle involves:

- a) *deblocking* of the 5'-hydroxyl group by treatment with dichloroacetic acid **4** (usually 3% in dichloromethane);
- b) *activation* with a tetrazole **5** solution
- c) *coupling* of the nucleoside phosphoramidite **6** to a 3'-growing oligonucleotide still bound on the support. The chain elongation occurs in 3' → 5' direction; the phosphoramidites are usually used in the 1.5 - 20-fold excess and due to their high reactivity, should be handled exclusively under inert reaction conditions;
- d) masking of the non-reacted 5'-OH groups (*capping*) by treatment with acetic anhydride and *N*-methylimidazole in order to avoid the formation of undesired sequences;
- e) *oxidation* of the tri-coordinated phosphite triester linkage to tetra-coordinated phosphate by treatment with iodine and water in the presence of bases such as pyridine.

The nucleotide chain is grown by reaction with the next nucleoside phosphoramidite after the *deprotection* step and when the desired length is achieved, *cleaved* from the solid support by treatment with 25% ammonia hydroxide solution at increased temperatures (usually within 5 hours at 55° C). During the cleavage step, all protective groups of exocyclic amines and the β-cyanoethyl group are removed. Depending on further application, DMT protecting group can be kept on or removed with dichloroacetic acid prior to the cleavage procedure. Since condensation does not proceed in quantitative yields (the yield *per* chain elongation step is mostly around 99%), short-chain oligonucleotides are present in addition to desired longer sequence within the final product. Therefore, the purification of synthesized oligonucleotides is required and this can be achieved either by reversed phase high performance liquid chromatography (HPLC) or by gel electrophoresis.

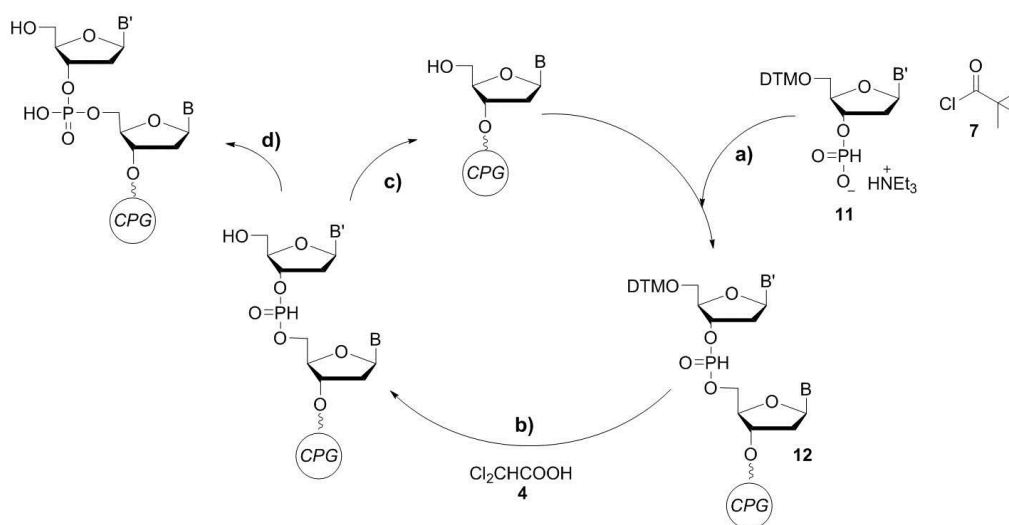
1.2.2 H-phosphonate Method for Oligonucleotide Synthesis

Though the first synthesis of oligonucleotide dimer using H-phosphonate chemistry was described by Hall, Todd and Webb in 1957,^[44] its use in the solid phase synthesis was only demonstrated three decades later by Garegg *et al.*^[45] and Froehler and Matteucci.^[46] H-phosphonates are mono- or diesters of phosphonic acid and can be prepared by activation of phosphonic acid with trimethylacetyl chloride **7** in pyridine and subsequent transesterification with a hydroxy terminated molecule **8** (Scheme 1.3)^[47] or employing other synthetic pathways.^[48] In solution, H-phosphonates exist as an equilibrium mixture of two tautomeric forms: a tetra-coordinated phosphonate **9** and a tri-coordinated phosphite **10** (Scheme 1.3).^[49]



Scheme 1.3 Synthesis and two tautomeric forms of the H-phosphonate, tetra-coordinated phosphonate **9** and tri-coordinated phosphite **10**.^[49]

Although the oxidation state of phosphorus atom in both forms is +3, the chemical reactivity is fundamentally different. Tri-coordinated species **10** reacts fast with various electrophiles, due to the presence of the lone electron pair at a phosphorus atom. In contrast, tetra-coordinated phosphonate **9** lacks a lone electron pair, which leads to a decreased reactivity towards electrophiles and consequently, to the improved stability and resistance to spontaneous oxidation. The chemistry of the phosphonate **9** is dominated by formation of a phosphoryl group (P=O), which is often a driving force of the reaction.^[48] The tautomeric equilibrium of both forms is almost completely shifted towards the tetra-coordinated H-phosphonate form **9**, permitting the synthesis of the phosphorus compounds without use of the protecting groups.^[49] At the same time, upon activation with appropriate activating reagents, such as trimethylacetyl chloride or 1-adamantanecarbonyl chloride, H-phosphonate monoesters **9** can efficiently undergo a nucleophilic substitution. The general synthetic cycle for the preparation of oligonucleotides by H-phosphonate method is depicted in Scheme 1.4.^[40]

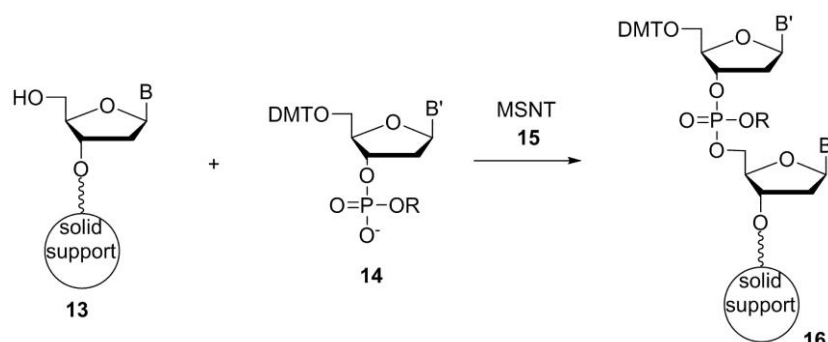


Scheme 1.4: Schematic illustration of the oligonucleotide synthesis cycle using H-phosphonate method; B, B' = nucleobases, DMT = 4,4'-dimethoxytrityl protecting group; a) condensation, b) detritylation, c) chain elongation, d) oxidation.

Following the detritylation step using dichloroacetic acid **4**, condensation is performed by addition of an appropriate nucleoside H-phosphonate **11** and an activating reagent trimethylacetyl chloride **7**, which results in the H-phosphonate diester **12**. Due to the stability of the H-phosphonate compound, oxidation at every cycle is not necessary and can be performed at the end of synthesis by treatment with an aqueous iodine in the presence of pyridine.^[40] Alternatively, the oxidation step can be performed under non-aqueous conditions providing modified oligonucleotides such as phosphoramidates,^[50] phosphorothioates,^[51] or phosphoroselenoates.^[52] By employing the solution of aqueous ammonia (25%), protecting groups of exocyclic amino groups are removed and the oligonucleotide is cleaved from the solid support. Despite the advantages of H-phosphonate method such as stability of nucleoside H-phosphonates, one-step oxidation and the ability to provide the backbone modified oligonucleotides, phosphoramidite method continues to be the most widely used due to its higher yields and fewer side products. However, the main appeal of the H-phosphonate approach lies in the stability of the coupling elements, which is advantageous when sensitive groups need to be introduced to the oligonucleotide.

1.2.3 Phosphate Triester Method for Oligonucleotide Synthesis

This method was first used in the 1970s to synthesize oligonucleotides using appropriate building blocks in solution, but can also be employed for the solid-phase synthesis.^[53] To achieve this, a protected nucleoside phosphodiester derivative **14** is allowed to react with the 5'-end of a support-bound nucleoside **13** to give a neutral phosphotriester (Scheme 1.5).^[54]



Scheme 1.5: Principle of the phosphate triester method for oligonucleotide synthesis using phosphodiester derivative **13** bound to the solid support and DMT protected phosphodiester **14** to give neutral dinucleotide **16**.

Different condensing agents such as mesitylene sulfonylnitrotriazole (MSNT) **15** or others,^[53b, 55] can be employed. However, due to long reaction times and large number of side reactions, the method is not used for the synthesis of oligonucleotides any longer.

Further developments of the oligonucleotide chemistry have largely been application driven. The more demanding applications required advanced modification strategies and sometimes, presence of multiple modifications within a single oligonucleotide. Novel, elegant chemistry solutions were developed in order to reduce the time and the costs of the synthesis. Structural modifications of the backbone, bases or sugars,^[24] but also conjugation with various compounds were performed on solid support or in the solution.^[56] However, it was soon clear that depending on the intended purpose, modified oligonucleotides need to be carefully designed in order to prevent the loss of their inherent biological and structural properties

1.3 Modification of Oligonucleotides with Various Functional Moieties

1.3.1 Oligonucleotide Modification on the Solid Support

Modification of oligonucleotides is mainly based on the phosphoramidite chemistry, which is utilized in commercial DNA synthesis. For the incorporation of modified phosphoramidites, but also in certain cases H-phosphonates derivatives (when the functional group, which needs to be added is not compatible with the phosphoramidite chemistry),^[47] during the automated synthesis, the nucleosidic or non-nucleosidic building blocks are synthesized, protected, and phosphitylated. As mentioned earlier, the phosphoramidite coupling reaction is water and oxygen sensitive requiring inert reaction conditions. When a modification of the nucleotide is required, this can be achieved by addition of the desired functional group either at the two ends (3'- and/or 5'-end) or within the sequences. In such way, various oligonucleotides were synthesized containing large number of functional moieties such as polyalkyl chains, cholesterol, azide, alkyne, dendrons and many others.^[57] Due to the availability of modified oligonucleotides containing optical tags such as fluorophores, significant advances could be made in DNA sequencing^[58] and *in vivo* gene detection.^[59] It will also be shown later within this thesis, how commercially available cyanine dye (Cy Dye) labeled oligonucleotides, prepared using cyanine phosphoramidites, can be employed for molecular recognition experiments.

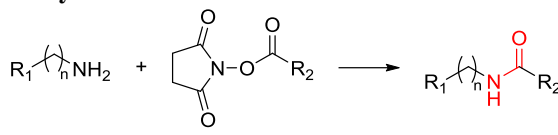
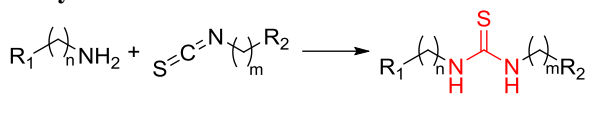
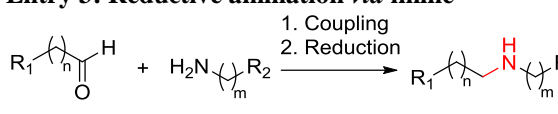
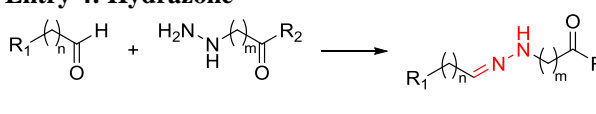
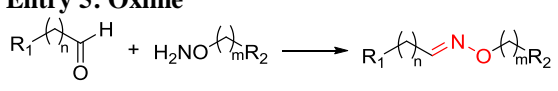
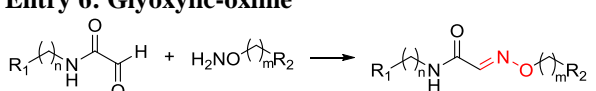
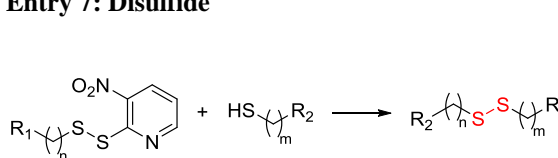
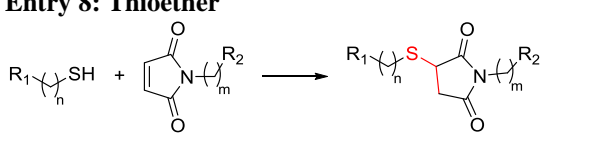
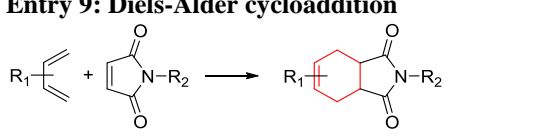
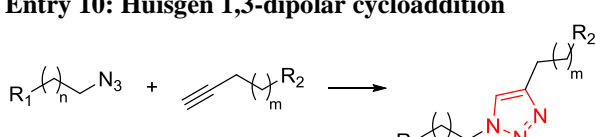
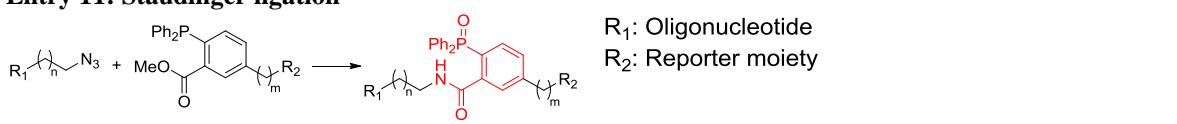
One of the major advantages of the solid support synthesis, besides the ease of purification, is that organic solvents can be used, enabling in such way a functionalization of hydrophilic oligonucleotides with hydrophobic groups.^[60] The solvent used in commercial synthesizer is anhydrous acetonitrile, therefore to be applied in an automated DNA synthesizer, the modifier phosphoramidites should have good solubility in acetonitrile. For molecules, which do not, the functionalization has to be handled manually and post-synthetically by employing the appropriate solvents.^[57a, 61]

Besides the reaction solvent, size of the modifier molecule has to be taken into account while planning the synthetic strategy, as the big molecules such as polymers can be sterically hindered, which makes active centers less accessible, resulting in low yields of coupling.^[61] Another disadvantage of the modification on the solid support is the challenging synthesis of desired modifiers, as not every conceivable phosphoramidite can be prepared using organic chemistry strategies or is commercially available. It should be noted that the solid support modification of oligonucleotides and addition of various functional groups, extends beyond the phosphoramidite or H-phosphonate chemistry. For example, amino- or aldehyde- terminated oligonucleotides, which are still bound to the solid support, can further be reacted with additional functional units such as activated carboxylic acid or amino terminated compounds.^[62] Finally, once the modification is achieved, modified DNA can be cleaved from the solid support by use of various reagents depending on the sensitivity of the modifier group.

1.3.2 In-solution Modification of Oligonucleotides

Another modification strategy, the in-solution coupling, involves pre-synthesis on the solid support and the purification of oligonucleotides, which usually contain smaller functional groups, and further modification using non-covalent or covalent strategies. As DNA is stable and fully functional in aqueous solutions, the disadvantage of this strategy is the limited number of modification methods, which can be performed in water. Furthermore, the in-solution conjugation usually requires an excess of the reagents and extensive purification, which is associated with product loss. However, the in-solution strategies are particularly suitable for conjugation with hydrophilic molecules such as various biomolecules (proteins, peptides), which are not compatible with organic solvents.^[11c] Table 1.1. summarizes the most employed approaches for chemical linkage of modified oligonucleotides in solution.

Table 1.1: Commonly employed linkages/reactions for in-the solution oligonucleotide conjugation. Adapted with permission from [56].^[56]

<p>Entry 1: Amide</p> 	<p>Entry 2: Thiourea</p> 
<p>Entry 3: Reductive amination via imine</p> 	<p>Entry 4: Hydrazone</p> 
<p>Entry 5: Oxime</p> 	<p>Entry 6: Glyoxylic-oxime</p> 
<p>Entry 7: Disulfide</p> 	<p>Entry 8: Thioether</p> 
<p>Entry 9: Diels-Alder cycloaddition</p> 	<p>Entry 10: Huisgen 1,3-dipolar cycloaddition</p> 
<p>Entry 11: Staudinger ligation</p>  <p>R₁: Oligonucleotide R₂: Reporter moiety</p>	

Amide bond formation is one of the most widely used synthetic strategies for post synthetic DNA modification. A standard procedure for the amide coupling involves the *in situ* activation of the carboxylic acid using activating reagents 1-ethyl-3-(3-

dimethylaminopropyl)carbodiimide (EDC) or *N*-hydroxysuccinimid (NHS) and subsequent coupling to amino-terminated DNA. Using such strategy, Lapiene *et al.* derivatized amino-modified oligonucleotide with a maleimide moiety using a heterobispecific cross linker sulfoSMCC (sulfosuccinimidyl-4-(*N*-maleimidomethyl)cyclohexane-1-carboxylate). The maleimide functionalized oligonucleotide could then be employed in further conjugation reactions with different fluorescent proteins.^[63] The drawback of the amide coupling reaction is that the nucleophilic nature of the amino group depends on the pH, meaning that at lower pH the amino group is protonated, which reduces the reactivity towards electrophiles.

Other widely used linkage method is the nucleophilic addition between thiol modified oligonucleotide and maleimide containing molecules. This strategy has extensively been used for the preparation of semisynthetic protein-DNA conjugates, in which the maleimide moiety is first introduced to the protein and subsequently conjugated with thiol modified oligonucleotides.^[64] In addition to maleimide-thiol coupling, other click-chemistry strategies, such as the Cu[I]-catalyzed azides-alkyne Huisgen cycloaddition (CuAAC), which is high-yielding, bioorthogonal and does not result in side products, has been employed for DNA modification.^[65] The effect of the cytotoxic copper catalysts, which limits the *in vivo* applications of CuAAC, can be minimized by use of Cu[I]-stabilizing ligands such as tris(benzyltriazolylmethyl)amine (TBTA) and tris(3-hydroxypropyltriazolylmethyl)amine (THPTA).^[66] Further developments in the azide-alkyne cycloaddition strategies also resulted in a copper-free strain-promoted alkyne-azide cycloaddition (SPAAC), which employs strained cyclooctynes and their derivatives.^[67] Cu-free reaction conditions allowed for Huisgen click reactions to be used *in vivo* with cultured cells, live zebrafish and mice. In the last decade, several excellent reviews were published concerning the application of click chemistry reactions for DNA modification, which shows their extraordinary applicability and versatility.^[68] Recently, Bauer and coworkers prepared a small library of bi-functional linkers, which allowed for protein-DNA conjugation employing CuAAC and SPAAC.^[9c] CuAAC reaction was also utilized by Isobe *et al.* for the synthesis of DNA analogues, in which the backbone phosphates were replaced by triazole moieties.^[69] Observed increase in double helix melting temperature demonstrated, that the prepared artificial oligonucleotide analogues have higher stability.^[69] Finally, Timper and colleagues also used click chemistry for the immobilization of alkyne functionalized DNA onto the azide modified silica surface to allow for preparation of the metal wires by gold deposition, enabling new developments in the use of DNA nanotechnology for design of electronic devices.^[70]

Besides azide-alkyne cycloaddition, Diels-Alder reaction between an electron-donating diene and the electron-withdrawing dienophile groups as well as Staudinger ligation between an azide and phosphane group were employed for the DNA conjugation. Generally, due to their stability, dienes are usually incorporated into oligonucleotides during the automated DNA synthesis and subsequently reacted with a range of dienophiles. In such way, Fruk and colleagues used Diels-Alder cycloaddition to label furan DNA with a spectroscopic reporter, benzotriazole dye containing a maleimide dienophile, to allow for detection of DNA at very low, femtomolar concentration.^[71] Highly selective and efficient labeling of DNA with fluorophores was also achieved by Wang *et al.* employing Staudinger ligation in which azido labeled DNA was reacted with fluorescein derivatized phosphane affording modified DNA in 90% yield.^[72] The advantage of using described cycloaddition reactions and Staudinger ligation is not only their high efficiency, absence of the side products and mild reactions conditions, but also their bioorthogonality as the employed reactive moieties are not present in the biomolecules (if not introduced on purpose). Therefore, DNA labeling or conjugation reactions using unprotected oligonucleotides can also be achieved in complex biological environments and *in vivo*.^[73]

For modification of oligonucleotides that are longer than those accessible by chemical synthesis (>100 bases), enzyme facilitated reactions such as enzymatic ligation or polymerase chain reaction (PCR) can be applied. These strategies are also useful for ligation of short native or modified oligonucleotides to other macromolecules such as proteins, polymers, fatty acids or another oligonucleotides, for which traditional routes of covalent modification fail due to the low yields. In one such application, Kjems and colleagues used terminal deoxynucleotidyl transferase (TdT) enzyme for direct enzymatic ligation of native DNA to nucleotide triphosphates coupled to peptides, proteins, dendrimers and PEGs.^[74] Furthermore, the same strategy was used for covalent attachment of nucleotide triphosphate activated streptavidin and G3.5 PAMAM dendrimer to a DNA origami platform.^[74]

As described above, a range of versatile strategies for modification of nucleic acids has been developed. The ability to synthesize, characterize and manipulate DNA opened many novel routes to applications in genomics, molecular biology, molecular engineering and nanobiotechnology. Especially for the latter two fields, DNA is widely used as a structural and functional element for the assembly of nanostructures, in design of antisense therapeutics and for development of microarray and biosensors technology. In order to use DNA for a specific

application, it needs to be modified taking into account the goal of the application and available resources.

Within this thesis DNA was functionalized with light activatable functional groups to enable the temporally and spatially resolved conjugation of DNA to various surfaces such as metallic nanoparticles and silicon wafers, which could further be employed both for development of new hybrid materials or biosensors. Following chapter will explore the importance of DNA coated surfaces and different strategies to achieve their design.

1.4 DNA Coated Surfaces

Functionalization of different surfaces with DNA has become significantly important due to its applications in diagnosis of infectious or genetic diseases, gene expression analysis, single nucleotide polymorphism (SNP) detection and mutation analysis, drug discovery, DNA sequencing, forensic science and sensing.^[75] Due to its physicochemical stability and ability to introduce different modifications to the backbone, DNA was immobilized on various surfaces such as gold, glass, silicon, polymer and other materials.^[76] A number of DNA microarray devices,^[77] new hybrid materials such as DNA-nanoparticle conjugates,^[78] but also various biological sensors^[76b] was developed in the past decades. The applications are commonly based on DNA directed immobilization (DDI): after immobilization of the specific oligonucleotides on the surface, hybridization of the complementary strands can be used to attach the whole range of functional molecules. Commonly used immobilization methods to prepare DNA coated surfaces are physisorption, chemisorption and covalent attachment and they will be addressed in the following sections.

1.4.1 Physisorption of DNA onto Charged Surfaces

Physisorption, as a method of surface modification with oligonucleotides, takes an advantage of the negatively charged DNA backbone, which can be adsorbed onto positively charged surfaces. Deposited oligonucleotides are randomly oriented due to their unspecific interaction with the surface at several points along the backbone (Figure 1.3.).

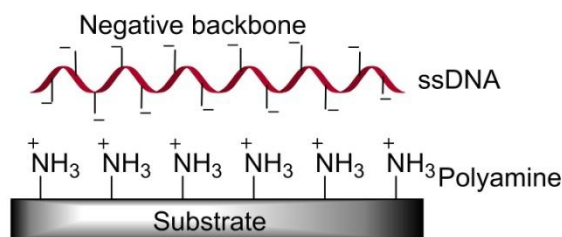


Figure 1.3: Physical adsorption of the negatively charged single stranded DNA onto the positively charged amino-functionalized glass substrate.^[79]

This is considered as the main disadvantage as it results in a weak interaction and a high background signal due to a highly unspecific adsorption. Still, such approach has been used in certain applications. For example, Xu and colleagues designed an electrochemical DNA sensor by immobilizing a single-stranded DNA (ssDNA) onto a chitosan-modified platinum electrode by physical adsorption.^[80] The ability of the sequence-specific DNA detection was confirmed by successful hybridization with the complementary strand. Wongkaew and colleagues demonstrated an effective DNA based voltammetric electrochemical detection method for a verification of the specific pathogenic infection within plants such as destructive crop disease, the sugarcane white leaf (SCWL).^[81] The SCWL-ssDNA, immobilized by electrostatic interactions on a chitosan modified glassy carbon electrode, could be used for identification of different DNA sequences from SCWL plants, mosaic virus infected sugarcane and healthy sugarcane plants. The successful hybridization of immobilized SCWL-ssDNA with a complementary strand from the infected plant probe was confirmed by cyclic and differential pulse voltammetry.

However, although this strategy does not involve any prior modification of the oligonucleotide, but only an introduction of charged moieties to the surface, it provides random orientation and only weak attachment of DNA, which can be easily removed by washing steps or by use of detergents.

1.4.2 Chemisorption of Modified DNA

Chemisorption is the substrate selective bonding of atoms or molecules to the solid surface.^[82] For example, sulfur containing substances including thiols, dialkylsulfides and dialkyldisulfides are known to be chemisorbed with high affinity onto gold.^[83] Therefore, gold surfaces can be coated with DNA by introduction of sulfur containing moieties into oligonucleotides. Furthermore, due to the absence of the sulfur atoms in natural DNA, this

approach was shown to be highly selective for the site-specific attachment of oligonucleotides onto surfaces. In 1996, Mirkin and colleagues showed for the first time that thiol-terminated DNA can be attached to gold nanoparticles (NPs) and subsequent aggregation of the particles can be induced by addition of the complementary strand.^[84] The prepared NP-DNA conjugates were highly stable at ambient conditions and could be stored and used over the prolonged period of time. However, when heated above 60 °C or treated with competing thiol reagents such as dithiothreitol (DTT) or β -mercaptoethanol, bound thiol oligonucleotide dissociated from NP surface. To overcome this problem, Letsinger and colleagues developed dithiane phosphoramidites and introduced them to oligonucleotides.^[85] Dithiane containing oligonucleotides form two gold-sulfur bonds with NP surface resulting in the more stable conjugates. In the meanwhile, DNA-NP conjugates have been used for the alternative DNA delivery in gene silencing applications^[86] and in the design of biosensors and bioelectronic devices.^[87]

Strong interactions between gold surface and thiol terminated oligonucleotides were also employed in fabrication of DNA nanostructures i.e. by AFM-based lithography.^[88] Applying the higher shear force on the AFM tip, the alkanethiol molecules within a self-assembled monolayer on the planar gold surfaces are displaced allowing for the thiol terminated oligonucleotides to adsorb onto the exposed gold area. This principle is called AFM nanografting and can result in DNA lines as narrow as 10 nm.^[88] The grafting approach was recently used by Castronovo and colleagues for the investigation of enzyme/DNA interactions within nanografted DNA patches of different density, demonstrating that the enzymatic activity is inhibited when the DNA density is higher than a certain threshold density.^[89] The AFM based methodology can be particularly interesting for preparation of biosensors and in one such approach, Bano and colleagues utilized nanografted DNA patterns for DNA directed immobilization of proteins to afford protein arrays for further sensing applications.^[90]

Chemisorption approach is a useful DNA immobilization strategy, however for some applications, in particular for a design of DNA microarrays, a covalent binding of molecules is preferred due to the stronger attachment. In addition, for many applications, the use of gold surfaces is not cost effective.

1.4.3 Covalent Attachment of DNA onto Various Surfaces

Covalent attachment is widely used strategy for the DNA immobilization onto surfaces as it relies on the conjugation of the chemically modified DNA to the activated surface by

formation of the stable covalent bonds. This allows a single point attachment of oligonucleotides in a region-selective manner with good surface coverage. Moreover, the oligonucleotide-surface bond remains stable towards high temperature and high salt concentration, which are often required in subsequent washing procedures or applications. Various strategies for the covalent attachment of oligonucleotides were developed, and many are overlapping with the DNA modification strategies summarized in Table 1.1. For the choice of the right surface chemistry, several aspects should be considered: a) the linkage between surface and oligonucleotide should be *chemically stable*, b) selected linker should ensure *efficient hybridization* and *minimize the steric interference* with the surface, c) *non-specific interaction* of oligonucleotides with surface should be *minimized* or eliminated and d) the reaction should be compatible with *aqueous conditions*.

In order to choose the right modification strategy, firstly, the application requirements should be considered. For microarray technology, glass slides are usually employed to prepare chips, while biosensors often require immobilization of DNA onto surface of various nanoparticles (gold, silver, magnetic or semiconducting) or noble metal electrodes. Self-assembly of larger devices might require use of both metals and polymers. The chemistry employed to coat such surfaces with DNA will depend largely on the surface material.

Glass and silicon surfaces, which are employed for microarray fabrication can be functionalized by use of organosilanes, which have been shown to be a very efficient reagents to introduce various functional groups to the glass surface.^[91] Different organosilane derivatives have been developed to date and the most widely used are shown in Figure 1.4.

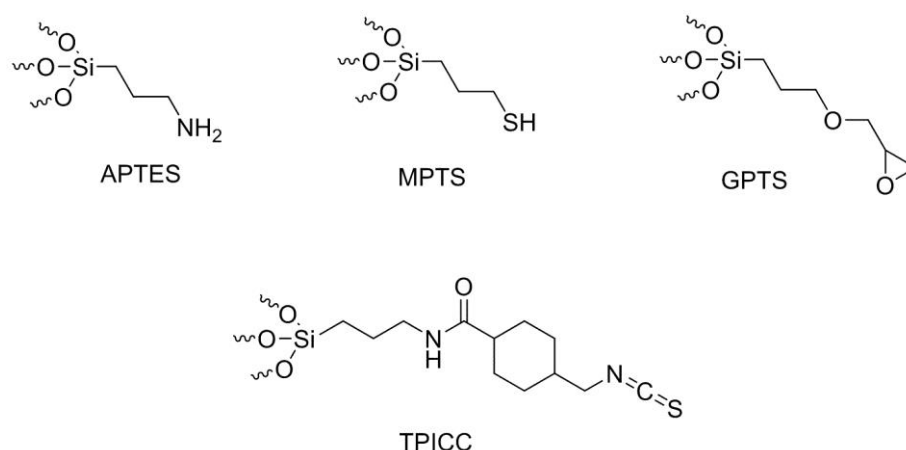


Figure 1.4: Most commonly used organosilane reagents for functionalization of glass and silicon surfaces. APTES = (3-aminopropyl)triethoxysilane, MPTS = (3-mercaptopropyl)trimethoxysilane, GPTS = (3-glycidopropyl)triethoxysilane, TPICC = *N*-(3-triethoxysilylpropyl)-4-(isothiocyanatomethyl)cyclohexane-1-carboxamide.

(3-Aminopropyl)triethoxysilane (APTES) is widely used for the introduction of amino groups on glass and silicon surfaces.^[92] APTES has also been shown to form covalently attached self-assembled monolayer (SAM) on aluminium oxide and gold surfaces.^[93] Recently, hydroxy functionalized multi-walled carbon nanotubes were silanized using APTES in order to improve the dispersion and interfacial interaction in composites.^[94] Once introduced to the surface, amine groups can further be derivatized with appropriately modified oligonucleotides.^[95] Using *N*-(3-triethoxysilylpropyl)-4-(isothiocyanatomethyl) cyclohexane-1-carboxamide (TPICC), Misra *et al.* introduced isothiocyanate moieties onto the glass surface to allow for the immobilization of self-quenched amino modified DNA hairpin, which fluorescence is restored upon hybridization with the complementary DNA.^[96] In a study by Sethi and colleagues, aminoalkyl, mercaptoalkyl and phosphorylated *ss*DNA were first reacted with (3-glycidoxypropyl) trimethoxysilane (GOPTS) using nucleophilic epoxide ring opening, and the resulting conjugates were subsequently immobilized onto the glass surface employing the silanization strategy to obtain DNA microarray.^[97] Fabricated microarray showed high immobilization efficiency (36-40%), high signal-to-noise ratio (98) and high hybridization ability. Silanization procedure was also utilized for the functionalization of glass with the maleimide moiety. Such surfaces can further react with thiolated DNA by thioether linkage^[98] as well as with the diene functionalized DNA *via* Diels-Alder cycloaddition.^[99] In addition, Rozkiewitz and colleagues reported a straightforward method to immobilize acetylene-modified oligonucleotides onto the azide terminated glass substrate employing click chemistry and microcontact printing.^[100] Glass slides were first silanized with 11-bromoundecyltrichlorosilane and subsequently treated with saturated sodium azide solution in order to replace bromide groups with azide. In the next step, acetylene modified oligonucleotides were physisorbed onto the dendrimer functionalized PDMS stamps and immobilized to the azide substrate by click reaction induced by microcontact printing.

Activation of various surfaces by silanization was also used for the fabrication of DNA biosensors. For example, an indium tin oxide glass (ITO) electrode was silanized with APTES and then reacted with the aldehyde modified complementary oligonucleotide by Schiff base formation.^[101] To obtain such electrodes, amide bond formation was also employed whereas the ITO surface was first functionalized with carboxyl moieties using 3-phosphonopropionic acid and subsequently reacted with amino terminated oligonucleotides by EDC/NHS coupling.^[102] Strategy employing amide coupling was also successfully used to immobilize amino terminated oligonucleotides onto a polycarbonate-gold nanoelectrodes^[103] and onto

carboxyl group coated CdSe/ZnS quantum dots (QD).^[104] To design DNA biosensors, Chen and colleagues recently utilized Diel-Alder cycloaddition reaction by first adding the maleimide dienophile to silver NPs and subsequently reacting them with diene modified DNA strands.^[105]

In general, covalent attachment represents a powerful tool for the immobilization of oligonucleotides onto various surfaces, enabling not only fabrication of the stable functional constructs, but also covering the wide range of surfaces and available functional groups. However, this strategy requires the activation of the reaction partners by different reagents, which can affect the yields and the subsequent hybridization of the complementary strands. Within this thesis, we have investigated sub-group of covalent strategies, namely photochemical reactions for attachment of DNA to various surfaces. Photochemical reactions are particularly interesting as they enable spatial and temporal control over the immobilization by use of light. Next section will give an overview of the mechanism and types of photochemical reactions further described in Results and Discussion.

1.4.4 Photochemical Reactions for the DNA Immobilization

Photochemical reactions are chemical reactions, caused by absorption of ultraviolet, visible or infrared irradiation.^[106] According to the first law of photochemistry the light of a particular wavelength must be absorbed for photochemical process to occur. After absorption of light, the molecule is promoted from its ground state (S_0) to a higher energy state (S_1), which in turn can undergo different physical and chemical processes. These are summarized in Jablonski diagram shown in (Figure 1.5).^[107]

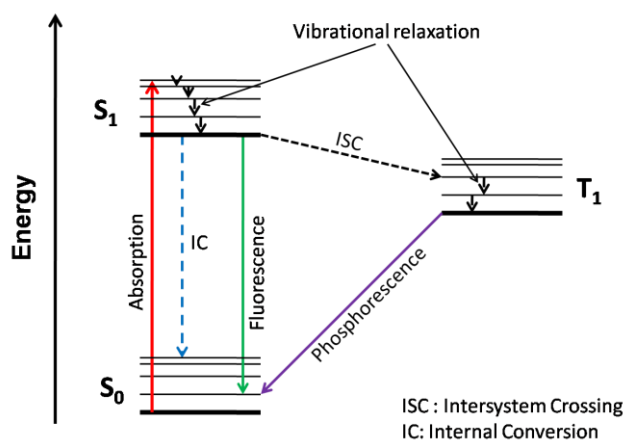


Figure 1.5: Schematic depiction of the Jablonski diagram including electronic excitation *via* absorption, radiative relaxation processes such as fluorescence and phosphorescence, and non-radiative processes such as internal conversion, intersystem crossing and vibration relaxation.

According to Frank-Condon-Principle, the excited molecule interacts with the surrounding molecules under energy loss and eventually reaches the vibrational ground state S_1 . Further loss of excess energy can happen through several physical routes including fluorescence, internal conversion, phosphorescence and energy transfer to another molecule. Internal conversion of excited states to lower energy states of the same multiplicity ($S_1 \rightarrow S_0$) takes place fast with loss of heat energy. Alternatively, the transition to the ground state can take place under light emission (fluorescence). The transition from excited single state S_1 to a lower energy triplet state T_1 is termed intersystem crossing. After relaxation to the ground T_1 state the radiative decay (phosphorescence) can occur including the transition from T_1 to S_0 . Importantly, the excited state energy can also initiate a chemical reaction such as elimination, cyclization, addition, electron transfer, cleavage, isomerization or rearrangement. Photochemical reactions can allow for the constructions of thermodynamically disfavored products like small rings, overcoming large activation barriers. Moreover, since the chemical reaction takes place exclusively after interaction with light, it can be controlled in a temporal and spatial manner. This poses a significant advantage for application of DNA as a structural or functional building material, in catalysis, for gene regulation and molecular diagnostics (DNA microarrays).

To guide the immobilization of oligonucleotides or affect their properties with light, different strategies have been developed. Generally, they can be divided into photoswitching and photocaging strategies and the use of photo-activatable groups.^[108] Photoswitching is based on the ability of molecules to undergo isomerization reactions upon light irradiation and in such way enabling structural changes of the systems they are coupled to. The most prominent molecule used for the photoswitching studies is azobenzene, which undergoes photochemically induced and a wavelength controlled *cis/trans* isomerization of the N=N bond. Once introduced to the oligonucleotides, it can affect the hybridization ability. Asanuma and colleagues found that *trans*-azobenzene units intercalate into duplex DNA structures through π - π interactions, leading to cooperative stabilization of the DNA duplex.^[109] On the other hand, *cis*-azobenzene lacks such affinity and therefore leads to helix destabilization. In the meanwhile, different approaches based on azobenzene switches have been developed.^[108a] Yan and colleagues employed visible-light-stimulated stabilization of duplex DNA by *trans*-azobenzene and duplex separation by UV-stimulated photoisomerization of *trans*-benzene to *cis*-benzene for the photoregulation of gold nanoparticles aggregation.^[110]

In case of photocaging, the regulation of the molecular processes with light is achieved by introduction of the photolabile protecting groups, either on the nucleobases, which affects the Watson-Crick base pairing, or on the ribose, the phosphodiester backbone, or internally.^[108a] To achieve that, a plethora of the photocleavable groups has been developed.^[111] For example, Deiters and colleagues added 6-nitropiperonyloxymethyl-caged thymidine to phosphorothioate oligonucleotides, antisense agents, which hybridize sequence specifically to mRNAs inhibiting translation and potentially leading to mRNA degradation through RNase H. Addition of the caging group decreases the antisense activity, which can be restored by its removal upon irradiation with UV light at 365 nm.^[112]

Light activation and photocaging have been used for the first to allow *in situ* preparation of DNA microarrays at the beginning of 1990s.^[113] Design procedure is based on the conventional phosphoramidite synthesis of oligonucleotides but employs light to activate each consecutive step in the oligonucleotide synthesis. First, hydroxyl derivatized glass substrate is reacted with the base, protected with a photocleavable protecting group at the 5'-end (Figure 1.6).

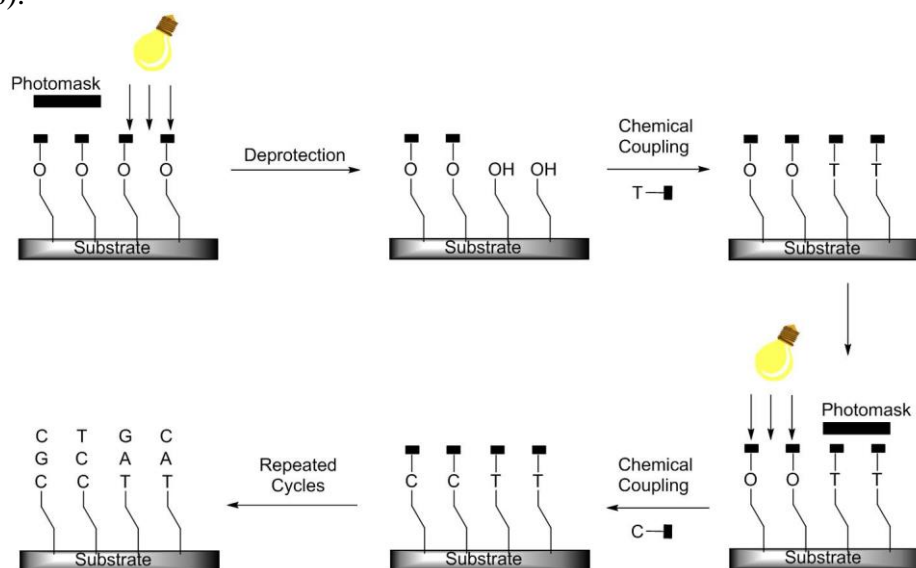


Figure 1.6: Scheme of the *in situ* photolithographic preparation of the oligonucleotides directly on the surface. Based on [79].^[79]

Subsequently, light is allowed to pass through a photolithographic mask with a high spatial resolution to enable photodeprotection to which another 5'-protected building block is added. In the following step, a new mask is used for site specific irradiation to generate next pattern of hydroxyl groups and the chemical cycle is repeated. In this way, the oligonucleotide chains of desired sequence and length are prepared. This method has revolutionized microarray

methodology as it enables the generation of small microarrays of high density (10^6 sequences/cm²).^[79] The success of this strategy depends on several factors such as efficiency of photocleavage procedure, the accuracy of mask alignment and the yields of phosphoramidite coupling steps. However, the method is burdened with some drawbacks, namely, low coupling yields, no quality and purification control of the generated arrays, long fabrication time, requirement for the expensive photo-masks and sophisticated instrumentation. In order to improve efficiency of the photocleavage procedure various photolabile protecting groups such as benzoyl-2-(2-nitrophenyl)-propoxycarbonyl and thiophenyl-2-(2-nitrophenyl)-propoxycarbonyl were introduced.^[114] In addition, the elaborate masks were replaced by a light projection from a digitally controlled array of micromirrors.^[115] Recently, Sack and colleagues presented an optimized photolithographic microarray fabrication procedure, using very photosensitive protecting group thiophenyl-NPPOC, which shortened the photodeprotection and coupling time resulting in a six-fold reduction in array fabrication time.^[116]

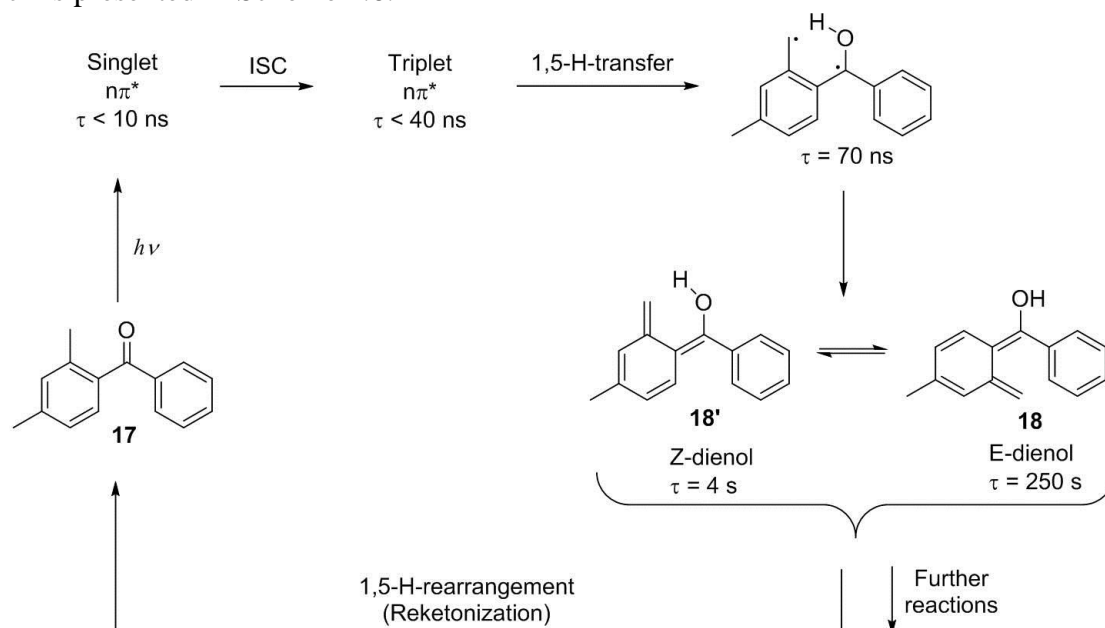
Another approach makes use of the chemical reactions in which photo-activatable moiety is attached to the DNA and allowed to react with various functional groups on surfaces. In such way, Koch and colleagues immobilized anthraquinone modified oligonucleotides on microtiter wells.^[117] In its excited state, anthraquinone is highly reactive towards C-H containing substrate and could be attached to various surfaces such as polystyrene, polycarbonate, polypropylene, Teflon and silylated glass. In another approach, formation of the light activated thioether linkage was used to immobilize thiol-DNA onto epoxy-functionalized silicon-substrate *via* UV irradiation (365 nm).^[118] The spatial control was achieved by employing the shadow mask. Additionally, light-induced thiol-ene and thiol-yne reactions were utilized by the same group for the immobilization of the thiolated DNA on alkene or alkyne functionalized silicon surface.^[119]

Within this thesis, light-induced Diels-Alder reaction and light-induced nitrile imine mediated tetrazole-ene cycloaddition were employed to control the reactions by light, and both reactions are discussed in the following section.

1.4.4.1 Light-induced Diels-Alder Cycloaddition

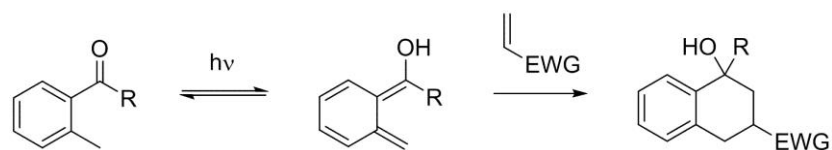
Light-induced Diels-Alder reaction is a [4+2] cycloaddition reaction between light-activated dienols, photoenols, which are formed *via* tautomerization of *o*-alkylphenylketones or *o*-alkylbenzaldehydes under UV irradiation, and dienophiles.

Photoenolization, the light-induced dienol formation, was first reported by Yang and Rivas in 1961.^[120] They obtained dienol **18** of the *ortho* substituted benzophenone (*o*-dimethyl benzophenone) **17** instead of expected photochemical reduction product benzopinacol in the presence of hydrogen donors. Such dienol readily reacted with dimethyl acethylenedicarboxylat to give Diels-Alder cycloadduct in excellent yields.^[120] After extensive flash photolysis investigations, Porter and Tchir proposed a photoenolization mechanism for this reaction, which is presented in Scheme 1.6.^[121]



Scheme 1.6: Photoenolization mechanism of 2,4-dimethylbenzophenone **17**. After absorption of light, excited singlet state is formed, which undergoes intersystem conversion (ISC) to the corresponding triplet state. After the internal 1,5-H-transfer di-radical species is formed followed by formation of E and Z dienol isomers **18** and **18'**. Both isomers can undergo the 1,5-rearrangement (also termed reketonization) yielding the starting ketone. Additionally, E-isomer can undergo Diels-Alder cycloaddition or electrocyclic reactions. The figure was adapted with permission from [121].^[121]

The initial $n\pi^*$ singlet state, which is formed after a photon absorption by 2,4-dimethylbenzophenone **17**, is extremely short-lived (lifetime $\tau < 10$ ns) and undergoes intersystem crossing to the corresponding triplet state, which exhibits a lifetime of $\tau < 40$ ns. The triplet state decays to a transient di-radical species ($\tau = 70$ ns) under 1,5-hydrogen transfer, which then undergoes the recombination with delocalised π -electrons of the aromatic ring and result in formation of E- and Z-isomeric dienols **18** and **18'**. E-dienol **18** exhibits longer lifetime (250 s) due to the unfavored internal tautomerization to starting ketone in aprotic solvents (1,5-hydrogen rearrangement) and can therefore, be employed for subsequent reactions such as Diels-Alder cycloaddition or electrocyclic reactions.^[121-122] The general reaction scheme for the light-induced Diels-Alder cycloaddition is depicted in Scheme 1.7.



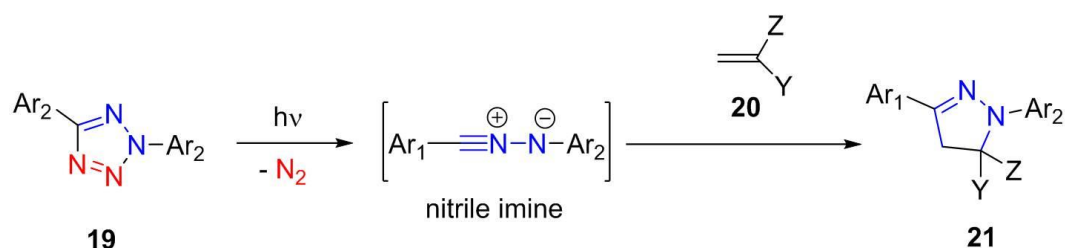
Scheme 1.7: General reaction scheme for the light-induced Diels-Alder cycloaddition of *o*-methyl benzaldehyde/benzophenone with an electron deficient dienophile; R = H, Ph; EWG = electron withdrawing group.

After the light absorption, reactive dienol is formed, which readily undergoes cycloaddition reactions with electron-deficient dienophiles, such as maleimide, the driving force of the reaction being the restored aromaticity. Although the photoenolization of *o*-methyl/phenyl ketones and aldehydes has been employed in organic chemistry for a long time,^[122-123] it was only recently applied in polymer chemistry and wider by group of Barner-Kowollik.^[124] In their initial study, two polymers each containing either *o*-methyl benzophenone or maleimide group have been conjugated *via* light-induced cycloaddition reaction under irradiation with a compact fluorescence lamp (36 W, $\lambda_{\text{max}} = 320$ nm) in toluene.^[124] Inspired by the success and high efficiency of the block copolymer formation, the same strategy was applied to the preparation of the tri-block polymers and wider.^[125] Further numerous studies led to the synthesis of the more reactive photoenol precursor, 2-formyl-3-methylphenoxy (FMP) derivative, which could undergo a cycloaddition with less electron deficient acrylates.^[126] Moreover, due to its biocompatibility, FMP has also been applied to coupling of biomolecules. In one such example, maleimide functionalized peptide could successfully be immobilized to FMP modified silicon wafer in a spatially controlled manner, utilizing a shadow mask.^[126a] Furthermore, Bauer and colleagues recently employed FMP derivative for the light-induced conjugation of DNA with maleimide functionalized myoglobin.^[127]

1.4.4.2 Nitrile Imine-Mediated Tetrazole-Ene Cycloaddition (NITEC)

Another light-induced conjugation strategy used within this thesis and further described in Results and Discussion, employs tetrazoles as photo-activatable compounds. Photochemical reactions of tetrazole moiety have been studied extensively for the last 50 years and it was first reported by Huisgen and colleagues in 1967 employing 2,5-diphenyl tetrazole and methyl crotonate as reagents.^[128] Upon UV irradiation, 2,5-diphenyl tetrazole undergoes facile cycloreversion and generates a nitrile imine dipole *in situ*, which spontaneously reacts with methyl crotonate to afford fluorescent pyrazoline as a cycloproduct. Nitrile imine, unlike other dipoles, readily undergoes reaction with water, resulting in hydrozides, which is the reason for

its *in situ* formation.^[129] General reaction scheme between the tetrazole **19** and dienophile **20** to afford fluorescent pyrazoline **21** is given in Scheme 1.8.



Scheme 1.8: General reaction scheme for the light-induced NITEC between 2,5-diaryl tetrazole **19** and alkene dipolarophile **20** to afford fluorescent pyrazoline **21**.

For a long time, tetrazoles were mostly used for the synthesis of heterocycles and polymers,^[130] but in 2007, Lin *et al.* reported the use of tetrazole for synthetic and biological applications.^[131] Since then, his group has extensively studied the photo-induced chemistry of tetrazoles and reported on various tetrazole derivatives in order to achieve highly biocompatible systems.^[132] Recently, the tetrazole-based cycloaddition (often referred to as NITEC for nitrile imine-mediated tetrazole-ene cycloaddition) has successfully been employed to selectively functionalize an alkene encoded protein *in vivo* under irradiation ($\lambda_{\text{max}} = 302$ nm) and the reaction could be monitored in real time by following the formation of the fluorescent pyrazoline cycloadduct ($\lambda_{\text{Ex}} = 438/24$ nm, $\lambda_{\text{Em}} = 483/32$ nm).^[133] Furthermore, Lin and colleagues also prepared a panel of oligothiophene-based tetrazoles in order to shift the activation wavelength towards visible (405 nm) region. Such water soluble tetrazole was then employed for the real-time spatially controlled fluorescence imaging ($\lambda_{\text{Ex}} = 458$ nm, $\lambda_{\text{Em}} = 531\text{--}623$ nm) of microtubules in live mammalian cells.^[134] NITEC strategy was also used for polymer grafting onto tetrazole functionalized silicon wafers and cellulose,^[135] and for conjugation of the antifouling polymers to polydopamine surface.^[136] Recently, our group showed that maleimide modified oligonucleotides can be attached to the surface of the tetrazole coated gold nanorods and the coupling quantified by fluorescence measurement of the resulting product.^[137]

Such recent applications of both light triggered reactions prompted us to try to employ them for structuring of DNA on various surfaces and inspired the use of simpler, more efficient strategy for surface patterning based on precise delivery of light by means of laser writing.

1.5 Methods for DNA Surface Structuring

The physical and chemical character of DNA immobilization to various surfaces has been reviewed in previous sections. However, for biosensing and diagnostic application, precise structuring of the surfaces is often needed to allow for the immobilization of pre-programmed sequences in a controllable spatial manner. This can be achieved by careful choice of the oligonucleotide structuring/surface delivery methods. The most common techniques to enable design of DNA structured surfaces were summarized in an extensive review by Meyer and colleagues and are shown in Table 1.2.^[11d]

Table 1.2: Overview of different techniques used for surface structuring of oligonucleotides. Adapted with permission from [11d].^[11d]

Method	Patterning mode ^a	Transfer mode ^b	Multiplexing ^c	Minimal feature size ^d	Process time/speed ^e	Feature generation ^f
Dip-pen Nanolithography	Direct	Direct	Sequential	100 nm	1 s/feature	Serial
Nanografting	Direct	Self-assembly	Sequential	10 - 100 nm	800 nm/s	Serial
Microcontact Printing	Replicative	Direct	By spotting of stamp	5 - 50 μm	20 min/stamping	Parallel
Inkjet printing	Direct	Direct	Sequential	50 - 200 μm	n.a. ^g	Serial
Nano-pipetting	Direct	Direct	Sequential	800 nm	10 s/feature	Serial
Microfluidic patterning	Replicative	Self-assembly	Sequential	10 - 100 μm	4 h/chip	Parallel
Photolithographic in situ synthesis	Replicative	In situ synthesis	Massive	1 μm	60 - 360 s/frame	Parallel

^aPattern is generated directly or by intermediate structures like masks or molds (replicative)

^bDirect feature transfer of ssDNA, by self-assembly or in situ synthesis

^cArray with different sequences possible

^dSpot diameter or line width

^eFeature fabrication duration

^fParallel or serial (one after another) feature generation

^gNo values specified

Important parameters to guide the choice of the structuring methods are the size and the number of features which can be generated, as well as the multiplexing ability of the method, that is, the ability of producing patterns of different sequences. One of the approaches, the photolithographic *in situ* synthesis, which is characterized by high multiplexing ability was described in Section 1.4.4 (Figure 1.6). However, this method is highly demanding in terms of instrumental equipment.^[138] Another photolithographic processes such as immobilization of pre-synthesized oligonucleotides *via* photo-activatable linker uses shadow masks to introduce desired pattern. Such an approach has the advantage of the simultaneous exposure, but for every desired pattern a specific mask must be fabricated, the method is not capable of multiplexing and the resolution is restricted to several tens of micrometers. For conventional applications in bioanalytics, such as gene expression profiling, inkjet printing has been the method of choice to afford the fabrication of oligonucleotide microarrays bearing spots of $\geq 100 \mu\text{m}$ diameter. Within this method, sample droplets are delivered to pre-programmed sites. However, for the applications of microarrays for single cell studies, more elaborate array constructions with smaller feature sizes are required. Only few methods are capable of structuring the features smaller than $10 \mu\text{m}$ diameter and these include high resolution methods such as dip-pen nanolithography^[139], AFM nanografting (Section 1.4.2),^[90] nano-pipetting^[140] or microcontact printing (Section 1.4.3).^[141] However, these methods are often time consuming and either lack in multiplexing ability (nanografting) or patterning variety (microcontact printing).

To overcome some of the drawbacks of existing DNA structuring methods and enable one-step fabrication of arrays with various patterns using light-induced reactions, we employed a multi-photon strategy referred to as direct laser writing (DLW), which is based on multi-photon absorption by photopolymers and allows fabrication of computer-designed mm-sized 3D structures with sub-100 nm spatial resolution.^[142]

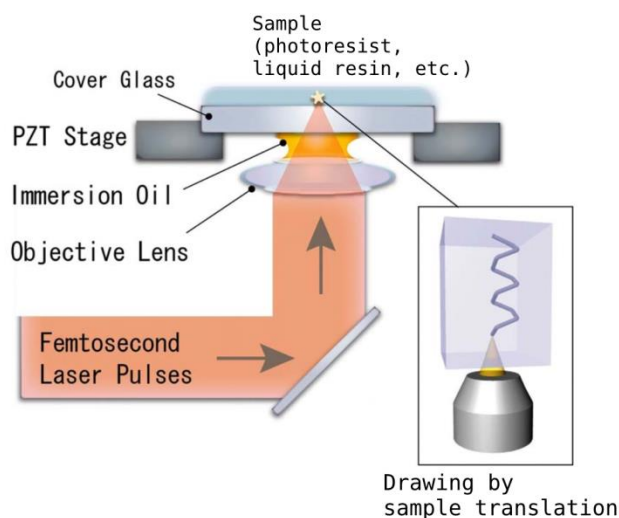


Figure 1.7: General experimental direct laser writing (DLW) setup. The inset shows the principle of drawing by a moving laser beam, which is focused onto the photoresist material. Adapted with permission from [143].^[143]

Figure 1.7 depicts a general experimental DLW setup. The beam of a femtosecond titanium sapphire oscillator is tightly focused inside the volume of transparent photopolymer solution, which is usually deposited on a supporting glass substrate. The laser light is absorbed *via* multi-photon absorption process at the focus, leading to a photo-polymerization within the absorbing material. By translating the focal spot inside the sample, arbitrary 3D structures can be fabricated. The translation can be achieved by using the high-accuracy translation stages controlled by piezo transducers or by moving the laser beam. Combination of the different light-induced chemical processes with the multi-photon absorption makes DLW technique highly suitable for various applications. Employing photo-polymerizable compounds, such as acrylates, but also organic-inorganic hybrid materials a number of components and devices has been fabricated such as photonic crystals,^[144] micromechanical and microfluidic devices,^[145] biomedical micro-devices and cell culture scaffolds.^[146] Recently, methacrylate modified polylactide was employed to fabricate high-resolution 3D structure to grow neuroblastoma cells, which preserved their viability and proliferation, indicating a good biocompatibility of the written structure, opening new routes for the use of such structures in the preparation of neuronal implants.^[147]

In addition to 3D fabrication, DLW can also be employed for the precise spatially resolved patterning on different surfaces. In this manner spatially controlled surface immobilization of functional polymers^[148] and gold nanoparticles,^[149] and as shown within this thesis DNA patterning could be performed.

2 Research Objectives

The aim of this thesis is to *establish light-induced conjugation strategies* to allow for DNA protein conjugation and surface immobilization in a controllable manner. DNA is a biopolymer, with the main role of being the genetic code carrier, and as with any other biomolecule, the chemical methods for its modification need to be mild (no temperature or pH extremes, no catalysts, or harsh reagents), proceed readily in aqueous solutions and be bioorthogonal. Besides its major role in genetics, DNA double helix formation between two DNA strands has been shown to be remarkably efficient way for immobilization of various moieties onto different surfaces, a process known as DNA directed immobilization. This requires an attachment of single stranded short DNA onto the desired surface, and a subsequent hybridization with the complementary strand. To achieve that, besides above requirements, chosen chemical strategy also needs to allow for the formation of a stable, covalent surface linkage in a controllable and reproducible way.

Within this thesis, two conjugation strategies should be employed, *the light-induced Diels-Alder cycloaddition* and the *nitrile imine-mediated tetrazole-ene cycloaddition* (NITEC). They were selected because they are bioorthogonal, do not require harsh conditions or catalysts, proceed well in aqueous media, although with different level of efficiency and can be triggered “on-demand” by light. To respond to irradiation, DNA needs to bear a light-activatable groups, which should be added to a short single stranded oligonucleotide using different modification approaches such as phosphoramidite, H-phosphonate or amide coupling to select for the most efficient. Two different photo-activatable photoenol moieties 2,5-dimethylbenzophenone and 2-methoxy-6-methylbenzaldehyde as well as 2,5-diphenyl tetrazole should first be derivatized with appropriate functional group and subsequently incorporated at 5'-end of oligonucleotides. The ability of the modified oligonucleotides to undergo *light-induced reactions should then be investigated by kinetic studies*, employing a model, small ene-containing molecule, to select for the most suitable light-induced reaction to be used for *preparation of DNA-protein conjugates* and *DNA coated surfaces employing direct laser writing strategy*.



3 Results and Discussion

3.1 Synthesis of the Photo-Activatable Oligonucleotides

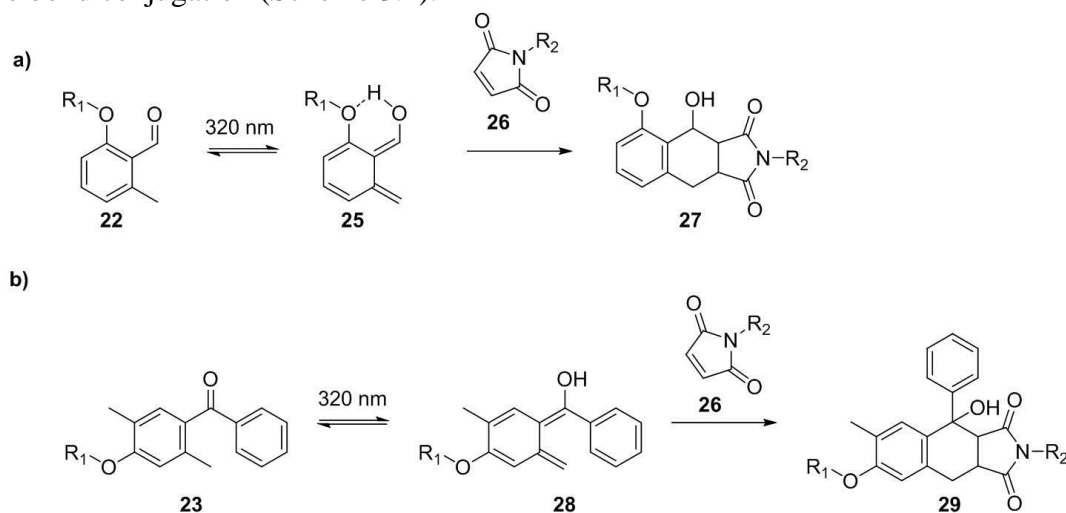
Various strategies have been employed for the light-induced regulation of oligonucleotide synthesis and reaction, although they could be grouped into three distinct approaches.^[108] One involves the use of the light sensitive protecting groups within the key locations such as nucleobases, ribose or phosphodiester as well as 5'- and 3'-end. The introduced modification blocks the inherent function of these groups by use of protecting functional groups (photo-caging), which can then be restored by use of light. This process is inherently irreversible. The other involves introduction of the light activatable molecular species to oligonucleotide, which undergo reversible isomerization reactions of double bonds or unimolecular pericyclic reactions upon irradiation (photo-switching).^[108a] The incorporated molecules change their conformation affecting the hybridization ability of the oligonucleotide and the process is reversible (switchable). Third approach employs light to control oligonucleotides and other biomolecules within the cells, typically neurons, which have been genetically modified in order to express light-sensitive ion channels.^[108a]

Within this thesis, new strategy was explored in which the advantages of first two approaches were employed. The isomerizable moiety was incorporated within oligonucleotides not for its steric effects, but for the reactive isomer formed upon irradiation to be further employed in modification reactions with various molecular species. As such, a photo-activatable 2-methoxy-6-methylbenzaldehyde **22** and 2,5-dimethylbenzophenone derivative **23**, which form reactive dienols, photoenols (PE) described in Section 1.4.4.1, were utilized. The generated reactive dienols can be trapped by electron deficient dienophiles in a Diels-Alder cycloaddition reaction. Resembling the photo-caging strategy, individual building elements of oligonucleotide were not protected, but rather protected reactive moiety was added to the oligonucleotide. The caging group can be removed by irradiation affording reactive group to further engage in coupling reactions. For this approach, tetrazole derivative **24**, which generates nitrile imine species upon photolysis and nitrogen release, was employed. Nitrile imines are reactive intermediates and undergo 1,3-dipolar cycloaddition reactions with various dipolarophiles. Both photoenol and tetrazole strategies can be, as it is shown further in the thesis, be used to link the oligonucleotides with other molecules in controllable manner using light as a trigger.

For the incorporation of these photo-activatable groups standard phosphoramidite and H-phosphonate methods, but also amide coupling *via* *N*-hydroxysuccinimide (NHS) ester were employed. The following section describes the synthesis of novel photo-activatable oligonucleotide building blocks, and their introduction to oligonucleotides by solid phase synthesis.

3.1.1 Phosphoramidite Method

As described in Section 1.4.4.1, photoenolization combined with subsequent Diels-Alder trapping, represents an effective method for the light controlled molecule association. Diverse photoenol precursors at different reaction conditions were screened by group of Prof. Barner-Kowollik for their applicability in a light-induced Diels-Alder cycloaddition reaction and are described elsewhere.^[150] In these studies, 2-methoxy-6-methylbenzaldehyde **22** and 2,5-dimethylbenzophenone **23** were found to give highest yields and fastest rate of reaction under mild reaction conditions.^[150] Photoenol **25** which is generated by irradiation of 2-methoxy-6-methylbenzaldehyde **22** is stabilized by internal hydrogen bonds and therefore less unstable in his activated state and longer available for further reactions, resulting in better product yields as shown in the case of the Diels-Alder cycloaddition with maleimide **26**. In case of 2,5-dimethylbenzophenone **23** the stabilization of the photoenol species **28** results from a double bond conjugation (Scheme 3.1).

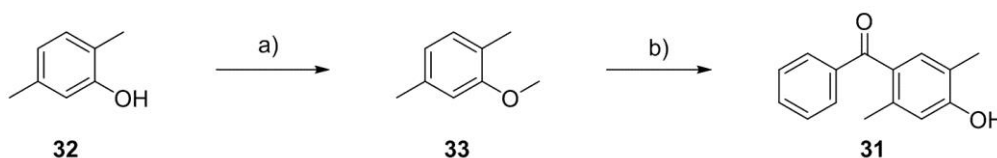


Scheme 3.1: Light-induced photoenol formation and its subsequent Diels-Alder cycloaddition reaction with maleimide moiety using a) 2-methoxy-6-methylbenzaldehyde **22** and b) 2,5-dimethylbenzophenone **23** as a photoenol precursor.

The photoenols,¹ especially **22**, which was found to be the most efficient, were used for various applications including polymer-polymer conjugations,^[126b, 151] immobilization onto different surfaces^[126a, 149, 152] and the design of 3D micro scaffolds.^[153] In addition, the light-induced conjugation strategy based on Diels-Alder cycloaddition of photoenols has been shown to be biocompatible, since it can be performed in aqueous media at ambient temperature. In one such study, maleimide functionalized peptide was covalently bound to photoenol coated silicon surfaces in a patterned way using a shadow mask.^[126a] In addition, biosurfaces such as hyaluronan film and cellulose were functionalized with photoenol moiety and patterned with maleimido-poly(trifluoroethyl methacrylate) and maleimido-peptide.^[154] Following this ground breaking work of Prof. Barner-Kowollik *et al.*, we explored the use of the photoenol based conjugation strategy to DNA functionalization and structuring.

Initially, Bauer *et al.* derivatized an oligonucleotide with 4((2-formyl-3-methylphenoxy)methyl)benzoic acid **30** through amide coupling using HBTU/HOBt as coupling reagents onto amino terminated oligonucleotide.^[126a, 127] The photoenol modified DNA was then conjugated to a protein myoglobin containing maleimide groups by light-induced Diels-Alder cycloaddition resulting in the functional protein-DNA conjugate. However, this approach resulted in the low yields of PE modified DNA, so we decided to explore another, more convenient strategy based on the use of phosphoramidites.

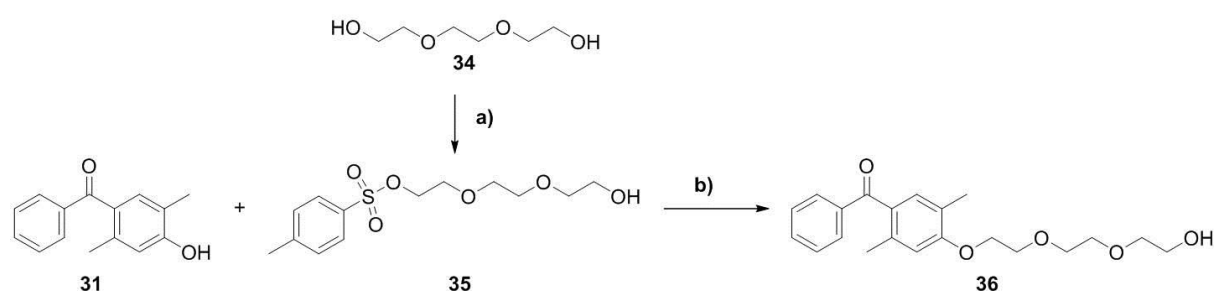
Phosphoramidite approach, described in Section 1.2.1, was employed for tethering the photoenol moiety to a 5'-end of oligonucleotide using automated solid phase synthesis, commonly employed for preparation of modified oligonucleotides. This method allows the direct introduction of photoenol moiety to various non-modified sequences during the automated process using DNA synthesizer. The procedure employs phosphoramidite building blocks containing desirable functional groups together with the range of reagents in a sequence of reactions, which result in DNA synthesis and desired modification.^[43]



Scheme 3.2: Synthesis of photoenol PE1 **31**; a) NaOH, CH₃I, THF, 50 °C, 16 h; H₂O, 88%; b) AlCl₃, benzoyl chloride, 0 °C - RT, CH₂Cl₂, 60h, 10%.

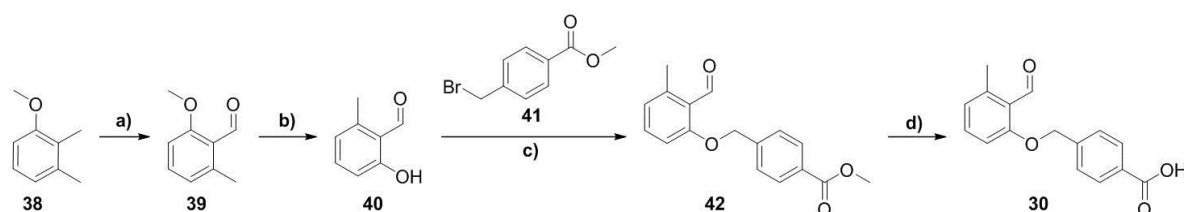
¹For the sake of convenience 2,5-dimethylbenzophenone **23** and 2-methoxy-6-methylbenzaldehyde **22** are called photoenols, PE1 and PE2, in the following text.

To achieve this with photo-activatable groups, phosphoramidites bearing photoenol moiety need to be synthesized and the first step was the preparation of photoenols PE1 **31** (Scheme 3.2)^[155] and PE2 **37** (Scheme 3.5) adapting the literature procedures. Firstly, 2,5-dimethylphenol **32** was etherified using methyl iodide as reported by Paptchikhine and co-workers,^[155] which was then followed by Friedel-Crafts acylation and methyl ether cleavage using AlCl₃ as a catalyst.^[126a] In order to improve the solubility and to allow for more steric freedom for further ligation reactions, the prepared photoenol PE1 **31** was derivatized with a three-membered glycol unit in a nucleophilic substitution of tosylated triethylene glycol **35** (Scheme 3.3).^[156] This resulted in modified photoenol **36** obtained in 87% yield.^[126a]



Scheme 3.3: Synthesis of triethylene glycol derivatized PE1 **36**; a) 4-methylbenzenesulfonyl chloride, CH₂Cl₂, 0 °C - RT, 16 h, 21%; b) K₂CO₃, LiBr, 18-crown-6, MeCN, reflux, 24 h, 87%.

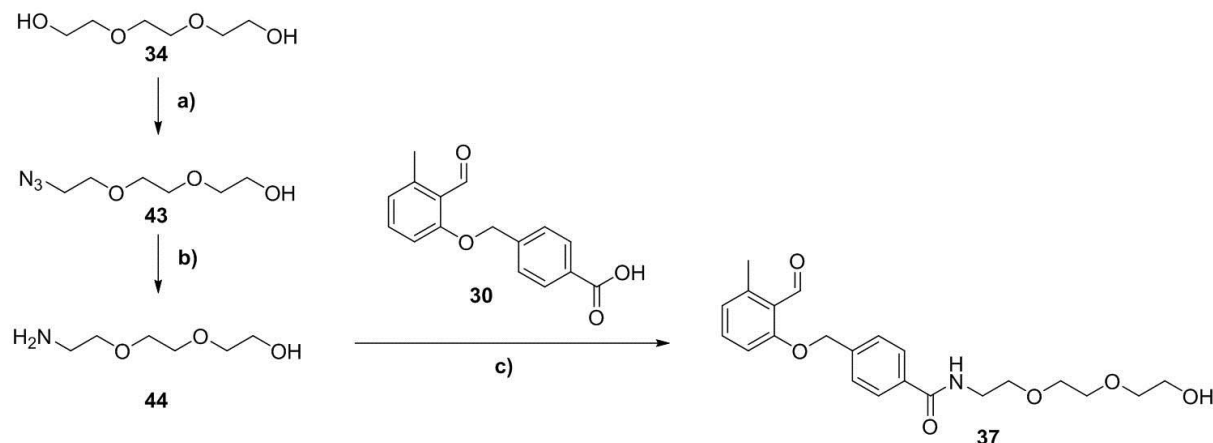
The second photoenol **30**, that contained carboxylic acid functional group was synthesized according to the literature procedure in four steps (Scheme 3.4).^[126a]



Scheme 3.4: Synthesis of 4-((2-formyl-3-methylphenoxy)methyl)benzoic acid **30** (PE2); a) K₂S₂O₈, CuSO₄, MeCN/H₂O (1:1, v/v), 100 °C, 30 min, 51%; b) AlCl₃, CH₂Cl₂, 0 °C, RT, 16 h, 48%; c) K₂CO₃, methyl 4-(bromomethyl)benzoate **41**, 18-crown-6, acetone, 40 °C, 16 h, quantitative; d) NaOH, CH₂Cl₂/MeOH (5:1, v/v), RT, 16 h, 85%.

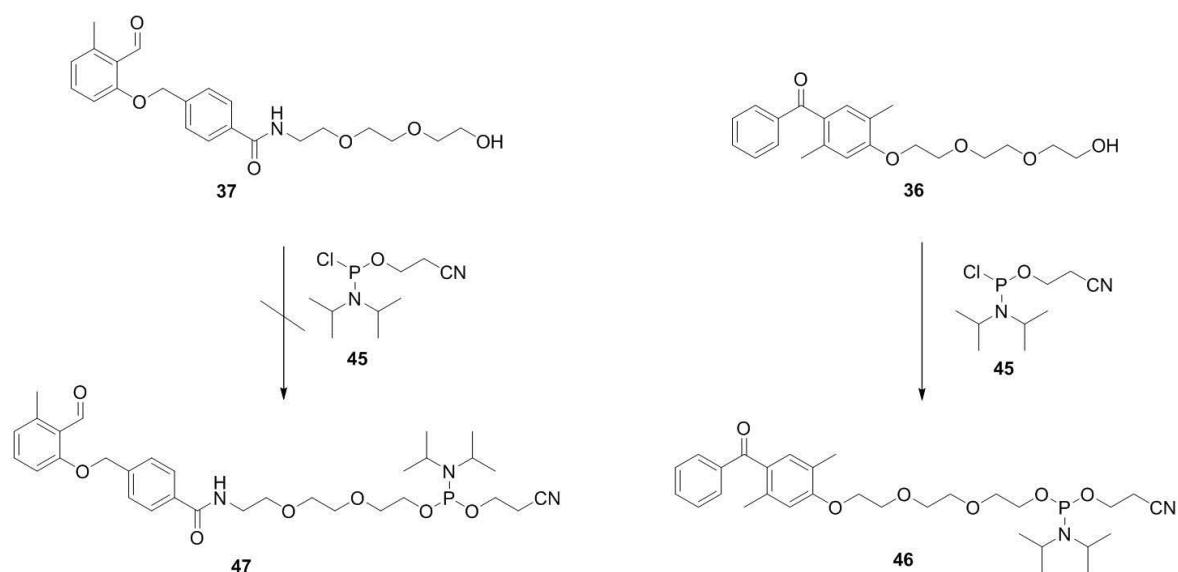
For the preparation of phosphoramidite, a hydroxyl group is required to bind to the phosphorus atom. Hydroxyl group is already introduced to PE1 **31** through triethylene glycol, while it was added to PE2 **30** through amide coupling with the bifunctional linker containing amine and hydroxyl group **44** (Scheme 3.5).^[9c] The amide coupling was performed using

1-hydroxybenzotriazole (HOBt), *N,N'*-dicyclohexylcarbodiimide (DCC) and *N*-hydroxysuccinimide (NHS) as coupling reagents resulting the product **37** with a yield of 47%.^[157]



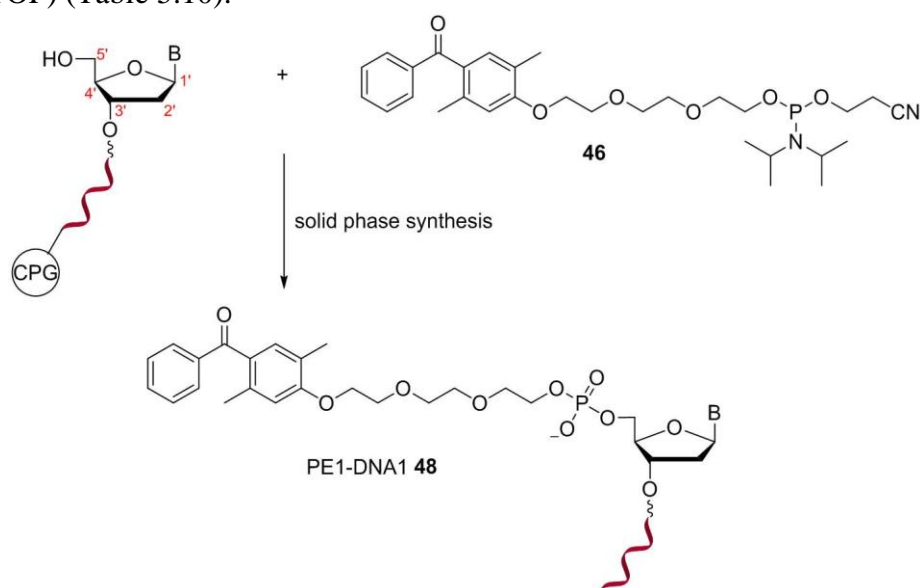
Scheme 3.5: Synthesis of triethylene glycol derivatized PE2 **37**; a) methanesulfonyl chloride, THF, 0 °C - RT, 16 h, NaN₃, EtOH, reflux, 24 h, 26%; b) Pd(OH)₂/C, H₂, EtOAc, RT, 16 h, 94%; c) HOBt, DCC, NHS, DMF, RT, 24 h, 47%.

En route to phosphoramidite, synthesized bifunctional photoenol precursors PE1 **36** and PE2 **37** were phosphitylated using 2-cyanoethyl *N,N*-diisopropylchlorophosphoramidite reagent **45** following the reported literature procedure.^[158] The crude PE1 phosphoramidite **46** was characterized by ³¹P-NMR and mass spectrometry and used in the next step without further purification. The reaction of PE2 **37** with the phosphitylating reagent **45** was not successful even after several attempts. Although a small phosphoramidite **47**, peak was observed in ³¹P-NMR spectrum, mass analysis using Electron Ionization Mass Spectrometry (EI-MS) showed that only an oxidized species [(**47**+O+2H)⁺] is present.



Scheme 3.6: Synthesis of photoenol-phosphoramidites **47** (left) and **46** (right); DIPEA, CH_2Cl_2 , 0 °C - RT, 2 h.

To afford modified DNA, PE1-phosphoramidite **46** was dissolved in an anhydrous acetonitrile, mounted onto a DNA synthesizer following by the standard synthesis protocol with prolonged coupling time of 560 s (standard coupling time 96 s). The photoenol modified oligonucleotide PE1-DNA1 **48** (Scheme 3.7) was obtained after high-performance liquid chromatography (HPLC) purification with a yield of 38%. The identity of the product was confirmed by Matrix-Assisted Laser Desorption Ionization - Time of Flight mass spectrometry (MALDI-TOF) (Table 5.10).



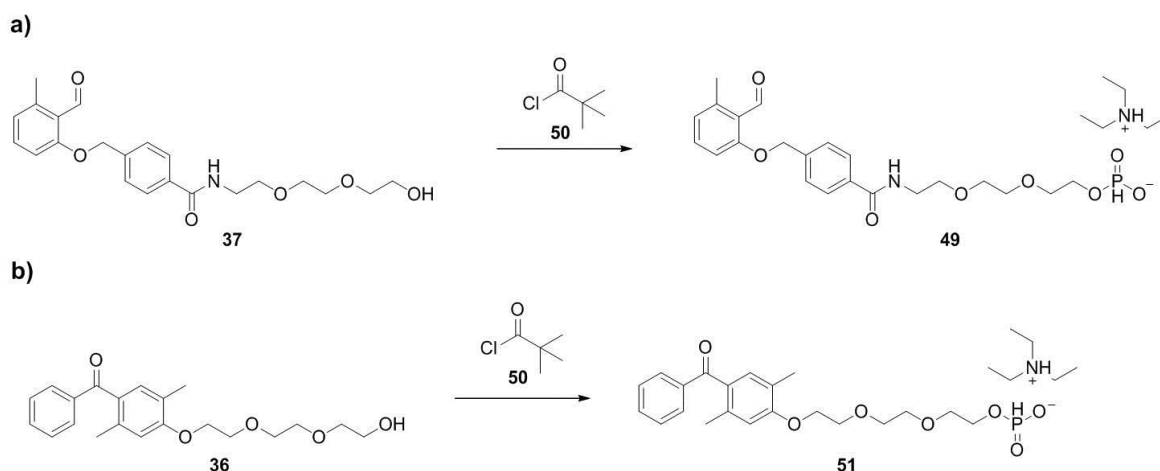
Scheme 3.7: Solid phase synthesis of the oligonucleotide PE1-DNA1 **48** containing photo-activatable 5'-end employing DNA synthesizer.

Due to the general instability of phosphoramidite and inability to obtain photoenol phosphoramidite PE2 **47** in applicable yields, another DNA incorporation strategy using H-phosphonate derivative (details on the methodology are given in Section 1.2.2) was explored.

3.1.2 H-Phosphonate Strategy for PE-DNA Preparation

In order to circumvent the observed oxidation of phosphorus during the synthesis of PE2-phosphoramidite **47**, another more stable phosphorus containing DNA building block, namely H-phosphonate photoenol **49** was prepared. As described in Section 1.2.2, H-phosphonates are mono- or diesters of phosphonic acid. These trivalent P(III) compounds with a tetrahedral geometry contain a phosphoryl group (P=O) and a hydrogen atom bonded to the phosphorus atom. Due to the lack of the lone electron pair on the phosphorus center, H-phosphonates are more resistant towards oxidation than most P(III) compound and therefore easier to handle, in particular during the purification steps. At the same time, upon activation, for example with trimethylacetyl chloride **50**, H-phosphonates monoesters can undergo nucleophilic substitution with hydroxyl containing molecules, such as nucleosides or another hydroxyl containing compound, to give the desired nucleoside H-phosphonate.^[40, 49]

To afford PE2 H-phosphonate **49**, the triethylene glycol derivatized photoenol **37** was used as a precursor. First, the procedure described by Froehler and co-workers, employing PCl_3 , *N*-methyl morpholine and triazole as an activating reagent was used for the synthesis **49**, but was not successful in our hands.^[159] However, the desired product **49** could be obtained using the synthetic procedure reported by Dougan and colleagues, which involved the reaction with phosphonic acid.^[47]



Scheme 3.8: Synthesis of the photoenol-H-phosphonates **49** and **51**; phosphonic acid, pyridine, trimethylacetyl chloride **50**, RT, 2 h; triethylammonium bicarbonate buffer.

Phosphonic acid was dissolved in anhydrous pyridine and added under inert atmosphere to **37** and after a complete dissolution, trimethylacetyl chloride **50** was added and the mixture stirred for two hours at ambient temperature. After quenching with triethylammonium bicarbonate buffer the solvents were removed and the product **49** was obtained as a triethylammonium salt with a yield of 68% (Scheme 3.8). Same procedure was employed to obtain PE1-H-phosphonate **51** (Scheme 3.8).

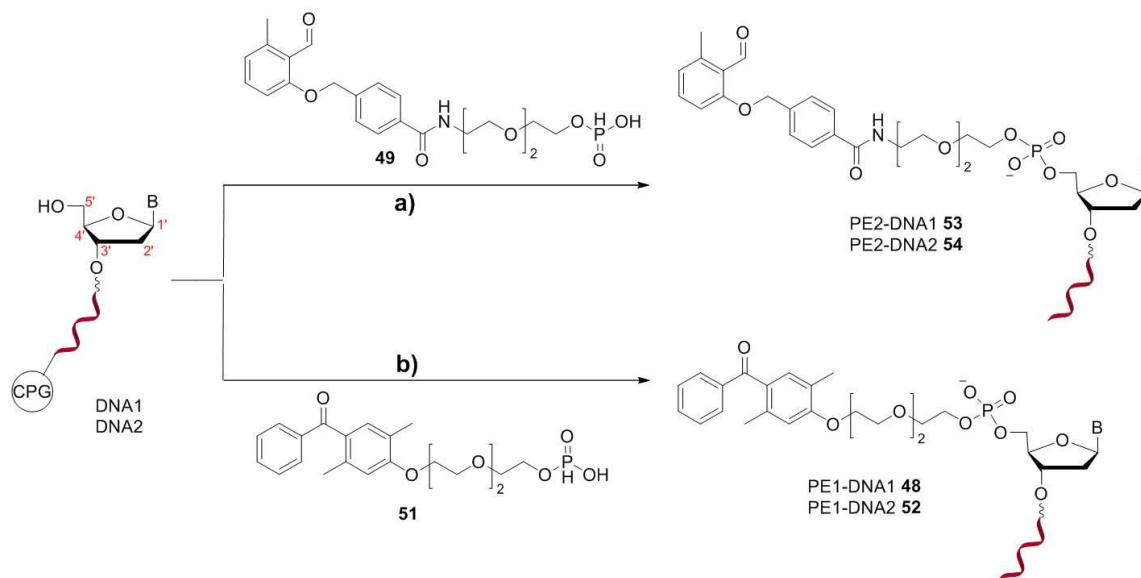
The introduction of the photoenol-H-phosphonates **49** and **51** to DNA was performed manually by direct coupling to commercially available CPG-bound oligonucleotides DNA1 and DNA2. Different reaction conditions were tested in order to improve the product yield and these are summarized in Table 3.1.

Table 3.1: Overview of different reaction conditions for the coupling of H-phosphonate **51** to DNA1.

Nr.	H-phosphonate/ eq.	Trimethylacetyl chloride/ eq.	Adamantyl chloride/ eq.	Reaction time, temp.	Yield
1	29.0	13.0	-	30 min RT	2%
2	185	20.0	-	3 h RT	3%
3	52.0	-	58.0	30 min RT	-
4	365	143	-	16 h 39 °C	36%

The best results were achieved employing the procedure 4, which involved heating at 39 °C for 16 h. The reaction was performed by addition of PE H-phosphonate **51** to the CPG-bound oligonucleotide in a mixture of anhydrous acetonitrile/pyridine (1:1, v/v) followed by addition of trimethylacetyl chloride **50** solution (0.100 M) and stirring at elevated temperature. After the washing steps, resulting PE1-DNA1 **48** was treated with standard oxidizing solution containing 0.02 M iodine in THF/pyridine/water (7:2:1) (10 min), washed with acetonitrile and cleaved from the solid support by incubation in 25% aqueous ammonia solution. After HPLC purification, the photoenol modified oligonucleotide PE1-DNA1 **48** was obtained with 36% yield. Additionally, another sequence, DNA2, was functionalized with PE1 **36** using the same

procedure and obtained with 41% yield. The products were analyzed by MALDI-TOF mass spectrometry (Table 5.10). The syntheses of PE2-DNA1 **53** and PE2-DNA2 **54** were performed using the optimized reaction conditions described above, however the oxidation time needed to be decreased (3min instead of 10 min) to avoid the oxidation of aldehyde moiety of PE2.



Scheme 3.9: H-phosphonate method for the synthesis of the photoenol modified oligonucleotides a) PE2-DNA1 **53** or PE2-DNA2 **54** and b) PE1-DNA1 **48** or PE1-DNA2 **52**; solid phase synthesis.

PE2-DNA1 **53** and PE2-DNA2 **54** were purified by HPLC in 43% and 38% yield respectively. The analysis was performed by MALDI-TOF mass spectrometry (Table 5.10).

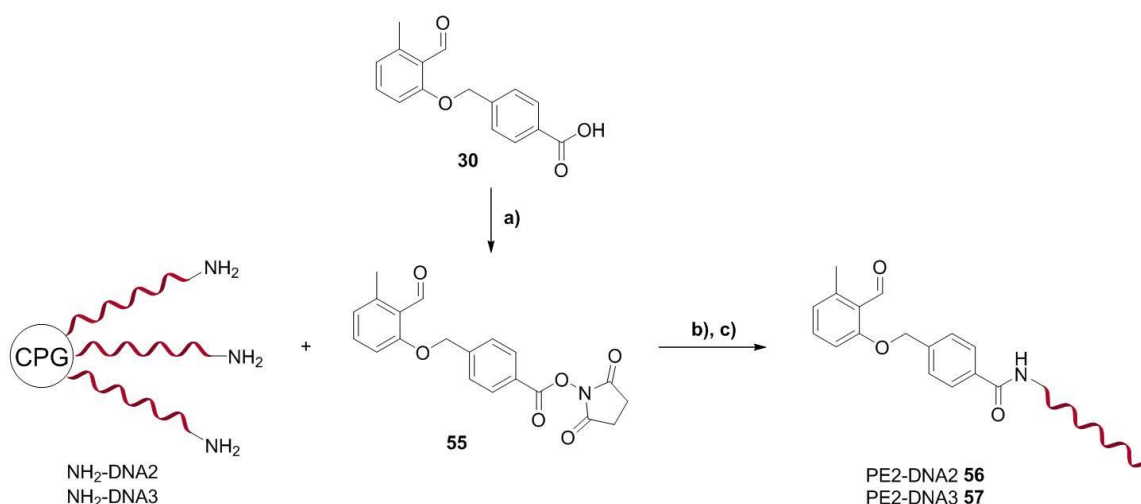
To explore, if the yields of reaction can be improved as well as to find the most suitable modification procedure for range of different DNA sequences, amide coupling of photoenol NHS derivative to amino modified DNA1 and DNA2 was performed. Amide coupling was an important strategy also to enable coupling of another photo-activatable species, tetrazole (Tz), as the preparation of tetrazole phosphoramidite or H-phosphonate derivatives would involve the complex synthetic procedure, so simpler alternatives were of huge advantages.

3.1.3 Amide Coupling Strategy for the Preparation of PE- and Tz-DNA.

Amide bond, one of the most common covalent linkages present in a wide variety of synthetic and natural compounds,^[160] is formally a product of the condensation reaction between a carboxylic acid and an amino group.^[161] However, the amidation reaction does not occur spontaneously as the elimination of water requires high temperature (> 200 °C),^[162] which is not compatible with many substances. Therefore, the activation of the precursor,

namely carboxylic acid, is a necessary step. The common procedure to achieve that includes the conversion of OH group of a carboxylic acid into a good leaving group prior to its reaction with amino functionality. In the past decades, enzymatic catalysis has also been explored and used as an alternative to the traditional organic synthesis procedures, although enzymes are not suitable for the wide use, as they require mild reaction condition and controllable environment consisting, of aqueous solutions.^[163]

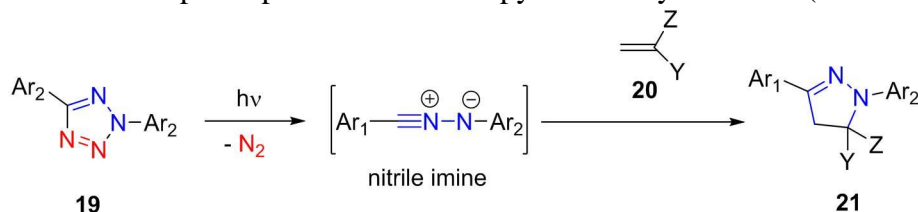
However, a plethora of activation methods and coupling strategies has been developed over the time, to be used in variety of synthetic procedures.^[161, 164] One of them, used in this thesis, is the activation of the acid functionality by treatment with DCC and NHS, the procedure, first applied for the peptide synthesis by Anderson and co-workers.^[165] In short, photoenol is derivatized to NHS ester by DCC/NHS activation in THF at ambient temperature, purified by column chromatography and subsequently employed in reaction with amino terminated oligonucleotide (Scheme 3.10), bound to the solid support (CPG-DNA), as we have found out previously, that yields can be improved if CPG bound DNA is used in amide coupling.^[166] The solid support strategy was the method of choice as the coupling reaction in solution was low yielding, due to the bad solubility of prepared NHS esters of PE2 and Tz in aqueous solutions. The solubility could be improved by introduction of ethylene glycol units to the photo-activatable compounds. However, the solid support strategy provided good yields and therefore was employed for the preparation of PE2 and Tz modified oligonucleotides.



Scheme 3.10: Synthesis of PE2-NHS ester **55** and amide coupling to NH₂-DNA2/DNA3; a) NHS, DCC, THF, 0 °C - RT, 16 h, quantitative; b) DIPEA, DMF, 40 °C, 2 h; c) 25% NH₃, 55 °C, 5 h.

The yields of the coupling reaction could be improved when the reaction was performed at 40 °C, instead at ambient temperature. PE2 modified sequences DNA2 and DNA3 were deprotected and cleaved from the solid support using the 25% aqueous ammonia solution and obtained in yields of 35% and 40% respectively after HPLC purification.

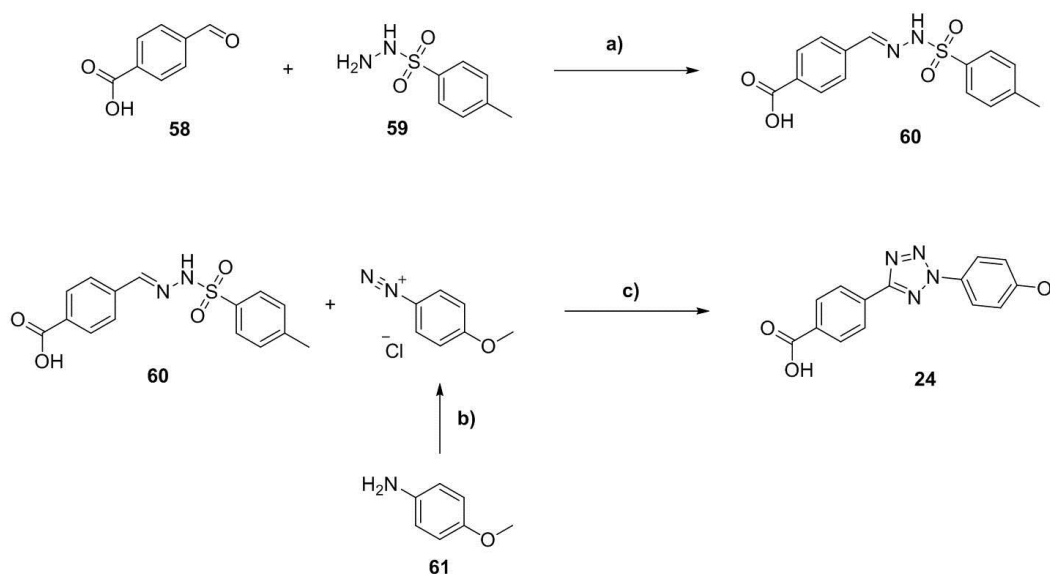
The amide coupling strategy *via* NHS ester was also used for the modification of oligonucleotides with photo-activatable tetrazole moiety (please refer to Section 1.4.4.2 for more details). Photo-induced reaction of tetrazole, namely 2,5-diphenyltetrazole, was for the first time reported in 1967 by Huisgen and co-workers. They described a cycloaddition reaction between 2,5-diphenyltetrazole and methyl crotonate upon UV irradiation.^[128] The proposed mechanism involved a cycloreversion of 2,5-diphenyltetrazole upon irradiation, resulting in the release of nitrogen and the formation of intermediate nitrile imine dipole, which subsequently reacted with an alkene dipolarophile to afford the pyrazoline cycloadduct (Scheme 3.11).



Scheme 3.11: Principle of the light-induced nitrile imine-mediated tetrazole-ene cycloaddition (NITEC) between 2,5-substituted tetrazole **19** and alkene dipolarophile **20**.

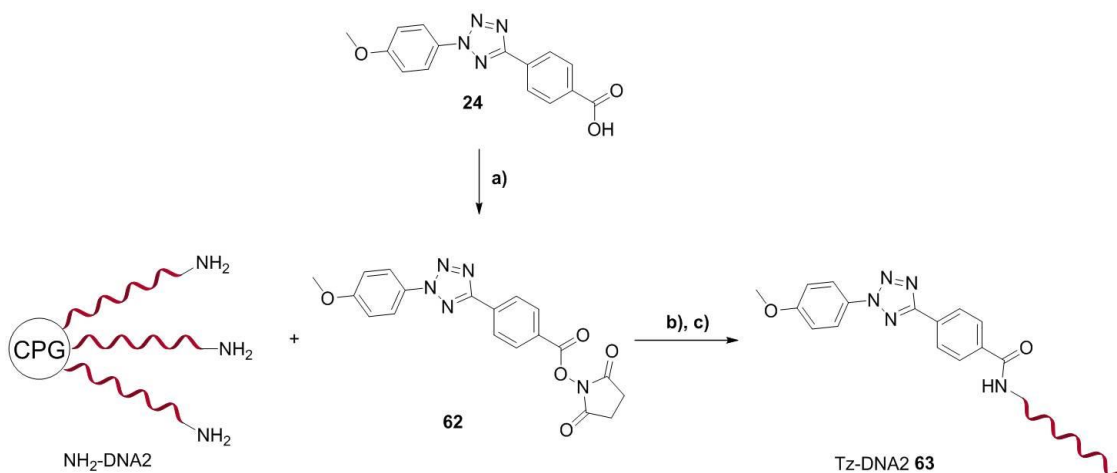
This reaction was initially done in benzene. Decades later, Lin and co-workers further developed the nitrile imine-mediated tetrazole-ene cycloaddition (NITEC), which can be performed in aqueous solution,^[131] and could be used for "stapling" of the peptide side chains,^[167] for fast (≤ 1 min) and selective protein modification in biological media,^[168] and investigation of the protein dynamics and function in live cells.^[169] Recently, Arndt and co-workers prepared tetrazole modified DNA by phosphoramidite procedure and performed subsequent "photoclick" reaction with maleimide functionalized Cy[®]3 dye.^[170] They introduced the photo-activatable tetrazole moiety at an internal oligonucleotide position by modifying nucleotides, which led to low yields of obtained cycloadducts, a result of the poor accessibility of the photo-reactive group. For our applications such approach is not suitable, as we aimed at designing surface immobilized DNA and require fast and high yielding reaction strategy. At the same time, we require 3' or 5' modification, for which amide coupling of amino terminated DNA is particularly suitable. To obtain tetrazole modified DNA, 4-(2-(4-methoxyphenyl)-2*H*-tetrazol-5-yl)benzoic acid **24**, which was shown to decrease the activation energy and allows the activation using UVA (≈ 320 nm) light, advantageous for biological applications, due to its lower damaging effect, was first synthesized.^[136] The synthesis was performed using optimized

literature procedure in three steps resulting the tetrazole carboxylic acid **24** with 51% overall yield (Scheme 3.12).



Scheme 3.12: Synthesis of tetrazole carboxylic acid **24**; a) EtOH, reflux, 30 min, 81%; b) HCl, NaNO₂, 0 °C, H₂O/EtOH (1:1, v/v); c) pyridine, -10 °C, 30 min, RT, 16 h, 62% (51% overall).

The acid moiety was subsequently converted to NHS ester employing the DCC/NHS procedure and coupled with amino-terminated oligonucleotide bound to CPG (Scheme 3.13).



Scheme 3.13: Synthesis of Tz-NHS ester **62** and amide coupling to NH₂-DNA₂; a) NHS, DCC, THF, 0 °C - RT, 16 h, quantitative; b) DIPEA, DMF, RT, 2 h; c) 25% NH₃, 55 °C, 5 h.

After the cleavage and purification, tetrazole modified oligonucleotide **63** was obtained with yield of 44% and the product identity verified by MALDI-TOF mass spectrometry (Table 5.11).

In conclusion, three different approaches were developed for the introduction of photoactivatable moieties to DNA on solid support. First, phosphoramidite photoenol building

elements were synthesized, employing novel triethylene glycol bifunctional linker containing OH group to enable the photoenol modification. As phosphoramidite preparation was not successful for all photoenol precursors, due to the sensitivity of the reaction to oxidation during the purification steps, another more robust strategy employing H-phosphonates was explored, which resulted in preparation of the H-phosphonate photoenol derivative, successfully used to obtain photoenol modified oligonucleotide in high yield. Finally, to extend the toolbox of available methodologies and enable addition of wider variety of photo-activatable molecules, NHS esters of both photoenol and tetrazole were synthesized for modification of solid phase bound DNA through amide coupling. All three strategies have their advantages and disadvantages and could be used as complementary methods to apply to different moieties depending on the application and availability of the starting materials. Photoenol and tetrazole containing oligonucleotides were successfully prepared and conditions and kinetics of the photo-induced cycloaddition will be discussed in the following section.

3.2 Kinetic Study of Light-Induced Cycloaddition Reactions

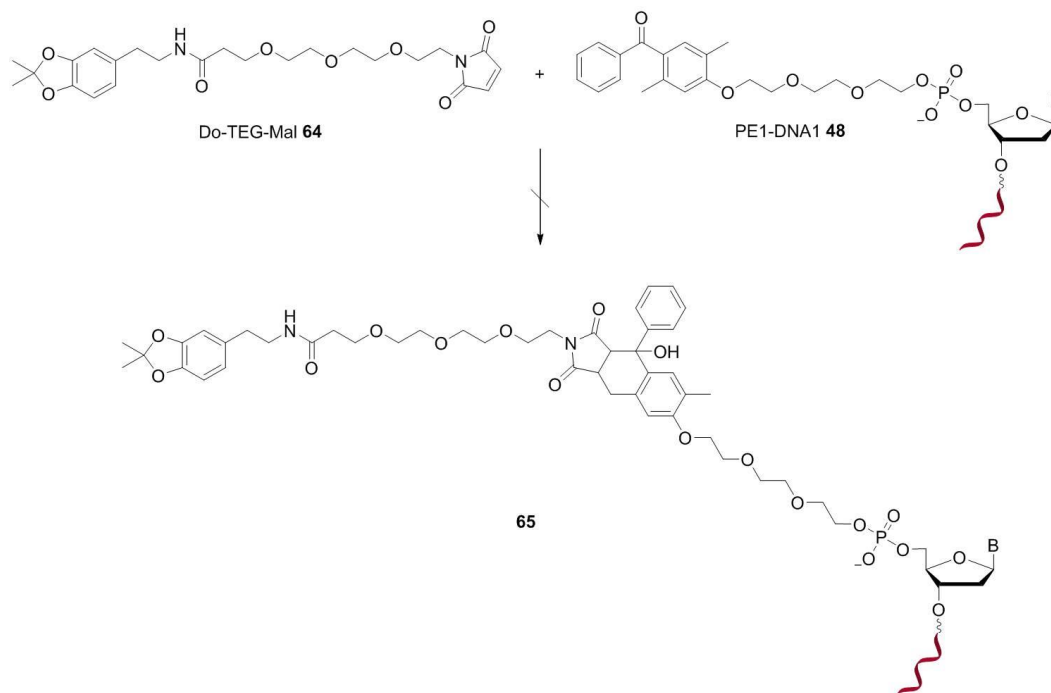
In order to investigate the ability and conditions, under which light-induced cycloaddition reaction can be used in future applications of DNA conjugation to biological molecules or surface structuring, it is important to thoroughly study the test reactions with smaller dienophiles. Reactions involving oligonucleotides require mild conditions in aqueous medium and therefore need to be carefully optimized. Protic solvents, such as water reduce the lifetime of reactive photoenol species, required for successful light-induced cycloaddition reaction.^[122] However, Pauloehrl and co-workers reported the successful cycloaddition reaction between photoenol **30** and maleimide modified peptide in aqueous acetonitrile (phosphate buffer/acetonitrile (1:3), v/v) indicating that the reaction can be optimized by adjusting the ratio of aprotic to protic solvents and by allowing for a longer reaction time (2 h for water/acetonitrile mixture as compared to 15 min for pure acetonitrile).^[126a] Another issue, which needs to be taken into account and might pose the critical obstacle is the use of UV irradiation ($\lambda_{\text{max}} = 317 \text{ nm}$) required for enolization process. Namely, UV light can be detrimental to the DNA.^[171] In general, exposure to UV irradiation can damage DNA either by direct DNA excitation or indirect mechanisms involving excitation of other chromophores present in the DNA environment (for example chromophores such as quinone, flavin or porphyrin within the cells).^[172] The direct excitation leads to the formation of cyclobutane pyrimidine dimers and other photoproducts, which are implicated in cytotoxic, carcinogenic and mutagenic effects of

UV-C and UV-B radiation.^[173] The radiation at longer wavelengths (UV-A or visible light), which will not be significantly absorbed by DNA, can generate excited photosensitizers within the biological medium, which can in turn cause oxidation or breakage of the DNA strands either directly or through the intermediates such as singlet oxygen or other reactive oxygen species.^[174] To minimize such effects, it is necessary to investigate the effect of irradiation on DNA, employed in presented studies. This was indeed done in Fruk group by irradiation of amino modified oligonucleotides by UV light ($\lambda_{\text{max}} = 320 \text{ nm}$) commonly used for photoactivation of *o*-methylbenzaldehyde.^[127] Results obtained from gel electrophoresis and HPLC studies have shown that there is no significant damaging effect to short oligonucleotides used in our applications upon prolonged irradiation (up to 16 hours). In their study of UV damaging effect, Schreier and co-workers explored dimerization process for all-thymine (T) oligonucleotides by a femtosecond time-resolved infrared spectroscopy and could ascertain that the ultrafast photoreaction between two thymines (~1 picosecond) takes place if the bases are properly oriented at the time of light absorption.^[175] However, oligonucleotides used in our work contain varied base sequence, ensuring the stability under UV irradiation. To make sure that significant amount of oxygen is removed from the solution, to minimize the possible generation of reactive species,^[176] all of the reaction samples were deoxygenated by purging with argon prior to irradiation. The deoxygenation was also performed to avoid the reaction of photoenol intermediate **25** with oxygen and production of cyclic peroxide.^[177]

To confirm the previous results obtained in the group and ensure that there are no damaging effects of UV radiation, studies on non-modified and photoenol and tetrazole modified oligonucleotides were performed. In addition, kinetic studies of light-induced cycloaddition reaction between photoenol or tetrazole modified oligonucleotides and maleimide containing molecules were performed by HPLC, gel electrophoresis and ESI-MS.

3.2.1 Light-Induced Cycloaddition of PE-DNA with the Model Maleimide

To assess the reactivity of synthesized photoenol or tetrazole modified oligonucleotides, model reactions with dopamine maleimide Do-TEG-Mal **64**, synthesized by Dr. Ishtiaq Ahmed, were performed. A solution of 1.00 eq. PE1-DNA1 **48** and 4.00 eq. Do-TEG-Mal **64** in a mixture of water/acetonitrile (1:1, v/v) was deoxygenated with argon for 15 min and subsequently irradiated using a 320 nm light source for 16 hours (Scheme 3.14).



Scheme 3.14: Model photoreaction between PE1-DNA1 **48** (1.00 eq.) and Do-TEG-Mal **64** (4.00 eq.); water/acetonitrile (1:1, v/v), 320 nm, RT, 16 h.

Excess of **64** was removed by gel filtration. After reduction of solvent in vacuum, the reaction mixture was analyzed by HPLC (Figure 3.1).

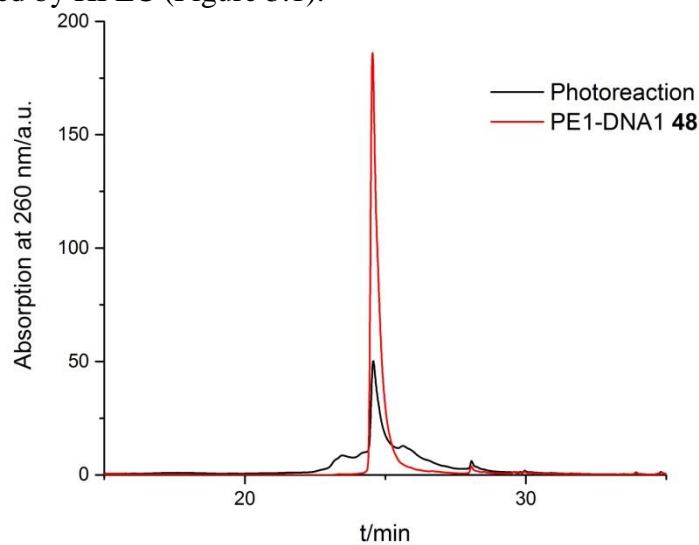
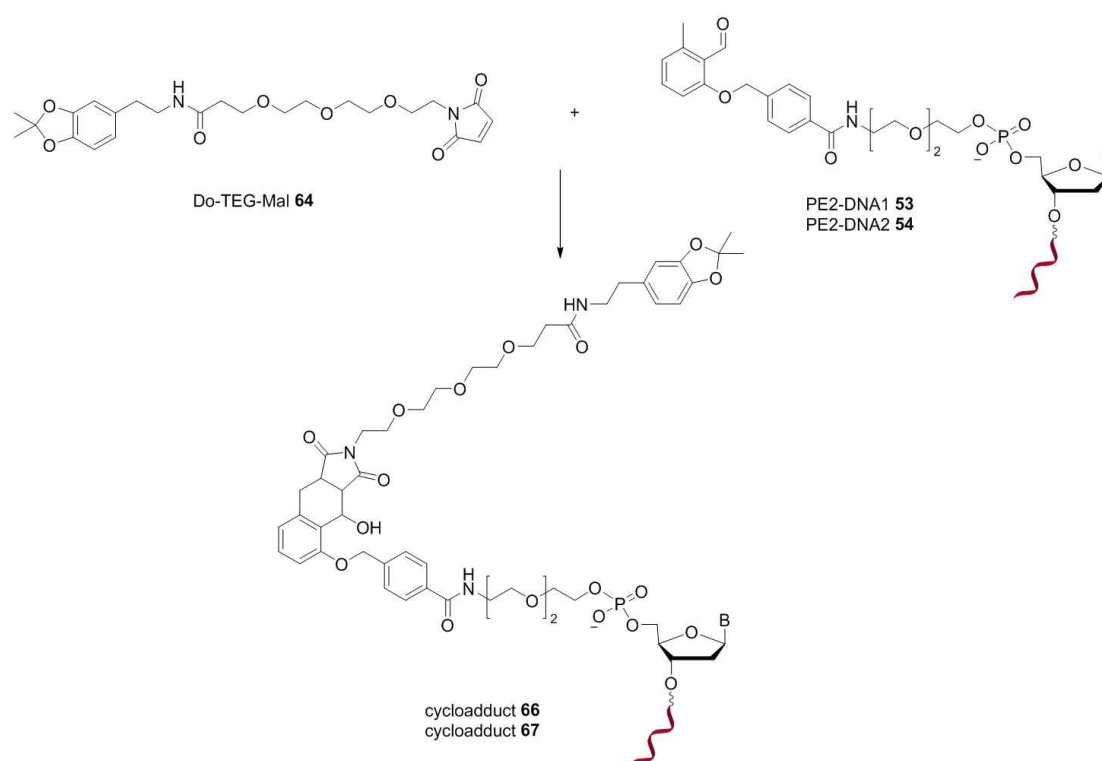


Figure 3.1: Overlay of HPLC chromatograms of PE1-DNA1 **48** and photoreaction between PE1-DNA1 **48** and Do-TEG-Mal **64**.

No cycloadduct was obtained, but new shoulder peaks were observed in irradiated samples. As their intensity or retention time did not change after prolonged irradiation (46h) and changed conditions, they were not investigated further. The reaction was also performed at different reaction conditions including decreased and increased amounts of maleimide **64** (0.25 eq., 4.00 eq. and 50.0 eq.) and different solvent systems, such as water/DMSO (1:1) or

DMF, but no cycloadduct was detected. We attribute this to the effect of the protic solvent on the enolization process of PE1 derivative. However, when we used PE2 **30**, previously employed for modification of peptides,^[126a] desired cycloadduct was identified. Using two different DNA sequences, PE2-DNA1 **53** and PE2-DNA2 **54** for light-induced addition of Do-TEG-Mal **64** in water/acetonitrile (1:1, v/v) ($\lambda_{\text{max}} = 320 \text{ nm}$) respective cycloadducts (Scheme 3.15) could be obtained and characterized using MALDI-TOF and gel electrophoresis (Figure 3.2).



Scheme 3.15: Model reaction between PE2-DNA1 **53** or PE2-DNA2 **54** and Do-TEG-Mal **64**; 1.00 eq. PE2-DNA1 or PE2-DNA2, 1.00 eq. Do-TEG-Mal, water/acetonitrile (1:1, v/v), 320 nm, RT, 16 h.

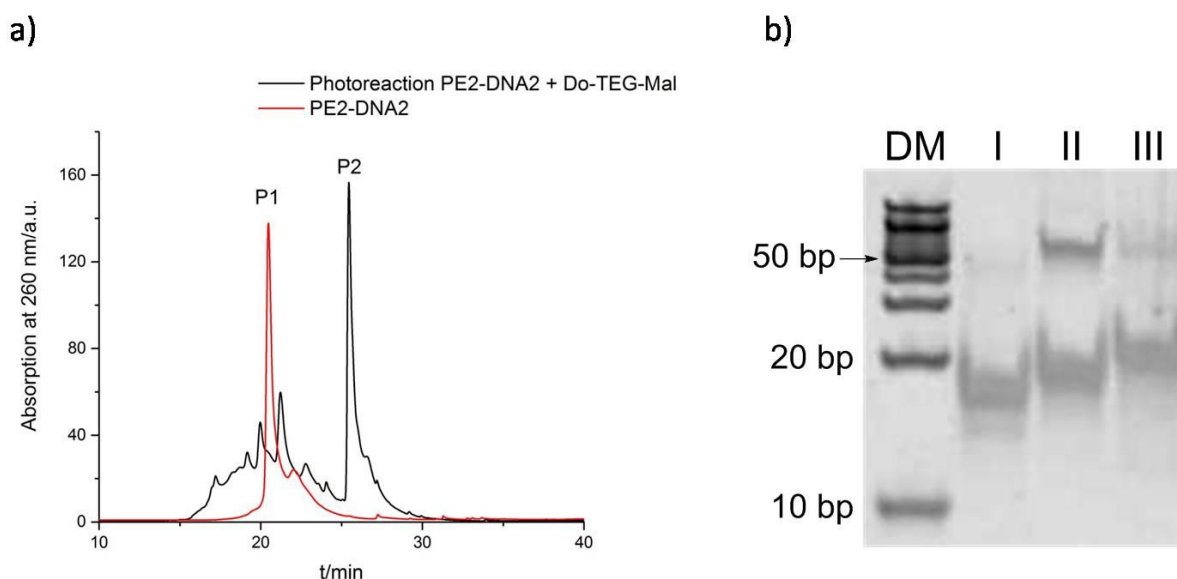


Figure 3.2: Analysis of photoreaction between PE2-DNA2 **54** and **64**; a) HPLC chromatograms of PE2-DNA2 (P1) and photoreaction (P2); b) native PAGE analysis of photoreaction, DM: 10 bp DNA marker, I: DNA2, II: PE2-DNA2, III: cycloadduct **67**; gel conditions: 21% polyacrylamide, 100 V, 2 h, running buffer: 1×TBE, SYBR Gold staining.

As it can be seen from the overlay of HPLC chromatograms (Figure 3.2a), new peak at the retention time of 25.7 (P 2, 35%) can be detected, which was assigned to cycloadduct **67** by MALDI-TOF mass spectrometry (Table 5.12). The chromatogram section between 16 and 25 min contains residues of starting PE2-DNA2 **54** and new additional peaks, which were not present in the control reactions with non-modified oligonucleotide (Figure 3.3a, II) or when reaction is performed in dark (Figure 3.3a, IV).

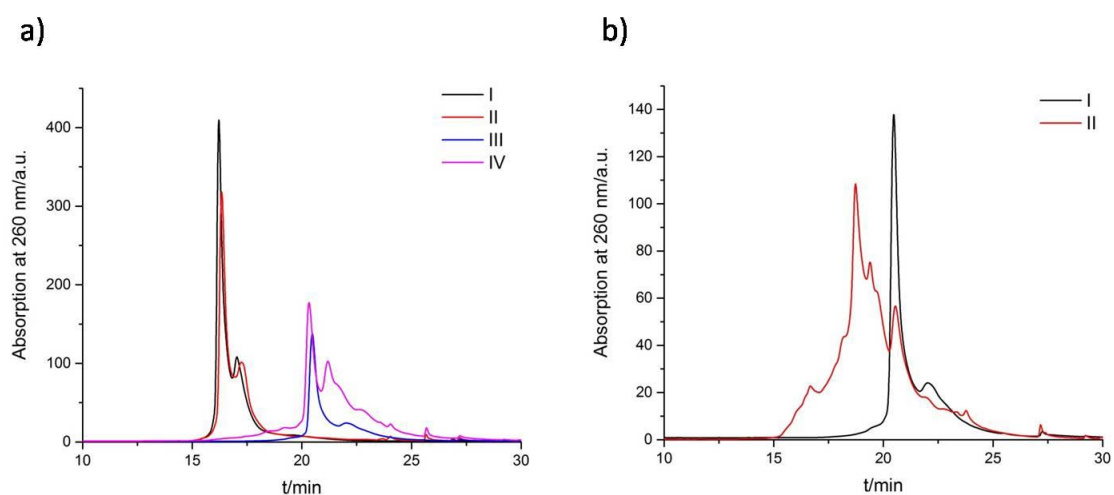


Figure 3.3: HPLC chromatograms of control reactions; a) I: DNA2 only; II: DNA2 irradiated with Do-TEG-Mal **64** at 320 nm for 16 h; III: PE2-DNA2 **54** only; IV: PE2-DNA2 **54** incubated with Do-TEG-Mal for 16 h in the dark; b) I: PE2-DNA2 **54** without irradiation, II: PE2-DNA2 **54** after irradiation with 320 nm light for 16 h.

However, upon irradiation of PE2-DNA2 **54** in the absence of any other reagents (Figure 3.3b, II), additional peaks, indicating the presence of side products, can clearly be observed. We attribute these side products to the intramolecular interactions most probably between photoenol moiety and double bonds within nucleobases, although due to the time constraints the side reactions have not been further investigated at this point. Gel electrophoresis analysis of cycloadduct in comparison to non modified DNA2 and PE2-DNA2 **54** was additionally performed. As it can be seen in Figure 3.2b, the electrophoretic mobility of oligonucleotides decreases for cycloadduct (lane III) in comparison with DNA2 (I) and PE2-DNA2 **54** (II) due to the change in molecular weight. Additional band with decreased electrophoretic mobility can be observed in lanes II and III, which can be attributed to a dimer formation (ca. 50 bp), a common effect observed in short DNA sequences cleaved from the solid support. It should be noted that the dimer band is also present in the lane I corresponding to a commercial, unmodified DNA, although at much lower intensity due to the extensive purification. As an additional confirmation of the dimer hypothesis, the electrophoretic mobility of this band remains same in all samples indicating that there is no hindering functional group present, which could impair the reaction.

To investigate whether the change of the DNA sequence influence the outcome of the reactions, PE2-DNA1 **53** was allowed to react with model maleimide under the same conditions and the results are shown in Figure 3.4.

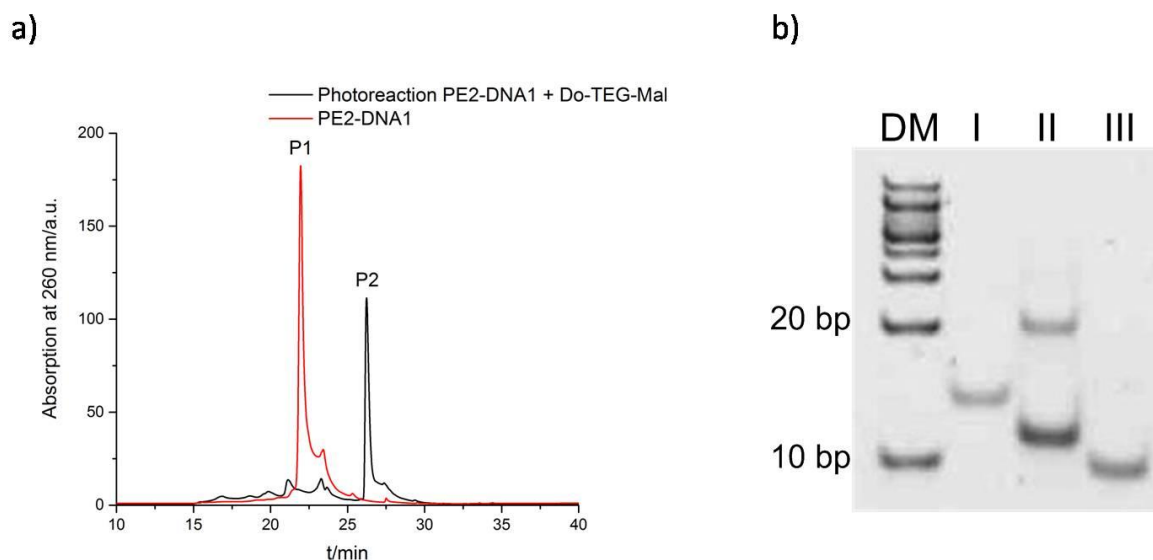


Figure 3.4: Analysis of photoreaction between PE2-DNA1 **53** and **64**; a) HPLC chromatograms of PE2-DNA1 (P1) and of photoreaction (P2); b) native PAGE analysis of photoreaction, DM: 10 bp DNA marker, I: cycloadduct **66**, II: PE2-DNA1, III: DNA1; gel conditions: 21% polyacrylamide, 100 V, 1.5 h, running buffer: 1×TBE, SYBR Gold staining.

As it can be seen, cycloaddition proceeds with high yield of product formation (P2, 93%) and negligible amount (7%) of side products (region between 15–25 min). Control reactions (Figure 3.5) show trends similar to PE2-DNA2 **54** reaction. Larger amount of side product is formed upon irradiation of PE2-DNA1 **53** without the presence of maleimide, indicating the intramolecular reaction.

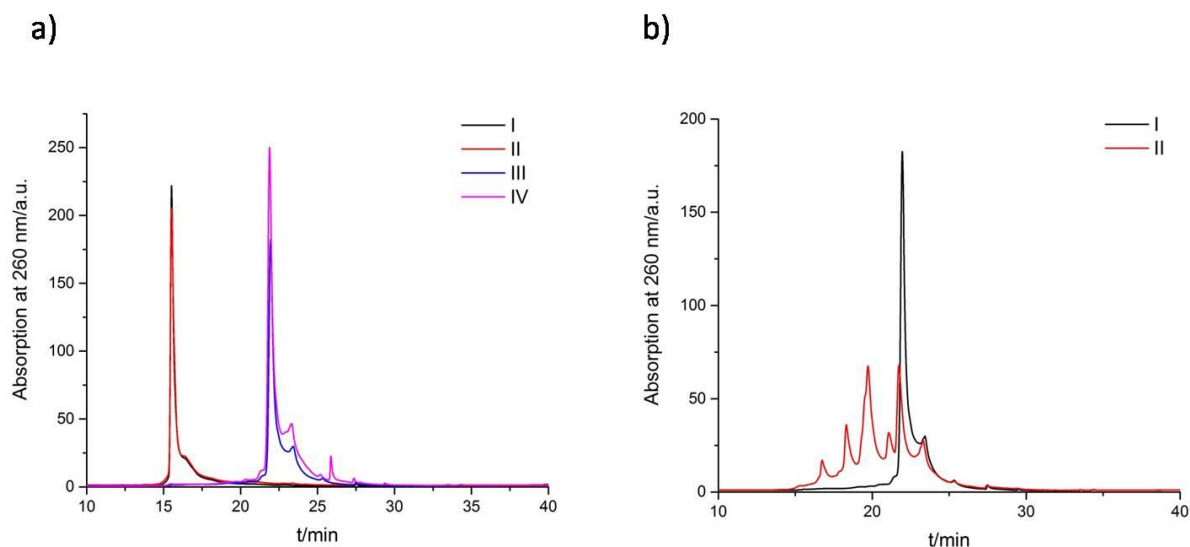


Figure 3.5: HPLC chromatograms of control reactions; a) I: DNA1 only; II: DNA1 and Do-TEG-Mal **64** irradiated at 320 nm for 16 h, III: PE2-DNA1 **53** only, IV: PE2-DNA1 **53** incubated with Do-TEG-Mal **64** for 16 h in the dark; b) I: PE2-DNA1 **53** only, II: PE2-DNA1 **53** irradiated at 320 nm for 16 h.

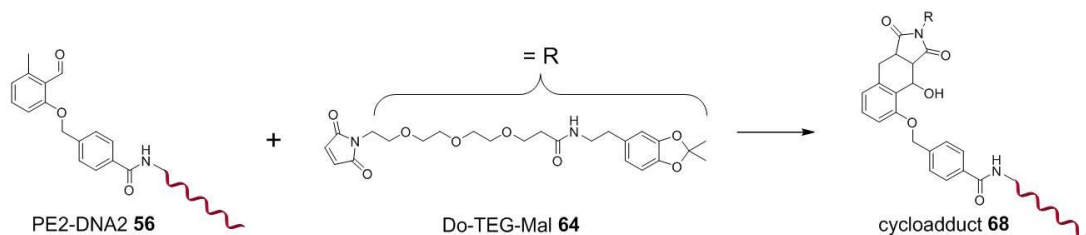
Gel electrophoresis (Figure 3.4b) confirms the presence of cycloadduct of higher molecular weight (low mobility, lane I) after irradiation. Unlike for DNA2, additional peak, which can be attributed to a dimer, is present only in the lane containing PE2-DNA1 **53** (lane 2), most probably due to the limitation of the HPLC purification of shorter oligonucleotides (DNA1 contains 12 bases as compared to DNA2 with 22 bases).

3.2.2 Photoenol- vs. Tetrazole-DNA Photoreaction with Model Maleimide

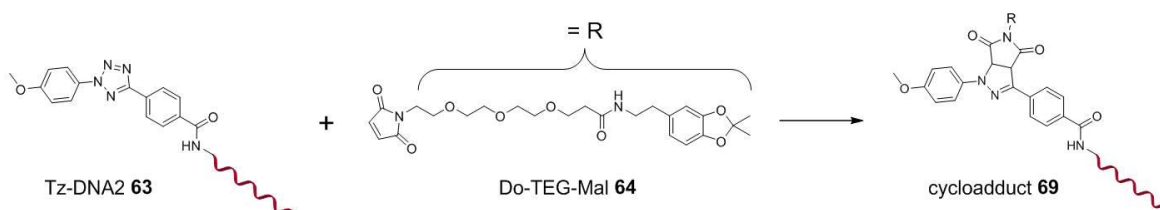
In order to assess the rate of reaction as well as the suitability of light-induced cycloadditions for DNA modification and conjugation, model reactions with maleimide were performed under same conditions using both PE2-DNA2 **56** and **64** and Tz-DNA2 **63** and **64** (Scheme 3.16). In such way, direct comparison of the kinetic parameters and yields could be obtained and most suitable reaction employed in further applications. Photo-induced cycloadditions were performed using equimolar quantities of reagents in water/DMSO mixture (3:2, v/v) under irradiation with a 320 nm light source for 2 h. DMSO was employed for the photoreactions instead of acetonitrile, as it has a lower vapor pressure and thus, ensures a slower

evaporation under irradiation of small volumes, which is an important requirement for DNA structuring applications where small volumes of reagents are required.

a)



b)



Scheme 3.16: Model photoreaction between a) PE2-DNA2 **56** or b) Tz-DNA2 **63** and Do-TEG-Mal **64** studied to obtain kinetic parameters. 1.00 eq. **56** or **63** and 1.00 eq. **64** respectively, solvent: water/DMSO (3:2, v/v), irradiation at 320 nm, RT, 2 h.

The reaction mixtures were worked up as described in previous section and purified by HPLC. PE2-DNA2 cycloadduct **68** was obtained and characterized as discussed in Section 3.2.1. The HPLC chromatogram of the photoreaction of tetrazole modified DNA2 **63** and maleimide is shown in Figure 3.6. Several distinct peaks can be observed. Peak P4 with retention time of 26.1 min (22% yield) was assigned to the expected cycloadduct **69** by MALDI-TOF mass spectrometry (Table 5.13).

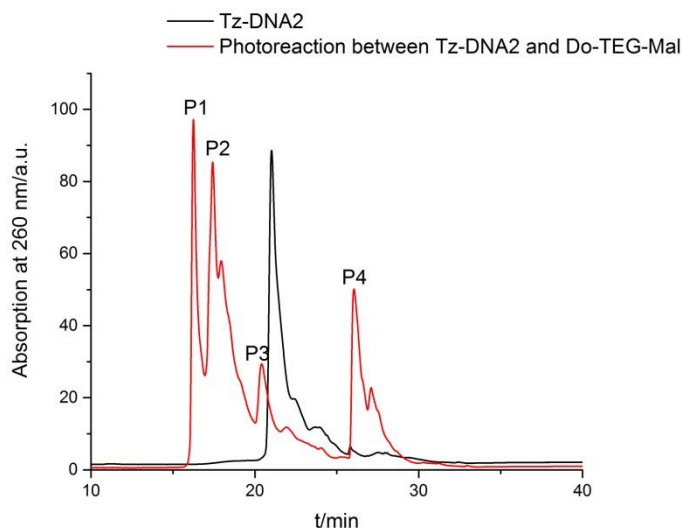


Figure 3.6: HPLC chromatogram of Tz-DNA2 **63** (1.00 eq.) and model reaction with maleimide **64** (1.00 eq).

Peaks P1 (16.2 min), P2 (around 17.4) and P3 (20.4) correspond to the side products of irradiation of Tz-DNA2 **63** with UV light. Attempt was made to decipher the possible products, however the analysis of the peaks P1 and P2 by MALDI-TOF has shown that a species with m/z ratio of 7218 g/mol is present which does not correspond to the starting material **63** ($m/z = 7349$) nor any literature deduced side product and due to the time constraints was not analyzed further. However, the reaction conditions were optimized to minimize or fully remove the occurrence of the side products. To achieve that photoreactions were tested using different amounts of maleimide and different irradiation times. First, 15.0 eq. of maleimide dienophile **64** were added to the solution of PE2-DNA2 **56** and Tz-DNA2 **63** and irradiated with 320 nm light source for 3 hours and the reaction mixtures were analyzed by HPLC and gel electrophoresis (Figure 3.7).

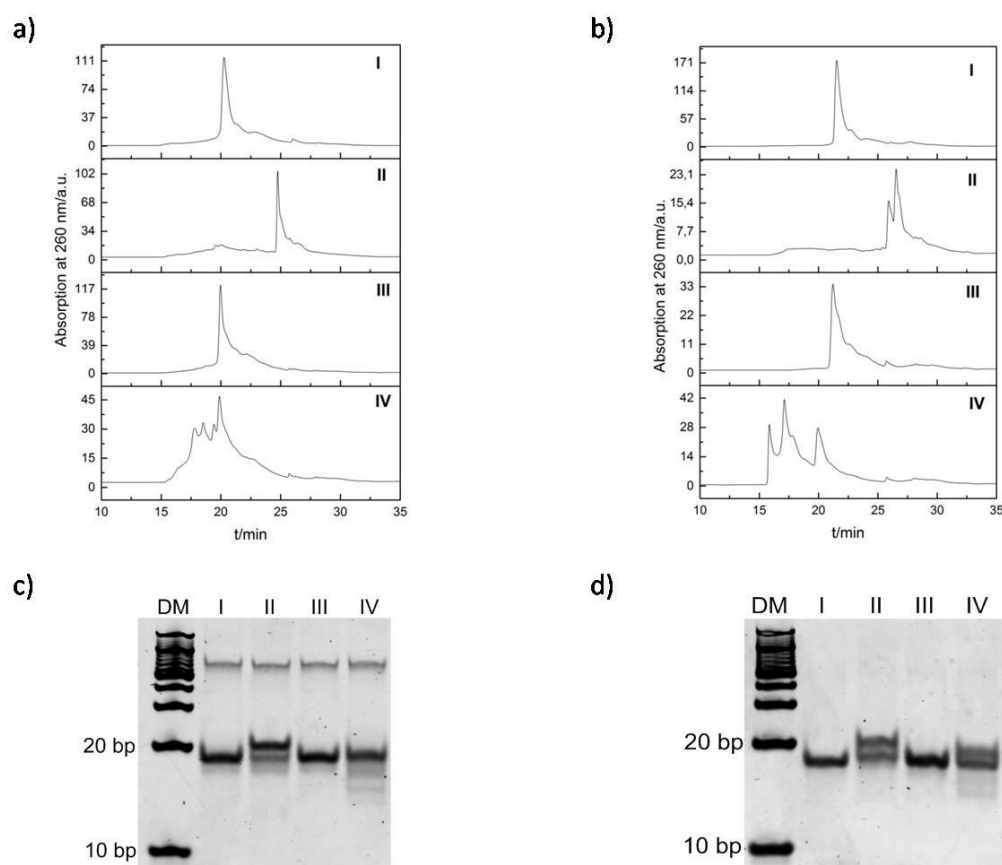


Figure 3.7: Photoreaction of PE2-DNA2 **56** (a, c) and Tz-DNA2 **63** (b, d) with 15.0 eq. of Do-TEG-Mal **64** under 320 nm irradiation for 3 h. HPLC chromatograms of PE2-DNA2 (a) and Tz-DNA2 (b) show I: PE2-DNA2 or Tz-DNA2 only; II: photoreaction; III: photoreaction after 3 h incubation in the dark; IV: irradiation of PE2-DNA2 and Tz-DNA2 without maleimide; c) and d) correspond to the gel electrophoretic analysis of the PE2-DNA2 and Tz-DNA2 photoreactions respectively. DM: 10 bp DNA marker, gel conditions: 21% polyacrylamide, 100 V, 2 h, running buffer: 1×TBE, SYBR Gold staining.

HPLC chromatograms of both photoreactions in the presence of 15.0 eq. of maleimide **64** as well as the control reactions show trends, already described for equimolar reactions. However, it can be observed that use of larger amount of dienophile minimizes the appearance of the side products (16–25 min region, see Figure 3.2 in Section 3.2.1), indicating that the photoreaction is strongly preferred in the presence of an excess of dienophile **64**. Controls, incubated in the dark, do not show any cycloadduct presence, while the irradiation of DNA, containing photo-activatable groups, indicates the presence of internal cycloaddition products discussed previously. Two peaks (Figure 3.7b, II) and corresponding two bands (Figure 3.7d, II) are observed in HPLC and gels respectively, after photoreaction of Tz-DNA2 **63** with excess maleimide **64**. In addition to the cycloadduct **69**, the band II contains a band with higher electrophoretic mobility also present in lane IV corresponding to the side product of Tz-DNA2 **63** irradiation. This indicates that both maleimide cycloaddition and

internal photo-induced side reaction occur within the irradiated reagent mixture. No reaction takes place when the reaction mixture is kept in dark confirming that the presence of the light source is a crucial requirement.

In order to determine the optimal dienophile amount and irradiation time, the kinetic studies of PE2-DNA2 **56** and Tz-DNA2 **63** reactions with 5.00 eq. and 15.0 eq. dienophile **64** were performed. The solutions were mixed and the analysis of the reaction mixture performed after specific intervals of irradiation (0 min, 15 min, 30 min, 1 h and 3 h). Comparison of HPLC chromatograms (Figure 3.8a, b) of reactions with different amounts of dienophile shows that in both cases the reactions are completed after 15 min irradiation, though around 16% reactant remained non-reacted. The reaction mixtures were additionally analyzed by ESI mass spectrometry, resulting in spectra of 4-, 5-, 6- and 7-fold charged ions assigned to reactant **56**, and photoadduct **68**. The abundance ratios of the ions confirms the results obtained by HPLC analysis. The amount of non-reacted PE2-DNA2 **56** is approximately 16% in both reactions and does not decrease with prolonged irradiation time.

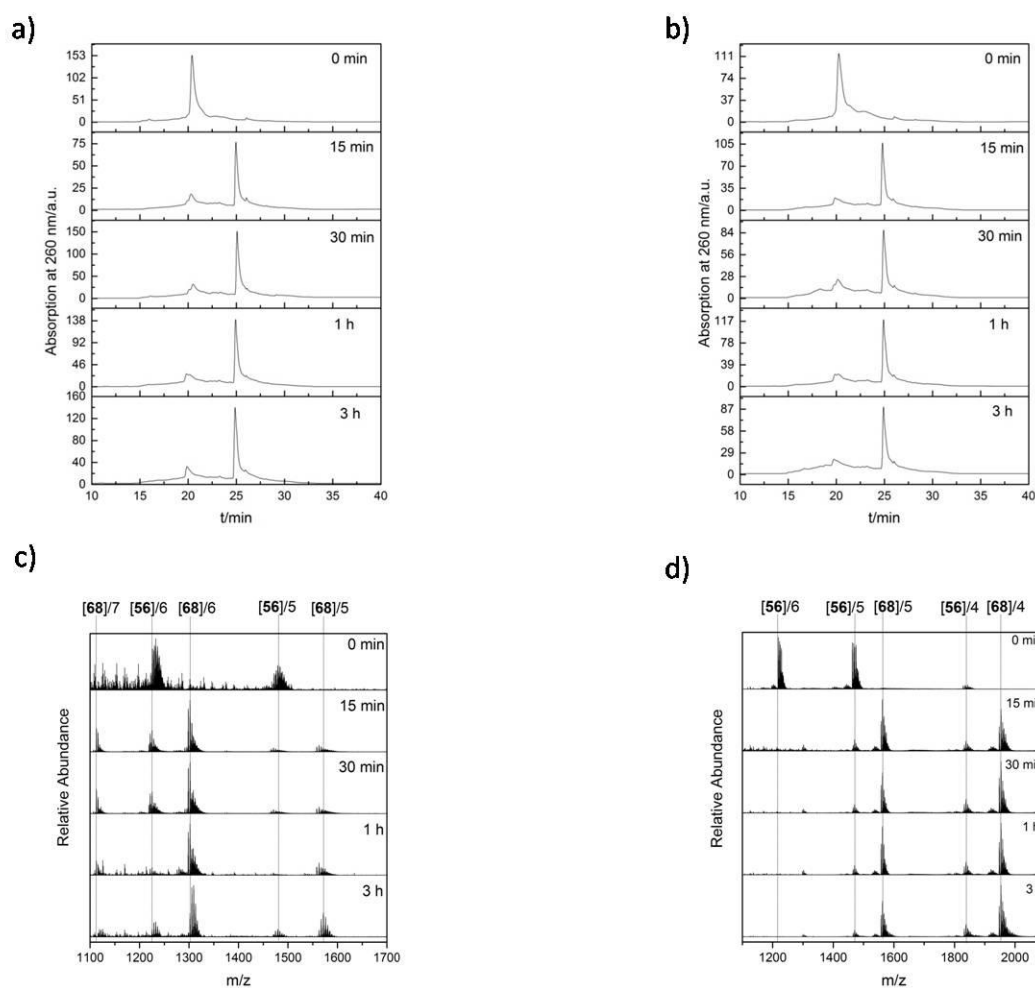


Figure 3.8: Kinetic study of the photoreaction between PE2-DNA2 **56** and Do-TEG-Mal **64**. HPLC chromatograms and ESI-MS data for 5.00 eq. (a, c) and 15.0 eq. (b, d) Do-TEG-Mal **64**. Irradiation was performed with a 320 nm light sources for 0 min, 15 min, 30 min, 1 h and 3 h.

Increasing the amount of dienophile to 100 eq. did not further improve the reaction yield, as confirmed by HPLC analysis (Figure 3.9).

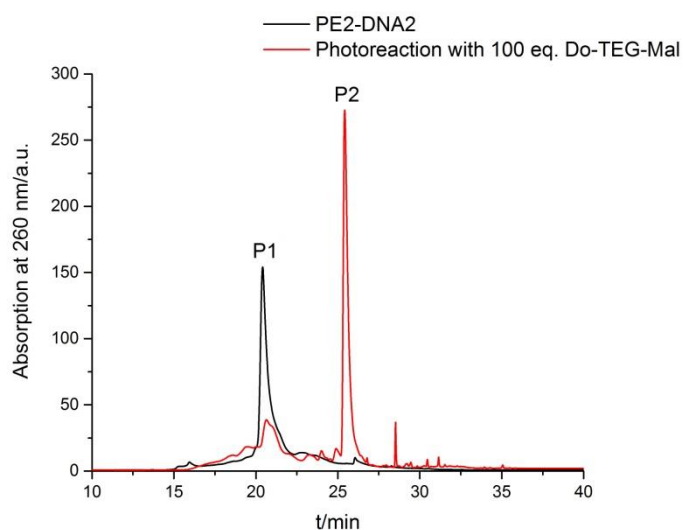


Figure 3.9: HPLC chromatograms of PE2-DNA2 **56** (P1) and photoreaction between **56** and 100 eq. Do-TEG-Mal **64** (P2).

To get more insight into the kinetics of the photoenol-DNA reaction, more detailed study was performed using ESI-MS (Figure 3.10).

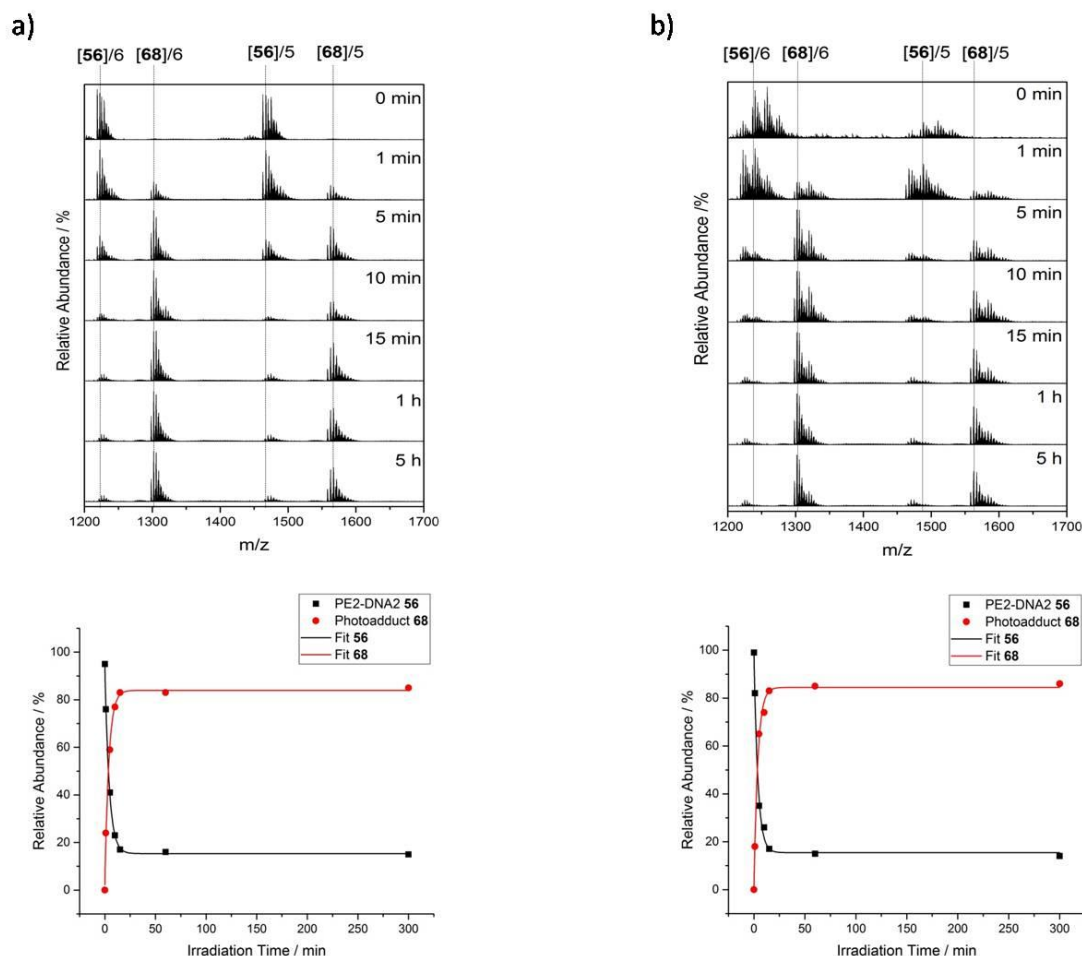


Figure 3.10: ESI-MS spectra (top) and the kinetic plots derived from the integration of the corresponding mass spectra (bottom) for photoreaction of PE2-DNA2 **56** with a) 5.00 eq. and b) 15.0 eq. of Do-TEG-Mal **64** at different irradiation times with 320 nm light.

The mass spectra in Figure 3.10 (top) show 5-fold and 6-fold charged ions of reactant with $m/z = 1467.2625$ and $m/z = 1222.5521$, and of photoadduct with $m/z = 1567.0983$ and $m/z = 1301.9206$ (determined by the most abundant isotopes of the isotopic patterns), indicating that the reaction is completed by 10 min irradiation. Approximately 16% of non-reacted **56** is still present after the reaction and this does not change with the time of irradiation, as already observed in HPLC. Kinetic plots (Figure 3.10, bottom), obtained by integration of the mass spectra peaks and plotting the percentage values as a function of time, indicate excellent agreement of the experimental data points with an exponential fit for both 5.00 eq. or 15.0 eq. reactions pointing out towards pseudo first-order kinetics.

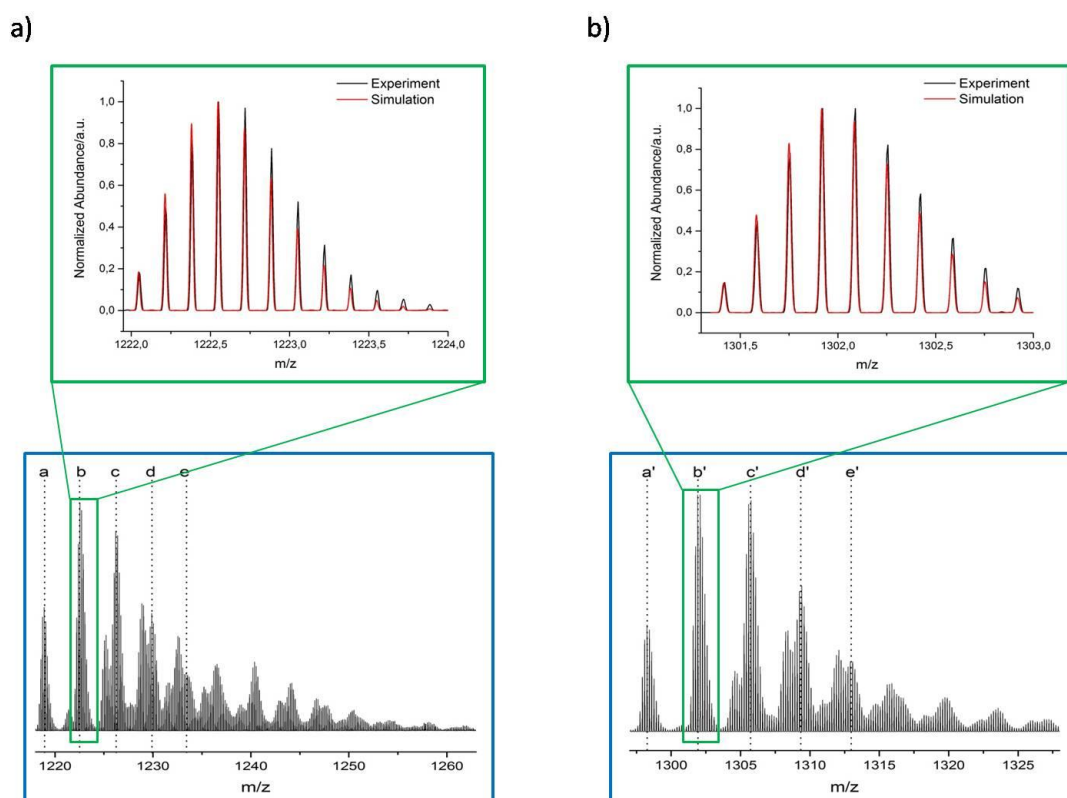


Figure 3.11: Expansion of the ESI mass spectrum region (bottom) and comparison between experimental and simulated data (top) for a) reactant **56** (m/z range: 1221.9 - 1224.0) and b) photoadduct **68** (m/z range: 1301.50 - 1303.0).

In addition, detailed analysis of the isotopic pattern of the most abundant isotopes of reactant and of the product and the comparison to their simulated isotopic pattern (Figure 3.11) provides unambiguous evidence for the successful generation of the desired cycloadduct. Furthermore, experimentally obtained m/z values of the reactant **56** and photoadduct **68** and their sodium adducts are in excellent agreement with the theoretically calculated, expected exact mass values ($\Delta m/z < 0.0100$, Table 3.2).

Table 3.2: Peak assignment of the ESI mass spectra of reactant **56** from $m/z = 1218.0$ to $m/z = 1263.0$ (a–e) and photoadduct **68** from $m/z = 1297.0$ to $m/z = 1328.0$ (a'–e'). Peak labels correspond to the spectra shown in Figure 3.11. Both experimental and theoretical m/z values and their differences ($\Delta m/z$) are shown.

Ion assignment	Sum formula	m/z_{expt}	m/z_{theor}	$\Delta m/z$
a	$[\text{C}_{240}\text{H}_{289}\text{N}_{95}\text{O}_{133}\text{P}_{22}]^{6+}$	1218.8905	1218.8841	0.0064
b	$[\text{C}_{240}\text{H}_{288}\text{NaN}_{95}\text{O}_{133}\text{P}_{22}]^{6+}$	1222.5521	1222.5477	0.0044
c	$[\text{C}_{240}\text{H}_{287}\text{Na}_2\text{N}_{95}\text{O}_{133}\text{P}_{22}]^{6+}$	1226.2140	1226.2114	0.0026

d	$[\text{C}_{240}\text{H}_{286}\text{Na}_3\text{N}_{95}\text{O}_{133}\text{P}_{22}]^{6+}$	1229.8765	1229.8750	0.0015
e	$[\text{C}_{240}\text{H}_{285}\text{Na}_4\text{N}_{95}\text{O}_{133}\text{P}_{22}]^{6+}$	1233.5382	1233.5387	0.0005
a'	$[\text{C}_{264}\text{H}_{321}\text{N}_{97}\text{O}_{141}\text{P}_{22}]^{6+}$	1298.2589	1298.2534	0.0055
b'	$[\text{C}_{264}\text{H}_{320}\text{NaN}_{97}\text{O}_{141}\text{P}_{22}]^{6+}$	1301.9206	1301.9171	0.0035
c'	$[\text{C}_{264}\text{H}_{320}\text{Na}_2\text{N}_{97}\text{O}_{141}\text{P}_{22}]^{6+}$	1305.7491	1305.7487	0.0004
d'	$[\text{C}_{264}\text{H}_{319}\text{Na}_3\text{N}_{97}\text{O}_{141}\text{P}_{22}]^{6+}$	1309.4111	1309.4123	0.0012
e'	$[\text{C}_{264}\text{H}_{318}\text{Na}_4\text{N}_{97}\text{O}_{141}\text{P}_{22}]^{6+}$	1313.0731	1313.0760	0.0029

Kinetic study of the photoreaction between Tz-DNA2 **63** and Do-TEG-Mal **64** was performed in a same manner as described above using 5.00 eq. or 15.0 eq. of dienophile **64** in water/DMSO (3:2, v/v) and irradiation for 0 min, 15 min, 30 min, 1 h and 6 h or 3 h, followed by purification by HPLC and MS characterization (Figure 3.12a-d).

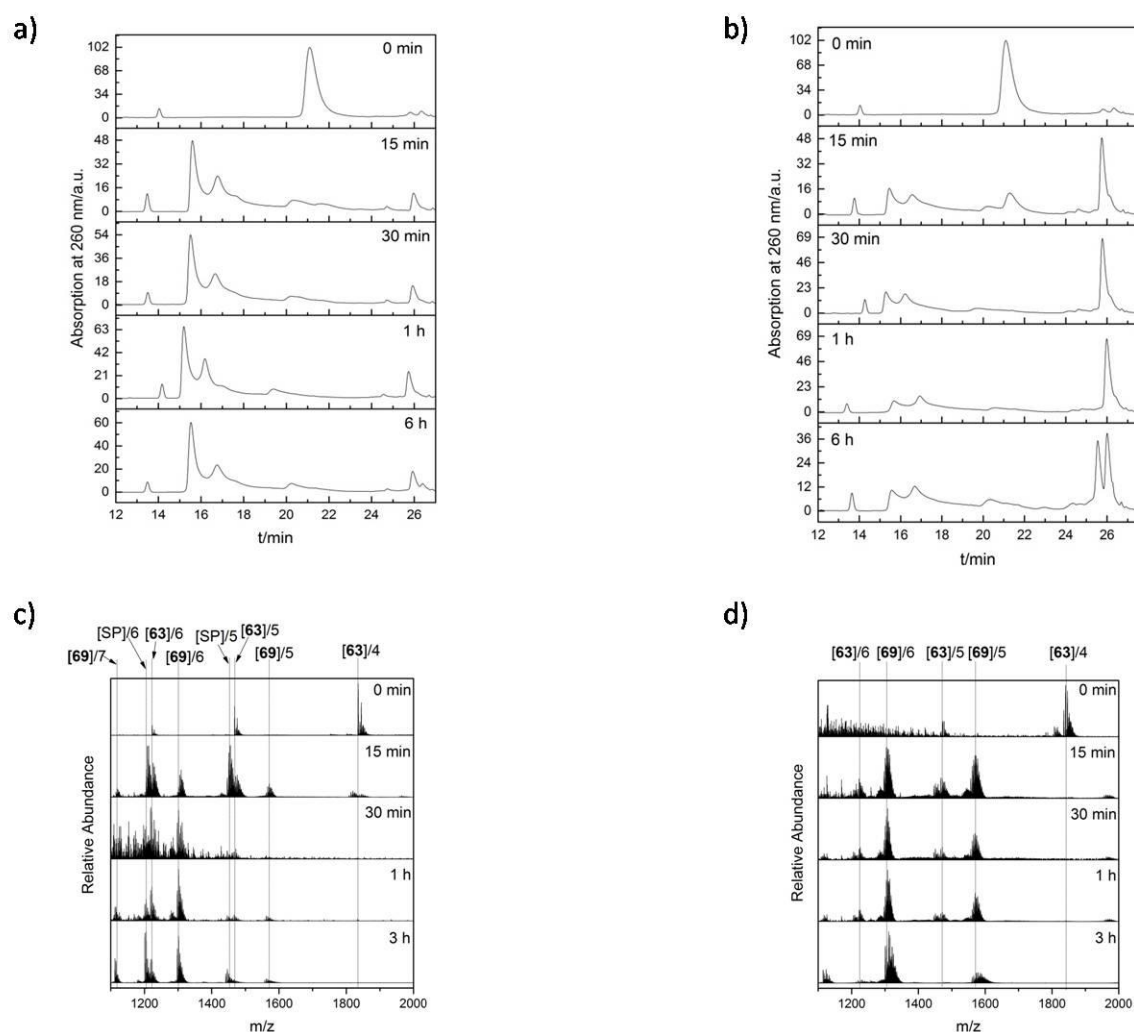


Figure 3.12: Kinetic study of the photoreaction between Tz-DNA2 **63** and 5.00 eq. (a, c) and 15.0 eq. (b, d) of Do-TEG-Mal **64** using HPLC (top) and ESI-MS mass spectrometry (bottom) at different irradiation time.

The HPLC analysis of the photoreaction (Figure 3.12a, b) indicates that the reaction is completed after 30 min for both 5.00 eq. and 15.0 eq. dienophile **64**, which is longer than in the case of PE2-DNA2 **56**. However, when 5.00 eq. of dienophile is added, side products (SP) (70%), represented by the fractions with a retention times of 15.5 min and 16.7 min, were mainly detected with merely 14% photoadduct **69** (the fraction at $t = 26.0$ min). With the increase of the dienophile amount to 15.0 eq. more photoadduct is obtained (80%) as compared to 17% of the side products, indicating the product promoting effect of the increased equivalents of dienophile. The reactions were also analyzed by ESI mass spectrometry, resulting in mass spectra (Figure 3.12c and d) with 4-, 5-, 6- and 7-fold charged ions, assigned to reactant **63**, photoadduct **69** and additional unidentified species, most probably the side products, which prevail in reaction mixture, containing 5.00 eq. of dienophile **64** and are considerably reduced

for 15.0 eq. **64**. Attempt was made to decrease the amount of the side products and the amount of dienophile increased to 100 eq., but this did not change the overall outcome (Figure 3.13).

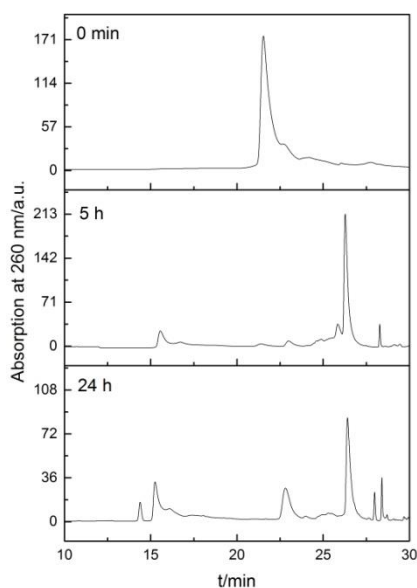


Figure 3.13: HPLC chromatograms of the reaction between Tz-DNA2 **63** and 100 eq. dienophile **64** after 0 min, 5 h and 24 h irradiation.

When irradiation time was increased to 24 h (Figure 3.13), it was observed that prolonged irradiation resulted in appearance of additional side products ($t = 14.4$ min and 22.8 min), probably stemming from the UV caused damage or species present in the reactions mixture. As such long irradiation times will not be used for further applications, but the experiment was performed out of scientific curiosity, these newly formed side products were not investigated further.

Detailed kinetic analysis by ESI-MS (Figure 3.14, top) showed the same trend as observed above, namely that the amount of side product is significantly increased when smaller amounts of dienophile is present (17% for 5.00 eq.), but only 5% is present for 15.0 or more equivalents, indicating that the larger amounts of dienophiles should be used in case of Tz-DNA2 **63**. This is unlike PE2-DNA2 **56** reaction where there is no significant increase in the cycloadduct yield upon the addition of 15.0 eq. of dienophile **64** and no side products are present in significant amount. Previous photoreaction of Tz-DNA2 **63** with 5.00 eq. dienophile **64** resulted almost exclusively side product, as determined by peak integration of HPLC spectra. In this case, however, the integration of undefined peaks from ESI mass spectra resulted a value of 17%. The difference can be attributed to the inaccuracy in the preparation of dienophile solution (caused by weighing), which was always freshly prepared in small

amounts. However, it should be noted, that for the dienophile amount ≥ 15.0 eq. the photoreaction is strongly preferred.

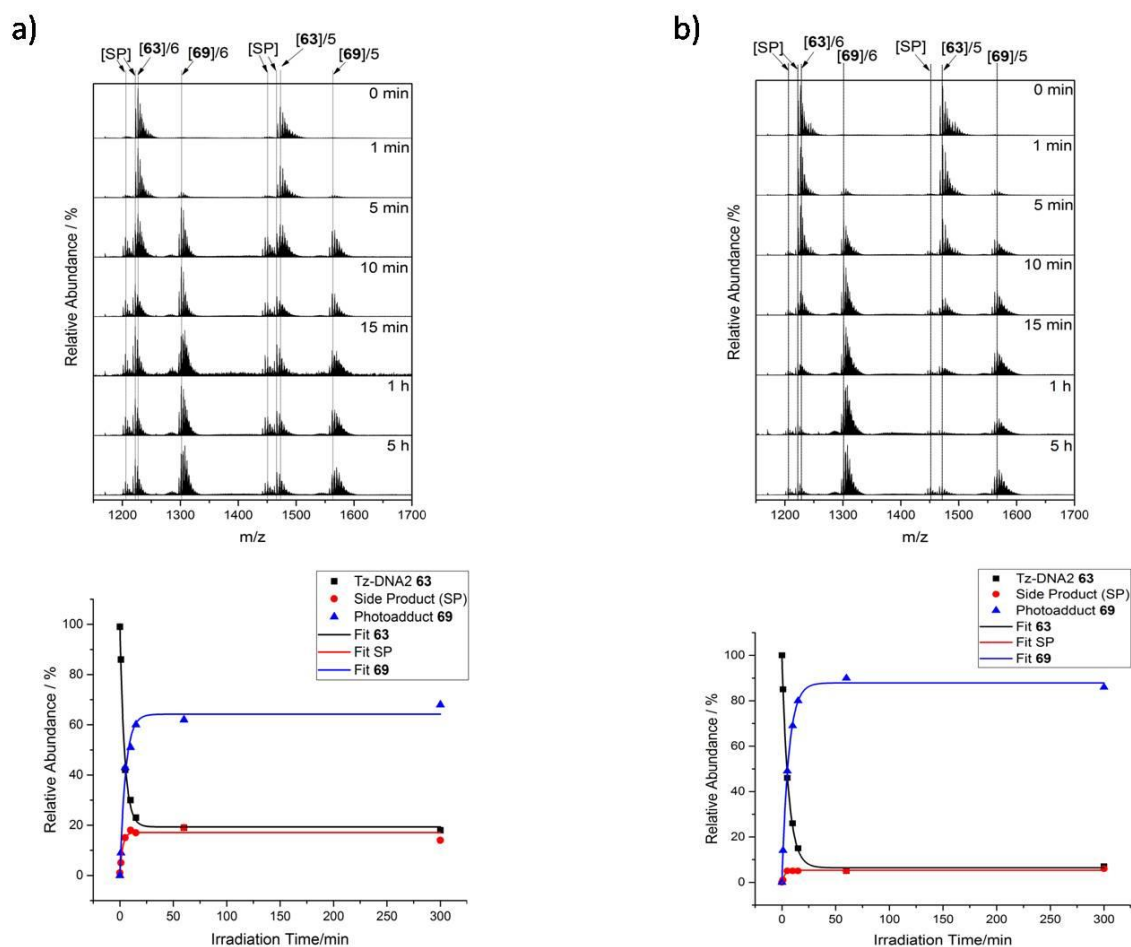


Figure 3.14: ESI-MS spectra (top) and the kinetic plots derived from the integration of the corresponding mass spectra (bottom) for photoreaction of Tz-DNA2 **63** with a) 5.00 eq. and b) 15.0 eq. of Do-TEG-Mal **64** at different irradiation times with 320 nm light.

Figure 3.14 (bottom) shows the plots of integrated MS peak values as a function of irradiation time, indicating the reaction completions after 30 min. The experimental data points show an excellent agreement with an exponential fit for both reactions with 5.00 eq. or 15.0 eq. dienophile **64**.

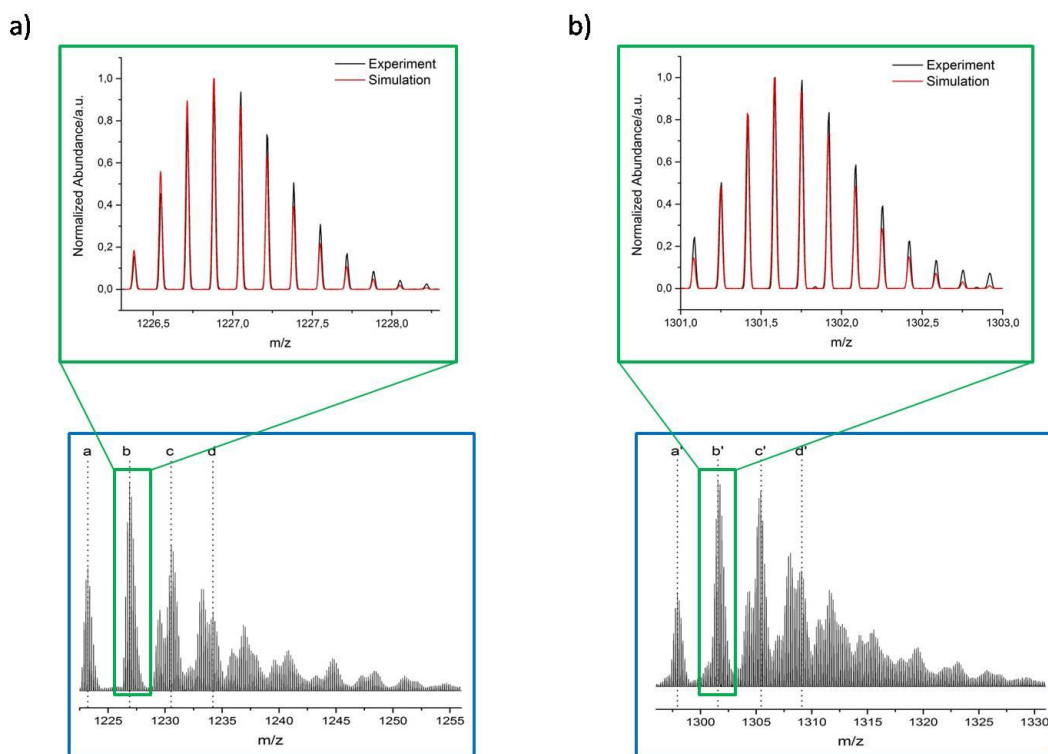


Figure 3.15: Expansion of the ESI mass spectrum region (bottom) and comparison between experimental and simulated data (top) for a) Tz-DNA2 **63** (m/z range: 1226.3 - 1228.3) and b) photoadduct **69** (m/z range: 1301.0 - 1303.0).

The detailed analysis of the isotopic pattern (Figure 3.15, bottom) of the most abundant isotopes of Tz-DNA2 **63** (m/z range of 1222.5 - 1256.0) and photoadduct **69** (m/z range of 1296.0 - 1331.0) and the comparison to their simulated isotopic pattern (Figure 3.15, top) provides evidence for the successful generation of the desired cycloadduct. Furthermore, experimentally obtained m/z values of the reactant **63** and photoadduct **69** and their sodium adducts are in excellent agreement with the theoretically calculated, expected exact mass values ($\Delta m/z < 0.0100$, Table 3.3).

Table 3.3: Peak assignment of the ESI mass spectra of reactant **63** from $m/z = 1222.5$ to $m/z = 1235.5$ (a - d) and photoadduct **69** from $m/z = 1296.0$ to $m/z = 1311.0$ (a' - d'). Peak labels correspond to the spectra shown in Figure 3.15. Both experimental and theoretical m/z values and their differences ($\Delta m/z$) are shown.

Ion assignment	Sum formula	m/z_{expt}	m/z_{theor}	$\Delta m/z$
a	$[\text{C}_{239}\text{H}_{287}\text{N}_{99}\text{O}_{132}\text{P}_{22}]^{6+}$	1223.2224	1223.2177	0.0047
b	$[\text{C}_{239}\text{H}_{286}\text{NaN}_{99}\text{O}_{132}\text{P}_{22}]^{6+}$	1226.8839	1226.8813	0.0026
c	$[\text{C}_{239}\text{H}_{285}\text{Na}_2\text{N}_{99}\text{O}_{132}\text{P}_{22}]^{6+}$	1230.5456	1230.5450	0.0006
d	$[\text{C}_{239}\text{H}_{284}\text{Na}_3\text{N}_{99}\text{O}_{132}\text{P}_{22}]^{6+}$	1234.2080	1234.2086	0.0006
a'	$[\text{C}_{263}\text{H}_{319}\text{N}_{99}\text{O}_{140}\text{P}_{22}]^{6+}$	1297.9250	1297.9193	0.0057
b'	$[\text{C}_{263}\text{H}_{318}\text{NaN}_{99}\text{O}_{140}\text{P}_{22}]^{6+}$	1301.5863	1301.5830	0.0033
c'	$[\text{C}_{263}\text{H}_{317}\text{Na}_2\text{N}_{99}\text{O}_{140}\text{P}_{22}]^{6+}$	1305.2482	1305.2466	0.0016
d'	$[\text{C}_{263}\text{H}_{316}\text{Na}_3\text{N}_{99}\text{O}_{140}\text{P}_{22}]^{6+}$	1308.9107	1308.9103	0.0004

Photoreactions of oligonucleotides labeled with two photo-activatable groups (PE2-DNA2 **56** and Tz-DNA2 **63**) were thoroughly studied using HPLC chromatography, gel electrophoresis and ESI-MS to optimize the reactions conditions, explore existence of the side products and get insight into the kinetics, in particular the most suitable equivalents of reagents and reaction time to obtain desired cycloadduct. Reactions using PE1 derivative were not successful due to the disfavored photoenolization process in aqueous (protic) media and this derivative was not further explored. Photoreactions employing PE2 modified oligonucleotides resulted in photoadducts obtained in good yields (35% for 1.00 eq. of dienophile), and the yields could be additionally improved by increasing the dienophile amount to 5.00 eq. (84%). Side products were observed only when starting PE2-DNA2 is irradiated by UV light in absence of dienophile, indicating a possible intramolecular cyclization. However, side product is not present in the significant amount when dienophile is added, indicating the preference for the photocyclization reaction. In contrast, side products can be detected when photoreaction with Tz-DNA2 is performed, although the amount decreases with addition of more dienophile (more than 15.0 eq.). Detailed ESI-MS and HPLC study also showed that photoenol reaction is faster (completion at 10 min) as compared to tetrazole (completion at 30 min), in which the side

products are not eliminated by either the addition of dienophile excess or prolonged irradiation time. According to the insights, gained from this study, PE2 modified oligonucleotide **56** represent the most appropriate reagent for the light-induced cycloaddition reactions, as confirmed by its use in different applications, such as light triggered DNA conjugation presented in the following chapter.

3.3 Photoenol Modified Oligonucleotides in DNA Bioconjugation and Structuring

3.3.1 Light-Induced Conjugation of PE2-DNA2 **54 to Horseradish Peroxidase (HRP)**

Conjugation of artificial oligonucleotides with proteins provides multifunctional constructs for the applications in bionanotechnology. Such construct have both the intrinsic functions of proteins, which can vary from catalysis^[178] and signaling and small molecule transfer^[179] to structuring^[180] and highly specific structural addressability of DNA, due to the Watson-Crick base pairing. Variety of synthetic strategies were developed for the covalent and non-covalent conjugation of the nucleic acids and proteins.^[11c] This section presents the use of previously described light-induced conjugation for oligonucleotides, which was for the first time demonstrated by our group by two independent studies employing different proteins, myoglobin and horseradish peroxidase, presented herewith.^[127]

Horseradish peroxidase (HRP, Figure 3.17a) is biotechnologically very important protein and one of the most potent peroxidases, used in various assays and biosensing applications.^[181] Taking into account its significance, it is not surprising that various methods have been published to enable its conjugation and we have attempted to extend the chemical toolbox by exploring light-induced cycloaddition methodology. Although it was shown, that the irradiation with UV light, necessary to cause the light-induced coupling, does not affect the structure and function of DNA, native structure of proteins has been reported to be more sensitive.^[182] Therefore, prior to light-induced coupling of PE2-DNA2 **54**, the study of HRP under UV light irradiation was performed. A solution of HRP in PBS/acetonitrile (3:2, v/v) was deoxygenated by purging with argon and irradiated under UV lamp ($\lambda_{\max} = 320$ nm) at ambient temperature for 16 hours. After buffer exchange by gel filtration columns, solution was analyzed by denaturing polyacrylamide gel electrophoresis (sodium dodecyl sulfate polyacrylamide gel electrophoresis, SDS-PAGE) shown in Figure 3.16.

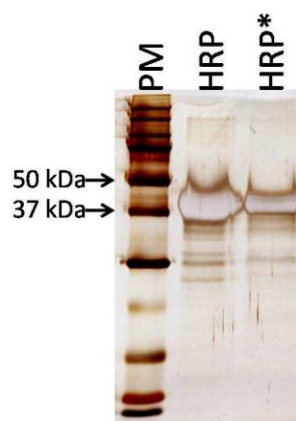


Figure 3.16: SDS-PAGE characterization of irradiated horseradish peroxidase HRP* in comparison to non-irradiated HRP. Conditions: 12% SDS-PAGE; Running buffer: 1xSDS-running buffer; Voltage: 30 min at 80 V, 1 h at 100 V; Staining: silver staining; Loading: 25.0 pmol; PM: protein marker (Precision Plus Protein Dual Xtra Standards, BioRad).

Both samples (irradiated HRP* and non-irradiated HRP) show the same electrophoretic mobility (bands between 37 kDa and 50 kDa) and no additional bands for irradiated HRP* could be detected, indicating that there is no significant structural damage of the protein under used irradiation conditions. Consequently, HRP could be employed in the light-induced cycloaddition reaction. HRP, like any other native protein, does not contain natural dienophile groups and to enable [4+2] photocycloaddition reaction with PE2-DNA2 **54**, must first be modified with dienophile moiety. This can be achieved using heterobifunctional linker sulfosuccinimidyl 4-(*N*-maleimidomethyl)cyclohexane-1-carboxylate **70** (sSMCC) (Figure 3.17b), which selectively reacts with lysine residues on the protein surface.^[183]

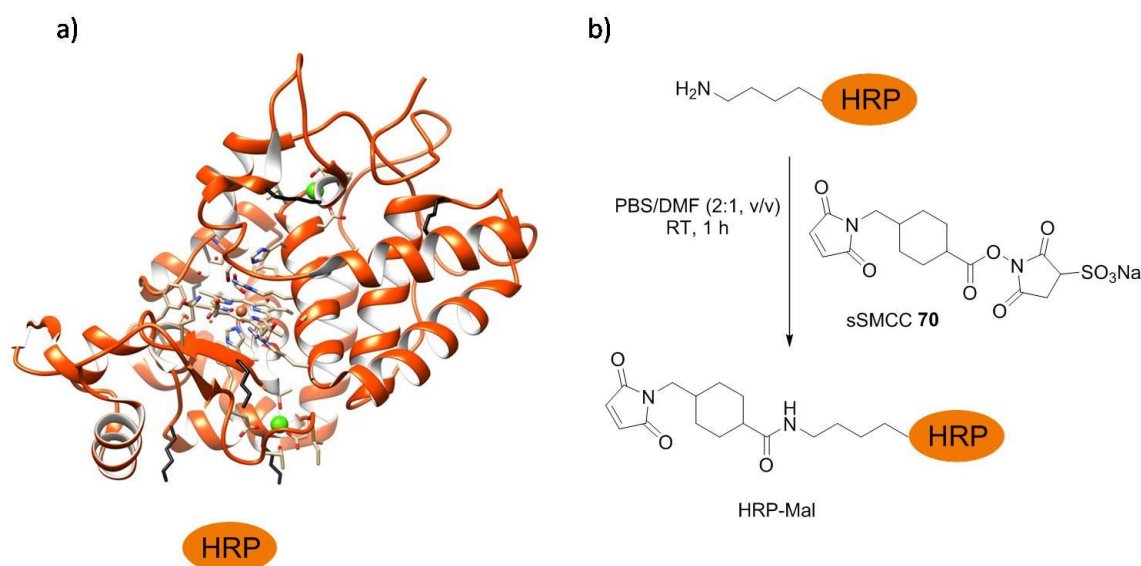
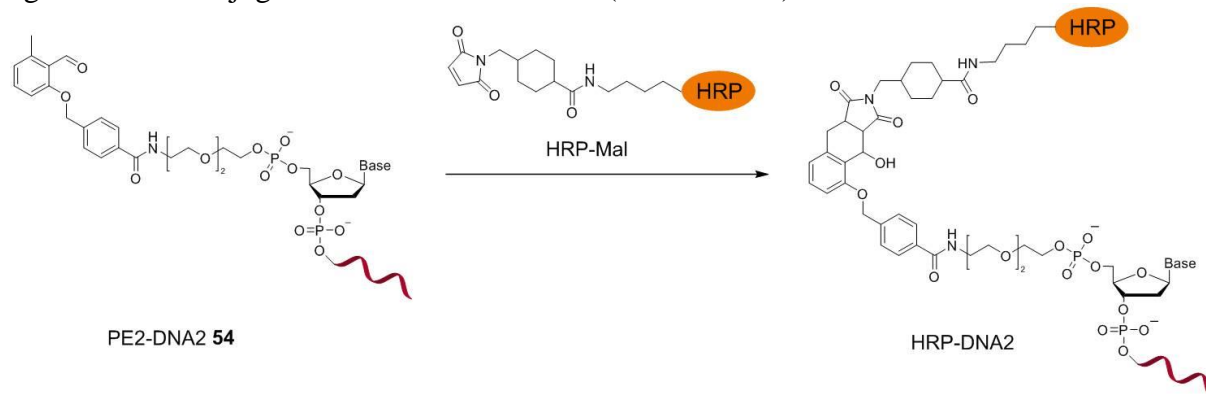


Figure 3.17: a) HRP structure with lysine moieties (black sticks); graphics was created using a software UCSF Chimera 1.11rc and 1W4W data from the protein data bank; b) modification of lysine moieties of HRP with sSMCC **70**.

To achieve the amide coupling, 33.2 nmol HRP in PBS buffer (pH = 6.0) were incubated with 2.00 mg sSMCC in DMF for 1 hour at ambient temperature. Excess sSMCC removed by gel filtration and the maleimide functionalized HRP was directly employed in a light-induced conjugation with PE2-DNA2 **54** (Scheme 3.17).



Scheme 3.17: Light-induced conjugation of PE2-DNA2 **54** and maleimide functionalized HRP (HRP-Mal); PBS/acetonitrile (3:2, v/v), $\lambda_{\text{max}} = 320$ nm, 16 h, RT.

For the photoreaction a mixture of 2.00 nmol PE2-DNA2 **54** and 2.20 nmol of fresh prepared HRP-Mal in 500 μL of PBS/ CH_3CN solution (3:2, v/v) was deoxygenated by purging with argon for 15 minutes and subsequently irradiated under UV lamp ($\lambda_{\text{max}} = 320$ nm) at ambient temperature, followed by chromatographic purification using fast protein liquid chromatography (FPLC). The collected fractions F1 and F2 exhibit the absorption at 260 nm and 403 nm, which are characteristic of DNA and HRP respectively (Figure 3.18a).^[184] Fraction F3, which contains several peaks, shows absorption exclusively at 260 nm, which is typically for DNA^[185] and most probably represents non-reacted PE2-DNA2 **54** and related side products. Characterization of the collected fractions was performed by native PAGE (12.5% PA gel, 30 min at 80 V, 90 min at 100 V in tris/glycin running buffer, Figure 3.18 b) using SYBRGold[®] staining for oligonucleotides and silver staining for HRP. Bands responding positively to both staining strategies contain HRP-DNA2 conjugates.

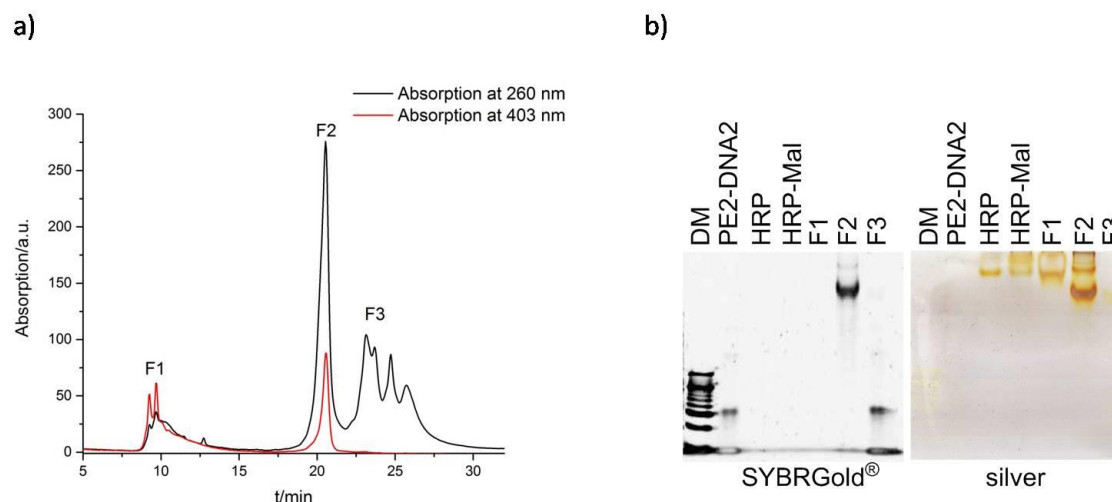


Figure 3.18: a) FPLC chromatogram of HRP-DNA2 conjugate purification; absorption detection at 260 nm (black curve) and 403 nm (red curve); b) native PAGE characterization of the FPLC fractions F1, F2 and F3 in comparison to PE2-DNA2 **54**, HRP and HRP-Mal; DM: 10 bp DNA marker; oligonucleotide and protein band visualization by SYBRGold® and silver staining respectively.

As it can be seen in Figure 3.18b, F1 fraction contains only HRP moiety and has the same electrophoretic mobility as HRP-Mal indicating that non reacted HRP-Mal is present in this fraction. Band F2 was assigned to HRP-DNA2 conjugate, as it shows the higher electrophoretic mobility in comparison to non-modified HRP or HRP-Mal, due to the increased negative charge after the coupling to PE2-DNA2 **54**. Additionally, it could be stained by both SYBRGold® and silver staining methods, confirming the presence of both DNA and protein. Beside the main product additional band with a lower electrophoretic mobility, similar to HRP-Mal, was detected in F2, indicating that small amount of residual HRP-Mal, which could not be separated from the main product, due to the chosen conditions is isolated together with the main product. Choice of different purification conditions could allow for better separation of both fractions. However, this was not an important requirement for this study and the product was used, as obtained from single FPLC purification. Band F3 shows the same electrophoretic mobility as PE2-DNA2 **54** and could be visualized exclusively by SYBRGold®, therefore it can be assigned to the non-reacted PE2-DNA2 **54**.

In order to explore the selectivity of the photoreaction, a number of control reactions was performed, such as the incubation of PE2-DNA2 **54** and HRP-Mal in the dark (Figure 3.19 a), irradiation of PE2-DNA2 **54** and non-modified HRP (Figure 3.19 b) alone, irradiation of non-modified DNA2 and HRP-Mal (Figure 3.19 c) and irradiation of non-modified DNA2 and non-modified HRP (Figure 3.19 d). The reactions were performed at the same reaction conditions as those used in previously described photoreaction (Scheme 3.17).

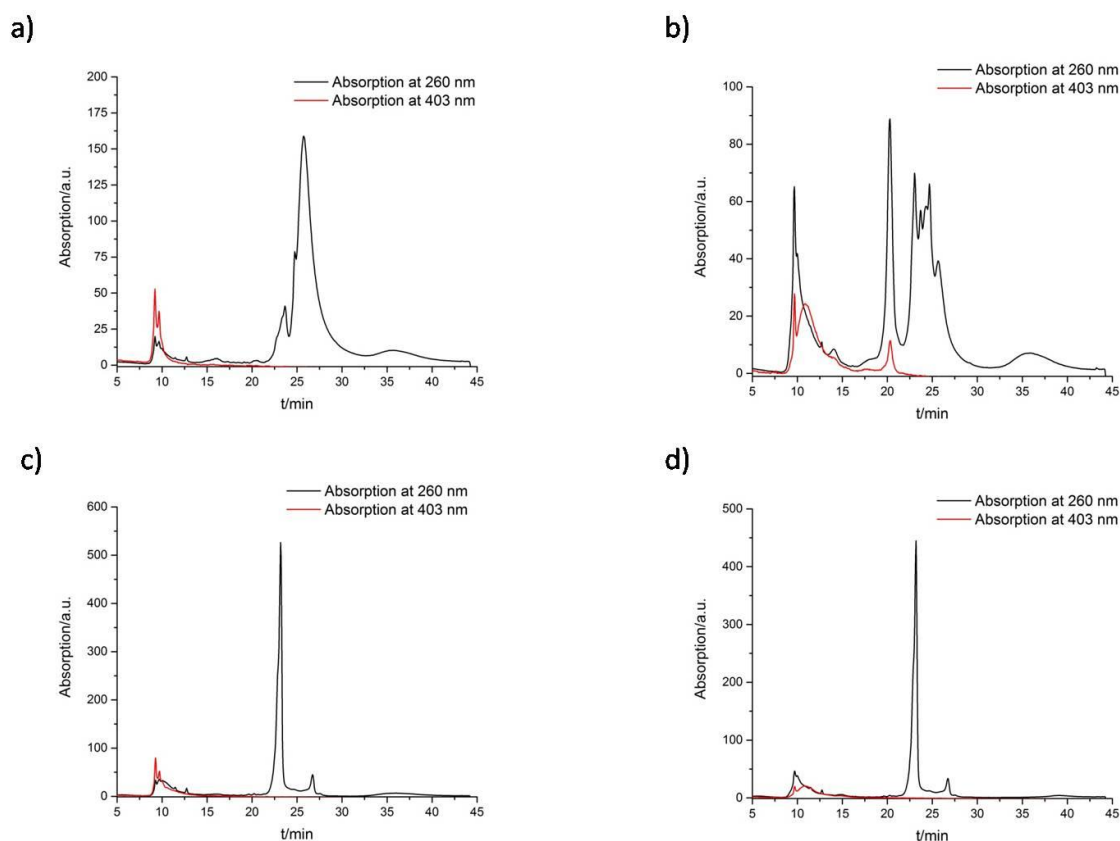


Figure 3.19: FPLC chromatograms of control reactions: a) incubation of PE2-DNA2 **54** and HRP-Mal for 16 h in the dark; b) irradiation of PE2-DNA2 **54** and HRP for 16 h at 320 nm; c) irradiation of DNA2 and HRP-Mal for 16 h at 320 nm; d) irradiation of DNA2 and HRP for 16 h at 320 nm. The black curve represents the absorption at 260 nm (DNA) and the red curve the absorption at 403 nm (HRP).

In case of the irradiation of non-modified HRP with PE2-DNA2 **54**, an insignificant amount of conjugate HRP-DNA2 was obtained, indicating, that a low yielding side reaction occurs between a photoenol moiety and amino acids of the protein. Recently, Siti and colleagues described the formation of the conjugation product when PEG-tetrazole is irradiated with native HRP and other proteins.^[186] Further investigations revealed that the light-induced cycloaddition reaction occurs exclusively with proteins/peptides containing tryptophan residue. Presumably, the side product in our case results from the reaction between tryptophan residue of HRP and photoenol moiety of PE2-DNA2 **54**. Due to very low amounts of side product (Figure 3.19b), isolation was not possible to enable instrumental analysis at this point and it was not further investigated.

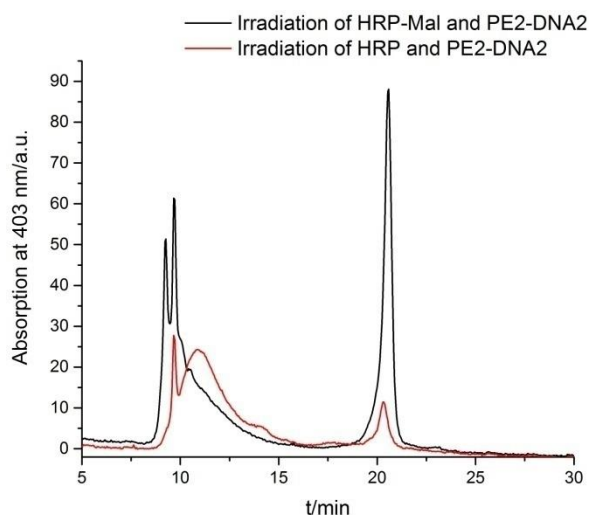


Figure 3.20: FPLC chromatograms of HRP-DNA2 obtained in the photoreaction between PE2-DNA2 **54** and HRP-Mal (black curve) and of the side product obtained after irradiation of PE2-DNA2 **54** and HRP (red curve).

The absence of HRP-DNA2 conjugate in other control reactions indicates the high specificity of the light-induced cycloaddition reaction between photoenol and maleimide modified biomolecules.

In order to explore if the inherent functions of DNA and HRP are preserved in the HRP-DNA2 conjugate, the hybridization ability of DNA, which is crucial for the DNA directed immobilization (DDI), as well as catalytic activity of HRP were tested. For the hybridization ability tests, purified HRP-DNA2 conjugate was incubated with a 10-fold excess of complementary oligonucleotide cDNA2 and, additionally, with a fluorescein labeled complementary strand 6-FAM-cDNA2 in a tris/EDTA/NaCl hybridization buffer. The reaction was performed for 16 hours at ambient temperature and subsequently analyzed by 12.5% polyacrylamide gel electrophoresis (Figure 3.21).

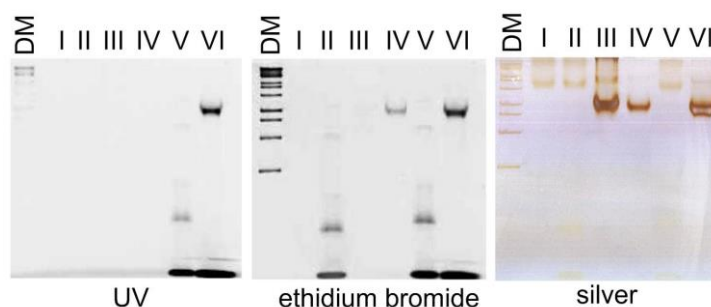


Figure 3.21: Native PAGE analysis of hybridization of HRP-DNA2 with complementary strands cDNA2 and 6-FAM-cDNA2, DM: 1kb DNA-marker, I: native HRP; II: control reaction (HRP+DNA2+cDNA2), III: HRP-DNA2 conjugate, IV: HRP-DNA2+cDNA2, V: control reaction (HRP+DNA2+6-FAM-cDNA2), VI: HRP-DNA2+6-FAM-cDNA2; Conditions: 12.5% PAGE; Running buffer: tris/glycine; Voltage: 30 min at 80 V, 90 min at 100 V; Loading: 25.0 pmol; DM: 1kb DNA marker; Visualization: UV irradiation, ethidium bromide and silver staining.

For the visualization of bands, UV irradiation, ethidium bromide and silver staining were performed. For the control reactions non-modified HRP was incubated with PE2-DNA2 **54** and cDNA2 or 6-FAM-cDNA2. The resulted gel was first analyzed under UV irradiation, which allows the detection of 6-FAM-cDNA2. Subsequently, the gel was stained with ethidium bromide in order to visualize the hybridized strands and finally silver staining was performed for the protein staining. As it can be seen in Figure 3.21, only the bands in lane IV and VI, which were loaded with hybridized samples, could be visualized with all three methods confirming the successful hybridization of HRP-DNA2 conjugate and preservation of the inherent DNA function.

In order to assess the peroxidase activity of the HRP-DNA2 conjugate, Amplex[®]Red assay was employed. Amplex[®]Red assay relies on HRP mediated transformation of colorless non-fluorescent Amplex Red (*N*-acetyl-3,7-dihydroxyphenoxazine) to pink, highly fluorescent resorufin ($\lambda_{\text{ex}} = 530 \text{ nm}$, $\lambda_{\text{em}} = 590 \text{ nm}$) in presence of H_2O_2 (Figure 3.22 a).

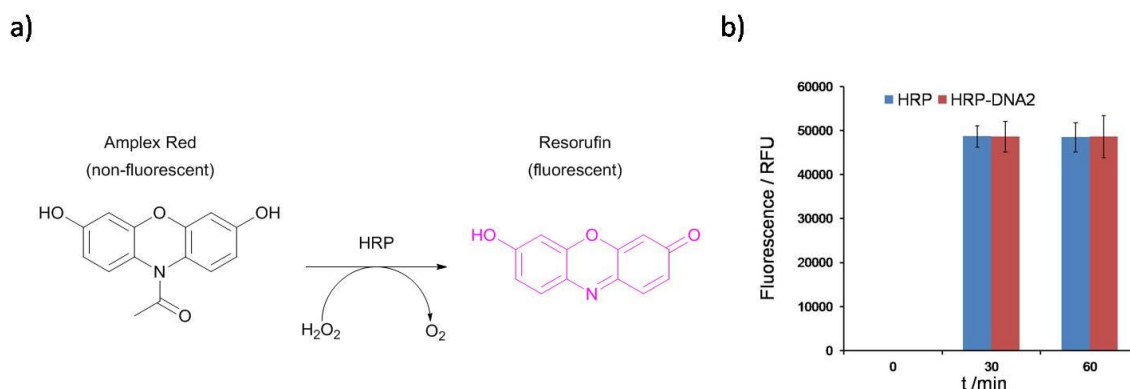


Figure 3.22: a) Principle of the peroxidase activity assay using Amplex Red and HRP in the presence of H_2O_2 ; b) the average of fluorescence intensity as a function of time after 0 min, 30 min and 60 min reaction duration obtained by Amplex[®]Red assay using native HRP (blue bar) or HRP-DNA2 conjugate (red bar).

The fluorescence signal intensity of the product was measured as a function of time and used as the confirmation of HRP activity, as the reaction does not proceed without the presence of the protein. Five measurements were performed for each sample of non-modified HRP and HRP-DNA2 conjugate over a period of one hour. The fluorescence intensity obtained in the presence of native HRP (blue bar) and HRP-DNA2 conjugate (red bar) is shown in Figure 3.22b. There is no difference in the intensity when both species are compared, indicating the high peroxidase activity of the conjugate, which is not affected by presence of conjugated DNA.

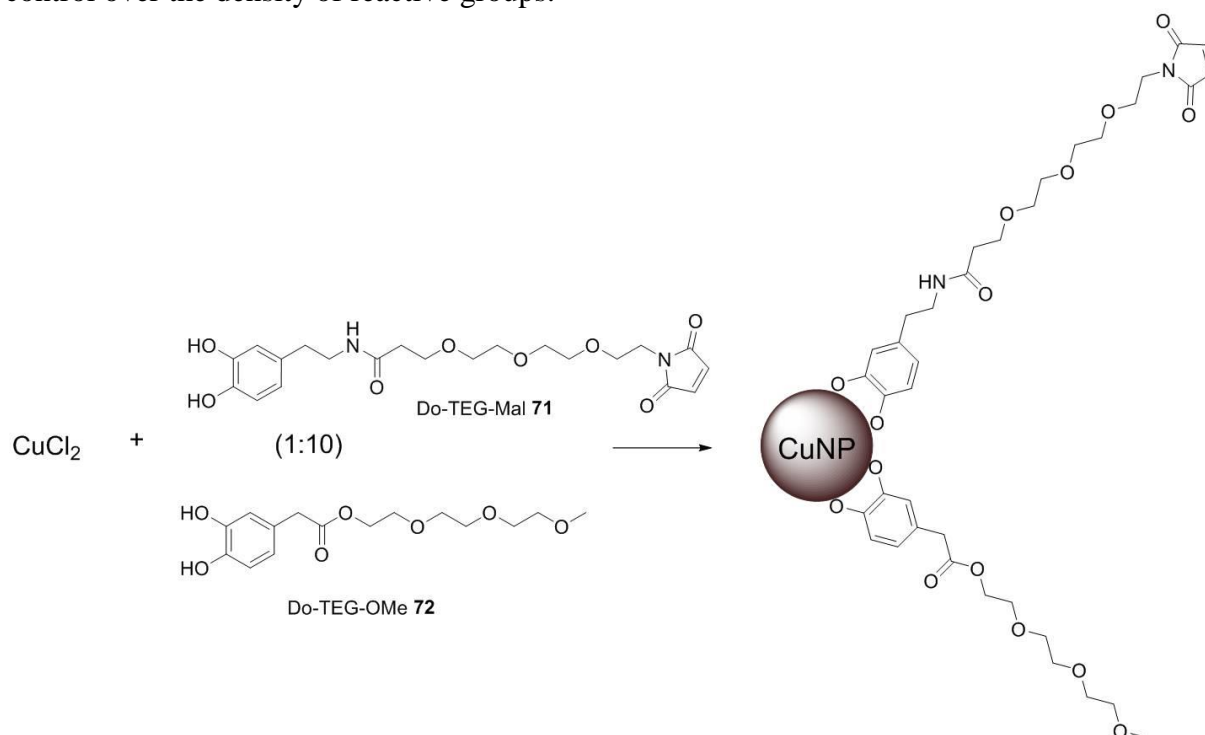
In conclusion, the light-induced conjugation strategy could successfully be applied for the conjugation of the photoenol modified oligonucleotide to a maleimide containing proteins such as horseradish peroxidase. After conjugation, the inherent functions of both DNA (hybridization ability) and HRP (enzymatic activity) were preserved, as shown by hybridization tests and Amplex[®]Red peroxidase activity assay. Successful conjugation of photoenol modified oligonucleotides to HRP inspired us to employ this mild and easily controllable reaction for modification of another class of catalysts, namely inorganic nanoparticles, which are playing increasing role in various applications beyond material design. Following section addresses the use of the light-induced reaction for the conjugation of maleimide functionalized copper nanoparticles with PE2-DNA2 **54**.

3.3.2 Light-Induced Biofunctionalization of Maleimide Coated Copper Nanoparticles

Functionalization of nanoparticles with biomolecules such as DNA, allows for the use of such composites in variety of applications. They can be employed as building blocks for nano-assembly or drug delivery vectors, structure design and the development of sensors and nanodevices^[187] as they possess both the recognition property of DNA and the unique optical, magnetic, electronic, mechanical and chemical properties of nanomaterials.^[188] Among DNA conjugated nanomaterials, gold nanoparticles (Au NPs) are best characterized and most widely used for various applications.^[189] In contrast, DNA conjugates with copper nanoparticles (Cu NPs) have not been yet reported, although Cu NPs have a range of highly desirable electronic and catalytic properties. Recently, double stranded DNA was utilized as a template for the synthesis of Cu- NPs,^[190] but the surface of Cu NPs has rarely been functionalized, most probably due to the inherent instability of Cu under ambient conditions and its oxidation, which changes the properties of nanomaterials. In the last decades, Cu NPs became more attractive to the science community because of their fascinating properties such as high catalytic activity, high conductivity and optical properties,^[191] but also because of the high natural abundance and low costs of copper. Till now, Cu NPs have been shown to be able to generate reactive oxygen species (ROS), which can be employed for the activation of HRP,^[192] and have shown a potential in design of catalysts,^[193] antibacterial materials,^[194] electronic materials^[195] and sensors.^[196] All of these prompted researchers to develop methods for the preparation of stable Cu and Cu-based nanomaterials.^[193] However, there is still a lack of synthetic procedures for modification of Cu NP surface, in particular attachment of biomolecular species such as

oligonucleotides, which could be, for instance, used for assembly of novel catalytic or optoelectronic platforms. Within this section, the use of light-induced cycloaddition reaction in design of DNA-Cu NPs is presented and discussed.

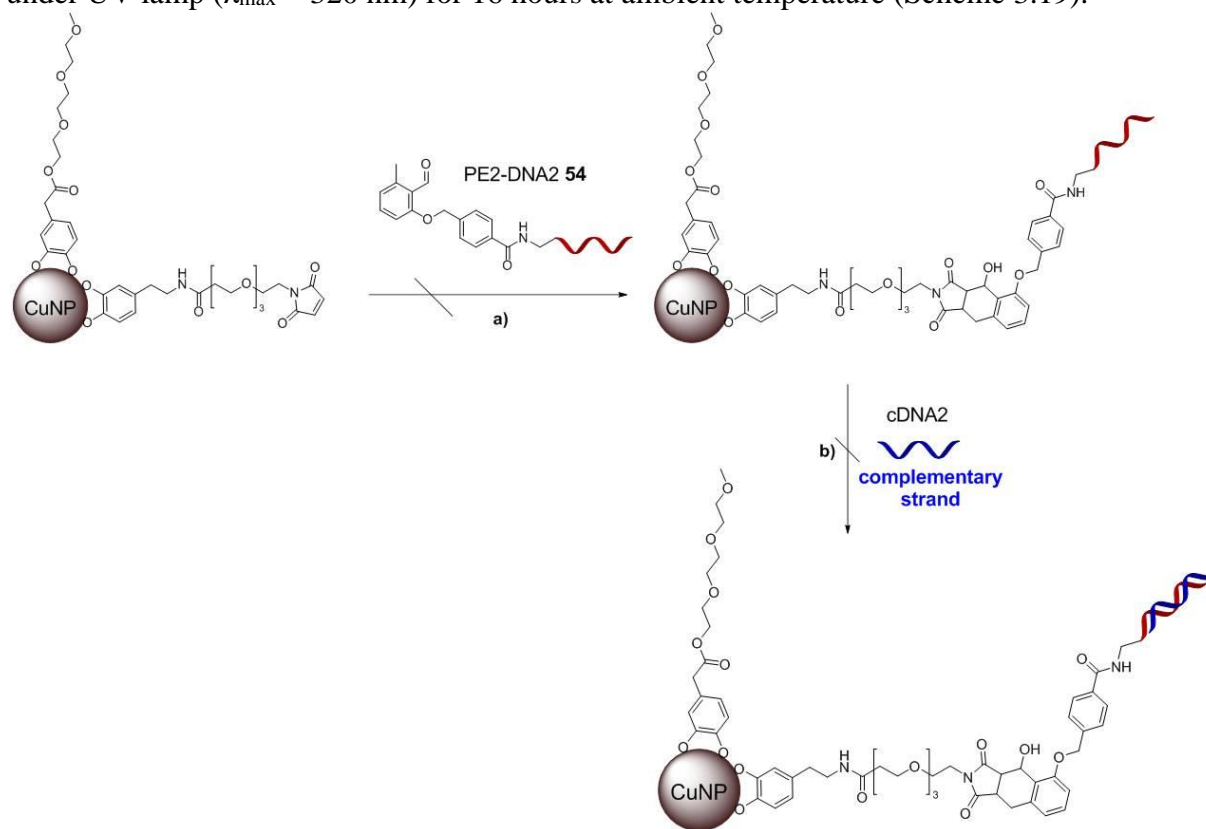
Originally, a strategy was developed within our group (by Dr. Cheng Chen) to prepare stable maleimide functionalized Cu NPs by employing catechol containing dopamine-based linkers.^[192] Using dopamine based linkers, several different dopamine derivatives were employed in addition to dopamine-maleimide. Of those, we have decided to use dopamine/maleimide, containing triethylene glycol group (Do-TEG-Mal **71**, prepared by Dr. Ishtiaq Ahmed) to minimize the steric hindrance on the surface, for the preparation of CuNPs. To further increase the access of the maleimide group for cycloaddition by minimizing surface crowding effect, a 1:10 ratio of maleimide containing to inert (without maleimide) dopamine linker was used for one-pot synthetic procedure (Scheme 3.18). As reported by Susumu *et al.* a combination of reactive and inert linker generally improves the colloidal stability and enable control over the density of reactive groups.^[197]



Scheme 3.18: Schematic illustration for the synthesis of maleimide functionalized copper nanoparticles; water/acetonitrile (1:1, v/v), 80 °C, 8 h.

Procedure, published by Chen *et al.*, was used to prepare and characterize stable Cu NPs.^[192] To test if the maleimide capped Cu NPs can undergo the light-induced reaction with photoenol modified DNA, they were mixed with a solution of PE2-DNA2 **54** in

water/acetonitrile (1:1, v/v), deoxygenated by purging with argon for 15 min and irradiated under UV lamp ($\lambda_{\text{max}} = 320$ nm) for 16 hours at ambient temperature (Scheme 3.19).



Scheme 3.19: Light-induced cycloaddition reaction between PE2-DNA2 **54** and maleimide functionalized copper nanoparticles and subsequent hybridization with a complementary oligonucleotide cDNA2; a) water/acetonitrile (1:1, v/v), $\lambda_{\text{max}} = 320$ nm, 16 h; b) 20 mM MgCl_2 , 16h, RT.

In addition, a control reaction was performed by incubating PE2-DNA2 **54** with maleimide containing CuNPs for 16 h at ambient temperature without irradiation. After purification by centrifugation, hybridization test for both reactions was performed by incubation of Cu NPs with a 10-fold excess of complementary cDNA2 in a 20 mM MgCl_2 solution at ambient temperature for 16 h. All reaction mixtures were subsequently analyzed by 0.8% agarose gel electrophoresis (Figure 3.23).

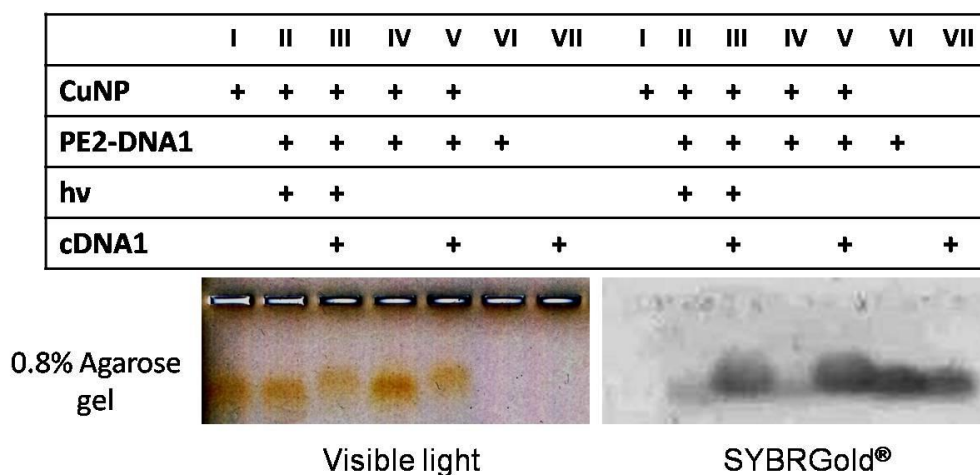


Figure 3.23: Agarose gel (0.8%) electrophoresis study of photoreaction between PE2-DNA2 **54** and maleimide Cu NPs nanoparticles at 320 nm. Visualization of bands was afforded by use of the visible and UV light after SYBRGold[®] staining of DNA. Gels were exposed to 100 V for 15 min in 0.5xTBE buffer.

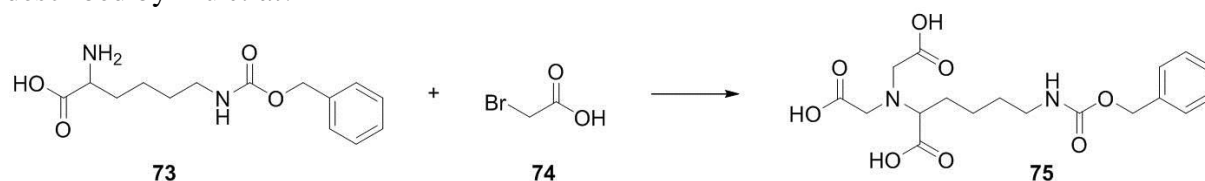
As seen from Figure 3.23, the electrophoretic mobility can be observed in all bands, containing Cu NPs, and the slight change is noticeable for bands corresponding to photoreaction (lane II) and that for control reaction (lane IV), performed in the dark. SYBRGold[®] staining is positive indicating that PE2-DNA2 **54** is present in both bands and DNA is interacting with Cu NPs unselectively. After addition of cDNA2 to explore the hybridization ability of bound DNA, a change in the mobility of the bands is observed (III and V) confirming the successful hybridization. However, there is no noticeable difference between the reaction and the control indicating that PE2-DNA2 **54** interacts with Cu NP in a non-specific way, most probably due to the electrostatic interaction of positively charged Cu NPs surface (zeta potential = 10.2 ± 1.18 mV)^[192] and negatively charged oligonucleotide backbone. There is also a possibility that PE group reacts as an anchor for Cu ions on the surface of NPs, however this hypothesis was not tested.

In order to remove any nonspecifically bound DNA, different washing steps were performed including wash steps with water at ambient temperature and at 40 °C, multiple washing steps with 20 mM and 200 mM NaCl solutions both at ambient temperature and 60 °C. Additionally, the photoreactions were performed in 20 mM, 40 mM and 200 mM NaCl_{aq}/acetonitrile (1:1, v/v) solutions in order to minimize the electrostatic interactions. However, the photoreaction was not successful using this particular system. Therefore, another Cu NP anchoring linker was explored to afford stable Cu NPs with surface attached maleimide groups, which could further be used for photoreactions.

Carboxylic acid groups and polyols have strong affinities for the metal surface and different synthetic methods, employing L-ascorbic acid,^[198] citric acid,^[199] oleic acid^[200] and

other^[201] have been used as a stabilizing agents for Cu NPs. Recently, nitrilotriacetic acid has been employed as a chelator for the extracellular synthesis of copper nanoparticles by thermoanaerobic bacteria.^[202] Combining strong affinity to copper with availability (derivatives were synthesized in the group) and simple modification route, nitrilotriacetic acid derivative **81** has been employed for the synthesis of Cu NPs.

For the initial experiments derivative **75** was prepared using synthetic procedure described by Liu *et al.*^[203]



Scheme 3.20: Synthesis of the nitrilotriacetic acid derivative **75** for CuNP coating; NaOH, 0 °C - RT, 16 h; 50 °C, 2 h, 50%.

In a nucleophilic substitution reaction a lysine derivative **73** was reacted with a bromoacetic acid **74** yielding 50% nitrilotriacetic acid derivative **75** (NTA) as a white solid (Scheme 3.20). Subsequently, the product **75** was employed for the Cu NPs synthesis using the modified procedure described by Kind and co-workers.^[199] $\text{CuCl}_2 \cdot 2\text{H}_2\text{O}$, dissolved in diethylene glycol, was reduced with NaBH_4 in the presence of **75** at 100 °C under inert atmosphere. Different ratios of copper salt, NaBH_4 and **75** were used to prepare batches of NTA coated Cu NPs (Figure 3.24a). After the addition of reducing agent, the color of the reaction solution turned from blue to black, indicating the formation of NPs, which were washed with an isopropanol/ethanol mixture (1:1, v/v) by centrifugation and resuspended in DMSO.

a)

$\text{CuCl}_2 \cdot 2\text{H}_2\text{O}$	NTA Linker 75	NaBH_4	Stability
1.00 eq.	1.00 eq.	4.00 eq.	-
1.00 eq.	0.100 eq.	8.00 eq.	2 h
1.00 eq.	0.200 eq.	8.00 eq.	7 days
1.00 eq.	0.680 eq.	8.00 eq.	-

b)

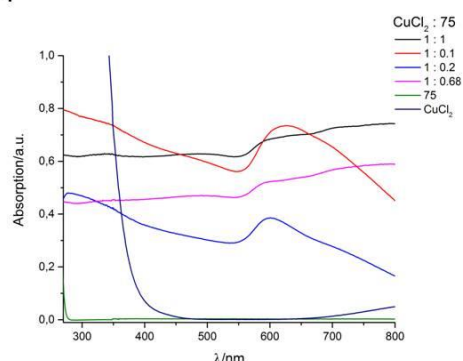
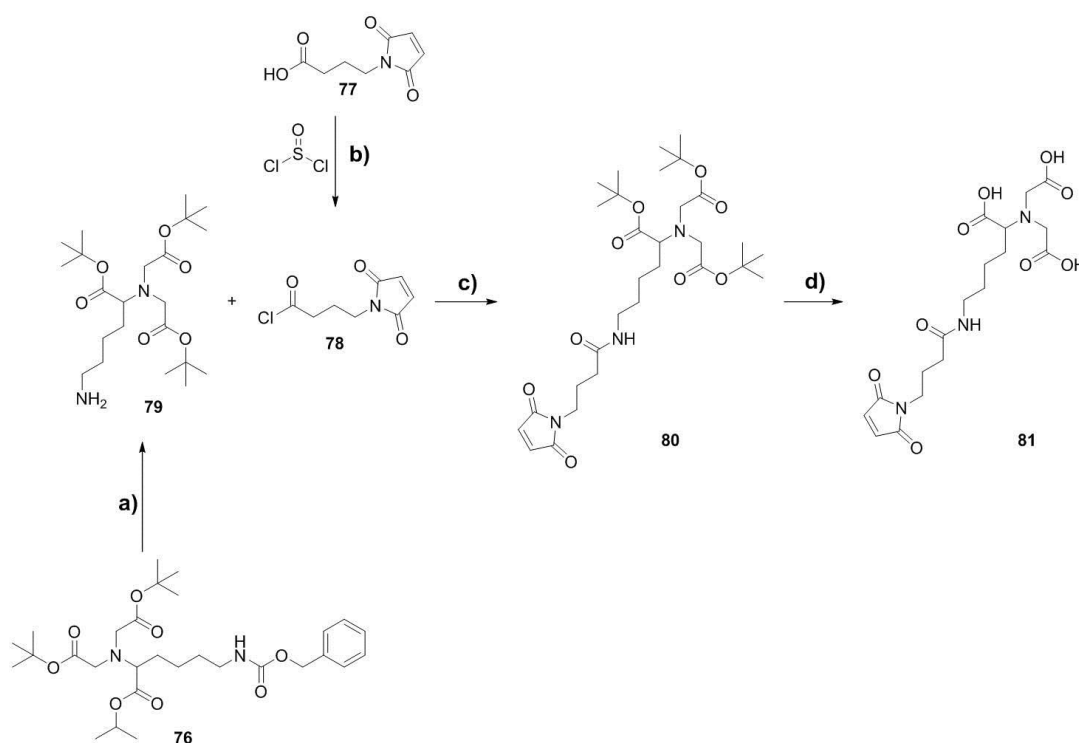


Figure 3.24: Tested reactant ratios a) for the synthesis of Cu-NTA nanoparticles and b) UV-Vis characterization of the obtained Cu-NTA nanoparticles.

Since Cu⁰ nanoparticles exhibit a characteristic localized surface plasmon resonance in the visible spectral range,^[204] the presence of Cu NPs can be confirmed by UV-Vis spectroscopy. Therefore, the UV-Vis spectra of copper suspensions in DMSO were recorded (Figure 3.24b) and the obtained spectra for the reactions with 0.100 eq. and 0.200 eq. NTA linker **75** showed absorption bands with $\lambda_{\text{max}} = 628$ nm and 607 nm, confirming the presence of Cu NPs.^[199, 204] NPs prepared using 0.200 eq. of NTA **75** showed higher stability than those prepared with 0.100 eq., which precipitated on the bottom of the vial after 2 hours.

In order to employ the light induced cycloaddition for DNA modification of Cu NPs, they need be derivatized with dienophile groups. To afford that, NTA derivative containing maleimide group was prepared. In the first step amino group of the NTA derivative **76**, synthesized by Dr. Ishtiaq Ahmed, was deprotected by palladium catalyzed hydrogenolysis.^[203] Then 4-maleimidobutyric acid **77**, was derivatized to acid chloride by refluxing with thionyl chloride.^[205] Obtained substances **78** and **79** were coupled by amidation reaction^[205] and finally the desired maleimide functionalized nitrilotriacetic acid **81** (NTA-Mal) was obtained after the deprotection of carboxylic groups by treatment with trifluoroacetic acid (Scheme 3.21 a - d).^[206]



Scheme 3.21: Synthesis of NTA-Mal **81**; a) Pd/C, H₂, MeOH, 5 h, RT, 95%; b) benzene, 70 °C, 2 h, 99%; c) triethylamine, CH₂Cl₂, inert atmosphere, 0 °C - RT, 16 h, 84%; d) TFA, CH₂Cl₂, 0 °C, 2 h at RT, 98%.

The obtained NTA-Mal **81** (98% in the last step) was subsequently employed for synthesis of Cu NPs. To prepare maleimide functionalized Cu NPs, 1.00 eq. $\text{CuCl}_2 \cdot 2\text{H}_2\text{O}$ in diethylene glycol was reduced with NaBH_4 (8.00 eq.) in the presence of 0.200 eq. NTA-Mal **81** at 100 °C. The color change from blue to black confirmed the formation of Cu NPs, which were subsequently characterized by UV-Vis spectroscopy (Figure 3.25).

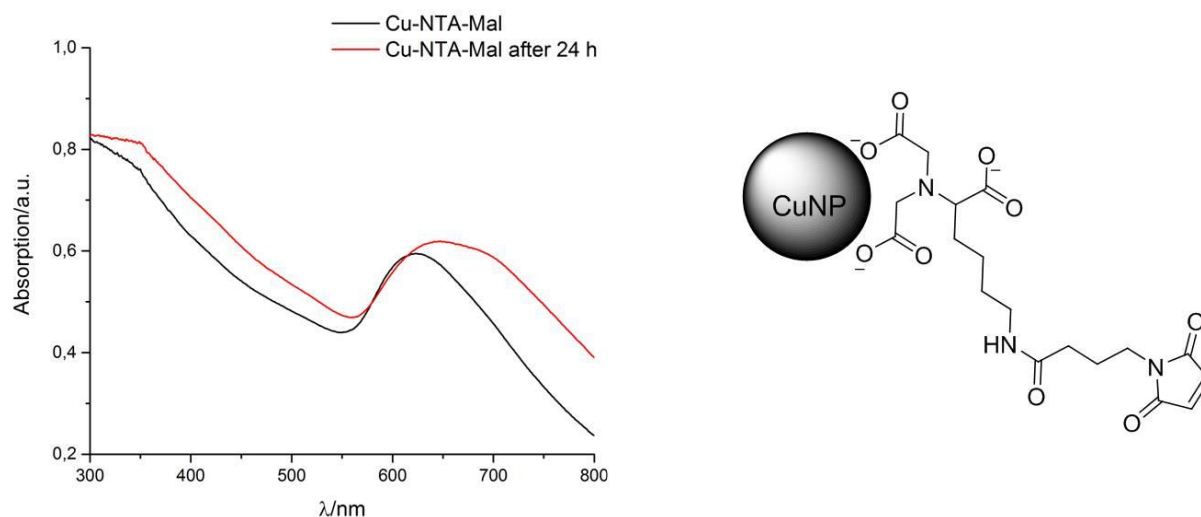


Figure 3.25: UV-Vis characterization of Cu-NTA-Mal immediately after the synthesis (black curve) and after 24 h of storage (red curve).

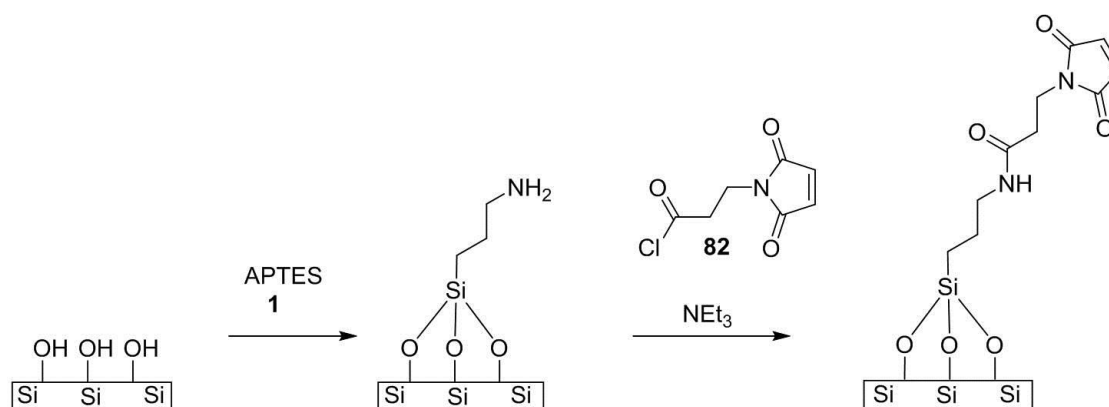
As seen in Figure 3.25, the UV-Vis spectra showed plasmon band at 623 nm characteristic for Cu NPs. Upon storage the band broadens and undergoes the red shift indicating the formation of Cu_2O layer on the NP surface.^[204] Due to the time constraints and experimental study of DNA surface structuring, further attempts to stabilize the NPs and study the photoreactions were not undertaken.

In conclusion, maleimide coated Cu NPs were prepared using both dopamine maleimide and nitrilotriacetic acid (NTA) maleimide anchoring strategies. Although initial results on photoreaction with PE2-DNA2 **54** were promising in case of dopamine Cu NPs, control reactions indicated that there is a strong, but non-specific binding of DNA to the NP surface, due to the electrostatic interactions between positively charged Cu NPs and negatively charged DNA backbone. To avoid the non-specific binding and afford stable maleimide coated Cu NPs, novel linker, based on NTA moiety, was employed to prepare Cu NPs, however they were not stable enough to perform further experiments. Additional studies were not conducted, due to the time constraints but, research student starting in Fruk group in 2016 will continue and build upon this initial, promising work and optimize the system for future applications.

Final section discusses one of the main focuses of this thesis, namely use of light-induced reactions for surface structuring with DNA.

3.3.3 Light-Induced Reactions for Spatially Controlled Immobilization of DNA

DNA has found numerous applications as a structural and functional element in design of biological assays,^[207] biosensors,^[208] nanomotors and optoelectronic devices.^[4a, 4b, 209] Different attachment strategies have been developed in order to obtain DNA functionalized surfaces, with different types of covalent binding, being most widely used. In general, such binding can be achieved by use of oligonucleotides, modified with a terminal functional group, which can selectively bind to the surface of interest.^[210] Using different structuring techniques such as dip-pen nanolithography,^[139] photolithography^[138] or *in situ* DNA chemical synthesis,^[138] single or many DNA sequences can be immobilized to design functional surfaces.^[113, 211] Among the developed structuring techniques, photolithography is nowadays considered as a routine tool in research laboratories,^[212] due to the relative ease of control over the structural features and positions of the molecules by use of the shadow mask.^[213] This is particularly important for design of biosensors and there is an ongoing search for covalent strategies that would ease the fabrications process.^[119a, 214] Due to advantages such as orthogonality and the ability to selectively pattern surfaces simply by UV irradiation, light-induced Diels-Alder cycloaddition is an excellent candidate for a surface modification strategy.^[126a, 149, 151b, 152] As discussed in previous sections, the reaction proceed under mild reaction conditions and provides quantitative or near-quantitative yields. Although it was mainly used for surface structuring of polymers, it was also shown that it can be employed as an elegant and facile method for the anchoring of biomolecules, such as peptides, onto different surfaces.^[126a, 154] Herewith we also, for the first time, show that this type of photoreaction can be employed for the covalent attachment of photoenol modified oligonucleotide PE2-DNA2 **54** onto a maleimide functionalized silicon surface. For this purpose silicon wafers were first functionalized with a maleimide moiety in a two step procedure employing (3-aminopropyl)triethoxysilane (APTES) **1** and 4-maleimidopropanoyl chloride **82** (Scheme 3.22).^[215]



Scheme 3.22: Maleimide functionalization of silicon wafer using a two step approach employing (3-aminopropyl)triethoxysilane (APTES) **1** and 4-maleimidopropanoyl chloride **82**.

To enable a spatial control, a shadow mask with a wave patterns, as shown in Figure 3.26, was employed.

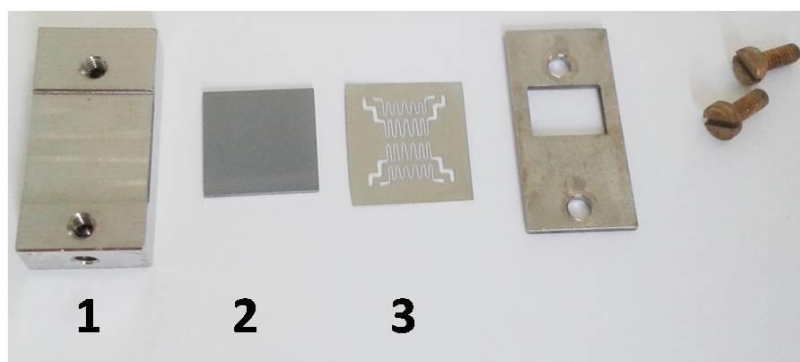


Figure 3.26: Photograph of the sample holder (1), silicon wafer (2) and shadow mask with a wave pattern (3), employed for the spatially controlled immobilization of PE2-DNA2 **54**.

Maleimide functionalized silicon wafer was covered with a mask, mounted in a sample holder, placed into the 1.75 μM PE2-DNA2 **54** solution (PBS/acetonitrile, 1:1, v/v), deoxygenated by purging with argon for 15 min and subsequently irradiated in a photoreactor.

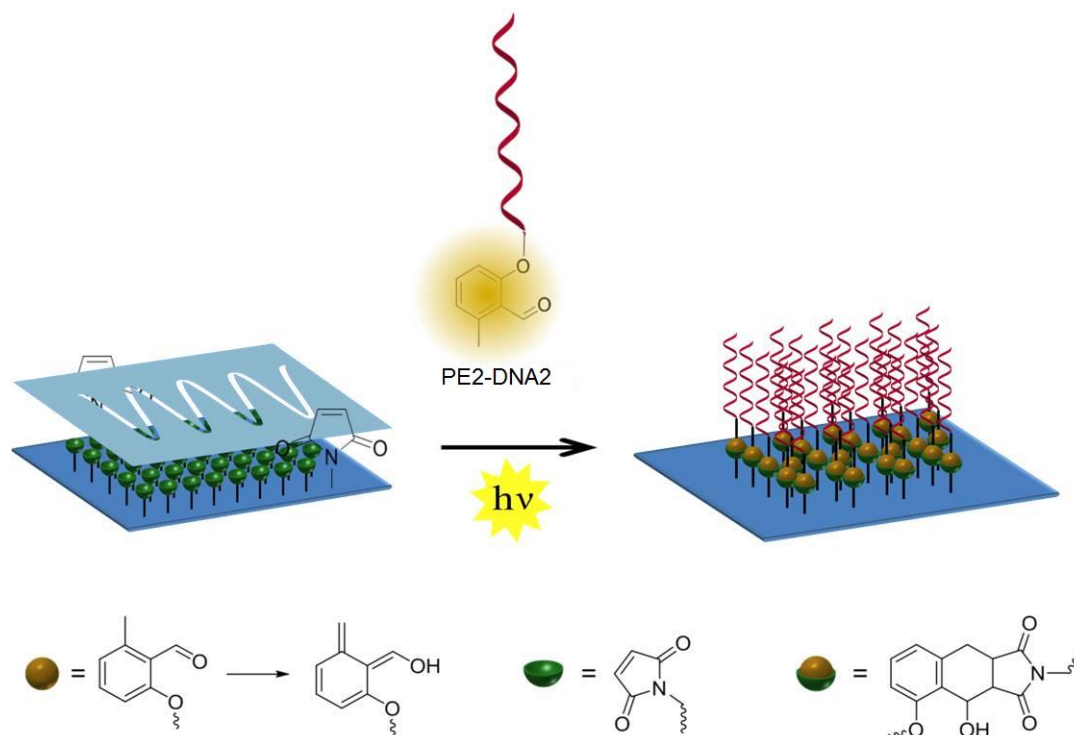


Figure 3.27: Schematic illustration of the spatially controlled light-induced immobilization of PE2-DNA2 **54** on maleimide functionalized silicon wafer.

Successful light-induced immobilization of PE2-DNA2 **54** was confirmed by Time-of-Flight Secondary Ion Mass Spectrometry (ToF-SIMS). Figure 3.28a depicts the ToF-SIMS image resulting from the sum of characteristic species assigned to nucleic acid ($m/z = 96.95$ (H_2PO_4^-), $m/z = 150.01$ (G^- , guanine), $m/z = 125.02$ (T^- , thymine), $m/z = 134.03$ (A^- , adenine) and $m/z = 110.01$ (C^- , cytosine)). The mass fragments corresponding to the DNA could only be found in the irradiated area thus confirming the site-specific immobilization of PE2-DNA2 **54**. In order to verify that DNA was not attached by non-specific interactions, control reaction was performed by irradiation of non-modified DNA2 at the same reaction conditions. The DNA characteristic mass fragments could not be found by ToF-SIMS analysis indicating that DNA was not attached to the surface (Figure 3.28b).

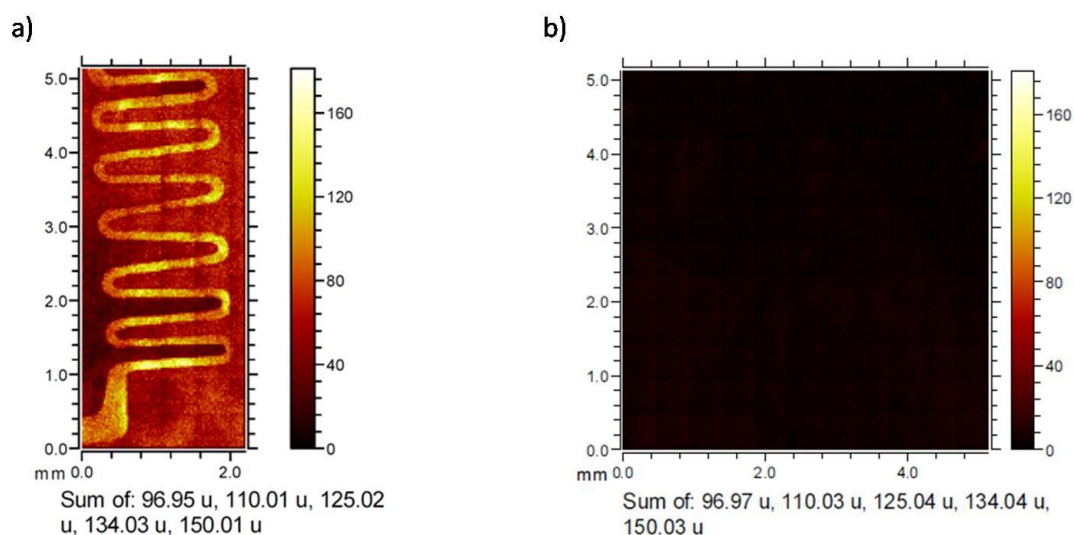


Figure 3.28: ToF-SIMS imaging of photo-patterned PE2-DNA2 **54** a) derived from the sum of the signals detected at 96.95 (H_2PO_4^-), 150.01 (G^-), 125.02 (T^-), 134.03 (A^-) and 110.01 (C^-) and ToF-SIMS imaging of photo-patterned non-modified DNA2 b) derived from the sum of the signals detected at 96.97 (H_2PO_4^-), 150.03 (G^-), 125.04 (T^-), 134.04 (A^-) and 110.03 (C^-) assigned to fragments of the corresponding oligonucleotides. Adapted with permission from [216].^[216]

To explore if the inherent function of the surface immobilized oligonucleotide was preserved, the PE2-DNA2 **54** containing surface was incubated with a complementary oligonucleotide cDNA2 (Figure 3.29a), labeled with a commercially available fluorophore Cy[®]3 ($\lambda_{\text{ex}} = 550 \text{ nm}$, $\lambda_{\text{em}} = 570 \text{ nm}$). In addition, a control reaction was performed by incubation of PE2-DNA2 **54** modified silicon wafer with a non-complementary Cy[®]3 labeled oligonucleotide Cy[®]3-DNA4 and both samples were studied using fluorescence microscopy.

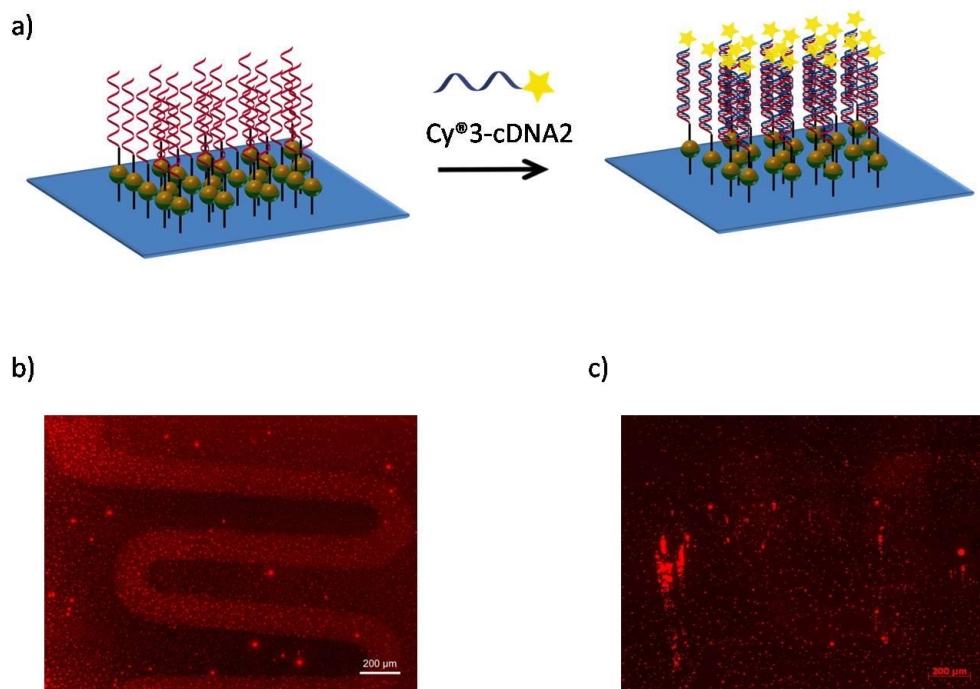


Figure 3.29: a) Schematic illustration of the hybridization of the PE2-DNA2 **54** modified silicon surface with a Cy³ labeled complementary oligonucleotide Cy³-cDNA2; b) fluorescence image of hybridized Cy³-cDNA2; c) fluorescence image of the control hybridization with a non-complementary Cy³ labeled oligonucleotide Cy³-cDNA4. Adapted with permission from [216].

As shown in Figure 3.29b the surface incubated with a complementary strand indicates a clear fluorescence pattern in the areas containing immobilized PE2-DNA2 **54**, as opposed to the lack of the pattern observed in the control sample (Figure 3.29c). Due to the overnight hybridization in high concentration of Cy³-cDNA2 and Cy³-DNA4 solutions (50.0 μM), DNA aggregates, seen as a small circular fluorescent deposits, were detected on both (reaction and control) surfaces. Further optimization of the hybridization conditions such as lower concentration of a complementary oligonucleotide or shorter hybridization times and additional washing steps as well as other hybridization buffer should be employed in future experiment in order to avoid the DNA aggregates formation.

However, successful spatially controlled immobilization of PE2-DNA2 **54** on maleimide functionalized silicon wafers, confirmed by ToF-SIMS analysis, was demonstrated. The preservation of inherent functions of immobilized oligonucleotides was confirmed by selective hybridization with a complementary strand. This allows for further applications of such surfaces for the immobilization of different species such as nanoparticles or proteins by DNA directed immobilization.

As proof-of-concept study was successful, light-induced immobilization strategy has further been employed for the more precisely patterning technique, which does not involve the use of mask but involves direct patterning by Direct Laser Writing (DLW).

3.3.4 Photo-Encoding of Maleimide Surfaces with DNA by Direct Laser Writing

Some bioanalytical applications, such as studies of the single cells or protein-protein interactions, require precise positioning of these species and for DNA directed immobilization to be used for these applications, DNA anchoring arrays are required features size smaller than 10 μm . As mentioned in previous section, various DNA patterning techniques including dip-pen nanolithography,^[139] nanografting,^[217] nano-pipetting^[218] or microcontact printing^[141] have been developed in last decades for the fabrication of precise DNA structures smaller than 1 μm , but they all have their advantages and disadvantages depending on a particular application. Direct Laser Writing (DLW) by multiphoton polymerization has emerged as a powerful printing technology, which allows fabrication of 3D structures with sub-100 nm resolution.^[142c, 219] DLW is based on multi-photon absorption by photopolymers.^[142] The beam of a femtosecond titanium sapphire oscillator is tightly focused inside the volume of transparent photopolymer solution, causing it to polymerize at specific positions by multiphoton absorption. By moving the laser beam or the substrate, depending on the desired pattern design, one can fabricate large variety of different patterns. The home-built direct laser writing setup, employed in this study (Figure 3.30), is based on a tunable titanium sapphire oscillator, delivering 150 fs pulses at a center wavelength of 700 nm. The beam intensity is controlled by an acousto-optical modulator (AOM) and is focused through an oil immersion objective lens with an numerical aperture of 1.4. The sample is held by a 3D piezo stage, that allows for its relative translation with respect to the laser beam focus. An additional CCD camera is used for monitoring the writing process and sample alignment.

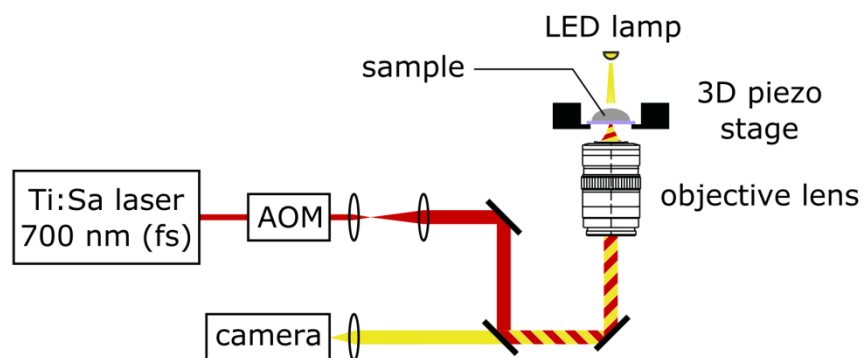


Figure 3.30: The home-built DLW setup for multiphoton microfabrication.

The used photoresist consists of at least two components: a monomer or a mixture of monomers, which polymerize to provide the final polymer, and a photoinitiator, which absorbs the laser light and induces the polymerization. There are two types of photoinitiators which are employed for DLW: the cationic photoinitiators (used for the polymerization of epoxides or vinyl ethers)^[220] and most commonly used radical photoinitiators, such as benzophenone and its derivatives, employed for the polymerization of acrylates and vinyl ethers.^[221] The photoresists can be divided in positive-tone photoresist^[222] (the structures are fabricated by focusing a laser beam into a solid resist, thereby dissolving the exposed regions) and negative-tone photoresist (the polymer structure is solidified from a solution in an exposed volume).^[223] The mostly employed negative photoresists are acrylate materials,^[142a, 224] the epoxy-based photoresist SU-8,^[143] hybrid materials^[225] and hydrogels.^[226] Furthermore, biological material including bovine serum albumin (BSA), fibrogen, fibronectin and collagen have been employed for the multiphoton polymerization.^[227] For example, Sun and colleagues used BSA as a building block for the fabrication of a novel soft diffractive optic, so called microscale kinoform phase-type lens, which might find applications in preparation of flexible and stretchable photonics and optics or bioimplantable devices.^[228] In addition, Melissinaki and colleagues employed methacrylate modified polylactide to fabricate high-resolution 3D structure and grown neuroblastoma cells, which preserved their viability and proliferation, indicating a good biocompatibility of the written structure, opening new routes to the use of such structures for preparation of neuronal implants.^[147] Recently, Richter and colleagues employed Diels-Alder photopolymerization and DLW for the immobilization of biotin or benzylguanine containing molecules, which were then used for the binding of streptavidin or SNAP-GFP in a high-precisely manner.^[153a] The multiphoton-induced cycloaddition reaction was also employed for the fabrication of woodpile photonic crystals,^[229] immobilization of

functionalized gold nanoparticles,^[149] for the coating of preformed 3D polymeric microstructures,^[230] for the wavelength selective polymer network formation of end-functional star polymers^[148a] and others.^[231] However, DLW by multiphoton-induced Diels-Alder cycloaddition for DNA structuring is for the first time demonstrated within this thesis.

3.3.4.1 DNA Array Prepared by DLW Using Single DNA Sequence

For the immobilization of oligonucleotides onto maleimide functionalized glass surface *via* Direct Laser Writing (DLW), photoenol modified PE2-DNA2 **56**, was employed. As described in Section 3.2.2, the kinetic studies of this light-induced cycloaddition showed that the reactions is fast, proceeds in high yields and can be performed in water/DMSO solution (3/2. v/v). This is an important fact, as solvents employed in DLW should have low volatility to avoid the concentration changes and reactant precipitation (or salt precipitation, if the buffer needs to be used) during the sample exposure, and water/DMSO mixture represents an appropriate solvent mixture, due to the low vapor pressure of both solvents.^[232] The home-built DLW setup² we have used, employs a laser tuned to 700 nm center wavelength for targeted two-photon excitation. An absorption maximum for PE2 moiety is at $\lambda_{\text{max}} = 317$ nm. Previously described photoreactions were successfully performed using UV irradiation from compact low-pressure fluorescent lamp with $\lambda_{\text{max}} = 320 \text{ nm} \pm 30 \text{ nm}$ and therefore, selected laser wavelength ensures the efficient multiphoton absorption, required for the photoreaction.

To fabricate the DNA microstructures by DLW,³ a droplet of 10.0 μM **56**, dissolved in a mixture of 1.00 mM NaCl_{aq}/DMSO (3:2, v/v), was placed on a glass surface (Figure 3.31a), previously cleaned, activated and functionalized with 4-maleimidobutyryl chloride **78**. For the initial experiments, simple square pattern consisting of ten squares (50 \times 50 μm) was written by exposing PE2-DNA2 **56** solution to the excitation laser. The squares were written at different laser powers (20, 18, 16, 14, 12, 10, 8, 6, 4 and 2 mW) with four passes per square and a writing speed of 100 $\mu\text{m s}^{-1}$.

²The home-built DLW setup was assembled by Dr. Joachim Fischer, Institute of Nanotechnology, Karlsruhe Institute of Technology (KIT).

³DLW procedure was performed by Patrick Müller, Institute of Applied Physics, and Dr. Alexander Quick, Institute for Technical Chemistry and Polymer Chemistry, Karlsruhe Institute of Technology (KIT).

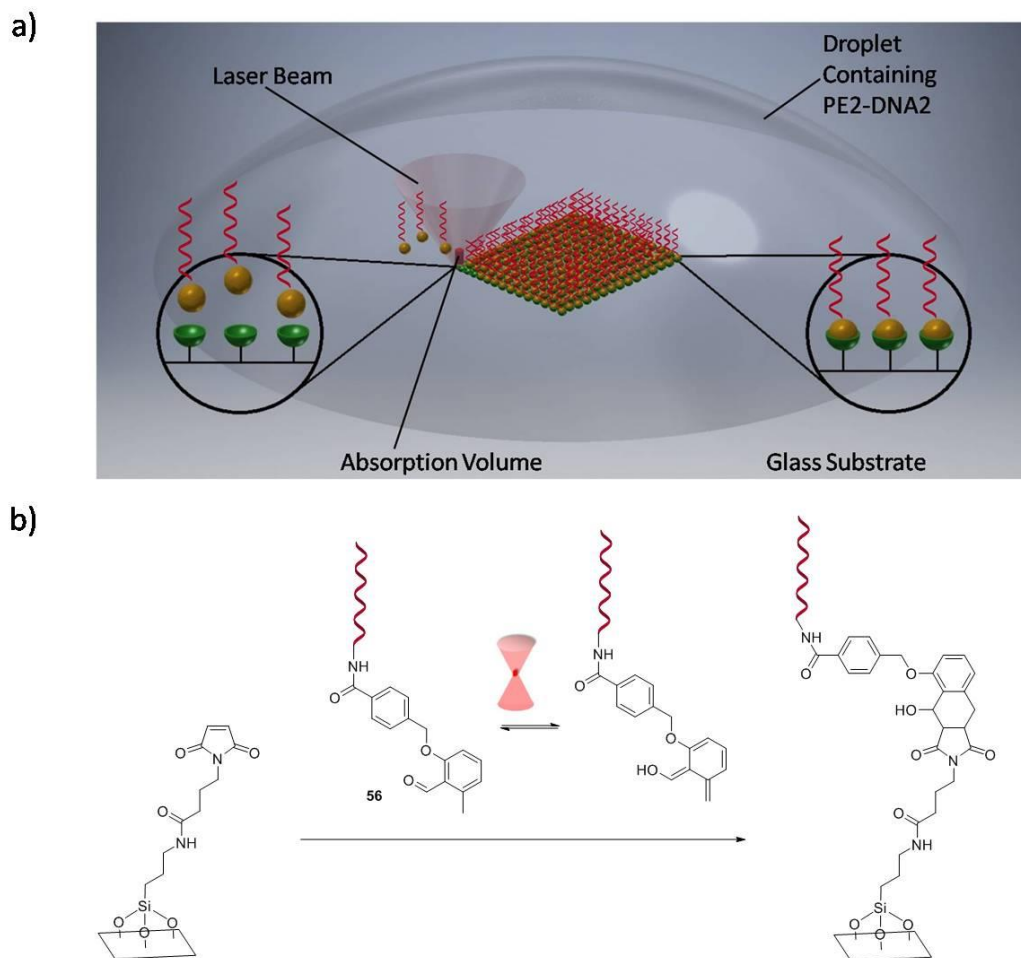


Figure 3.31: a) Principle of the light-induced PE2 DNA2 **56** immobilization using direct laser writing (DLW); b) Photoenolization of **56**, induced by laser light absorption, and subsequent [4+2] cycloaddition with maleimide moiety bound to the surface.

Subsequently, PE2- DNA2 **56** functionalized surfaces were washed in order to remove the non-reacted starting material **56** and analyzed by ToF-SIMS. Figure 3.32a depicts the resulted image of measured PO_2^- signal, which represents a characteristic mass fragment of DNA.^[233] Ten squares with high PO_2^- signal intensity corresponding to the written pattern were observed. However, despite the multi-step washing procedure, a relatively high background PO_2^- signal has been detected, probably stemming from non-specific attachment of **56** due to the electrostatic interactions between positively charged amino groups on the surface and negatively charged DNA backbone. To avoid this, the writing and washing conditions were optimized in the follow up experiments. In order to assess the hybridization ability of the immobilized oligonucleotides, the modified surfaces were incubated in a $3.00 \mu\text{M}$ Cy[®]3-cDNA2 solution in TE-Mg buffer for 16 hours. The surfaces were washed with ultrapure

water (MQ water), TETBS buffer and again in MQ water, rinsed with fresh MQ water and dried under a stream of nitrogen.

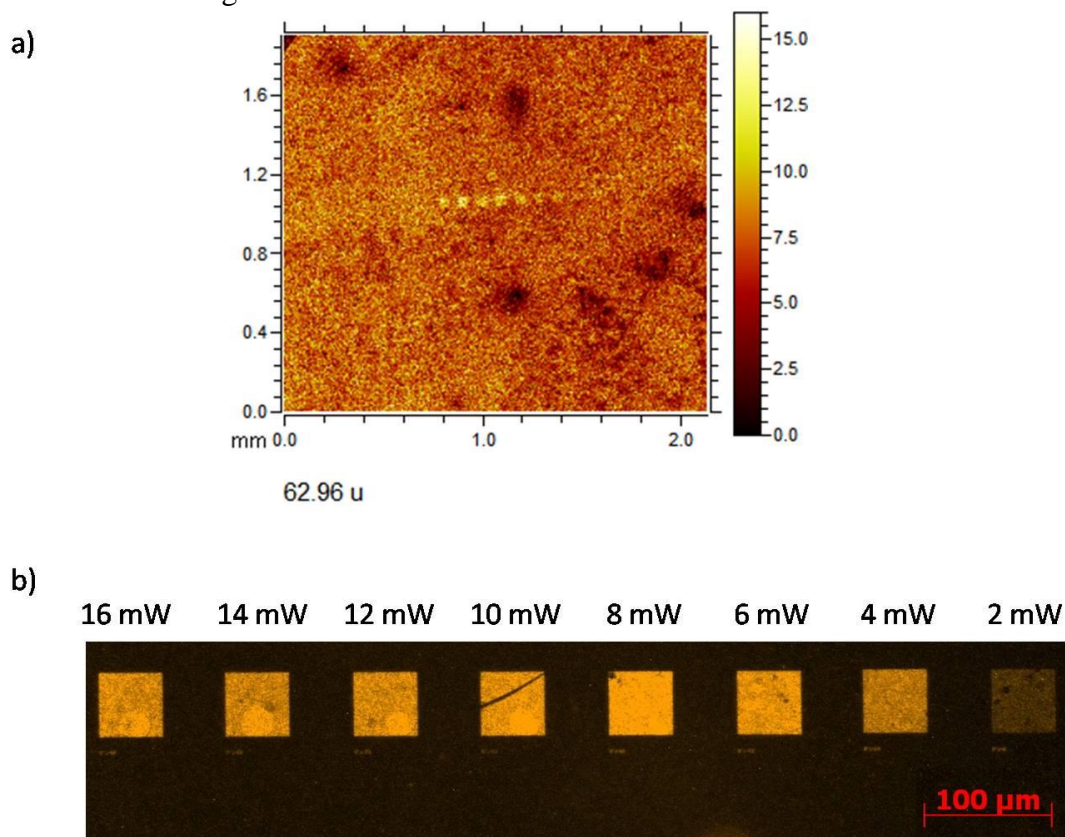


Figure 3.32: a) ToF-SIMS image of PO_2^- ion of PE2-DNA2 **56** immobilized on maleimide functionalized glass surface *via* DLW; b) fluorescence image of hybridized Cy[®]3-cDNA2 squares, written by employing the laser power of 2 - 16 mW.

The fluorescence detection of hybridized oligonucleotides was performed by fluorescence microscopy and as it can be seen from Figure 3.32b, the fluorescence image of eight clearly distinguishable and regular squares can be observed, confirming the high hybridization rate of complementary fluorescent DNA to immobilized oligonucleotides. It should be noted that the fluorescence intensity increases with the increase in the laser power. This is a consequence of more PE2 moieties being activated at higher power, leading to higher yield of reaction with the surface maleimide groups. However, at the laser power above 8 mW, a decrease of fluorescence intensity was observed indicating the possible DNA damage and lower density of immobilized DNA. In order to optimize the DLW procedure, different conditions were tested and are summarized in the following paragraphs.

3.3.4.2 Optimization of the DLW Procedure: Dose and Resolution Tests

In order to establish the best writing conditions, dose tests were performed. For this purpose, a group of 2D lines was written using a 10.0 μM PE2-DNA2 **56**, dissolved in 0.5 \times SSC buffer (pH 7.0)/DMSO (3:2, v/v) mixture and scanning speed of 100 $\mu\text{m s}^{-1}$. Three fields (100 \times 100 μm) of lines were constructed by 1-fold, 2-fold and 4-fold scanning repetition. Throughout the line pattern, the laser power was linearly increased from 0 to 20 mW from the bottommost to the topmost line. From the left line to the right line of each field the value of the vertical axis (z position) was increased resulting in the focal point position being inside the glass substrate for the leftmost line and above the surface inside the DNA solution for the rightmost line. Thus incorrect detection of the glass interface can be compensated. For the visualization of the written DNA pattern the surface was washed (10 min in 2 \times SSC + 0.2% SDS (2 \times), 10 min in 2 \times SSC, 15 min in 0.1 \times SSC + 0.1% SDS and 10 min in MQ water) and subsequently incubated in 200 nM Cy[®]3-cDNA2 dissolved in TETBS/TE-Mg (1:1, v/v) buffer mixture at ambient temperature for 16 h. The excess of complementary oligonucleotide was removed by washing with MQ water, TETBS and again with MQ water.

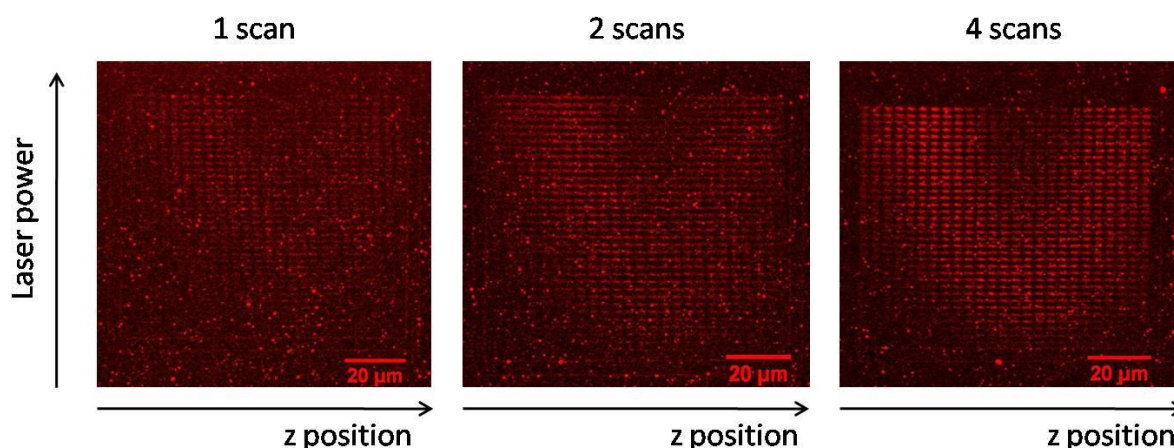


Figure 3.33: Fluorescence images of hybridized Cy[®]3-cDNA2 of 2D line fields constructed by 1-fold, 2-fold and 4-fold scanning repetition; z position change from left to the right, laser power increasing linearly from bottom to top from 0 to 20 mW.

Subsequently, the surface was dried under a stream of nitrogen and analyzed by fluorescence microscopy (Figure 3.33).⁴ As expected, no lines could be observed for the focal point position far from the interface and for low laser powers and the most intense lines were observed for the 4-fold scanned field (right image in Figure 3.33). Unfortunately, the employed hybridization conditions resulted in DNA aggregates formation. To find the most suitable hybridization conditions, hybridization at different concentrations of Cy[®]3-cDNA2 and

⁴Fluorescence measurements were performed by Patrick Müller, Institute of Applied Physics, Karlsruhe Institute of Technology (KIT).

incubation times in combination with various washing and surface blocking procedures were performed (not shown). Finally, the best results could be obtained using the conditions below:

Concentration of 56 in

0.5×SSC(pH 7.0)/DMSO (3:2, v/v): 10 μM

Writing speed: 100 $\mu\text{m s}^{-1}$

Scan number: 4-fold

Laser power: 6 mW

Washing steps after DLW: 10 min in 2×SSC + 0.2% SDS (2×)

10 min in 2×SSC

15 min in 0.1×SSC + 0.1% SDS

10 min in MQ water

Blocking before hybridization: 45 in (5×SSC, 0.1% SDS, 1% BSA) at 42°C, than rinsing with MQ water

Hybridization: 200 nM Cy[®]3-cDNA2 or 200 nM Cy[®]5-cDNA3 in TETBS buffer, 1.5 h at RT

Washing steps after hybridization: 5 min in 2×SSC + 0.2% SDS (2×)

10 min in 0.1×SSC + 0.1% SDS

5 min in 2×SSC

5 min in MQ water

Employing the optimized reaction conditions resolution tests were performed in order to determine the resolution limit for the given DLW system. In such an experiment, line arrays were fabricated with varying line distance, ranging from 1.00 μm to 0.400 μm (from bottom to the top). Additionally, the laser power was varied from 0.40 mW to 24 mW (from left to the right). Around the line array a frame and text labels were written by 1-fold scan using a writing speed of 100 $\mu\text{m s}^{-1}$. After the laser writing was performed, the sample was treated using optimized blocking, hybridization and washing steps and analyzed by fluorescence microscopy (Figure 3.34).

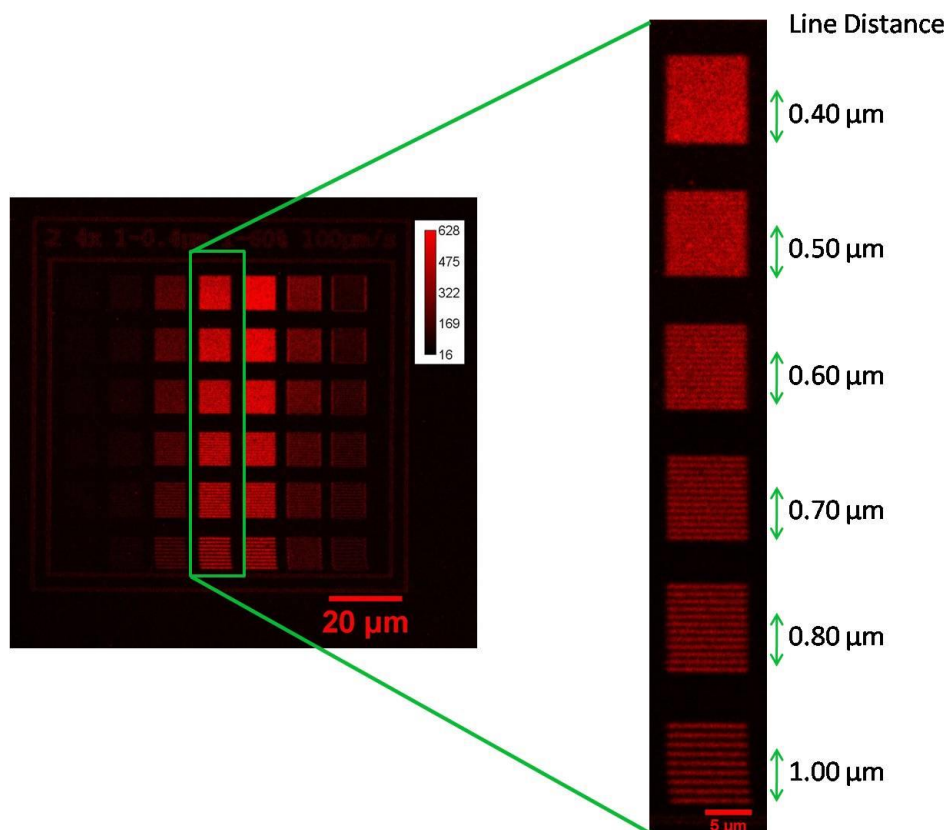


Figure 3.34: Fluorescence images of Cy³-cDNA2 hybridised to PE2-DNA2 immobilized onto the 2D line array written by DLW using 4-fold scanning repetition and the speed of $100 \mu\text{m s}^{-1}$. Laser power was increased from left to the right: 0.4 mW, 0.8 mW, 2 mW, 4 mW, 8 mW, 16 mW and 24 mW. Zoomed section is the column, written using 4mW laser power and different distances between the line segments (image on the right).

As it can be seen from Figure 3.34, strongly fluorescent images are obtained for regions written using 4 and 8 mW laser power, and no fluorescent signals are detected in the areas without immobilized DNA, demonstrating that precise and well defined patterns can be prepared using our strategy. Weaker fluorescence signal are observed at the lower and higher laser power, confirming our hypotheses that this is due to the low activation level of the photoenol containing DNA, or its damage, respectively. When the segment written with 4mW laser power is magnified, clearly defined, $0.478 \pm 0.047 \text{ nm}$ wide lines (this was determined using ImageJ software using the fluorescence intensity profile across the lines) can be observed up to the line distance of $0.60 \mu\text{m}$. The arrays with smaller line distance could not be resolved by the employed confocal optical microscope. Further investigations by *e.g.* Atomic Force Microscopy (AFM) would be conceivable, but were not performed at this point. Rather, a more challenging issue of highly resolved, multi-sequence array fabrication was addressed and it is presented in the following section. .

3.3.4.3 DLW for Multi-DNA Array Preparation

The simplest multi-DNA array was designed using two different DNA sequences. For this purposes additional 22mer oligonucleotide sequence DNA3 was functionalized with PE2 moiety (procedure described in Section 3.1.3) and employed in DLW experiments. The fabrication of two-sequence array was performed in three writing steps. First, a $100 \times 100 \mu\text{m}$ polymer frame (Figure 3.35) was written using a solution of polymerization reagents tetraphotoenol **83** and maleimide containing methacrylate derivative **84** in γ -butyrolacton/acetophenone mixture, synthesized by Dr. A. S. Quick.^[229]

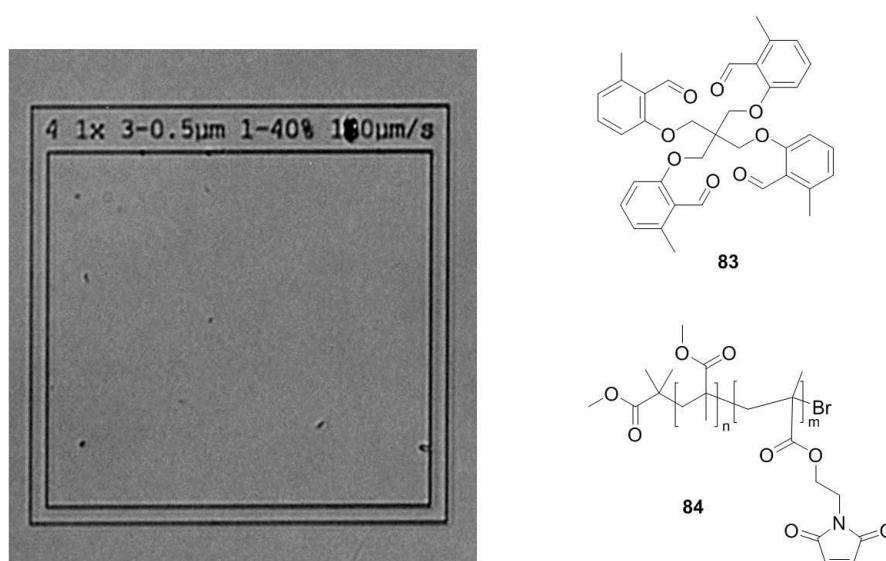


Figure 3.35: Microscopic of $100 \times 100 \mu\text{m}$ image of polymer frame written by DLW utilizing **83** and **84** as polymerization reagents.

Such polymer frame is visible by an employed CCD camera and is used as a reference point for the later spatial control of the writing position. In the next step, first DNA sequence, PE2-DNA2 **56**, is written within the polymer frame using the optimized, but slightly changed, reaction conditions (higher concentration of the PE2-DNA2 **56** solution ($30.0 \mu\text{M}$ instead of $10.0 \mu\text{M}$) and a slower writing speed ($50 \mu\text{m s}^{-1}$ instead of $100 \mu\text{m s}^{-1}$) were employed. A reference point relative to the left lower corner of the polymer frame was fixed as a starting point of the laser writing position and a 2D line array consisting of four columns of three line segments with different line spacing ($8.00 \mu\text{m}$, $6.00 \mu\text{m}$ and $4.00 \mu\text{m}$, from bottom to top) was fabricated (Figure 3.36). Additionally, a 2×2 checkerboard pattern with $10 \times 10 \mu\text{m}$ squares was written on the right hand side of the frame. Following this step, a third writing step was performed to immobilize the second sequence PE2-DNA3 **57**. This was done only after

previously defined writing start point has been localized employing a 3D piezo stage and CCD camera.

The line pattern of the second sequence was programmed in such way to be written between the lines of the first sequence. Finally, multi DNA array was washed, surfaces blocked and immobilized DNA was allowed to hybridize with corresponding complementary DNA sequences, Cy[®]3-cDNA2 and Cy[®]5-cDNA3, labeled with two different flourophores. (Figure 3.36).

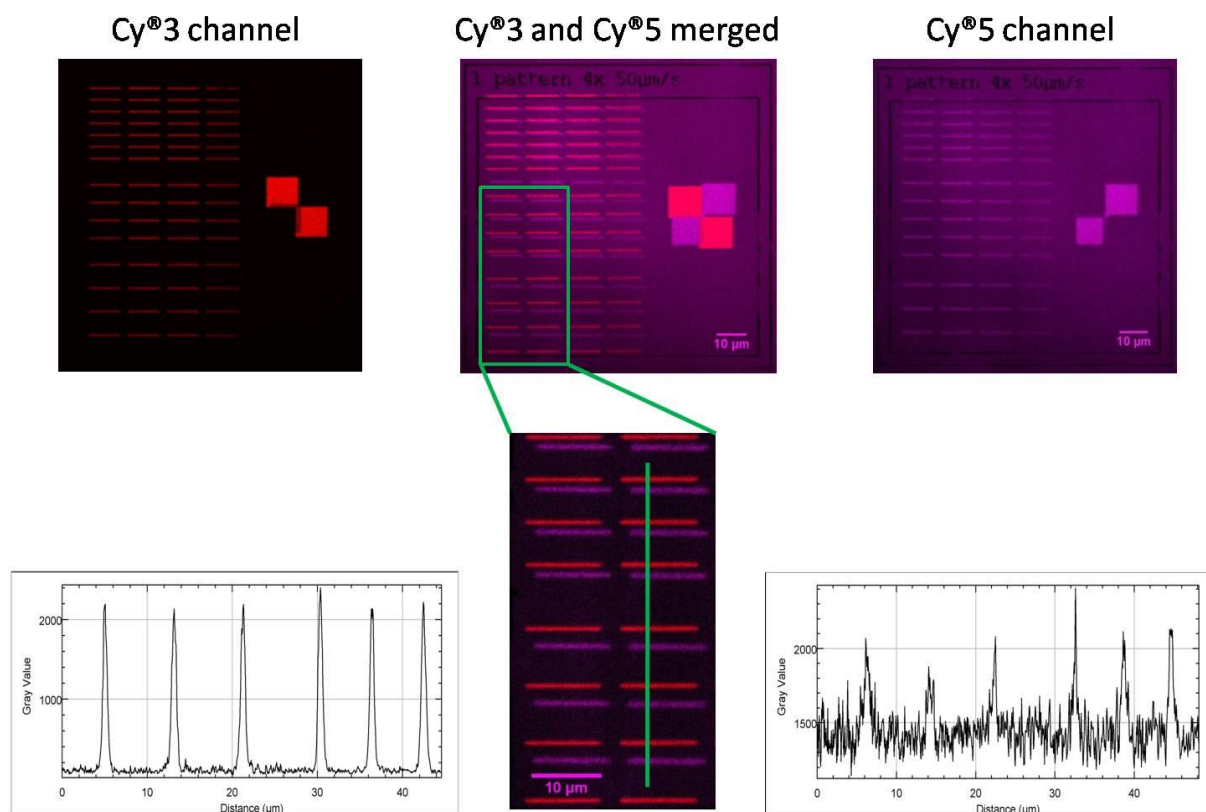


Figure 3.36: Top: fluorescence images of the two DNA sequence patterns for Cy[®]3 (left), Cy[®]5 (right) and merged signals (middle). Bottom: magnification of the four lower line segments of the merged image image and fluorescence intensity profiles along the green line for Cy[®]3 lines (left) and for Cy[®]5 (right) lines to illustrate the regularity of the line pattern. Cy[®]3 ($\lambda_{\text{ex}} = 550 \text{ nm}$, $\lambda_{\text{em}} = 570 \text{ nm}$; Cy[®]5 ($\lambda_{\text{ex}} = 649 \text{ nm}$, $\lambda_{\text{em}} = 666 \text{ nm}$).

Strong, clearly distinguishable fluorescent signals could be detected for different sequences and the quality of the lateral resolution is additionally confirmed by the intensity profile along the patterned structure (Figure 3.36, bottom left and right). It should be noted, that the lines of the second DNA sequences are slightly shifted to the right due to the limitations of employed piezo stage during the writing procedure. However, larger structures such as 3×3 (10×10 µm) or 2×2 (45×45 µm) checkerboard pattern could be reproduced in exact agreement with the programmed design (Figure 3.37).

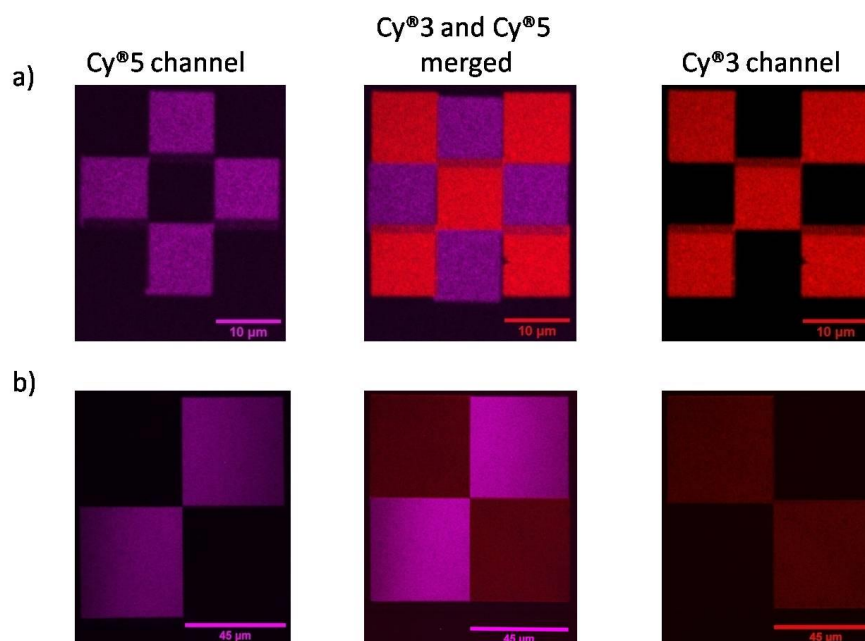


Figure 3.37: Fluorescence images of a) 3×3 (10×10 μm) and b) 2×2 (45×45 μm) checkerboard pattern containing two different sequences hybridized with corresponding Cy[®]5 and Cy[®]3 complementary DNA. Merged patterns are shown in the middle. Laser power : 6 mW, writing speed 50 μm s⁻¹.

In addition, high and well defined fluorescent regions confirm, that fabrication of multiplex DNA using light-induced cycloaddition and DLW is not only possible, but it results in functional surfaces as confirmed with high level of DNA hybridization and well-resolved patterns, which can be readjusted to the needs of a particular application. We were also interested in exploring if other species, in particular protein, could be immobilized onto such patterns through DNA directed immobilization. But prior to this experiments, the hybridization limits of DNA arrays was studied by incubating DNA2 patterns with different amounts of Cy[®]3-cDNA2 solutions (1.00 pM, 100 pM, 1.00 nM and 1.00 μM). This is important as some of the species, which might be used for array preparation through DDI are present in small amounts and this strategy might not be suitable if not enough DNA on the surface is available for hybridization.

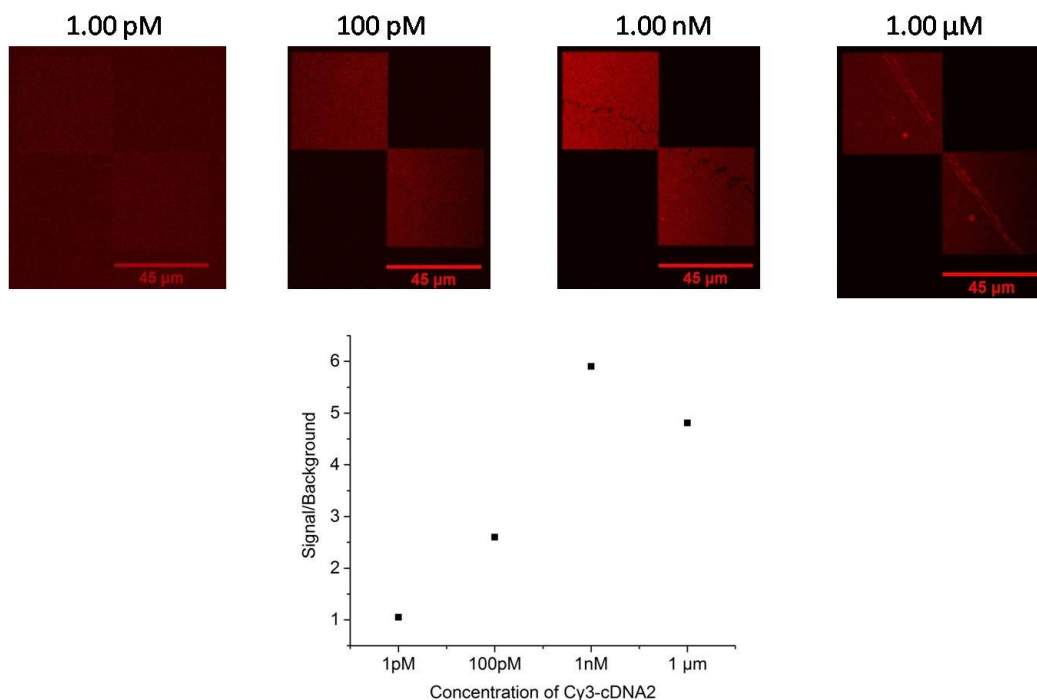


Figure 3.38: Fluorescence images of PE2-DNA2 **56** containing surfaces incubated with Cy[®]3-cDNA2 of different concentrations (1.00 pM, 100 pM, 1.00 nM and 1.00 μM).

Figure 3.38 shows the results of the hybridization study, clearly indicating that the best fluorescence signal intensity can be obtained when 1.00 nM Cy[®]3-cDNA2 is used and higher concentration lead to a decreased intensity due to the crowding effects. It should be noted his results are by no means to be taken as a strict rule, since the hybridization ability will depend on the size and charge of the DNA conjugate (as seen in the next paragraph). However, it can be considered as a concentration guide to determine the concentration range for hybridization onto the DLW array patterns.

In order to test the applicability of two sequence arrays for the DNA directed immobilization of proteins, HRP-cDNA2 conjugate (synthesized using the procedure reported by Kukolka *et al.*^[234]) was hybridized onto the surface of the 2×2 (45×45 μm) checkerboard pattern containing both DNA2 and DNA3 sequences by incubating the pattern in 100 nM HRP-cDNA2 solution in PBS buffer at ambient temperature for 2 h. The hybridization was also attempted using 1.00 nM solution, however as noted earlier, the hybridization ability depends on the properties of DNA conjugate and in case of HRP, the optimum solution concentration was found to be 100 nM. After extensive washing, the hybridized pattern was analyzed by ToF-SIMS, focusing on the detection of the iron content. Namely, HRP contains heme cofactor, which might be expected to give distinct iron signal. However, no iron could be detected, most

probably due to the low concentration of the protein on the surface and the hindrance of the heme by the protein shell.

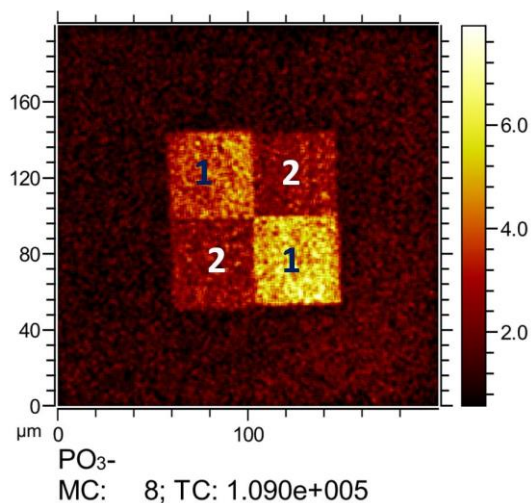


Figure 3.39: ToF-SIMS image of PO₃⁻ ion of 2×2 checkerboard pattern containing PE2-DNA2 (1) and PE2-DNA3 (2) after hybridization with HRP-cDNA2.

However, we have obtained phosphate ion signals (PO₃⁻), which were more intense in the square patterns containing PE2-DNA2. This means that the higher DNA content is present in this region, indicating the presence of complementary sequence containing HPR moiety (Figure 3.39). We have additionally tried to label immobilized HRP with heavy iodine according to the published procedures, but this was not successful in our hands and additional experiments were not performed due to the time constraints. In addition, another protein, widely used streptavidin (STV) was hybridized onto two-pattern array using 100 nM STV-cDNA2^[234] solution. To prove that STV is bound onto array, we employed the strong biotin binding affinity of this protein (association constant ca. $10^{15} \text{ dm}^3 \text{ mol}^{-1}$)^[235] and exposed the STV bound surface to fluorophore labeled biotin (300 nM solution of Atto550-biotin). As a control, PE2-DNA2 array without STV-cDNA2 conjugate was incubated with Atto550-biotin to ensure that there is no unspecific binding on labeled biotin to DNA surface. As it can be seen in Figure 3.40, only the pattern, to which STV is hybridized, showed high fluorescence intensity stemming from the bound biotin, proving that the protein is successfully hybridized and capable of undergoing the binding event with biotin.

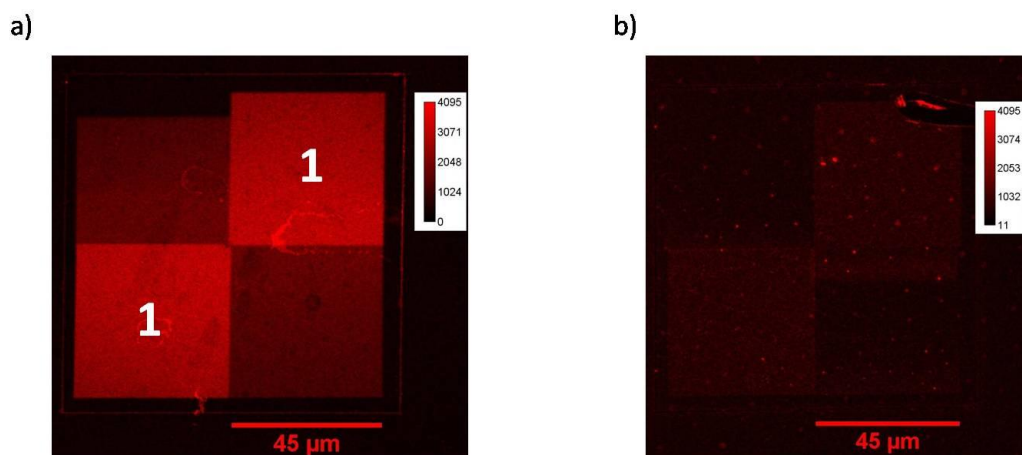


Figure 3.40: Fluorescence images of Atto550-biotin bound to a) two sequence pattern containing immobilized STV-cDNA2 (squares labeled 1) and b) STV free surface. (Atto550: $\lambda_{\text{ex}} = 554$ nm, $\lambda_{\text{em}} = 576$ nm).

Low fluorescence intensity can be observed in control regions containing DNA only (but not in the surrounding empty area) most probably due to the electrostatic interaction of cationic fluorophore Atto550 and anionic oligonucleotide backbone. This issues can be resolved in the future by use of other labeling fluorophores and more intense washing steps.

In conclusion, distinct patterns of photoenol containing oligonucleotides were successful created by use of photoactivation ability of direct laser writing and following reaction with the maleimide modified glass surface. Both line array and checkered pattern arrays were designed using single and multi-DNA sequences. Hybridization studies have shown, that immobilized DNA is fully functional and can be used for subsequent DNA directed immobilization of different species. This was confirmed by successful hybridization of DNA containing small molecules (fluorophores) and proteins (HRP and STV). In addition, a clearly defined and highly resolved (lines within the line pattern were still clearly resolved at 600 nm interline distance) patterns can be programmed and written opening new possibilities for surface structuring for application in biosensing and material design.

4 Summary and Outlook

Within this thesis, DNA was covalently coupled to the protein and different surfaces using novel light-induced strategies based on photoenol and tetrazole chemistry. To enable light-induced cycloaddition, oligonucleotides were first functionalized with photo-activatable groups: 2,5-dimethylbenzophenone (PE1) and 2-methoxy-6-methylbenzaldehyde (PE2) for Diels-Alder cycloaddition and tetrazole (Tz,) for NITEC using phosphoramidite, H-phosphonate and amide coupling methods. Further, the ability of modified oligonucleotides to undergo light-induced reactions was studied in details using model dienophile, Do-TEG-Mal. Reactions with PE1-DNA1 (performed in aqueous solutions due to the DNA stability and solubility requirements) were not successful as the presence of protic solvents favors reketonization of PE1 group.^[122] In contrast, PE2-DNA2 and Tz-DNA2 could successfully be converted to desired cycloadducts in high yields. However, side products were detected when the reaction with Tz-DNA2 was performed, although their amount could be decreased by addition of the larger amount of dienophile (15.0 eq). Detailed ESI-MS and HPLC studies also showed that the light-induced reaction of PE2-DNA2 is faster (completed after 10 min) than of tetrazole-DNA, in which the side products are not eliminated by either the excess of dienophile or prolonged irradiation time.

Taking into account the reaction kinetics and the absence of the side products, PE2-DNA2 was further used for coupling to the protein horseradish peroxidase (HRP). Resulting conjugate retained inherent functions of both the DNA and HRP as confirmed by DNA hybridization and Amplex[®]Red peroxidase activity assay. In addition, to extend the application of the light-triggered reactions to surface biofunctionalization, the modification of copper nanoparticles (Cu NPs), which have excellent electronic and catalytic properties and a huge potential for design of electronic and biosensing devices, with DNA was attempted. For this purpose, two different bi-functional linkers containing maleimide for light-induced cycloaddition, and dopamine and nitrilotriacetic acid (NTA), respectively, were prepared for stabilization of Cu NPs. Although initial coupling results with PE2-DNA2 and dopamine-maleimide coated Cu NPs were promising, control reactions indicated that there is a strong, non-specific binding of DNA to the NP surface. On the other hand, CuNPs containing NTA bound maleimide were not stable enough to perform light triggered coupling. However, further studies should be conducted to afford stable Cu-NTA-Mal NPs, and these should involve the

optimization of the solvent composition and introduction of polyethylene glycol unite to NTA-Mal linker in order to improve the solubility and decrease the steric hindering of surface functional groups.

Finally, the light-induced Diels-Alder cycloaddition was successfully employed for the controlled immobilization of PE2-DNA2 onto maleimide functionalized silicon and glass surfaces. Initial experiments, performed utilizing a shadow mask, resulted in a DNA wave pattern with line thickness of 200 μm after irradiation with 320 nm light. However, much improved resolution and significant increase in the pattern variety was achieved by use of Direct Laser Writing (DLW) technique combined with multiphoton-induced cycloaddition. Fully functional line patterns containing multiple DNA sequences with the resolution of 600 nm were structured and successfully hybridized with fluorophore labeled complementary strands. This indicated that DNA directed immobilization on patterned surface can be performed, which was additionally confirmed by immobilization of DNA-HRP and DNA-streptavidin (STV) protein conjugates. Successful immobilization was confirmed either indirectly through monitoring of the phosphate signal by TOF-SIMS or by use of the fluorescent protein binding substrates. Further experiments, which were not performed due to the time constrains, should focus on the simultaneous immobilization of multiple functional proteins such as cell receptor proteins and design of i.e. ordered cell patterns either for the cell studies or the growth of artificial tissues.

In conclusion, it has been shown for the first time that light-induced Diels-Alder cycloaddition, based on the photoenol chemistry can be used not only for the preparation of DNA-protein conjugates, but also for the precise structuring of DNA on various surfaces. Remarkable resolution and variety of patterns can be achieved by combination of the light-induced reactions and direct laser writing technology, which might open new avenues for use of DNA surfaces in bionanotechnology, in particular design of cell arrays and preparation of bio-inspired materials.

5 Experimental Part

5.1 Materials and Methods

5.1.1 Chemicals

Triethylene glycol ($\geq 99\%$, Sigma-Aldrich), anhydrous *N,N*-dimethylformamide (DMF, $\geq 99.8\%$, Sigma-Aldrich), dichloromethane (DCM, $\geq 99.8\%$, VWR), 1-hydroxybenzotriazole hydrate (HOBt, $\geq 97\%$, Sigma Aldrich), *N,N'*-dicyclohexylcarbodiimide (DCC, 99%, Sigma-Aldrich), *N*-hydroxysuccinimide (NHS, 98%, Sigma-Aldrich), methanol (MeOH, 99.8%, VWR), phosphorous acid (H_3PO_3 , 99%, Sigma-Aldrich), anhydrous pyridine (99.8%, Sigma-Aldrich), trimethylacetyl chloride (99%, Sigma-Aldrich), acetonitrile (MeCN, 99.9%, VWR), anhydrous acetonitrile (MeCN, 99.8%, Sigma-Aldrich), triethylamine (NEt_3 , $\geq 99\%$, Sigma-Aldrich), 4-(*N*-maleimidomethyl)cyclohexane-1-carboxylic acid 3-sulfo-*N*-hydroxysuccinimide ester sodium salt (sulfo-SMCC, powder, Sigma-Aldrich), horseradish peroxidase (HRP, type VI-A, Sigma-Aldrich), oxidizing solution (0.02 M iodine in THF/pyridine/water (7:2:1), Link Technologies), oligonucleotides **DNA1**, **DNA2**, **NH₂-DNA2** and **NH₂-DNA3** on solid support, **cDNA2**, **6-FAM-cDNA2**, **Cy@3-cDNA2**, **Cy@5-cDNA3**, **SH-cDNA2** and **Cy@3-DNA4** as purified lyophilized solid (Sigma-Aldrich, for sequences refer to Table 5.1) were used as received. Protein marker, Precision Plus Protein™ Dual Xtra Standards, was purchased from Bio-Rad. DNA marker, O'Range Ruler 10 bp DNA Ladder, was purchased from ThermoFisher Scientific. Ultrapure water produced with a Milli-Q Advantage A10 system was used in all experiments. Triethyl ammonium bicarbonate buffer (TEAB buffer, 2 M, pH 7.5) was prepared by bubbling of gaseous CO_2 into 2 M aqueous solution of triethylamine until the pH of this solution reaches pH 7.5. Gel filtration NAP5 and NAP10 columns and Vivaspin sample concentrators were purchased from GE Healthcare (Germany).

DNA sequences

Table 5.1: Sequences and extinction coefficients of used oligonucleotides.

Name	Sequence (5'-3') and 5'-modification	ϵ [L* mol^{-1} * cm^{-1}]
DNA1	5'-GGTGAAGAGATC-3'	127600
DNA2	5'-GTGGAAAGTGGCAATCGTGAAG-3'	228100
NH₂-DNA2	5'-[AminoC6T]- GTGGAAAGTGGCAATCGTGAAG-3'	228100
NH₂-DNA3	5'-[AminoC6T]- GGTCCGGTCATAAAGCGATAAG-3'	225100
cDNA2	5'-CTTCACGATTGCCACTTTCCAC-3'	191700
6-FAM-cDNA2	5'-[6FAM]-CTTCACGATTGCCACTTTCCAC-3'	191700
Cy[®]3-cDNA2	5'-[Cyanine3]-CTTCACGATTGCCACTTTCCAC-3'	191700
Cy5[®]-cDNA3	5'-[Cyanine5]-CTTATCGCTTTATGACCGGACC-3'	
Cy[®]3-DNA4	5'-[Cyanine3]CCTGCTTATGTTTCCGATGTGC-3'	193400
SH-cDNA2	5'-[ThiC6]CTTCACGATTGCCACTTTCCAC-3'	191700

Buffers

Table 5.2: Buffers and the corresponding recipes.

Buffer	Composition
5×TBE	450 mM Tris/HCl, 450 mM Borsäure, 10 mM EDTA, pH 8-8.3
1×PBS	16.7 mM KH ₂ PO ₄ , 83.3 mM K ₂ HPO ₄ , 150 mM NaCl, pH 7.3
TETBS	20 mM Tris/HCl, 150 mM NaCl, 5 mM EDTA-Na ₂ ·2H ₂ O, 0.05% Tween-20, pH 7.5
DNA loading buffer(6×)	10 mM Tris, 60 mM EDTA, 0.03% bromophenol blue, 0.03% xylene cyanol, 60% glycerin, pH 7.6

Nanoparticle loading buffer (6×)	10 mM Tris, 60 mM EDTA, 60% glycerin, pH 7.6
SDS loading buffer (4×)	50 mM Tris, 8% SDS, 40% glycin, 20% mercaptoethanol, 5mg/mL bromophenol blue
Stacking gel buffer	0.5 M Tris, pH 6.8
Separating gel buffer	1.5 M Tris, pH 8.8
PAGE running buffer	25 mM Tris, 192 mM glycin
SDS running buffer	25 mM Tris, 250 mM glycin, 0.1% SDS
20×SSC	3 M NaCl, 0.3 M trisodium citrate
Glycin-NaOH buffer	add 50 mM NaOH to 50 mM glycin until pH reach 8.5
Anion exchange buffer A	20 mM Tris/HCl, pH 8.3 or 6.3
Anion exchange buffer B	20 mM Tris/HCl, 1 M NaCl, pH 8.3 or 6.3
HPLC elution buffer	0.1 M NH ₄ OAc

5.1.2 Instruments and Methods

Nuclear magnetic resonance spectroscopy (NMR)

NMR spectroscopy was performed using following instruments:

¹H-NMR (250 MHz), ¹³C-NMR (63 MHz): *Bruker AC 250*

¹H-NMR (300 MHz), ¹³C-NMR (75 MHz): *Bruker AVANCE 300*

¹H-NMR (400 MHz), ³¹P-NMR (100MHz), ¹³C-NMR (100 MHz): *Bruker AVANCE 400*

¹H-NMR (500 MHz), ¹³C-NMR (126 MHz): *Bruker AVANCE DRX 500*

Samples were dissolved in CDCl₃, DMSO-d₆, methanol-d₄ or CD₃CN. The δ-scale is referenced to tetramethylsilane (TMS) or phosphoric acid as the internal standards. The chemical shift δ is expressed in "ppm" and the coupling constant *J* is in "Hz".

Mass Spectrometry (MS)

The mass of the compounds was measured by Fast Atom Bombardment Mass Spectrometry (FAB-MS) or Electron Ionization Mass Spectrometry (EI-MS) using Finnigan MAT95 mass spectrometer. Analyses of oligonucleotides were performed by Matrix-Assisted Laser Desorption Ionization - Time of Flight Mass Spectrometry (MALDI-TOF) using Autoflex III SmartBeam™ (Nd:YAG laser (355 nm) with a repetition rate of 200 Hz)

spectrometer from Bruker Daltonics in the linear negative mode; used matrix: a 9:1 mixture of saturated 3-hydroxypicolinic acid and 0.44 M diammonium hydrogen citrate. Fragments can be identified according to their mass-to-charge ratios (m/z), and the intensity of the signals represents the relative abundance of the ions. The most intense signal is the base peak, which is assigned an abundance of 100%.

EI-MS: abbreviation for the molecular ion $[M]^+$.

FAB-MS: abbreviation for the protonated molecular ion $[M+H]^+$.

MALDI-TOF: abbreviation for the molecular ion $[M]$.

Electrospray Ionization Mass Spectrometry (ESI-MS)⁵

Mass spectra were recorded on a Q Exactive (Orbitrap) mass spectrometer (ThermoFisher Scientific, San Jose, CA, USA) equipped with an HESI II probe. The instrument was calibrated in the m/z range 74 – 1822 using premixed calibration solutions (Thermo Scientific). A constant spray voltage of 2.9 kV and a dimensionless sheath gas of 10 were applied. The capillary temperature and the S-lens RF level were set to 320 °C and 68.0, respectively. The oligonucleotide samples were dissolved with a concentration of 10 μM in a mixture of water/acetonitrile (3:1, v/v) containing 0.5 % acetic acid and infused with a flow of 30 $\mu\text{L}\cdot\text{min}^{-1}$.

Time-of-Flight Secondary Ion Mass Spectrometry (ToF-SIMS)⁶

Time-of-Flight Secondary Ion Mass Spectrometry (ToF-SIMS) was conducted with a TOF.SIMS5 instrument (ION-TOF GmbH, Münster, Germany), equipped with a Bi cluster liquid metal primary ion source and a non-linear time-of-flight analyzer. The Bi source was operated in the bunched mode providing 0.7 ns Bi_3^+ ion pulses at 25 keV energy and a lateral resolution of approximately 4 μm . The short pulse length allowed high mass resolution to analyze the complex mass spectra of the immobilized organic layers. Images larger than the maximum deflection range of the primary ion gun of $500\times 500\ \mu\text{m}^2$ were obtained using the manipulator stage scan mode. Primary ion doses were kept below $10^{11}\ \text{ions}\cdot\text{m}^{-2}$ (static SIMS limit). Spectra were calibrated on the CH^- , CH_2^- , CH_3^- , or on the C^+ , CH^+ , CH_2^+ , and CH_3^+ peaks.

⁵ ESI-MS measurements were conducted by Dr. Michael Kaupp, Institute for Technical and Polymer Chemistry, Karlsruhe Institute of Technology (KIT).

⁶ ToF-SIMS measurements were conducted by Dr. Alexander Welle and Doris Abt, Institute for Technical Chemistry and Polymer Chemistry, Karlsruhe Institute of Technology (KIT).

Fourier Transform Infrared Spectroscopy (FTIR)

Fourier transform infrared spectra (FTIR) were recorded using Bruker "IFS-88" or Bruker ALPHA. For the sample preparation diffusive reflectance infrared Fourier transform (DRIFT) and attenuated total reflection (ATR) techniques were used. The absorption bands of functional groups in IR spectra are expressed in wavenumbers $\tilde{\nu}$ (cm⁻¹).

UV-Vis Spectroscopy

UV-Vis spectra were recorded on a Cary 300 Scan spectrophotometer (Varian Inc., Germany) and on a Cary 100 (Agilent Technologies) in the wavelength region 200–800 nm respectively.

Fluorescence microscopy

Fluorescence microscopy was performed using Axiovert 200M (Carl Zeiss) inverted microscope with Plan-Neofluar objective (magnification/numeric aperture 10x/0.16). For confocal fluorescence microscopy⁷ a commercial laser scanning microscope (Zeiss LSM 510 Meta) was employed. As excitation sources, a DPSS laser at 561 nm wavelength (Cyanine3 dye) and a helium-neon gas laser at 633 nm wavelength (Cyanine5 dye) were used. The sample was imaged through a 63x objective lens with a numerical aperture of 1.4.

High-Performance Liquid Chromatography (HPLC)

High-performance liquid chromatography (HPLC) was performed using HPLC system 1200 series of Agilent Technologies with degasser (G1322A), autosampler (G1329A), thermostated column compartment (G1316A), quaternary pump (G1311A), diode-array detector (G1315D), fraction collector (G1364C) and Zorbax Eclipse XDB-C18 column (dimensions 4.6×150 mm) from Agilent. Following purification conditions were used: eluent A 0.1 M NH₄OAc, eluent B acetonitrile, gradient 0–100% B over 40 min (Table 5.3), flowrate 1 mL/min, UV/Vis detection at 260 nm and 280 nm. Purification was verified by MS (MALDI-TOF).

⁷ Confocal fluorescence microscopy was conducted by Patrick Müller, Institute of Applied Physics, Karlsruhe Institute of Technology (KIT).

Table 5.3: Standard gradient for the purification of oligonucleotides by HPLC. Eluent A: 0.1 M ammonium acetate, eluent B: acetonitrile.

t / min	0	10	15	20	25	32	40	45
B / %	0	5	10	15	30	80	100	0

Fast Protein Liquid Chromatography (FPLC)

Protein purifications were performed on a GE Healthcare Äkta Explorer 900 FPLC System with a pump: P-900, detectors: Monitor UV-900 and Monitor pH/C-900, fraction collector: Frac-950 and MonoQ 5/50 GL anion exchange column (GE Healthcare, Germany). Used purification conditions: buffer A: 20 mM Tris, pH 8.3; buffer B: 20 mM Tris, 1 M NaCl, pH 8.3; gradient: linear increase of buffer B to 100 % in 30 minutes, flowrate: 1 mL/min, UV/Vis detection at 260 nm and 403 nm for the Äkta Explorer 900 FPLC System. Also another system was used: GE Healthcare Äkta pure 25 with HiTrap Q HP (5 mL) column. Used purification conditions: buffer A: 20 mM Tris, pH 6.3; buffer B: 20 mM Tris, 1 M NaCl, pH 6.3 respectively; gradient: linear increase of buffer B to 100% in 28 minutes, flowrate: 5 mL/min, UV-Vis detection at 260 nm and 403 nm.

Polyacrylamide Gel Electrophoresis (PAGE)

PAGE characterization was performed by using a Mini-Protean[®] Tetra System, which was connected to PowerPac[™] voltage source (BioRad, Germany). Native PAGE was used for the separation of DNA according to their size. 12 mL of 21% PA gel solution was prepared following the recipe from the Table 5.4. After polymerization of the gel solution, the glass plates were put into an electrophoresis system (Bio-Rad). Subsequently 1 μ L of loading buffer (6 \times) was added to 5 μ L of DNA sample and loaded into the wells. Gels were run in 1 \times TBE buffer at 100 V.

Table 5.4: Recipe for 21% PA gel.

Gel component	Volume
water	1.6 mL
5 \times TBE	2 mL
30% acrylamide and bis-acrylamide, solution 37.5:1	8.4 mL
ammonium persulfate solution (10% in water)	0.1 mL
tetramethylethylenediamine (TEMED)	0.004 mL

For the characterization of proteins and protein-DNA conjugates SDS-PAGE and non-denaturing PAGE consisting of stacking and separating gels were used. The recipes of 12% SDS- and 12.5% non-denaturing PA gels are listed in the Table 5.5 and Table 5.6 respectively. For the SDS-PAGE sample preparation 4 μL of SDS loading buffer (4 \times) were mixed with 12 μL Protein sample and heated for 5 minutes at 95°C. Then the samples were loaded into the wells and the gel was run for 30 minutes at 80 V and 1 hour at 100 V in SDS running buffer. For the mass reference 1 μL of the standard protein marker was added in one of the wells.

Table 5.5: Recipe for SDS-PA gel.

Gel component	SDS-Stacking gel (5%)	SDS-Separating gel (12%)
	Volume	Volume
water	2.20 mL	3.30 mL
30% acrylamide and bis-acrylamide, solution 37.5:1	0.67 mL	4.00 mL
0.5 M Tris/HCl, pH 6.8	1.00 mL	-
1.5 M Tris/HCl, pH 8.8	-	2.50 mL
10% SDS solution in water	0.04 mL	0.10 mL
10% ammonium persulfate solution in water	0.04 mL	0.10 mL
TEMED	0.004 mL	0.004 mL

For the non-denaturing PAGE sample preparation 1 μL of loading buffer (6 \times) was added to 5 μL of protein-DNA conjugate sample and loaded into the wells. The gel was run for 30 minutes at 100 V and 1.5 hours at 120 V in PAGE running buffer. For the mass reference 1 μL of the standard protein marker was added in one of the wells.

Table 5.6: Recipe for non-denaturing PA gel.

Gel component	Stacking gel (5%)	Separating gel (12%)
	Volume	Volume
water	2.40 mL	4.00 mL
30% acrylamide and bis-acrylamide, solution 37.5:1	0.561 mL	5.00 mL
0.5 M Tris/HCl, pH 6.8	0.428 mL	-

1.5 M Tris/HCl, pH 8.8	-	3.00 mL
10% ammonium persulfate solution in water	0.034 mL	0.06 mL
TEMED	0.0034 mL	0.006 mL

When the gel running was completed, the gel was transferred into a staining chamber. To prepare the staining solution for *ss*DNA or *ds*DNA was prepared by dissolving 3 μ L SYBR gold or ethidium bromide in 30 mL 1 \times TBE buffer. Bio-Rad Silver staining kit was used for protein staining. The images of the stained gels were taken under UV-irradiation by using a Bio-Rad Gel DocTM XR imaging system.

Agarose Gel Electrophoresis

Agarose gel was prepared by dissolving certain amount of agarose in 0.5 \times TBE buffer in a microwave oven. After cooling down the solution slightly it was casted in an electrophoresis system. After the formation of polymerized gel, 0.5 \times TBE buffer was added to the chamber. Then 3 μ L of nanoparticle loading buffer (6 \times) was added to 15 μ L samples and loaded into the wells. Gels were run at 100 V.

Setup for Photo-Induced Reactions

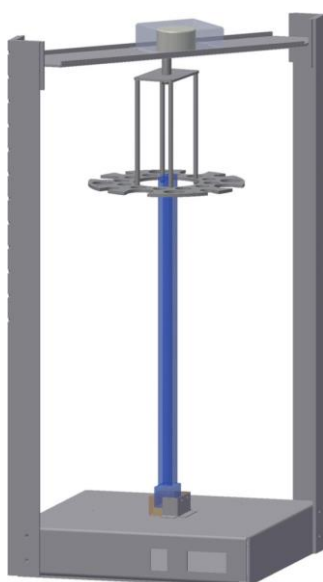


Figure 5.1: Drawing of the custom-built photoreactor employed in the current study.

The samples to be irradiated were crimped air-tight in headspace vials (20 mm, VWR, Germany) using SBR seals (VWR, Germany) with PTFE inner liner. The photoreactions were performed in a custom-built photoreactor (Figure 5.1), consisting of a metal disk which revolves at a distance of 40-50 mm around a compact low-pressure fluorescent lamp with $\lambda_{\text{max}} = 320 \text{ nm} \pm 30 \text{ nm}$ (36 W, Arimed B6, Cosmedico GmbH, Germany) (Figure 5.2).

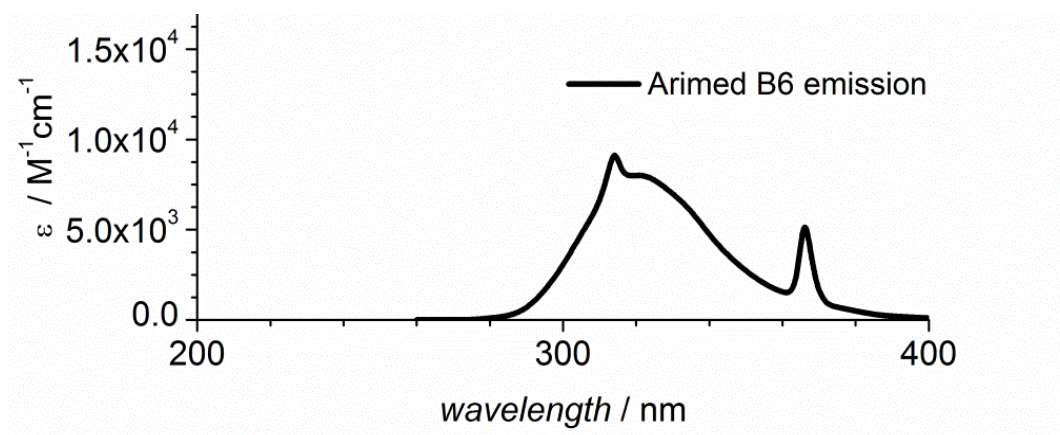


Figure 5.2: Emission spectrum of the employed compact low-pressure fluorescent lamp (36 w, Arimed B6, $\lambda_{\text{max}} = 320 \pm 30 \text{ nm}$).

For spatially controlled surface immobilization of **PE2-DNA2** maleimide functionalized surfaces were mounted into sample holders with mask before being immersed with the reaction solution.

Direct Laser Writing⁸

The home-built direct laser writing setup is based on a tunable Titanium Sapphire oscillator (Coherent Chameleon Ultra II) delivering 150 fs pulses at a center wavelength of 700 nm. The beam intensity is controlled by an acousto-optical modulator (AA Optic-Electronic). The laser beam is focused through an oil immersion objective lens with a numerical aperture of 1.4 (Leica HCX PL APO 100x/1.4-0.7 OILCS). The sample is held by a 3D piezo stage (Physik Instrumente (PI) GmbH und Co. KG) that allows for its relative translation with respect to the laser beam focus. An additional CCD camera is used for monitoring the writing process and sample alignment.

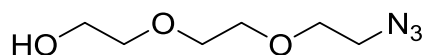
⁸ DLW was conducted by Patrick Müller, Institute of Applied Physics, and Dr. Alexander Quick, Institute for Technical Chemistry and Polymer Chemistry, Karlsruhe Institute of Technology (KIT).

5.2 Syntheses

The syntheses of the compounds *N*-(2-(2,2-dimethylbenzo[*d*][1,3]dioxol-5-yl)ethyl)-3-(2-(2-(2-(2,5-dioxo-2,5-dihydro-1*H*-pyrrol-1-yl)ethoxy)ethoxy)ethoxy)propan-amide^[236] **64**, 4-maleimidobutyric acid^[205] **77**, dopamine-triethylene glycol methyl ether^[236] **72** and di-tert-butyl 2,2'-((6-(((benzyloxy)carbonyl)amino)-1-(tert-butoxy)-1-oxohexan-2-yl)azanediyl) diacetate^[237] **76** was performed by Dr. Ishtiaq Ahmed, Centre for Functional Nanostructures, Institute for Biological Interfaces, Karlsruhe Institute of Technology (KIT), according to the literature procedures.

Syntheses of oligonucleotide modifiers.

2-(2-(2-Azidoethoxy)ethoxy)ethan-1-ol **43**

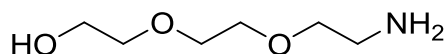


A solution of 15.2 g (101 mmol, 1 eq.) triethylene glycol and 10.8 mL (7.89 g, 77.9 mmol, 0.770 eq.) triethylamine in 100 mL THF was cooled to 0°C. Methanesulfonyl chloride 2.82 mL (4.17 g, 36.4 mmol, 0.360 eq.) was added dropwise and the reaction mixture was brought under stirring to the ambient temperature overnight. Solvents were removed and the residue was re-dissolved in 100 mL EtOH. Sodium azide 4.67 g (71.9 mmol, 0.710 eq.) was added and the reaction mixture was heated to 95°C under reflux overnight. After cooling to ambient temperature solvent was removed under reduced pressure and the residue was re-dissolved in 150 mL diethyl ether, washed three times with saturated NaCl solution. The organic layer was dried over sodium sulfate and the solvent was removed under reduced pressure. The crude product was purified by silica gel chromatography, CH/EtOAc (3:1, 2:1, (v/v), EtOAc), yielding 4.66 g (26.6 mmol, 26 %) of a yellow oil.

¹H-NMR (250 MHz, CDCl₃):

δ (ppm) = 3.39 (t, ³J = 5.2 Hz, 2H, CH₂N₃), 3.59 – 3.75 (m, 10 H, 5×CH₂).

2-(2-(2-aminoethoxy)ethoxy)ethan-1-ol **44**

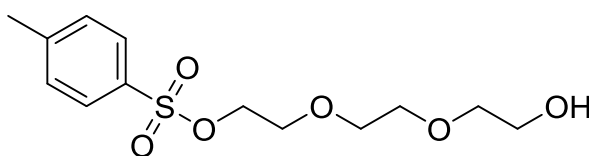


In a 100 mL three necked round bottom flask 1.50 g (8.56 mmol, 1.00 eq.) 2-(2-(2-azidoethoxy)ethoxy)ethan-1-ol **43** was dissolved in 50 mL EtOAc under inert atmosphere. Subsequently 200 mg Pd(OH)₂/C (10%) were added and the flask was flushed with hydrogen. The reaction mixture was stirred under hydrogen atmosphere at ambient temperature overnight. The mixture was filtered over celite in a sintered funnel to remove palladium and charcoal and the celite was washed with several portions of EtOAc. The solvent was removed under reduced pressure and 1.20 g (8.04 mmol, 94%) of amino terminated triethylene glycol **44** was obtained as a brown oil.

¹H-NMR (250 MHz, CD₃CN):

δ (ppm) = 2.72 – 2.81 (m, 2H, CH₂NH₂), 3.47 – 3.58 (m, 10 H, 5×CH₂).

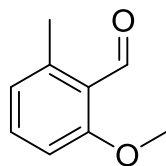
2-(2-(2-Hydroxyethoxy)ethoxy)ethyl 4-methylbenzenesulfonate **35**



A solution of 10.0 g (66.6 mmol, 1 eq.) triethylene glycol and 4.62 mL (3.37 g, 33.3 mmol, 0.500 eq.) triethylamine in 100 mL DCM was cooled to 0°C. A solution of 3.17 g (16.7 mmol, 0.250 eq.) 4-toluenesulfonyl chloride in 20 mL DCM was added dropwise and the reaction mixture was brought under stirring to the ambient temperature overnight. The reaction mixture was washed with saturated sodium bicarbonate solution 100 mL and the organic layer was dried over sodium sulfate. The solvent was removed under reduced pressure and the crude product was purified by silica gel chromatography, CH/EtOAc (2:1, 1:1, (v/v), EtOAc), R_f = 0.10 (CH/EtOAc, 1:1, v/v), yielding 6.20 g (20.4 mmol, 21%) of a colorless oil.

¹H-NMR (250 MHz, CDCl₃):

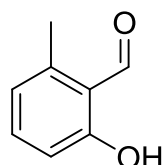
δ (ppm) = 2.43 (s, 3 H, CH₃), 3.53 – 3.59 (m, 6 H, 3×CH₂), 3.66 – 3.71 (m, 4 H, 2×CH₂), 4.15 (t, ³J = 4.7 Hz, 2H, CH₂OS), 7.33 (d, ³J = 8.1 Hz, 2 H, 2×Ar-H), 7.78 (d, ³J = 8.3 Hz, 2 H, 2×Ar-H).

2-Methoxy-6-methylbenzaldehyde 39^[126a]

A suspension of 5.00 g (36.7 mmol, 1.00 eq.) 2,3-dimethylanisole, 9.15 g (36.7 mmol, 1.00 eq.) copper(II) sulfate pentahydrate and 29.6 g (110 mmol, 3.00 eq.) potassium peroxydisulfate in 250 mL acetonitrile/water (1:1, v/v) was heated 20 min under reflux (reaction control by thin layer chromatography). The reaction mixture was cooled down to the ambient temperature and the non-dissolved copper salt was removed by filtration. DCM (100 mL) was added and the phases were separated. The aqueous phase was extracted two times with DCM (100 mL) and the combined organic layers were dried over sodium sulfate. After removal of solvent under reduced pressure, the crude product was purified by flash column chromatography (CH/EtOAc, (5:1, 4:1 (v/v))), $R_f = 0.54$ (CH/EtOAc (2:1, v/v)) yielding 3.32 g (22.1 mmol, 60 %) of a yellow oil.

¹H-NMR (250 MHz, CDCl₃):

δ (ppm) = 2.57 (s, 3 H, C_{arom}CH₃), 3.90 (s, 3 H, C_{arom}OCH₃), 6.82 (t, ³J = 7.8 Hz, 2 H, 2×Ar-H), 7.38 (t, ³J = 7.8 Hz, 1 H, Ar-H), 10.65 (s, 1 H, CHO).

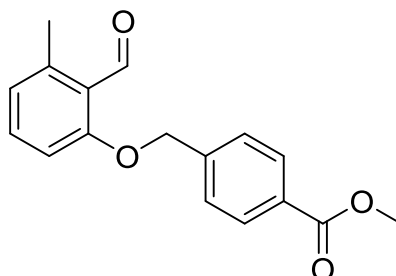
2-Hydroxy-6-methylbenzaldehyde 40

A solution of 3.32 g (22.1 mmol, 1.00 eq.) 2-methoxy-6-methylbenzaldehyde **39** in 50 mL anhydrous DCM was cooled down to 0 °C. AlCl₃ 8.85 g (66.4 mmol, 3.00 eq.) was added and the reaction mixture was stirred at ambient temperature overnight. The reaction was quenched with water and the phases were separated. The aqueous layer was extracted three times with DCM (100 mL). The combined organic layers were dried over sodium sulfate and the solvent was removed under reduced pressure. The crude product was purified by flash column chromatography (CH/EtOAc (100/1, v/v), $R_f = 0.24$ (CH/EtOAc (80:1, v/v)) yielding 1.60 g (11.7 mmol, 53 %) of a yellow solid.

¹H-NMR (300 MHz, CDCl₃):

δ (ppm) = 2.61 (s, 3 H, CH_3), 6.71 (d, $^3J = 7.4$ Hz, 1 H, Ar- H), 6.82 (d, $^3J = 8.5$ Hz, 1 H, Ar- H), 7.38 (t, $^3J = 8.1$ Hz, 1 H, Ar- H), 10.33 (s, 1 H, CHO), 11.92 (s, 1 H, $C_{arom}OH$).

Methyl 4-((2-formyl-3-methylphenoxy)methyl)benzoate **42**

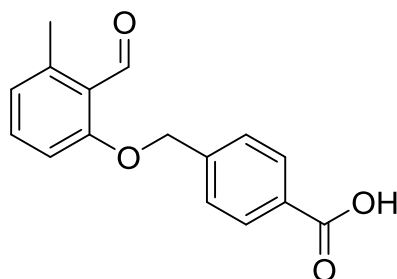


A solution of 1.00 g (7.34 mmol, 1.00 eq.) 2-hydroxy-6-methylbenzaldehyde **40**, 1.72 g (7.49 mmol, 1.02 eq.) of methyl-4-(bromomethyl)-benzoate, 1.50 g (11.0 mmol, 1.50 eq.) K_2CO_3 and 29.0 mg (110 μ mol, 0.0150 eq.) 18-crown-6 in 80 mL anhydrous acetone was stirred at 40 °C overnight. The reaction mixture was cooled to the ambient temperature, non-dissolved salt was filtered and the solvent was removed under reduced pressure. The residue was re-dissolved in 100 mL DCM/water (1:1, v/v) and acidified with 1 M HCl to pH 1. The aqueous layer was extracted three times with DCM (150 mL). The combined organic layers were dried over sodium sulfate and the solvent was removed under reduced pressure. The crude product was recrystallized from hexane/EtOAc (7:1, v/v) yielding 2.10 g (7.38 mmol, 100%) of a pale yellow solid.

1H -NMR (400 MHz, $CDCl_3$):

δ (ppm) = 2.58 (s, 3 H, $C_{arom}CH_3$), 3.92 (s, 3 H, $COOCH_3$), 5.21 (s, 2 H, CH_2), 6.84 (t, $^3J = 7.4$ Hz, 2 H, $2 \times Ar-H$), 7.36 (t, $^3J = 7.9$ Hz, 1 H, Ar- H), 7.49 (dt, $^3J = 8.5$ Hz, 2 H, $2 \times Ar-H$), 8.06 (dt, $^3J = 8.4$ Hz, $^4J = 1.8$ Hz, 2 H, $2 \times Ar-H$), 10.75 (s, 1 H, CHO).

MS (EI, 70 eV), m/z (%): 284 (32) [M^+], 149 (100), 121 (18).

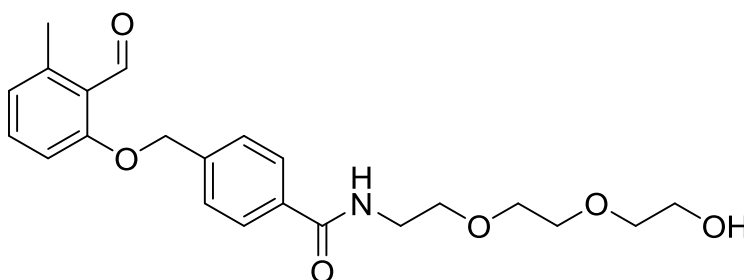
4-((2-Formyl-3-methylphenoxy)methyl)benzoic acid 30

A solution of 900 mg (22.5 mmol, 4.00 eq.) NaOH in 10 mL MeOH was added to a solution of 1.60 g (5.63 mmol, 1.00 eq.) methyl-4-((2-formyl-3-methylphenoxy)-methyl)benzoate **42** in 100 mL DCM. The reaction mixture was stirred at ambient temperature overnight. Solvents were removed under reduced pressure and the residue was re-dissolved in 100 mL DCM/water (1:1, v/v). The organic phase was extracted three times with water and the combined aqueous layers were acidified with 1 M HCl to pH 3. The aqueous layer was extracted three times with DCM (150 mL). The combined organic layers were dried over sodium sulfate and the solvent was removed under reduced pressure yielding 1.15 g (4.25 mmol, 76 %) of a yellow solid.

¹H-NMR (250 MHz, CDCl₃):

δ (ppm) = 2.52 (s, 3 H, CH₃), 5.39 (s, 2 H, CH₂), 6.90 (dt, ³J = 7.6 Hz, 1 H, Ar-H), 7.14 (d, ³J = 8.4 Hz, 1 H, Ar-H), 7.46 (t, ³J = 8.3 Hz, 1 H, Ar-H), 7.68 (d, ³J = 8.5 Hz, 2 H, 2×Ar-H), 8.09 (dt, ³J = 8.5 Hz, ⁴J = 1.8 Hz, 2 H, 2×Ar-H), 10.74 (s, 1 H, CHO).

MS (EI, 70 eV), *m/z* (%): 270 (36) [M⁺], 135 (100).

4-((2-Formyl-3-methylphenoxy)methyl)-N-(2-(2-(2-hydroxyethoxy)ethoxy)ethyl)benzamide 37

The synthesis was performed under inert conditions using the literature procedure.^[157] The solution of 100 mg (370 μmol , 1.00 eq.) 4-((2-formyl-3-methylphenoxy)methyl)benzoic acid **30** and 51.0 mg (377 μmol , 1.02 eq.) HOBt in 10 mL dry DMF was stirred for 10 minutes at room temperature. 78.0 mg (377 μmol , 1.02 eq.) DCC in 5 mL dry DMF were added and the solution was stirred for another 10 minutes, before 43.0 mg (377 μmol , 1.02 eq.) NHS in 10 mL dry DMF were added dropwise over a period of 30 minutes. The reaction was continued for 2 hours. The resulting NHS ester was added dropwise to a stirred solution of 61.0 mg (407 μmol , 1.10 eq.) 2-(2-(2-aminoethoxy)ethoxy)ethan-1-ol **44** in 10 mL dry DMF over a period of 45 minutes. The reaction mixture was stirred for 48 h at room temperature. The urea side product was removed by filtration and the crude product was transferred to chloroform. The organic solution was washed three times with saturated NaCl solution and deionized water. The organic phase was dried over Na_2SO_4 and the solvent removed under reduced pressure. The crude product was purified by silica gel chromatography, CH/EtOAc (3:1, 1:1, 1:2 (v/v), MeOH), $R_f = 0.14$ (EtOAc), yielding 69.8 mg (174 μmol , 47 %) of a yellow solid.

$^1\text{H-NMR}$ (300 MHz, CDCl_3):

δ (ppm) = 2.56 (s, 3 H, CH_3), 3.56 – 3.59 (m, 2 H, NHCH_2), 3.65 – 3.68 (m, 10 H, $5 \times \text{CH}_2$), 5.17 (s, 2 H, $\text{C}_{\text{arom}}\text{CH}_2\text{OC}_{\text{arom}}$), 6.83 (t, $^3J = 8.0$ Hz, 2 H, $2 \times \text{Ar-H}$), 7.34 (t, $^3J = 8.0$ Hz, 1 H, Ar-H), 7.46 (d, $^3J = 8.2$ Hz, 2 H, $2 \times \text{Ar-H}$), 7.84 (d, $^3J = 8.2$ Hz, 2 H, $2 \times \text{Ar-H}$), 10.71 (s, 1 H, CHO).

$^{13}\text{C-NMR}$ (100 MHz, CDCl_3):

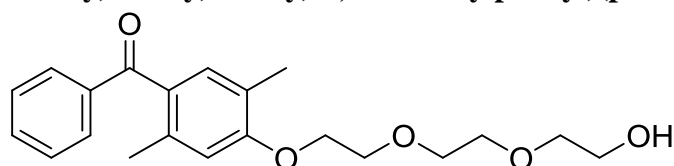
$\delta = 21.40$ (CH_3), 39.71 (NHCH_2), 61.47 (CH_2OH), 70.02 ($4 \times \text{CH}_2$), 110.31 (C-Ar), 123.52 (C_{quart} , $\text{C}_{\text{arom}}\text{CHO}$), 124.56 (C-Ar), 127.00 ($2 \times \text{C-Ar}$), 127.47 ($2 \times \text{C-Ar}$), 134.19 (C_{quart} , $\text{C}_{\text{arom}}\text{CONH}$), 134.40 (C-Ar), 139.63 (C_{quart} , $\text{C}_{\text{arom}}\text{CH}_2\text{OC}_{\text{arom}}$), 142.17 (C_{quart} , $\text{C}_{\text{arom}}\text{CH}_3$), 161.89 (C_{quart} , $\text{C}_{\text{arom}}\text{OCH}_2$), 167.09 (C_{quart} , CONH), 192.09 (C_{quart} , CHO).

IR (ATR Platinum):

$\tilde{\nu} = 3456$ (w, v (O-H)), 3319 (w, v (N-H)), 2890 (w, v (C-H)), 1688 (m, v (C-N), v (C=O)), 1644 (m, v (NHC=O), v (C=C)), 1537 (m, v (C-H)), 1271 (s, v (C-O)).

HR-MS (FAB, matrix: 3-NBA), m/z $[\text{M}+\text{H}]^+$ calculated for $\text{C}_{22}\text{H}_{28}\text{O}_6\text{N}_1$ 402.1911; found, 402.1912.

(4-(2-(2-(2-Hydroxyethoxy)ethoxy)ethoxy)-2,5-dimethylphenyl)(phenyl)methanone 36



A solution of 620 mg (2.74 mmol, 1.00 eq.) (4-hydroxy-2,5-dimethylphenyl)(phenyl)methanone **31**, 1.00 g (3.29 mmol, 1.20 eq.) of 2-(2-(2-hydroxyethoxy)ethoxy)ethyl 4-methylbenzenesulfonate **35**, 1.14 g (8.21 mmol, 3.00 eq.) K_2CO_3 , 7.00 mg (82.0 μmol , 0.0300 eq.) LiBr and 22.0 mg (82.0 μmol , 0.0300 eq.) 18-crown-6 in 80 mL anhydrous acetonitrile was heated under reflux overnight. The reaction mixture was cooled to the ambient temperature, non-dissolved salt was filtered and washed with acetone. The solvents were removed under reduced pressure. The crude product was purified by silica gel chromatography, CH/EtOAc (1:1, 1:2, 1:3 (v/v)), $R_f = 0.15$ (CH/EtOAc, 1:1, v/v), yielding 851 mg (2.37 mmol, 87 %) of a colorless oil.

$^1\text{H-NMR}$ (400 MHz, CDCl_3):

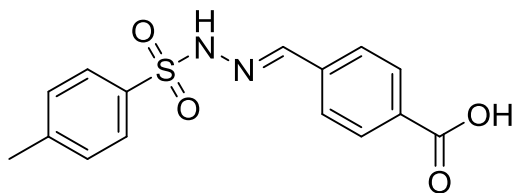
δ (ppm) = 2.17 (s, 3 H, CH_3), 2.36 (s, 3 H, CH_3), 2.49 (br, 1 H, OH), 3.62 (t, $^3J = 4.9$ Hz, 2 H, CH_2), 3.69 – 3.77 (m, 6 H, $3 \times \text{CH}_2$), 3.91 (t, $^3J = 4.9$ Hz, 2 H, CH_2), 4.20 (t, $^3J = 4.6$ Hz, 2 H, CH_2), 6.71 (s, 1 H, Ar-*H*), 7.15 (s, 1 H, Ar-*H*), 7.43 (t, $^3J = 7.8$ Hz, 2 H, $2 \times \text{Ar-}H$), 7.55 (tt, $^3J = 7.4$ Hz, $^4J = 1.2$ Hz 1 H, Ar-*H*), 7.75 (d, $^3J = 7.1$ Hz, 2 H, $2 \times \text{Ar-}H$).

$^{13}\text{C-NMR}$ (100 MHz, CDCl_3):

δ = 15.69 (CH_3), 20.55 (CH_3), 61.73 (CH_2OH), 67.65 ($\text{C}_{\text{arom}}\text{OCH}_2$), 69.70 (CH_2), 70.41 (CH_2), 70.97 (CH_2), 72.46 (CH_2), 113.56 (C-Ar), 123.35 (C_{quart} , $\text{C}_{\text{arom}}\text{CH}_3$), 128.22 ($2 \times \text{C-Ar}$), 129.96 ($2 \times \text{C-Ar}$), 130.30 (C_{quart} , CCO), 132.43 (C-Ar), 132.48 (C-Ar), 137.65 (C_{quart} , $\text{C}_{\text{arom}}\text{CH}_3$), 138.72 (C_{quart} , CCO), 158.51 (C_{quart} , $\text{C}_{\text{arom}}\text{O}$), 197.99 (C_{quart} , CO).

MS (FAB, matrix: 3-NBA), m/z (%): 359 (80) $[\text{M}+\text{H}]^+$, 105 (100).

4-((2-Tosylhydrazono)methyl)benzoic acid **60**



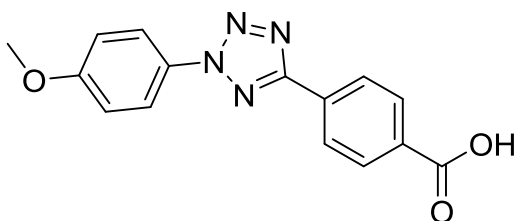
A mixture of 6.56 g (43.7 mmol, 1.00 eq.) 4-formylbenzoic acid and 8.14 g (43.7 mmol, 1.00 eq.) *p*-toluenesulfonyl hydrazide in 100 mL ethanol was heated under reflux for 30 min. The reaction mixture was diluted with 100 mL water and the precipitate was filtered off. The

solid was washed with 100 mL aqueous EtOH and dried under reduced pressure to give 11.3 g (35.3 mmol, 81%) of a colorless solid.

¹H-NMR (250 MHz, DMSO-d⁶):

δ (ppm) = 2.35 (s, 3 H, CH₃), 7.40 (d, ³J = 8.1 Hz, 2 H, 2×Ar-H), 7.66 (d, ³J = 8.4 Hz, 2 H, 2×Ar-H), 7.76 (d, ³J = 8.3 Hz, 2 H, 2×Ar-H), 7.93 (d, ³J = 8.3 Hz, 2 H, 2×Ar-H), 7.96 (s, 1 H, NCH), 11.69 (s, 1 H, NH).

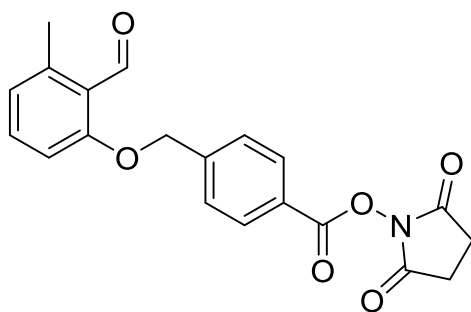
4-(2-(4-Methoxyphenyl)-2H-tetrazol-5-yl)benzoic acid **24**



In a 250 ml round bottom flask 4.00 g (32.5 mmol, 1.00 eq.) of *p*-anisidine were dissolved in a mixture of concentrated HCl (8.46 mL), H₂O (26.9 mL) and EtOH (26.9 mL) and cooled to 0°C. A cooled solution of 2.24 g (32.5 mmol, 1.00 eq.) NaNO₂ in 13.5 mL H₂O was added dropwise and stirred for 10 min at 0 °C. Formed diazonium salt solution was added dropwise to a solution of 10.3 g (32.5 mmol, 1.00 eq.) 4-((2-tosylhydrazono)methyl)benzoic acid **60** in 200 mL pyridine at the temperature between -10 °C and -5 °C over a period of 45 min. After complete addition, the solution was stirred at 0 °C for 30 min and at the ambient temperature overnight. The turbid solution was poured into a 10% aqueous HCl solution (500 mL), the precipitate was filtered off, washed with 500 mL EtOH and dried under reduced pressure to give 6.00 g (20.3 mmol, 62%) of a purple solid.

¹H-NMR (250 MHz, DMSO-d⁶):

δ (ppm) = 3.86 (s, 3 H, CH₃), 7.21 (dt, ³J = 9.1 Hz, ⁴J = 2.2 Hz, 2 H, 2×Ar-H), 8.06 (dt, ³J = 9.1 Hz, ⁴J = 2.2 Hz, 2 H, 2×Ar-H), 8.13 (dt, ³J = 8.5 Hz, ⁴J = 1.8 Hz, 2 H, 2×Ar-H), 8.25 (dt, ³J = 8.5 Hz, ⁴J = 1.8 Hz, 2 H, 2×Ar-H), 13.26 (br, 1 H, COOH).

2,5-Dioxopyrrolidin-1-yl 4-((2-formyl-3-methylphenoxy)methyl)benzoate 55

In a 50 mL two necked round bottom flask 100 mg (369 μmol , 1.00 eq.) 4-((2-formyl-3-methylphenoxy)methyl)benzoic acid **30** and 51.1 mg (440 μmol , 1.20 eq.) NHS were dissolved in 20 mL anhydrous THF under inert atmosphere. The reaction mixture was cooled to 0 °C and 91.6 mg (444 μmol , 1.20 eq.) DCC were added. The stirring was continued at ambient temperature overnight. After the filtration of DCU salt solvent was removed under reduced pressure and the crude product was purified by flush column chromatography DCM/MeOH (DCM, 99.5:0.5, 99:1 (v/v)), $R_f = 0.56$ (DCM/MeOH, 98:2, v/v), yielding 130 mg (353 μmol , 96 %) of a pale yellow solid.

$^1\text{H-NMR}$ (500 MHz, CDCl_3):

δ (ppm) = 2.59 (s, 3 H, CH_3), 2.91 (br, 4 H, $2\times\text{CH}_2$), 5.26 (s, 2 H, CH_2), 6.82 – 6.86 (m, 2 H, $2\times\text{Ar-H}$), 7.36 (t, $^3J = 8.0$ Hz, 1 H, Ar-H), 7.57 (d, $^3J = 8.2$ Hz, 2 H, $2\times\text{Ar-H}$), 8.16 (d, $^3J = 8.2$ Hz, 2 H, $2\times\text{Ar-H}$), 10.76 (s, 1 H, CHO).

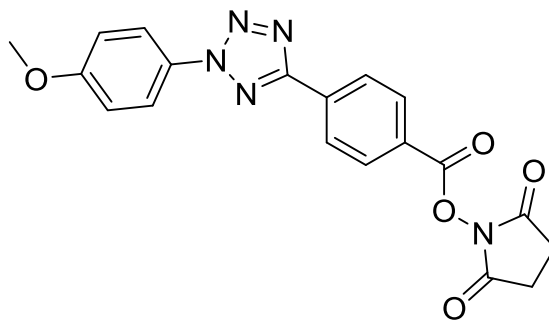
$^{13}\text{C-NMR}$ (126 MHz, CDCl_3):

$\delta = 21.44$ (CH_3), 25.65 ($2\times\text{CH}_2$), 69.56 (CH_2), 110.23 (C-Ar), 123.64 (C_{quart} , $\text{C}_{\text{aromCHO}}$), 124.84 (C-Ar), 127.02 ($2\times\text{C-Ar}$), 130.99 ($2\times\text{C-Ar}$), 134.39 (C-Ar), 142.37 (C_{quart} , $\text{C}_{\text{aromCH}_3}$), 143.73 (C_{quart} , $\text{C}_{\text{aromCH}_2}$), 161.47 (C_{quart} , C_{aromO}), 161.57 (C_{quart} , $\text{C}_{\text{aromCOO}}$), 169.16 ($2\times\text{C}_{\text{quart}}$, $2\times\text{CON}$), 191.79 (C_{quart} , CHO).

IR (ATR Platinum):

$\tilde{\nu} = 1763$ (w, ν (C=O)), 1730 (w, ν (C=ON), ν (C=OO)), 1685 (w, ν (C-N), ν (N-O)), 1575 (w, ν (C=C)), 1236 (w, ν (C-O)).

HR-MS (EI, 70 eV), m/z [M^+] calculated for $\text{C}_{20}\text{H}_{17}\text{O}_6\text{N}_1$ 367.1050; found, 367.1052.

2,5-Dioxopyrrolidin-1-yl 4-(2-(4-methoxyphenyl)-2H-tetrazol-5-yl)benzoate 62

In a 50 mL two necked round bottom flask 100 mg (338 μmol , 1.00 eq.) 4-(2-(4-methoxyphenyl)-2H-tetrazol-5-yl)benzoic acid **24** and 47.0 mg (405 μmol , 1.20 eq.) NHS were dissolved in 20 mL anhydrous THF under inert atmosphere. The reaction mixture was cooled to 0 °C and 84.0 mg (405 μmol , 1.20 eq.) DCC were added. The stirring was continued at ambient temperature overnight. After the filtration of DCU salt solvent was removed under reduced pressure and the crude product was purified by flush column chromatography DCM/MeOH (DCM, 99.5:0.5, 99:1 (v/v)), $R_f = 0.58$ (DCM/MeOH, 98:2, v/v), yielding 110 mg (279 μmol , 83 %) of a pink solid.

$^1\text{H-NMR}$ (500 MHz, CDCl_3):

δ (ppm) = 2.94 (br, 4 H, $2\times\text{CH}_2$), 3.90 (s, 3 H, CH_3), 7.07 (d, $^3J = 8.7$ Hz, 2 H, $2\times\text{Ar-H}$), 8.11 (d, $^3J = 8.7$ Hz, 2 H, $2\times\text{Ar-H}$), 8.29 (d, $^3J = 8.1$ Hz, 2 H, $2\times\text{Ar-H}$), 8.40 (d, $^3J = 8.1$ Hz, 2 H, $2\times\text{Ar-H}$).

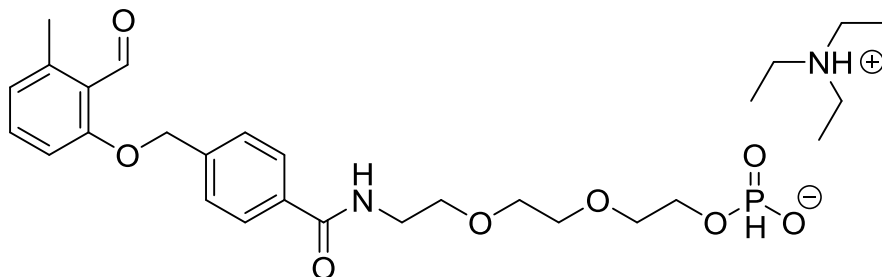
$^{13}\text{C-NMR}$ (126 MHz, CDCl_3):

$\delta = 25.69$ ($2\times\text{CH}_2$), 55.69 (CH_3), 114.76 ($2\times\text{C-Ar}$), 121.50 ($2\times\text{C-Ar}$), 126.54 (C_{quart} , C_{aromN}), 127.21 ($2\times\text{C-Ar}$), 130.21 (C_{quart} , $\text{C}_{\text{aromCOO}}$), 131.20 ($2\times\text{C-Ar}$), 133.26 (C_{quart} , C_{aromCN}), 160.77 (C_{quart} , C_{aromCO}), 161.39 (C_{quart} , C_{aromCN}), 163.63 (C_{quart} , COO), 169.11 (C_{quart} , $2\times\text{CON}$).

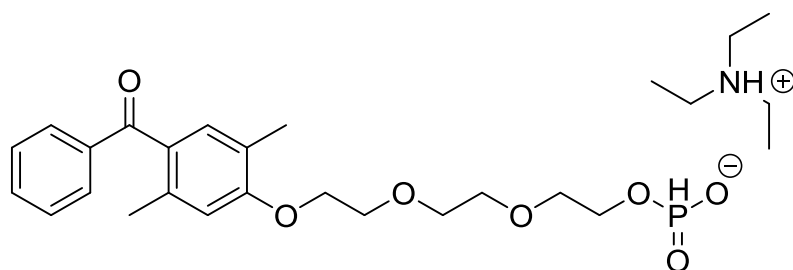
IR (ATR Platinum):

$\tilde{\nu} = 2940$ (vw, v (C-H)), 1765 (m, v (C=O)), 1730 (m, v (C=N), v (N=N), v (C=C)), (w, v (C=ON), v (C=OO)), 1512 (m, v (C=C)), 1200 (w, v (C-O)).

HR-MS (FAB, matrix: 3-NBA), m/z $[\text{M}+\text{H}]^+$ calculated for $\text{C}_{19}\text{H}_{16}\text{O}_5\text{N}_5$ 394.1146; found, 394.1144.

2-(2-(2-(4-((2-Formyl-3-methylphenoxy)methyl)benzamido)ethoxy)ethoxy)ethyl phosphonate triethylammonium salt **49**

Compound **49** was synthesized under inert conditions according to a reported method with slight modification.^[47] 4-((2-Formyl-3-methylphenoxy)methyl)-N-(2-(2-(2-hydroxyethoxy)ethoxy)ethyl)benzamide **37** 120 mg (299 μmol , 1.00 eq.) was dissolved in a solution of 1 M phosphorous acid in anhydrous pyridine (681 mg, 8.31 mmol, 27.7 eq. of H_3PO_3 dissolved in 9.80 ml pyridine). Pivaloyl chloride 202 μL (1.64 mmol, 5.50 eq.) was added dropwise to the reaction mixture. The solution became briefly opaque and was stirred for a further 2 hours. Once complete (TLC control), the reaction mixture was quenched by addition of TEAB buffer (8.40 mL, 2 M, pH 7.7) and was then extracted twice with DCM. The organic layers were combined and dried over Na_2SO_4 . The solvents were removed under reduced pressure to give the product **49** as a yellow thick oil, which was used in the next step without further purification. $^{31}\text{P-NMR}$ (100 MHz, CD_3CN): δ (ppm) = 3.78 (s, 1 P).

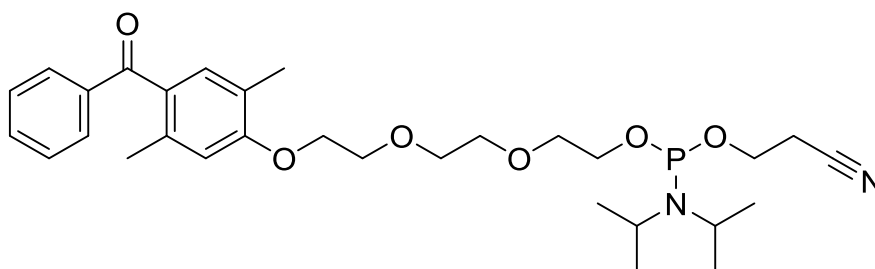
2-(2-(2-(4-Benzoyl-2,5-dimethylphenoxy)ethoxy)ethoxy)ethyl phosphonate triethylammonium salt **51**

Compound **51** was synthesized under inert conditions according to a reported method with slight modification.^[47] (4-(2-(2-(2-Hydroxyethoxy)ethoxy)ethoxy)-2,5-dimethylphenyl)(phenyl)methanone **36** 61.0 mg (170 μmol , 1.00 eq.) was dissolved in a solution of 1 M phosphorous acid in anhydrous pyridine (388 mg, 4.73 mmol, 27.7 eq. of H_3PO_3

dissolved in 5.57 ml pyridine). Pivaloyl chloride 115 μL (936 μmol , 5.50 eq.) was added dropwise to the reaction mixture. The solution became briefly opaque and was stirred for a further 30 minutes. Once complete, the reaction mixture was quenched by addition of TEAB buffer (3.88 mL, 2 M, pH 7.7) and was then extracted twice with DCM. The organic layers were combined and dried over Na_2SO_4 . The solvents were removed under reduced pressure to give the product **51** as a pale yellow semi-solid, which was used in the next step without further purification.

$^{31}\text{P-NMR}$ (100 MHz, CD_3CN): δ (ppm) = 3.47 (s, 1 P).

2-(2-(2-(4-Benzoyl-2,5-dimethylphenoxy)ethoxy)ethoxy)ethyl (2-cyanoethyl) diisopropylphosphoramidite **46**

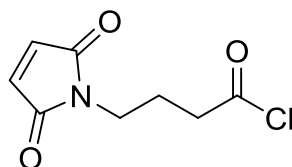


Compound **46** was synthesized under inert conditions using the procedure described by Ligeour and co-workers.^[238] DIPEA 199 μL (1.17 mmol, 2.00 eq.) and 2-cyanoethyl *N,N*-diisopropylchlorophosphoramidite 196 μL (879 μmol , 1.50 eq.) were added to a solution of 21.0 mg (586 μmol , 1.00 eq.) (4-(2-(2-(2-Hydroxyethoxy)ethoxy)ethoxy)-2,5-dimethylphenyl)(phenyl)methanone **36** in 3 mL of anhydrous CH_2Cl_2 and stirred 2 h at ambient temperature. The reaction mixture was washed with saturated NaHCO_3 solution and dried over Na_2SO_4 . The solvents were removed under reduced pressure to give the product **46** as a colorless semi-solid, which was used in the next step without further purification.

$^{31}\text{P-NMR}$ (100 MHz, CD_3CN): δ = 11.8; 18.2; 149.2.

Nanoparticle Linker Syntheses

4-Maleimidobutyryl chloride **78**

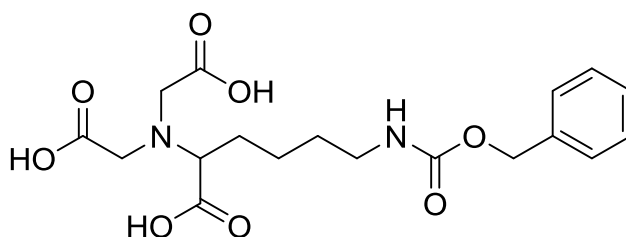


4-Maleimidobutyric acid (1.10 g, 6.01 mmol) was dissolved in benzene (10 mL) and thionyl chloride (1.00 mL) was added. The reaction mixture was refluxed for 2 h at 70°C. Subsequently, the benzene and non-reacted thionyl chloride were removed under reduced pressure yielding 1.10 g (5.46 mmol, 99%) of a white powder.

¹H-NMR (250 MHz, CDCl₃):

δ (ppm) = 1.98 (quint, ³J = 6.9 Hz, 2 H, CH₂), 2.92 (t, ³J = 7.2 Hz, 2 H, CH₂), 3.59 (t, ³J = 6.7 Hz, 2 H, CH₂), 6.72 (s, 2 H, 2×CH).

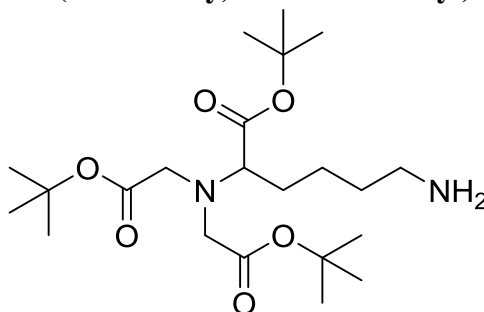
2,2'-((5-(((Benzyloxy)carbonyl)amino)-1-carboxypentyl)azanediyl)diacetic acid 75



In a 100 mL round bottom flask 6.96 g (50.1 mmol, 2.81 eq.) bromoacetic acid were dissolved in 15 mL of 2 M NaOH solution and cooled to 0 °C. Under vigorous stirring the solution of 5.00 g (17.8 mmol, 1.00 eq.) *N*(γ)-benzyloxycarbonyl-L-lysine in 15.0 mL of 2 M NaOH was added dropwise at 0 °C. After 2 h, the ice bath was removed and the reaction mixture was stirred at ambient temperature overnight. The solution was heated to 50 °C for 2 h. The reaction mixture was cooled to the ambient temperature and 48 mL of 1 M HCl solution was added. Formed crystals were filtered and re-dissolved in 1 M NaOH solution. The product precipitated out by the dropwise addition of 1 M NaOH solution and was collected by filtration yielding 3.54 g (8.93 mmol, 50%) of a white solid.

¹H-NMR (250 MHz, DMSO-d₆):

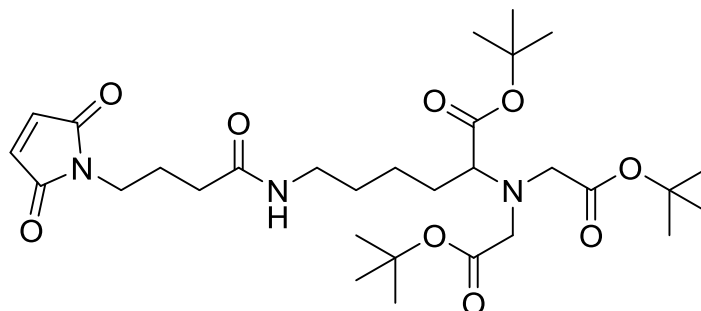
δ (ppm) = 1.32 – 1.44 (m, 4 H, 2×CH₂), 1.47 – 1.69 (m, 2 H, CH₂), 2.92 – 3.00 (m, 2 H, CH₂NH), 3.31 (t, ³J = 7.3 Hz, 1 H, NCHCH₂), 3.46 (dd, 4 H, (HOCOCH₂)₂N), 4.99 (s, 2 H, C_{arom}CH₂OCONH), 7.27 – 7.36 (m, 5 H, 5×Ar-H).

Di-tert-butyl 2,2'-((6-amino-1-(tert-butoxy)-1-oxohexan-2-yl)azanediyl)diacetate 79

In a 100 mL three necked round bottom flask 2.00 g (3.54 mmol, 1.00 eq.) di-tert-butyl 2,2'-((6-(((benzyloxy)carbonyl)amino)-1-(tert-butoxy)-1-oxohexan-2-yl)azanediyl) diacetate **76** was dissolved in 50 mL MeOH under inert atmosphere. Subsequently 200 mg Pd/C (10%) were added and the flask was flushed with hydrogen. The reaction mixture was completed after 5 h as monitored by TLC (CH/EtOAc (2:1, v/v)) and visualized by UV and ninhydrin staining. The mixture was filtered over celite in a sintered funnel to remove palladium and charcoal and the celite was washed with several portions of MeOH. The solvent was removed under reduced pressure and 1.45 g (3.37 mmol, 95%) of the compound **79** were obtained as a yellow oil.

¹H-NMR (400 MHz, CDCl₃):

δ (ppm) = 1.07 – 1.27 (m, 2 H, CH₂), 1.44 (s, 18 H, ((CH₃)₃COCOCH₂)₂N), 1.45 (s, 9 H, (CH₃)₃COCOCHN), 1.47 – 1.54 (m, 2 H, CH₂), 1.56 – 1.70 (m, 2 H, CH₂), 2.67 (t, ³J = 6.6 Hz, 2 H, CH₂), 3.30 (t, ³J = 7.4 Hz, 1 H, NCHCH₂), 3.45 (s, 2 H, (CH₃)₃COCOCH₂N), 3.47 (d, 2 H, (CH₃)₃COCOCH₂N).

Di-tert-butyl 2,2'-((1-(tert-butoxy)-6-(4-(2,5-dioxo-2,5-dihydro-1H-pyrrol-1-yl)butanamido)-1-oxohexan-2-yl)azanediyl)diacetate 80

In a 100 mL two necked round bottom flask 870 mg (2.02 mmol, 1.00 eq.) di-tert-butyl 2,2'-((6-amino-1-(tert-butoxy)-1-oxohexan-2-yl)azanediyl)diacetate **79** and 0.559 mL

(408 mg, 4.03 mmol, 2.00 eq.) triethylamine were dissolved in 50 mL anhydrous DCM under inert atmosphere. The reaction mixture was cooled to 0 °C and the solution of 1.22 g (6.05 mmol, 3.00 eq.) 4-(2,5-dioxo-2,5-dihydro-1*H*-pyrrol-1-yl)butanoyl chloride **78** in 20.0 mL of anhydrous DCM was added dropwise at 0 °C. The reaction mixture was warmed to the ambient temperature under stirring overnight. The solvent was removed under reduced pressure and the crude product was purified by flash column chromatography DCM/MeOH (DCM, 99:1, 99:2 (v/v)), $R_f = 0.75$ (DCM/MeOH, 9:1, v/v), yielding 1.01 g (1.69 mmol, 84 %) of a yellow oil.

¹H-NMR (400 MHz, CDCl₃):

δ (ppm) = 1.44 (s, 18 H, 6×CH₃), 1.45 (s, 9 H, 3×CH₃), 1.47 – 1.58 (m, 4 H, 2×CH₂), 1.59 – 1.66 (m, 2 H, CH₂), 1.93 (quint, ³*J* = 7.0 Hz, 2 H, CH₂), 2.17 (t, ³*J* = 7.3 Hz, 2 H, CH₂), 3.15 – 3.25 (m, 2 H, CH₂), 3.29 (t, ³*J* = 6.8 Hz, 1 H, CH), 3.42 (s, 2 H, CH₂), 3.45 (s, 2 H, CH₂), 3.55 (t, ³*J* = 6.7 Hz, 2 H, CH₂), 6.68 (s, 2 H, 2×CH).

¹³C-NMR (100 MHz, CDCl₃):

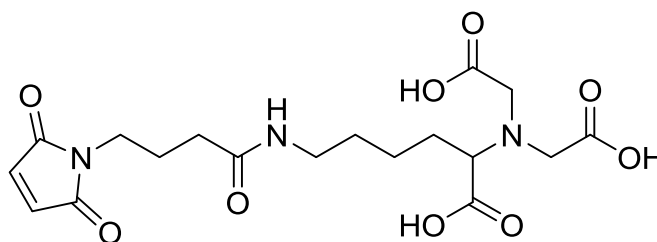
δ = 22.87 (CH₂), 24.81 (CH₂), 28.10 (6×CH₃), 28.19 (3×CH₃), 28.38 (CH₂), 29.79 (CH₂), 33.56 (CH₂), 37.30 (CH₂), 39.22 (CH₂), 53.89 (2×CH₂), 64.85 (CH), 80.73 (C_{quart}, 2×(OC(CH₃)₃)), 81.12 (C_{quart}, OC(CH₃)₃), 134.08 (C_{quart}, 2×CHCON), 170.74 (C_{quart}, 2×CH₂COO), 170.84 (C_{quart}, CHCOO), 171.79 (C_{quart}, CONH), 172.42 (C_{quart}, 2×CON).

IR (ATR Platinum):

$\tilde{\nu}$ = 2975 (w, v (C-H), v (N-H)), 1704 (s, v (C=O), v (C=C), δ (N-H)), 1365 (m, δ_s (C-H)), 1138 (s, v (C-O)).

HR-MS (FAB, matrix: 3-NBA), m/z [M+H]⁺ calculated for C₃₀H₅₀O₉N₃ 596.3542; found, 596.3543.

2,2'-((1-Carboxy-5-(4-(2,5-dioxo-2,5-dihydro-1*H*-pyrrol-1-yl)butanamido)pentyl)azanediyldiacetic acid **81**



In a 25 mL round bottom flask 100 mg (168 μmol , 1 eq.) di-tert-butyl 2,2'-((1-(tert-butoxy)-6-(4-(2,5-dioxo-2,5-dihydro-1*H*-pyrrol-1-yl)butanamido)-1-oxohexan-2-yl)azanediyl)diacetate **80** were dissolved in 5 mL DCM and the solution was cooled to 0 °C. Subsequently 1.00 mL TFA was added and the reaction mixture was stirred 3 h at the ambient temperature. The solvent was removed under reduced pressure and the rest of TFA was co-evaporated three times (30 mL) with toluene yielding 70.7 mg (165 μmol , 98%) of a yellow oil.

¹H-NMR (400 MHz, DMSO-*d*⁶):

δ (ppm) = 1.35 – 1.39 (m, 4 H, 2 \times CH₂), 1.46 – 1.62 (m, 2 H, CH₂), 1.69 (t, ³*J* = 7.2 Hz, 2 H, CH₂), 2.02 (t, ³*J* = 7.5 Hz, 2 H, CH₂), 2.93 – 2.98 (m, 2 H, CH₂), 3.36 – 3.42 (m, 5 H, 2 \times CH₂, CH), 3.57 – 3.60 (m, 2 H, CH₂), 6.70 (s, 2 H, 2 \times CH₂).

¹³C-NMR (100 MHz, DMSO-*d*⁶):

δ = 24.12 (CH₂), 28.75 (CH₂), 32.54 (CH₂), 36.35 (CH₂), 36.82 (2 \times CH₂), 38.26 (CH₂), 52.44 (CH₂), 53.18 (CH₂), 63.82 (CH), 134.39 (C_{quart}, 2 \times CHCON), 170.91 (C_{quart}, 2 \times CH₂COOH), 170.99 (C_{quart}, 2 \times CON), 172.37 (C_{quart}, CONH), 173.11 (C_{quart}, CHCOOH).

IR (ATR Platinum):

$\tilde{\nu}$ = 3085 (w, ν (O-H)), 2938 (w, ν (C-H), ν (N-H)), 1698 (s, ν (C=O), ν (C=C), δ (N-H)), 1407 (m, δ_s (C-H)), 1141 (s, ν (C-O)).

HR-MS (FAB, matrix: 3-NBA), *m/z* [M+H]⁺ calculated for C₁₈H₂₆O₉N₃ 428.1664; found, 428.1662.

5.3 DNA Modification

Phosphoramidite Method

The synthesis of the **PE1-DNA1 48** was performed on an Expedite 7/99 Synthesizer from PerSeptive Biosystems in a group of Prof. Dr. Hans-Achim Wagenknecht at the Institute for Organic Chemistry, Karlsruhe Institute of Technology (KIT) under the supervision of Claudia Stubinitzky using standard phosphoramidite coupling protocol (Table 5.7). Reagents and CPG (0.100 μmol) were purchased from ABI and Glen Research. The commercially available (Proligo) phosphoramidites of the natural DNA bases and the synthesized photoenol(1) phosphoramidite **46** were dissolved under inert atmosphere in absolute acetonitrile (67.0 mM and 100 mM respectively). The coupling reagents and the building blocks were conveyed in a pulsed mode with 16 μL per pulse. The coupling protocol contains the

information about the conveyed substance, the pulse number and the duration of single steps in seconds. The time period of 0 s represents the minimum time of a single step. Used coupling reagents:

- Dblk: 3% dichloroacetic acid in DCM
- Wsh: acetonitrile
- Act: 450 mM tetrazole in acetonitrile
- Caps: acetic anhydride in THF/pyridine (Cap A) and N-methylimidazole in THF/pyridine (Cap B)
- Ox: iodine in water/THF/pyridine

Table 5.7: Standard coupling protocol for natural bases with thymine (T) as example.

Coding	Function	Mode	Amount /Arg1	Time (s) /Arg2
\$Deblocking				
144	Index Fract. Coll.	NA	1	0
0	Default	WAIT	0	1.5
141	Trityl Mon. On/Off	NA	1	1
16	Dblk	PULSE	10	0
16	Dblk	PULSE	50	49
38	Diverted Wsh A	PULSE	40	0
141	Trityl Mon. On/Off	NA	0	1
38	Diverted Wsh A	PULSE	40	0
144	Index Fract. Coll.	NA	2	0
\$Coupling				
1	Wsh	PULSE	5	0
2	Act	PULSE	5	0
21	T+Act	PULSE	5	0
21	T+Act	PULSE	2	16
2	Act	PULSE	3	24
1	Wsh	PULSE	7	56
1	Wsh	PULSE	8	0
\$Capping				

12	Wsh A	PULSE	20	0
13	Caps	PULSE	8	0
12	Wsh A	PULSE	6	15
12	Wsh A	PULSE	14	0
\$Oxidizing				
15	Ox	PULSE	15	0
12	Wsh A	PULSE	15	0
\$Capping				
13	Caps	PULSE	7	0
12	Wsh A	PULSE	30	0

For the photoenol(1) phosphoramidite **46** the coupling time was enhanced from 96 s to 560 s. Table 5.8 shows the modified section "\$Coupling" of standard protocol.

Table 5.8: Coupling protocol for the photoenol phosphoramidite **46**.

\$Coupling				
1	Wsh	PULSE	5	0
2	Act	PULSE	5	0
22	46 +Act	PULSE	5	0
22	46 +Act	PULSE	2	120
2	Act	PULSE	4	240
1	Wsh	PULSE	7	200
1	Wsh	PULSE	8	0

The synthesized **PE1-DNA1 48** was cleaved from the resin and deprotected by incubation with 25% aqueous ammonia solution at 60 °C for 3 h. The resin was filtered off, washed with de-ionized water and the solvents were removed in vacuum concentrator. The crude **PE1-DNA1 48** was re-dissolved in de-ionized water (500 µL) and purified by HPLC. Product fraction was collected and the solvent was removed in vacuum concentrator. After re-dissolving in de-ionized water (1.50 mL), **PE1-DNA1 48** was quantified by the absorbance at 260 nm on a Cary 300 Scan spectrophotometer and analyzed by MALDI-TOF (Table 5.9) and gel electrophoresis (21% PA gel, 30 min at 100 V, 50 min at 120 V in TBE running buffer).

Table 5.9: MALDI-TOF MS results for the photoenol modified oligonucleotide **PE1-DNA1 48**, theoretical and found values in [g/mol].

	[M] _{theo} [g/mol]	[M] _{found} [g/mol]
PE1-DNA1 48	4154	4153

H-Posphonate Method

For the photoenol modification of **DNA** (205 nmol) H-phosphonates **51** and **49** were used following the procedure below.

The commercial dimethoxytrityl (DMT) protected oligonucleotide (1.00 eq.) on controlled pore glass (CPG) solid support was deprotected with dichloroacetic acid (3% in DCM). The reaction completion was followed by color change from orange-yellow to colorless. The solid support was washed several times with acetonitrile, dried and transferred to a previously silanized flask. The H-phosphonate (350 eq.) was dissolved in anhydrous CH₃CN/pyridine (1:1, v/v) (360 mM) under inert atmosphere and added to the CPG. Pivaloyl chloride (100 eq., 100 mM in anhydrous CH₃CN/pyridine (1:1, v/v)) was added and the reaction mixture was stirred at 39 °C for 16 hours. The reaction solution was removed by centrifugation and the solid support washed five times with CH₃CN (5 mL). After treatment with standard DNA synthesis oxidizing solution (500 µL) for 10 minutes in case of modification with photoenol **51** and for 3 minutes, when photoenol **49** was used, the CPG was washed five times with CH₃CN (5 mL). The PE-modified sequence was deprotected and cleaved from the solid support by incubation with 750 µL 25% ammonia solution at 55 °C for 5 hours. The supernatant was collected and the solvents removed in vacuum concentrator. Photoenol modified oligonucleotide was dissolved in water and purified by reversed phase HPLC. The main fractions were collected, concentrated in vacuum concentrator, quantified by the absorbance at 260 nm on a Cary 300 Scan spectrophotometer and characterized by MALDI-TOF (Table 5.10) and PA gel electrophoresis (21% PA gel, 30 min at 100 V, 50 min at 120 V in TBE running buffer).

Table 5.10: MALDI-TOF MS results for the photoenol modified oligonucleotides; theoretical and found values in [g/mol].

	[M] _{theo} [g/mol]	[M] _{found} [g/mol]
PE1-DNA1 48	4154	4156
PE2-DNA1 53	4197	4196
PE2-DNA2 54	7356	7354

Amide Coupling via Active Ester (NHS ester) Method.

The commercial dimethoxytrityl (DMT) protected **NH₂-DNA2** (or **NH₂-DNA3**) (175.3 nmol, 1.00 eq. (or 177.6 nmol, 1.00 eq.)) on controlled pore glass (CPG) solid support was deprotected with dichloroacetic acid (3% in DCM). The reaction completion was followed by color change from orange-yellow to colorless. The solid support was washed five times (5 mL) with acetonitrile, dried and transferred to an Eppendorf® Safe-Lock tube. In another tube 20.0 mg (54.4 μmol, 310 eq.) NHS ester **55** were dissolved in 300 μL anhydrous DMF under inert atmosphere and added to the CPG. Subsequently, 10 μL (7.60 μg, 58.8 nmol, 0.335 eq.) DIPEA were added and the reaction mixture was incubated at 40 °C for 2 h. The reaction solution was removed by centrifugation and the solid support washed five times with DMF (5 mL) and three times with acetonitrile (3 mL). The PE-modified sequence was deprotected and cleaved from the solid support by incubation with 750 μL 25% ammonia solution at 55 °C for 5 hours. The supernatant was collected and the solvents removed in vacuum concentrator. Photoenol modified oligonucleotide was dissolved in water and purified by reversed phase HPLC. The main fractions were collected, concentrated in vacuum concentrator, quantified by the absorbance at 260 nm on a Cary 300 Scan spectrophotometer and characterized by MALDI-TOF (Table 5.11) and PA gel electrophoresis 21% PA gel, 30 min at 100 V, 50 min at 120 V in TBE running buffer.

For the modification of **NH₂-DNA2** with tetrazole moiety same procedure as described above with slight modification was used. For the coupling step 40.0 mg (102 μmol, 580 eq.) NHS ester **62** were dissolved in 700 μL anhydrous DMF under inert atmosphere and added to the CPG. Subsequently, 10 μL (7.60 μg, 58.8 nmol, 0.335 eq.) DIPEA were added and the reaction mixture was incubated at ambient temperature for 2 h. After purification the product was quantified by the absorbance at 260 nm on a Cary 300 Scan spectrophotometer and characterized by MALDI-TOF (Table 5.11) and PA gel electrophoresis 21% PA gel, 30 min at 100 V, 50 min at 120 V in TBE running buffer.

Table 5.11: MALDI-TOF MS results for the photoenol/tetrazole modified amino terminated oligonucleotides; theoretical and found values in [g/mol].

	[M] _{theo} [g/mol]	[M] _{found} [g/mol]
PE2-DNA2 56	7323	7324
PE2-DNA3 57	7243	7232
Tz-DNA2 63	7349	7349

5.4 Photoreactions

Photo-Induced Cycloaddition between Photoenol Modified Oligonucleotides PE2-DNA1 53 and PE2-DNA2 54 and Dienophile 64

For the initial photo-induced cycloaddition reactions between photoenol modified oligonucleotide and maleimide linker **64** the following procedure was used. The mixture of 2.00 nmol PE-DNA and 2.00 nmol dienophile **64** in 1.00 mL H₂O/CH₃CN (1:1, v/v) was placed into the headspace vial, which was crimped air-tight as described above, degassed by purging with argon for 15 minutes and subsequently irradiated for 16 hours in the photoreactor at $\lambda_{\max} = 320$ nm. After the irradiation the solvents were removed under reduced pressure, the residue re-dissolved in water and purified by reversed phase HPLC. The collected fractions were characterized by MALDI-TOF (Table 5.12) and native PAGE (21% PA gel, 30 min at 100 V, 50 min at 120 V in TBE running buffer).

Table 5.12: MALDI-TOF MS results for the photo-cycloadducts **66** und **67**; theoretical and found values in [g/mol].

	[M] _{theo} [g/mol]	[M] _{found} [g/mol]
Cycloadduct 67	7832	7838
Cycloadduct 66	4673	4675

Photo-Induced Cycloaddition between Photoenol-/Tetrazole Modified Oligonucleotides PE2-DNA2 56/Tz-DNA2 63 and Dienophile 64.

For the photo-induced cycloaddition reactions between photoenol/tetrazole modified oligonucleotides and maleimide linker **64** and for the control experiments the following procedure was used. Different amounts of dienophile **64** (5 eq., 15 eq. and 100 eq.) were tested. The mixture of 2.00 nmol modified DNA and a certain amount of dienophile **64** (5 eq., 15 eq. or 100 eq.) in 500 μ L H₂O/DMSO (3:2, v/v) was placed into the headspace vial, which was crimped air-tight as described above, deoxygenated by purging with argon for 15 minutes and subsequently irradiated for 2 hours in the photoreactor at $\lambda_{\max} = 320$ nm. After irradiation the reaction mixture was passed through NAP-5 and NAP-10 columns and eluted with water in order to remove DMSO and the excess of **64**. The solution was concentrated under reduced pressure and the residue re-dissolved in water (300 μ L) and purified by reversed phase HPLC.

The collected fractions were characterized by MALDI-TOF (Table 5.13) and native PAGE 21% PA gel, 30 min at 100 V, 50 min at 120 V in TBE running buffer.

Table 5.13: MALDI-TOF MS results for the photo-cycloadducts **68** and **69**, theoretical and found values in [g/mol].

	[M] _{theo} [g/mol]	[M] _{found} [g/mol]
Cycloadduct 68	7796	7794
Cycloadduct 69	7794	7792

Photo-Induced Cycloaddition between Photoenol Modified Oligonucleotide PE2-DNA2 54 and HRP-Mal.

Photo-Induced Cycloaddition between Photoenol Modified Oligonucleotide **PE2-DNA2 54** and HRP-Mal as well as the control reactions were performed using the following procedure. First HRP was functionalized with maleimide group in the coupling reaction with sulfo-SMCC. Sulfo-SMCC (2.00 mg, 4.58 μ mol, 138 eq.) was dissolved in 100 μ L DMF and added to 200 μ L HRP solution (33.2 nmol, 1.00 eq., 166 μ M in PBS buffer, pH 6.0) and incubated for 1 hour at room temperature. The excess sulfo-SMCC was removed by filtration of the reaction mixture through NAP-5 and NAP-10 columns. The buffer was exchanged using PBS buffer pH 7.1 as eluent.

For the photoreaction a mixture of 2.00 nmol **PE2-DNA2 54** and 2.20 nmol of fresh prepared HRP-Mal in 500 μ L of PBS/CH₃CN solution (3:2, v/v) was placed into the headspace vial, which was crimped air-tight as described above, degassed by purging with nitrogen for 15 minutes and subsequently irradiated for 16 hours in the photoreactor at $\lambda_{\max} = 320$ nm (± 30 nm, 36 W, Arimed B6, Cosmedico GmbH, Germany). The reaction mixture was filtered through NAP-5 and NAP-10 columns to exchange the buffer to 20 mM Tris/HCl pH 8.3, concentrated by using 5 kDa Vivaspin and purified by anion exchange chromatography using MonoQ 5/50 GL column (buffer A: 20 mM Tris, buffer B: 20 mM Tris, 1 M NaCl; gradient: linear increase of buffer B to 100 % in 30 minutes, flowrate: 1 mL/min). The concentration and buffer exchange to PBS of collected fractions were carried out by using 5 kDa Vivaspin, the characterization of product fraction was performed by native PAGE 12.5% PA gel, 30 min at 80 V, 90 min at 100 V in Tris/glycin running buffer.

Stability Test for HRP under Irradiation at $\lambda_{\text{max}} = 320 \text{ nm}$ ($\pm 30 \text{ nm}$).

For the stability tests, a solution of native HRP (2.00 nmol) in a mixture of PBS/CH₃CN (3:2) (500 mL) was placed into the headspace vials, which was crimped air-tight as described above, degassed by purging with nitrogen for 15 minutes and subsequently irradiated in the photoreactor at $\lambda_{\text{max}} = 320 \text{ nm}$ ($\pm 30 \text{ nm}$) for 16 hours. In order to remove acetonitrile from the reaction mixture the solution was passed through NAP-5 and NAP-10 and eluted with PBS. Subsequently, the solution was concentrated by using 5 kDa Vivaspinn and analyzed by SDS-PAGE (12.5% SDS-PA gel, 30 min at 80 V, 1 h at 100 V in SDS/Tris/glycine running buffer).

Peroxidase Activity Tests for HRP and HRP-DNA2 Conjugate (*Amplex®Red Assay*).

Peroxidase activity tests for HRP and **HRP-DNA2** conjugate were performed in black 96 well microtiterplates using a Synergy microplate reader (BioTek) to record the fluorescence signals of resorufin ($\lambda_{\text{ex}} = 530 \text{ nm}$, $\lambda_{\text{em}} = 590 \text{ nm}$, sensitivity = 70), which was formed by the oxidation of Amplex Red. The mixture of 2 pmol (0.500 μL , 3.74 μM) HRP or 2 pmol (0.800 μL , 2.57 μM) **HRP-DNA2** in sodium phosphate buffer (pH 6.0) and 1 nmol (5.00 μL , 200 μM) H₂O₂ was added to the wells (5 wells per sample). To each sample 5 nmol (10.0 μL , 0.500 mM) Amplex®Red were added and the final volume of each sample was adjusted to 100 μL with sodium phosphate buffer (pH 6.0). The measurements were done over a time period of 1 h for every sample.

5.4.1 Kinetic Study of the Photo-Induced Cycloaddition Reaction.**General procedure**

A solution of photoenol/tetrazole modified oligonucleotide (24 nmol, 1.00 eq.) and **64** (120 nmol, 5.00 eq. or 360 nmol, 15.0 eq.) in 3.00 mL of water/DMSO mixture (3:2, (v/v)) was placed in a headspace vial (Pyrex, diameter 20 mm, VWR, Germany) in the dark. The vial was crimped air-tight using SBR seal (VWR, Germany) with PTFE inner liner and the solution was deoxygenated by purging with argon for 15 minutes. Subsequently, the reaction mixture was aliquoted in 5 different headspace vials (500 μL in each; the vials were flushed with argon and crimped air-tight) in a glove box and irradiated for 0 min, 15 min, 30 min, 1 h and 3 h by revolving around a compact low-pressure fluorescent lamp with $\lambda_{\text{max}} = 320 \text{ nm}$ at a distance of 40-50 mm in a custom-built photoreactor. Each reaction mixture was passed through NAP-5 and NAP-10 columns and eluted with water in order to remove DMSO and the excess of **64**.

Solvent was removed in vacuum concentrator and the residues were re-dissolved in 200 μ L water. One part of the solution (100 μ L) was analyzed by reversed phase HPLC. The other 100 μ L of each sample were mixed with 100 μ L of a mixture acetonitrile/water (1:1, (v/v)) and 1% AcOH, filtered with syringe filter (GHP Acrodisc® 13 mm syringe filter with 0.2 μ m GHP membrane from PALL Life Sciences) and analyzed by ESI-MS.

Irradiation of Tz-DNA2 63 and 100 eq. of dienophile 64.

A solution of **Tz-DNA2 63** (9.00 nmol, 1.00 eq.) and **64** (900 nmol, 100 eq.) in 1.50 mL of water/DMSO mixture (3:2, (v/v)) was placed in a headspace vial (Pyrex, diameter 20 mm, VWR, Germany) in the dark. The vial was crimped air-tight using SBR seal (VWR, Germany) with PTFE inner liner and the solution was deoxygenated by purging with argon for 15 minutes. Subsequently, the reaction mixture was aliquoted in 3 different headspace vials (500 μ L in each; the vials were flushed with argon and crimped air-tight) in a glove box and irradiated for 1 h, 5 h and 24 h by revolving around a compact low-pressure fluorescent lamp with $\lambda_{\text{max}} = 320$ nm at a distance of 40-50 mm in a custom-built photoreactor. Each reaction mixture was passed through NAP-5 and NAP-10 columns and eluted with water in order to remove DMSO and the excess of **64**. Solvent was removed in vacuum concentrator and the residues were re-dissolved in 200 μ L water. One part of the solution (100 μ L) was analyzed by reversed phase HPLC. The other 100 μ L of each sample were mixed with 100 μ L of a mixture acetonitrile/water (1:1, (v/v)) and 1% AcOH, filtered with syringe filter (GHP Acrodisc® 13 mm syringe filter with 0.2 μ m GHP membrane from PALL Life Sciences) and analyzed by ESI-MS.

The Detailed Time Resolution of the Photo-Induced Cycloaddition Reaction between the Photoenol/Tetrazole Modified Oligonucleotides and the Dienophile 64.

A solution of photoenol/tetrazole modified oligonucleotide (16.0 nmol, 1.00 eq.) and **64** (80.0 nmol, 5.00 eq. or 240 nmol, 15.0 eq.) in 4.00 mL of water/DMSO mixture (3:2, (v/v)) was placed in a headspace vial (Pyrex, diameter 20 mm, VWR, Germany) in the dark. The vial was crimped air-tight using SBR seal (VWR, Germany) with PTFE inner liner and the solution was deoxygenated by purging with argon for 15 minutes. Subsequently, the reaction mixture was aliquoted in 7 different headspace vials (500 μ L in each; the vials were flushed with argon and crimped air-tight) in a glove box and irradiated for 0 min, 1 min, 5 min, 10 min, 15 min, 1 h and 5 h by revolving around a compact low-pressure fluorescent lamp with

$\lambda_{\max} = 320 \text{ nm}$ at a distance of 40-50 mm in a custom-built photoreactor. Each reaction mixture was passed through NAP-5 and NAP-10 columns and eluted with water in order to remove DMSO and the excess of **64**. Solvent was removed in vacuum concentrator and the residues were re-dissolved in 100 μL water. Each sample was mixed with 100 μL of a mixture acetonitrile/water (1:1, (v/v)) and 1% AcOH, filtered with syringe filter (GHP Acrodisc® 13 mm syringe filter with 0.2 μm GHP membrane from PALL Life Sciences) and analyzed by ESI-MS.

5.4.2 Spatially Controlled Immobilization of PE2-DNA2 54 on Maleimide Functionalized Silicon Wafers.

For the spatially controlled immobilization of **PE2-DNA2 54**, maleimide functionalized silicon wafer⁹ was mounted into the sample holder with a shadow mask and placed into the **PE2-DNA2 54** solution (1.75 μM , 4.00 mL) in PBS/CH₃CN (1:1, v/v). The vial was crimped air-tight using SBR seals with PTFE inner liner. The solution was deoxygenated by purging with argon for 15 min and subsequently irradiated for 5 h by revolving around a compact low-pressure fluorescent lamp with $\lambda_{\max} = 320 \text{ nm}$ at a distance of 40-50 mm in a custom-built photoreactor. After irradiation, the mask was removed. The surface was rinsed with de-ionized water and sonicated in water for 10 s, in order to remove any possibly physisorbed material. The surface was subsequently washed with PBS buffer, MQ water, DMF, DMSO, again with MQ water and finally dried under a nitrogen stream. The surface was then analyzed by ToF-SIMS. For the control experiment the same procedure as described above was applied for the non-modified **DNA2**.

Hybridization of immobilized PE2-DNA2 54 with complementary Cy@3 labeled cDNA2.

The surface with immobilized **PE2-DNA2 54** was covered with a 50 μM solution of complementary **DNA2** labeled with Cy@3 dye ($\lambda_{\text{Exc}}=550 \text{ nm}$, $\lambda_{\text{Em}}=570 \text{ nm}$) in TETBS buffer (pH = 7.5) and incubated in the dark at ambient temperature overnight. The surface was then washed several times with MQ water, TETBS buffer and again with MQ water, dried under a nitrogen stream and analyzed by fluorescence microscopy. For the control experiment, the surface with immobilized **PE2-DNA2** was covered with non-complementary DNA4 labeled with Cy@3 dye using the same procedure as described above.

⁹ The functionalization of silicon wafers with maleimide moiety was conducted by Doris Abt, Institute for Technical Chemistry and Polymer Chemistry, Karlsruhe Institute of Technology (KIT), using the procedure described by Yameen *et al.*

5.4.3 Direct Laser Writing (DLW).

Cleaning and Functionalization of Glass Surfaces with Maleimide Moiety.

Substrate Preparation.

High precision microscope cover glasses (22×22 mm, 170±5µm, No. 1.5H) were cleaned with acetone wetted KimTech wipes, placed into the slides holder and heated in a solution of 40.0 mL 25% ammonia solution, 40.0 mL 30% H₂O₂ and 200 mL MQ water (1:1:5, v/v/v) in a glass chamber at 150 °C for 1 h. Each glass was thoroughly rinsed with MQ water, EtOH, MQ water and finally dried under a nitrogen stream. Glasses were placed on a glass Petri dish and exposed to oxygen plasma (300 W) for 5 min just before silanization.

APTES Functionalized Glass Substrates.

Silanization solution was prepared by mixing 93.005% MeOH (235 mL), 5% MQ water (12.5 mL), 0.005% glacial acetic acid (12.0 µL) and 1% APTES (2.50 mL). Plasma activated glasses were shaken in the silanization solution at ambient temperature for 1 h and finally thoroughly rinsed with EtOH and MQ water. The glass substrates were subsequently annealed at 100 °C for 1 h, kept under vacuum for 2 h and stored under inert atmosphere before maleimide functionalization.

Maleimide Functionalized Glass Substrates.

The APTES functionalized glass substrates were separately immersed in 55.0 mM CH₂Cl₂ solution of triethylamine (12.0 mL) in Falcon® 50 mL centrifuge tubes. Equal volume (12.0 mL) of a 50.0 mM solution of 4-maleimidobutyryl chloride **78** in anhydrous CH₂Cl₂ was added under inert atmosphere and the reaction was proceed at ambient temperature overnight. Maleimide functionalized substrates were thoroughly rinsed with CH₂Cl₂ and MeOH and additionally kept in MeOH overnight, in order to remove the quaternary triethylammonium salt. The substrates were rinsed with MeOH, dried under a nitrogen stream and stored under inert atmosphere at ambient temperature.

Dose and Resolution Tests

The maleimide functionalized glass slide was mounted in the DLW sample holder and a droplet of an immersion oil was placed on one glass side. The sample was placed into the DLW setup and a droplet of a freshly prepared, filtered (GHP Acrodisc® 13 mm syringe filter

with 0.2 μm GHP membrane from PALL Life Sciences) 10.0 μM solution of **PE2-DNA2 56** in 0.5 \times SSC (pH 7.0)/DMSO (3:2, v/v) was placed on maleimide functionalized glass side. On the same surface dose and resolution test were performed in the 100 \times 100 μm^2 squares respectively. For the dose tests 2 μm long lines were written with the scanning speed of 100 $\mu\text{m s}^{-1}$ and a scan number of 4 by linear increasing of laser power from 0 mW (bottom) to 20 mW (top) and variation of the laser focus position (z position) at the interface from -z (left) to +z (right). For the resolution tests a pattern of 6 \times 7 segments with 10 μm long lines and different distances between the lines were written by variation of the laser power from left to right (0.4 mW, 0.8 mW, 2 mW, 4 mW, 8 mW, 16 mW, 24 mW) and decrease of the line distance from bottom to top (1 μm , 0.8 μm , 0.7 μm , 0.6 μm , 0.5 μm , 0.4 μm). Sample development was performed by immersing the sample in 2 \times SSC, 0.2% SDS (20 mL, 10 min), after short sonication (5 s) the sample was immersed into 2 \times SSC (20 mL, 10 min), then into 0.1 \times SSC, 0.1% SDS (20 mL, 10 min) and finally rinsed thoroughly with MQ water and dried under a stream of nitrogen.

Hybridization of immobilized PE2-DNA2 56 with complementary Cy@3-cDNA2.

The surface with immobilized **PE2-DNA2 56** was blocked with BSA prior to hybridization. The sample was immersed in a solution of 5 \times SSC/SDS/BSA (98.9% / 0.1% / 1%) and incubated in a water bath at 43 $^{\circ}\text{C}$ for 1 h. Subsequently, the sample was rinsed thoroughly with MQ water and placed in TETBS buffer. A solution of **Cy@3-cDNA2** in TETBS buffer was heated to 95 $^{\circ}\text{C}$ for 5 min and added to the sample, so that the final concentration was 200 nM. The sample was incubated in the dark at ambient temperature for 1.5 h, washed by immersing in 2 \times SSC, 0.2% SDS (20 mL, 5 min), 2 \times SSC (20 mL, 5 min), in 0.1 \times SSC, 0.1% SDS (20 mL, 10 min) and finally rinsed thoroughly with MQ water and dried under a stream of nitrogen.

Writing of Two Different DNA Sequences.

In order to perform the writing of two different DNA sequences, a 3D polymer frame (100 \times 100 μm^2) as a visual reference object was written with tetraphotoenol photoresist. The tetraphotoenol was synthesized by Dr. Alexander Quick, Institute for Technical Chemistry and Polymer Chemistry, Karlsruhe Institute of Technology (KIT) using the previously reported procedure.^[229] The maleimide functionalized glass slide was mounted in the DLW sample holder and a droplet of an immersion oil was placed on one glass side. The sample was placed into the DLW setup and a droplet of a tetraphotoenol photoresist (27.3 mM in γ -

butyrolactone/acetophenone (1:1, v/v)) was placed on maleimide functionalized glass side. The frame was written with the scanning speed of $10 \mu\text{m s}^{-1}$ and 12.0 mW laser power. Sample development was performed by immersing the sample in acetone for several minutes. The sample was rinsed with acetone and MQ water, dried under a stream of nitrogen, mounted in the DLW sample holder and a droplet of an immersion oil was placed on one glass side. A droplet of a freshly prepared, filtered (GHP Acrodisc® 13 mm syringe filter with $0.2 \mu\text{m}$ GHP membrane from PALL Life Sciences) $30.0 \mu\text{M}$ solution of **PE2-DNA2 56** in $0.5\times\text{SSC}$ (pH 7.0)/DMSO (3:2, v/v) was placed on maleimide functionalized glass side. A pattern of line segments and checkerboard pattern were written with the scanning speed of $50 \mu\text{m s}^{-1}$, 4 scans and 6 mW laser power. Subsequently, the sample was developed by immersing in $2\times\text{SSC}$, 0.2% SDS (20 mL, 10 min), sonicated for 5 s, immersed into $2\times\text{SSC}$ (20 mL, 10 min), then into $0.1\times\text{SSC}$, 0.1% SDS (20 mL, 10 min) and finally rinsed thoroughly with MQ water and dried under a stream of nitrogen. Then the sample was mounted in the DLW sample holder and again the immersion oil was dripped on one glass side. The sample was placed into the DLW setup and a droplet of a freshly prepared, filtered $30.0 \mu\text{M}$ solution of **PE2-DNA3 57** in $0.5\times\text{SSC}$ (pH 7.0)/DMSO (3:2, v/v) was placed on maleimide functionalized glass side. The sample was positioned according to the previous writing settings and the patterns were completed with the second sequence. The sample was developed as described before.

Hybridization of immobilized PE2-DNA2 56 and PE2-DNA3 57 with complementary Cy@3-cDNA2 and Cy@5-cDNA3.

The surface with immobilized **PE2-DNA2 56** and **PE2-DNA3 57** was blocked with BSA prior to hybridization. The sample was immersed in a solution of $5\times\text{SSC}/\text{SDS}/\text{BSA}$ (98.9% / 0.1% / 1%) and incubated in a water bath at $43 \text{ }^\circ\text{C}$ for 1 h. Subsequently, the sample was rinsed thoroughly with MQ water and placed in TETBS buffer. A solution of **Cy@3-cDNA2** and **Cy@5-cDNA3** in TETBS buffer was heated to $95 \text{ }^\circ\text{C}$ for 5 min and added to the sample, so that the final concentration was 200 nM. The sample was incubated in the dark at ambient temperature for 1.5 h. The sample was washed by immersing in $2\times\text{SSC}$, 0.2% SDS (20 mL, 5 min), $2\times\text{SSC}$ (20 mL, 5 min), in $0.1\times\text{SSC}$, 0.1% SDS (20 mL, 10 min) and finally rinsed thoroughly with MQ water and dried under a stream of nitrogen.

5.4.4 Synthesis of Do-TEG-Mal 71 Coated Copper Nanoparticles.

Dopamine-maleimide coated copper nanoparticles were synthesized employing a literature procedure.^[236] A solution of 29.0 mg (125 μmol , 0.500 eq.) Do-TEG-Mal **71** and 39.0 mg (125 μmol , 0.500 eq.) dopamine-triethylene glycol methyl ether **72** (as an inert linker) in 4.00 mL $\text{CH}_3\text{CN}/\text{H}_2\text{O}$ (1:1, v/v) was heated under inert atmosphere to 80 °C. $\text{CuCl}_2 \cdot 2\text{H}_2\text{O}$ (42.0 mg, 250 μmol , 1.00 eq.) was dissolved in 1.00 mL $\text{CH}_3\text{CN}/\text{H}_2\text{O}$ (1:1, v/v) and added dropwise to the dopamine linkers solution. The reaction mixture was stirred at 80 °C for 10 h. Synthesized nanoparticles were analyzed by UV-Vis spectroscopy.

Synthesis of NTA 75 Coated Copper Nanoparticles.

A typical synthesis was performed under inert atmosphere in order to avoid moisture and oxygen during the reaction. In a 25 mL two necked round bottom flask $\text{CuCl}_2 \cdot 2\text{H}_2\text{O}$ (17.0 mg, 100 μmol , 1.00 eq.) and NTA**75** (33.7 mg, 85.0 μmol , 0.850 eq.) were dissolved in 5.00 mL diethylene glycol and heated to 100 °C. In another 5 mL round bottom flask 2.50 mL diethylene glycol were heated to 100 °C and at this temperature 18.9 mg (500 μmol , 5.00 eq.) NaBH_4 were added. The solution was added dropwise to the copper solution under vigorous stirring. The solution color turned from blue-green to brownish black due to the formation of copper nanoparticles. After slow cooling to ambient temperature, the as-prepared nanoparticles were collected by centrifugation and washed three times by centrifugation in a 1:1 mixture of EtOH and isopropanol. The washed nanoparticles were re-dispersed in isopropanol and analyzed by UV-Vis spectroscopy. Different copper/linker ratios were tested in order to investigate the stability of copper nanoparticles (Table 5.14).

Table 5.14: Reactant amounts used for the synthesis of CuNPs.

$\text{CuCl}_2 \cdot 2\text{H}_2\text{O}$	NTA Linker	NaBH_4	Stability
1.00 eq.	0.680 eq.	8.00 eq.	-
1.00 eq.	1.00 eq.	4.00 eq.	-
1.00 eq.	0.100 eq.	8.00 eq.	2 h
1.00 eq.	0.150 eq.	8.00 eq.	2 h
1.00 eq.	0.200 eq.	8.00 eq.	7 days
1.00 eq.	0.400 eq.	8.00 eq.	-

Synthesis of NTA-Mal **81 Coated Copper Nanoparticles.**

In a 25 mL two necked round bottom flask $\text{CuCl}_2 \cdot 2\text{H}_2\text{O}$ (21.3 mg, 125 μmol , 1.00 eq.) and NTA-Mal **81** (10.7 mg, 24.9 μmol , 0.200 eq.) were dissolved in 5.00 mL diethylene glycol and heated to 100 °C. In another 5 mL round bottom flask 2.50 mL diethylene glycol were heated to 100 °C and at this temperature 37.8 mg (999 μmol , 8.00 eq.) NaBH_4 were added. The solution was added dropwise to the copper solution under vigorous stirring. The solution color turned from blue-green to brownish black due to the formation of copper nanoparticles. After slow cooling to ambient temperature, the as-prepared nanoparticles were collected by centrifugation and washed three times by centrifugation from a 1:1 mixture of EtOH and DMSO. The washed nanoparticles were re-dispersed in DMSO and analyzed by UV-Vis spectroscopy.

6 Bibliography

- [1] a) R. Dahm, *Hum. Genet.* **2008**, *122*, 565-581; b) O. T. Avery, C. M. Macleod, M. McCarty, *J. Exp. Med.* **1944**, *79*, 137-158; c) E. Chargaff, E. Vischer, R. Doniger, C. Green, F. Misani, *J. Biol. Chem.* **1949**, *177*, 405-416; d) E. Chargaff, *Fed. Proc.* **1951**, *10*, 654-659; e) A. D. Hershey, M. Chase, *J. Gen. Physiol.* **1952**, *36*, 39-56; f) J. D. Watson, F. H. C. Crick, *Nature* **1953**, *171*, 737-738; g) J. H. Matthaei, O. W. Jones, R. G. Martin, M. W. Nirenberg, *Proc. Natl. Acad. Sci.* **1962**, *48*, 666-677; h) A. M. Maxam, W. Gilbert, *Proc. Natl. Acad. Sci.* **1977**, *74*, 560-564; i) J. Schmutz, J. Wheeler, J. Grimwood, M. Dickson, J. Yang, C. Caoile, E. Bajorek, S. Black, Y. M. Chan, M. Denys, J. Escobar, D. Flowers, D. Fotopulos, C. Garcia, M. Gomez, E. Gonzales, L. Haydu, F. Lopez, L. Ramirez, J. Retterer, A. Rodriguez, S. Rogers, A. Salazar, M. Tsai, R. M. Myers, *Nature* **2004**, *429*, 365-368.
- [2] a) I. Grissa, G. Vergnaud, C. Pourcel, *Nucl. Acids Res.* **2007**, *35*, W52-W57; b) E. R. Westra, D. C. Swarts, R. H. Staals, M. M. Jore, S. J. Brouns, J. van der Oost, *Annu. Rev. Genet.* **2012**, *46*, 311-339; c) A. Marchfelder, *RNA Biol.* **2013**, *10*, 655-658; d) W. Zhou, A. Deiters, *Angew. Chem. Int. Ed.* **2016**, *55*, 5394-5399.
- [3] a) N. A. W. Bell, U. F. Keyser, *Nat. Nanotechnol.* **2016**, *11*, 645-651; b) J. L. Kong, N. A. W. Bell, U. F. Keyser, *Nano Lett.* **2016**, *16*, 3557-3562; c) K. Gopfrich, C. Y. Li, I. Mames, S. P. Bhamidimarri, M. Ricci, J. Yoo, A. Mames, A. Ohmann, M. Winterhalter, E. Stulz, A. Aksimentiev, U. F. Keyser, *Nano Lett.* **2016**, *16*, 4665-4669; d) Y. R. Yang, Y. Liu, H. Yan, *Bioconjugate Chem.* **2015**, *26*, 1381-1395; e) J. List, E. Falgenhauer, E. Kopperger, G. Pardatscher, F. C. Simmel, *Nat. Commun.* **2016**, *7*, 12414-12419.
- [4] a) Y. C. Hung, W. T. Hsu, T. Y. Lin, L. Fruk, *Appl. Phys. Lett.* **2011**, *99*, 253301-253303; b) C. Y. Hung, W. T. Tu, Y. T. Lin, L. Fruk, Y. C. Hung, *J. Appl. Phys.* **2015**, *118*, 235503-235510; c) Y. W. Kwon, D. H. Choi, J. I. Jin, *Polym. J.* **2012**, *44*, 1191-1208.
- [5] N. C. Seeman, *J. Theor. Biol.* **1982**, *99*, 237-247.
- [6] H. Yan, T. H. LaBean, L. Feng, J. H. Reif, *Proc. Natl. Acad. Sci. USA* **2003**, *100*, 8103-8108.
- [7] W. M. Shih, J. D. Quispe, G. F. Joyce, *Nature* **2004**, *427*, 618-621.
- [8] P. W. Rothmund, *Nature* **2006**, *440*, 297-302.
- [9] a) L. Fruk, C. M. Niemeyer, *Angew. Chem. Int. Ed.* **2005**, *44*, 2603-2606; b) C. M. Niemeyer, B. Ceyhan, *Angew. Chem. Int. Ed.* **2001**, *40*, 3685-3688; c) D. M. Bauer, I. Ahmed, A. Vigovskaya, L. Fruk, *Bioconjugate Chem.* **2013**, *24*, 1094-1101; d) Z. Zhao, E. L. Jacovetty, Y. Liu, H. Yan, *Angew. Chem. Int. Ed.* **2011**, *50*, 2041-2044.
- [10] a) C. M. Niemeyer, L. Boldt, B. Ceyhan, D. Blohm, *Anal. Biochem.* **1999**, *268*, 54-63; b) P. K. Dutta, R. Varghese, J. Nangreave, S. Lin, H. Yan, Y. Liu, *J. Am. Chem. Soc.* **2011**, *133*, 11985-11993; c) G. Shtenberg, N. Massad-Ivanir, S. Engin, M. Sharon, L. Fruk, E. Segal, *Nanoscale Res. Lett.* **2012**, *7*, 443-448.
- [11] a) G. Shtenberg, N. Massad-Ivanir, L. Fruk, E. Segal, *ACS Appl. Mater. Interfaces* **2014**, *6*, 16049-16055; b) G. Shtenberg, N. Massad-Ivanir, O. Moscovitz, S. Engin, M. Sharon, L. Fruk, E. Segal, *Anal. Chem.* **2013**, *85*, 1951-1956; c) C. M. Niemeyer, *Angew. Chem. Int. Ed.* **2010**, *49*, 1200-1216; d) R. Meyer, S. Giselsbrecht, B. E. Rapp, M. Hirtz, C. M. Niemeyer, *Curr. Opin. Chem. Biol.* **2014**, *18*, 8-15.
- [12] J. W. de Vries, F. Zhang, A. Herrmann, *J. Control. Release* **2013**, *172*, 467-483.
- [13] a) K. E. Dunn, F. Dannenberg, T. E. Ouldrige, M. Kwiatkowska, A. J. Turberfield, J. Bath, *Nature* **2015**, *525*, 82-86; b) F. Dannenberg, K. E. Dunn, J. Bath, M.

- Kwiatkowska, A. J. Turberfield, T. E. Ouldrige, *J. Chem. Phys.* **2015**, *143*, 165102-165123.
- [14] a) Y. W. Kwon, C. H. Lee, D. H. Choi, J. I. Jin, *J. Mater. Chem.* **2009**, *19*, 1353-1380; b) M. R. Jones, N. C. Seeman, C. A. Mirkin, *Science* **2015**, *347*, 1260901-1260911; c) Y. C. Hung, D. M. Bauer, I. Ahmed, L. Fruk, *Methods* **2014**, *67*, 105-115.
- [15] Y. C. Hung, P. Mueller, Y. S. Wang, L. Fruk, *Nanoscale* **2012**, *4*, 5585-5587.
- [16] A. J. Steckl, *Nat. Photonics* **2007**, *1*, 3-5.
- [17] G. Roelfes, B. L. Feringa, *Angew. Chem. Int. Ed.* **2005**, *44*, 3230-3232.
- [18] B. M. Paterson, B. E. Roberts, E. L. Kuff, *Proc. Natl. Acad. Sci.* **1977**, *74*, 4370-4374.
- [19] M. L. Stephenson, P. C. Zamecnik, *Proc. Natl. Acad. Sci.* **1978**, *75*, 285-288.
- [20] J. B. Opalinska, A. M. Gewirtz, *Nature Rev.* **2002**, *1*, 503-514.
- [21] R. Juliano, M. R. Alam, V. Dixit, H. Kang, *Nucl. Acids Res.* **2008**, *36*, 4158-4171.
- [22] a) Y. Dorsett, T. Tuschl, *Nature Rev.* **2004**, *3*, 318-329; b) K. E. Maier, M. Levy, *Mol. Ther. Methods Clin. Dev.* **2016**, *5*, 16014.
- [23] E. S. Gragoudas, A. P. Adamis, E. T. Cunningham, Jr., M. Feinsod, D. R. Guyer, *N. Engl. J. Med.* **2004**, *351*, 2805-2816.
- [24] N. M. Bell, J. Micklefield, *ChemBioChem* **2009**, *10*, 2691-2703.
- [25] Y. Singh, N. Spinelli, E. Defrancq, *Curr. Org. Chem.* **2008**, *12*, 263-290.
- [26] S. D. Patil, D. G. Rhodes, D. J. Burgess, *AAPS J.* **2005**, *7*, E61-77.
- [27] a) H. Lonnberg, *Bioconjugate Chem.* **2009**, *20*, 1065-1094; b) T. S. Zatsepin, T. S. Oretskaya, *Chem. Biodivers.* **2004**, *1*, 1401-1417.
- [28] A. M. Michelson, A. R. Todd, *J. Chem. Soc.* **1955**, 2632-2638.
- [29] K. L. Agarwal, H. Buchi, M. H. Caruthers, N. Gupta, H. G. Khorana, K. Kleppe, A. Kumar, E. Ohtsuka, U. L. Rajbhandary, J. H. Van de Sande, V. Sgaramella, H. Weber, T. Yamada, *Nature* **1970**, *227*, 27-34.
- [30] H. Schaller, G. Weimann, H. G. Khorana, B. Lerch, *J. Am. Chem. Soc.* **1963**, *85*, 3821-3827.
- [31] G. S. Ti, B. L. Gaffney, R. A. Jones, *J. Am. Chem. Soc.* **1982**, *104*, 1316-1319.
- [32] M. Smith, H. G. Khorana, D. H. Rammner, I. H. Goldberg, *J. Am. Chem. Soc.* **1962**, *84*, 430-440.
- [33] E. L. Brown, R. Belagaje, M. J. Ryan, H. G. Khorana, *Methods Enzymol.* **1979**, *68*, 109-151.
- [34] a) R. L. Letsinger, M. J. Kornet, *J. Am. Chem. Soc.* **1963**, *85*, 3045-3046; b) R. L. Letsinger, K. K. Ogilvie, P. S. Miller, *J. Am. Chem. Soc.* **1969**, *91*, 3360-3365; c) R. L. Letsinger, K. K. Ogilvie, *J. Am. Chem. Soc.* **1969**, *91*, 3350-3355.
- [35] R. B. Merrifield, *J. Am. Chem. Soc.* **1963**, *85*, 2149-2154.
- [36] R. L. Letsinger, M. J. Kornet, V. Mahadevan, D. M. Jerina, *J. Am. Chem. Soc.* **1964**, *86*, 5163-5165.
- [37] a) M. H. Caruthers, *J. Biol. Chem.* **2013**, *288*, 1420-1427; b) S. L. Beaucage, M. H. Caruthers, *Tetrahedron Lett.* **1981**, *22*, 1859-1862.
- [38] a) R. L. Letsinger, J. L. Finnan, *J. Am. Chem. Soc.* **1975**, *97*, 7197-7198; b) R. L. Letsinger, W. B. Lunsford, *J. Am. Chem. Soc.* **1976**, *98*, 3655-3661.
- [39] L. J. McBride, M. H. Caruthers, *Tetrahedron Lett.* **1983**, *24*, 245-248.
- [40] S. Roy, M. Caruthers, *Molecules* **2013**, *18*, 14268-14284.
- [41] J. Katzhendler, S. Cohen, E. Rahamim, M. Weisz, I. Ringel, J. Deutsch, *Tetrahedron* **1989**, *45*, 2777-2792.
- [42] a) A. Vanaerschot, P. Herdewijn, H. Vanderhaeghe, *Nucleos. Nucleot.* **1988**, *7*, 75-90; b) L. Arnold, Z. Tocik, E. Bradkova, Z. Hostomsky, V. Paces, J. Smrt, *Collect. Czech. Chem. Commun.* **1989**, *54*, 523-532.
- [43] S. L. Beaucage, R. P. Iyer, *Tetrahedron* **1992**, *48*, 2223-2311.
- [44] R. H. Hall, A. Todd, R. F. Webb, *J. Chem. Soc.* **1957**, 3291-3296.

- [45] P. J. Garegg, I. Lindh, T. Regberg, J. Stawinski, R. Stromberg, C. Henrichson, *Tetrahedron Lett.* **1986**, 27, 4051-4054.
- [46] B. C. Froehler, M. D. Matteucci, *Tetrahedron Lett.* **1986**, 27, 469-472.
- [47] J. A. Dougan, A. K. Reid, D. Graham, *Tetrahedron Lett.* **2010**, 51, 5787-5790.
- [48] M. Sobkowski, A. Kraszewski, J. Stawinski, *Top. Curr. Chem.* **2015**, 361, 137-178.
- [49] A. Kraszewski, J. Stawinski, *Pure Appl. Chem.* **2007**, 79, 2217-2227.
- [50] B. Froehler, P. Ng, M. Matteucci, *Nucl. Acids Res.* **1988**, 16, 4831-4839.
- [51] S. Agrawal, J. Y. Tang, *Tetrahedron Lett.* **1990**, 31, 7541-7544.
- [52] J. Stawinski, M. Thelin, *J. Org. Chem.* **1994**, 59, 130-136.
- [53] a) J. C. Catlin, F. Cramer, *J. Org. Chem.* **1973**, 38, 245-250; b) S. A. Narang, H. M. Hsiung, R. Brousseau, *Methods Enzymol.* **1979**, 68, 90-98.
- [54] S. S. Jones, B. Rayner, C. B. Reese, A. Ubasawa, M. Ubasawa, *Tetrahedron* **1980**, 36, 3075-3085.
- [55] J. H. Vanboom, P. M. J. Burgers, P. H. Vandeursen, F. M. Derooy, C. B. Reese, *J. Chem. Soc. Chem. Commun.* **1976**, 167-168.
- [56] Y. Singh, P. Murat, E. Defrancq, *Chem. Soc. Rev.* **2010**, 39, 2054-2070.
- [57] a) L. Y. Wang, Y. Feng, Y. W. Sun, Z. B. Li, Z. Q. Yang, Y. M. He, Q. H. Fan, D. S. Liu, *Soft Matter*. **2011**, 7, 7187-7190; b) R. Kumar, A. El-Sagheer, J. Tumpene, P. Lincoln, L. M. Wilhelmsson, T. Brown, *J. Am. Chem. Soc.* **2007**, 129, 6859-6864; c) C. MacKellar, D. Graham, D. W. Will, S. Burgess, T. Brown, *Nucl. Acids Res.* **1992**, 20, 3411-3417; d) A. Roget, H. Bazin, R. Teoule, *Nucl. Acids Res.* **1989**, 17, 7643-7651.
- [58] E. Pettersson, J. Lundeberg, A. Ahmadian, *Genomics* **2009**, 93, 105-111.
- [59] R. B. Altman, D. S. Terry, Z. Zhou, Q. S. Zheng, P. Geggier, R. A. Kolster, Y. F. Zhao, J. A. Javitch, J. D. Warren, S. C. Blanchard, *Nat. Methods* **2012**, 9, 68-71.
- [60] M. Kwak, A. Herrmann, *Angew. Chem. Int. Ed.* **2010**, 49, 8574-8587.
- [61] Z. Y. Zhao, L. Y. Wang, Y. Liu, Z. Q. Yang, Y. M. He, Z. B. Li, Q. H. Fan, D. S. Liu, *Chem. Commun.* **2012**, 48, 9753-9755.
- [62] R. M. Franzini, F. Samain, M. Abd Elrahman, G. Mikutis, A. Nauer, M. Zimmermann, J. Scheuermann, J. Hall, D. Neri, *Bioconjugate Chem.* **2014**, 25, 1453-1461.
- [63] V. Lapiene, F. Kukulka, K. Kiko, A. Arndt, C. M. Niemeyer, *Bioconjugate Chem.* **2010**, 21, 921-927.
- [64] a) C. M. Niemeyer, T. Sano, C. L. Smith, C. R. Cantor, *Nucleic Acids Res.* **1994**, 22, 5530-5539; b) R. D. Joerger, T. M. Truby, E. R. Hendrickson, R. M. Young, R. C. Ebersole, *Clin. Chem.* **1995**, 41, 1371-1377.
- [65] a) H. C. Kolb, M. G. Finn, K. B. Sharpless, *Angew. Chem. Int. Ed.* **2001**, 40, 2004-2021; b) V. V. Rostovtsev, L. G. Green, V. V. Fokin, K. B. Sharpless, *Angew. Chem. Int. Ed.* **2002**, 41, 2596-2599.
- [66] T. R. Chan, R. Hilgraf, K. B. Sharpless, V. V. Fokin, *Org. Lett.* **2004**, 6, 2853-2855.
- [67] a) I. S. Marks, J. S. Kang, B. T. Jones, K. J. Landmark, A. J. Cleland, T. A. Taton, *Bioconjugate Chem.* **2011**, 22, 1259-1263; b) N. J. Agard, J. A. Prescher, C. R. Bertozzi, *J. Am. Chem. Soc.* **2004**, 126, 15046-15047.
- [68] a) P. M. E. Gramlich, C. T. Wirges, A. Manetto, T. Carell, *Angew. Chem. Int. Ed.* **2008**, 47, 8350-8358; b) A. H. El-Sagheer, T. Brown, *Chem. Soc. Rev.* **2010**, 39, 1388-1405; c) M. M. Haque, X. H. Peng, *Sci. China Chem.* **2014**, 57, 215-231.
- [69] H. Isobe, T. Fujino, N. Yamazaki, M. Guillot-Nieckowski, E. Nakamura, *Org. Lett.* **2008**, 10, 3729-3732.
- [70] J. Timper, K. Gutmiedl, C. Wirges, J. Broda, M. Noyong, J. Mayer, T. Carell, U. Simon, *Angew. Chem. Int. Ed.* **2012**, 51, 7586-7588.
- [71] L. Fruk, A. Grondin, W. E. Smith, D. Graham, *Chem. Commun.* **2002**, 2100-2101.
- [72] C. C. Wang, T. S. Seo, Z. Li, H. Ruparel, J. Ju, *Bioconjugate Chem.* **2003**, 14, 697-701.
- [73] C. S. McKay, M. G. Finn, *Chem. Biol.* **2014**, 21, 1075-1101.

- [74] R. S. Sorensen, A. H. Okholm, D. Schaffert, A. L. Kodal, K. V. Gothelf, J. Kjems, *ACS Nano* **2013**, *7*, 8098-8104.
- [75] a) M. Schena, D. Shalon, R. W. Davis, P. O. Brown, *Science* **1995**, *270*, 467-470; b) L. Wang, R. Luhm, M. Lei, *Adv. Exp. Med. Biol.* **2007**, *593*, 105-116; c) R. M. Shai, *Front. Biosci.* **2006**, *11*, 1414-1424; d) M. L. Bulyk, E. Gentalen, D. J. Lockhart, G. M. Church, *Nat. Biotechnol.* **1999**, *17*, 573-577; e) M. L. Bulyk, *Curr. Opin. Biotechnol.* **2006**, *17*, 422-430; f) J. Mintseris, M. B. Eisen, *BMC Bioinformatics* **2006**, *7*, 429; g) R. W. Wallace, *Mol. Med. Today* **1997**, *3*, 384-389; h) M. Schena, D. Shalon, R. W. Davis, P. O. Brown, *Science* **1995**, *270*, 467-470; i) D. J. Lockhart, E. A. Winzeler, *Nature* **2000**, *405*, 827-836; j) G. Ramsay, *Nat. Biotechnol.* **1998**, *16*, 40-44.
- [76] a) D. Peelen, L. M. Smith, *Langmuir* **2005**, *21*, 266-271; b) H. Cai, X. N. Cao, Y. Jiang, P. G. He, Y. Z. Fang, *Anal. Bioanal. Chem.* **2003**, *375*, 287-293; c) H. Sheng, B. C. Ye, *Appl. Biochem. Biotechnol.* **2009**, *152*, 54-65; d) D. Liu, R. K. Perdue, L. Sun, R. M. Crooks, *Langmuir* **2004**, *20*, 5905-5910; e) Y. Li, Z. Wang, L. M. Ou, H. Z. Yu, *Anal. Chem.* **2007**, *79*, 426-433; f) F. Fixe, M. Dufva, P. Telleman, C. B. Christensen, *Nucl. Acids Res.* **2004**, *32*, 9-16; g) F. Fixe, M. Dufva, P. Telleman, C. B. Christensen, *Lab on a chip* **2004**, *4*, 191-195.
- [77] M. R. Lockett, M. R. Shortreed, L. M. Smith, *Langmuir* **2008**, *24*, 9198-9203.
- [78] A. Heuer-Jungemann, P. K. Harimech, T. Brown, A. G. Kanaras, *Nanoscale* **2013**, *5*, 9503-9510.
- [79] D. Sethi, R. P. Gandhi, P. Kuma, K. C. Gupta, *Biotechnol. J.* **2009**, *4*, 1513-1529.
- [80] C. Xu, H. Cai, Q. Xu, P. He, Y. Fang, *Fresenius J. Anal. Chem.* **2001**, *369*, 428-432.
- [81] P. Wongkaew, S. Poosittisak, *Am. J. Plant. Sci.* **2014**, *5*, 2256-2268.
- [82] J. K. Norskov, *Rep. Prog. Phys.* **1990**, *53*, 1253-1295.
- [83] a) M. D. Porter, T. B. Bright, D. L. Allara, C. E. D. Chidsey, *J. Am. Chem. Soc.* **1987**, *109*, 3559-3568; b) P. E. Laibinis, G. M. Whitesides, *J. Am. Chem. Soc.* **1992**, *114*, 1990-1995; c) H. Sellers, A. Ulman, Y. Shnidman, J. E. Eilers, *J. Am. Chem. Soc.* **1993**, *115*, 9389-9401.
- [84] C. A. Mirkin, R. L. Letsinger, R. C. Mucic, J. J. Storhoff, *Nature* **1996**, *382*, 607-609.
- [85] R. L. Letsinger, R. Elghanian, G. Viswanadham, C. A. Mirkin, *Bioconjugate Chem.* **2000**, *11*, 289-291.
- [86] V. Sokolova, M. Epple, *Angew. Chem. Int. Ed.* **2008**, *47*, 1382-1395.
- [87] E. Katz, I. Willner, *Angew. Chem. Int. Ed.* **2004**, *43*, 6042-6108.
- [88] M. Z. Liu, N. A. Amro, C. S. Chow, G. Y. Liu, *Nano Lett.* **2002**, *2*, 863-867.
- [89] M. Castronovo, S. Radovic, C. Grunwald, L. Casalis, M. Morgante, G. Scoles, *Nano Lett.* **2008**, *8*, 4140-4145.
- [90] F. Bano, L. Fruk, B. Sanavio, M. Glettenberg, L. Casalis, C. M. Niemeyer, G. Scoles, *Nano Lett.* **2009**, *9*, 2614-2618.
- [91] T. G. Waddell, D. E. Leyden, M. T. DeBello, *J. Am. Chem. Soc.* **1981**, *103*, 5303-5307.
- [92] E. T. Vandenberg, L. Bertilsson, B. Liedberg, K. Uvdal, R. Erlandsson, H. Elwing, I. Lundstrom, *J. Colloid Interface Sci.* **1991**, *147*, 103-118.
- [93] a) D. G. Kurth, T. Bein, *Langmuir* **1995**, *11*, 3061-3067; b) A. Simon, T. Cohen-Bouhacina, M. C. Porte, J. P. Aime, C. Baquey, *J. Colloid Interface Sci.* **2002**, *251*, 278-283; c) H. L. Li, N. Perkas, Q. L. Li, Y. Gofer, Y. Koltypin, A. Gedanken, *Langmuir* **2003**, *19*, 10409-10413.
- [94] Y. X. Zhao, B. Wang, W. W. Chen, A. Li, G. Q. Zheng, C. T. Liu, J. B. Chen, C. Y. Shen, *Polym. Composite* **2016**, *37*, 1914-1923.
- [95] R. Moller, A. Csaki, J. M. Kohler, W. Fritzsche, *Nucleic Acids Res.* **2000**, *28*, E91.
- [96] A. Misra, M. Shahid, *Bioorg. Med. Chem.* **2009**, *17*, 5826-5833.
- [97] D. Sethi, A. Kumar, K. C. Gupta, P. Kumar, *Bioconjugate Chem.* **2008**, *19*, 2136-2143.
- [98] J. Choithani, P. Kumar, K. C. Gupta, *Anal. Biochem.* **2006**, *357*, 240-248.

- [99] H. A. Latham-Timmons, A. Wolter, J. S. Roach, R. Giare, M. Leuck, *Nucleos. Nucleot. Nucl.* **2003**, *22*, 1495-1497.
- [100] D. I. Rozkiewicz, J. Gierlich, G. A. Burley, K. Gutmiedl, T. Carell, B. J. Ravoo, D. N. Reinhoudt, *ChemBioChem* **2007**, *8*, 1997-2002.
- [101] Z. Q. Gao, N. C. Tansil, *Nucl. Acids Res.* **2005**, *33*, 123-130.
- [102] J. Das, J. A. Lee, H. Yang, *Langmuir* **2010**, *26*, 6804-6808.
- [103] M. Silvestrini, L. Fruk, P. Ugo, *Biosens Bioel.* **2013**, *40*, 265-270.
- [104] D. Zhou, L. Ying, X. Hong, E. A. Hall, C. Abell, D. Klenerman, *Langmuir* **2008**, *24*, 1659-1664.
- [105] C. Chen, L. Fruk, *RSC Adv.* **2013**, *3*, 1709-1713.
- [106] S. E. Braslavsky, *Pure Appl. Chem.* **2007**, *79*, 293-465.
- [107] D. Frackowiak, *J. Photochem. Photobiol. B* **1988**, *2*, 399-408.
- [108] a) C. Brieke, F. Rohrbach, A. Gottschalk, G. Mayer, A. Heckel, *Angew. Chem. Int. Ed.* **2012**, *51*, 8446-8476; b) G. Mayer, A. Heckel, *Angew. Chem. Int. Ed.* **2006**, *45*, 4900-4921; c) I. Ahmed, L. Fruk, *Mol. BioSyst.* **2013**, *9*, 565-570.
- [109] H. Asanuma, T. Ito, T. Yoshida, X. Liang, M. Komiyama, *Angew. Chem. Int. Ed.* **1999**, *38*, 2393-2395.
- [110] Y. Yan, J. I. Chen, D. S. Ginger, *Nano Lett.* **2012**, *12*, 2530-2536.
- [111] P. Klan, T. Solomek, C. G. Bochet, A. Blanc, R. Givens, M. Rubina, V. Popik, A. Kostikov, J. Wirz, *Chem. Rev.* **2013**, *113*, 119-191.
- [112] D. D. Young, H. Lusic, M. O. Lively, J. A. Yoder, A. Deiters, *ChemBioChem* **2008**, *9*, 2937-2940.
- [113] S. P. A. Fodor, J. L. Read, M. C. Pirrung, L. Stryer, A. T. Lu, D. Solas, *Science* **1991**, *251*, 767-773.
- [114] N. Kretschy, A. K. Holik, V. Somoza, K. P. Stengele, M. M. Somoza, *Angew. Chem. Int. Ed.* **2015**, *54*, 8555-8559.
- [115] a) C. Agbavwe, C. Kim, D. Hong, K. Heinrich, T. Wang, M. M. Somoza, *J. Nanobiotechnol.* **2011**, *9*, 57; b) S. Singh-Gasson, R. D. Green, Y. Yue, C. Nelson, F. Blattner, M. R. Sussman, F. Cerrina, *Nat. Biotechnol.* **1999**, *17*, 974-978; c) M. Sack, N. Kretschy, B. Rohm, V. Somoza, M. M. Somoza, *Anal. Chem.* **2013**, *85*, 8513-8517.
- [116] M. Sack, K. Holz, A. K. Holik, N. Kretschy, V. Somoza, K. P. Stengele, M. M. Somoza, *J. Nanobiotechnol.* **2016**, *14*, 14.
- [117] T. Koch, N. Jacobsen, J. Fensholdt, U. Boas, M. Fenger, M. H. Jakobsen, *Bioconjugate Chem.* **2000**, *11*, 474-483.
- [118] J. Escorihuela, M. J. Banuls, R. Puchades, A. Maquieira, *Bioconjugate Chem.* **2012**, *23*, 2121-2128.
- [119] a) J. Escorihuela, M. J. Banuls, S. Grijalvo, R. Eritja, R. Puchades, A. Maquieira, *Bioconjugate Chem.* **2014**, *25*, 618-627; b) J. Escorihuela, M. J. Banuls, R. Puchades, A. Maquieira, *J. Mater. Chem. B* **2014**, *2*, 8510-8517.
- [120] N. C. Yang, C. Rivas, *J. Am. Chem. Soc.* **1961**, *83*, 2213-2213.
- [121] G. Porter, M. F. Tchir, *J. Chem. Soc. Chem. Commun.* **1970**, 1372-1373.
- [122] P. G. Sammes, *Tetrahedron* **1976**, *32*, 405-422.
- [123] J. L. Segura, N. Martin, *Chem. Rev.* **1999**, *99*, 3199-3246.
- [124] T. Gruending, K. K. Oehlenschlaeger, E. Frick, M. Glassner, C. Schmid, C. Barner-Kowollik, *Macromol. Rapid Commun.* **2011**, *32*, 807-812.
- [125] M. Glassner, K. K. Oehlenschlaeger, T. Gruending, C. Barner-Kowollik, *Macromolecules* **2011**, *44*, 4681-4689.
- [126] a) T. Pauloehrl, G. Delaittre, V. Winkler, A. Welle, M. Bruns, H. G. Borner, A. M. Greiner, M. Bastmeyer, C. Barner-Kowollik, *Angew. Chem. Int. Ed.* **2012**, *51*, 1071-1074; b) M. Winkler, J. O. Mueller, K. K. Oehlenschlaeger, L. M. de Espinosa, M. A. R. Meier, C. Barner-Kowollik, *Macromolecules* **2012**, *45*, 5012-5019.

- [127] D. M. Bauer, A. Rogge, L. Stolzer, C. Barner-Kowollik, L. Fruk, *Chem. Commun.* **2013**, 49, 8626-8628.
- [128] J. S. Clovis, A. Eckell, R. Huisgen, R. Sustmann, *Chem. Ber.* **1967**, 100, 60-70.
- [129] A. Herner, Q. Lin, *Top. Curr. Chem.* **2016**, 374, 77-107.
- [130] a) A. Padwa, S. Nahm, E. Sato, *J. Org. Chem.* **1978**, 43, 1664-1671; b) R. Darkow, M. Yoshikawa, T. Kitao, G. Tomaschewski, J. Schellenberg, *J. Polym. Sci. Polym. Chem.* **1994**, 32, 1657-1664.
- [131] Y. Wang, C. I. Vera, Q. Lin, *Org. Lett.* **2007**, 9, 4155-4158.
- [132] Y. Wang, W. J. Hu, W. Song, R. K. Lim, Q. Lin, *Org. Lett.* **2008**, 10, 3725-3728.
- [133] W. Song, Y. Wang, J. Qu, Q. Lin, *J. Am. Chem. Soc.* **2008**, 130, 9654-9655.
- [134] P. An, Z. Yu, Q. Lin, *Chem. Commun.* **2013**, 49, 9920-9922.
- [135] M. Dietrich, G. Delaittre, J. P. Blinco, A. J. Inglis, M. Bruns, C. Barner-Kowollik, *Adv. Funct. Mater.* **2012**, 22, 304-312.
- [136] C. Rodriguez-Emmenegger, C. M. Preuss, B. Yameen, O. Pop-Georgievski, M. Bachmann, J. O. Mueller, M. Bruns, A. S. Goldmann, M. Bastmeyer, C. Barner-Kowollik, *Adv. Mater.* **2013**, 25, 6123-6127.
- [137] L. Stolzer, A. Vigovskaya, C. Barner-Kowollik, L. Fruk, *Chem. Eur. J.* **2015**, 21, 14309-14313.
- [138] M. C. Pirrung, *Angew. Chem. Int. Ed.* **2002**, 41, 1276-1289.
- [139] L. M. Demers, D. S. Ginger, S. J. Park, Z. Li, S. W. Chung, C. A. Mirkin, *Science* **2002**, 296, 1836-1838.
- [140] A. Bruckbauer, D. J. Zhou, L. M. Ying, Y. E. Korchev, C. Abell, D. Klenerman, *J. Am. Chem. Soc.* **2003**, 125, 9834-9839.
- [141] S. A. Lange, V. Benes, D. P. Kern, J. K. Horber, A. Bernard, *Anal. Chem.* **2004**, 76, 1641-1647.
- [142] a) C. N. LaFratta, J. T. Fourkas, T. Baldacchini, R. A. Farrer, *Angew. Chem. Int. Ed.* **2007**, 46, 6238-6258; b) S. Maruo, J. T. Fourkas, *Laser Photonics Rev.* **2008**, 2, 100-111; c) M. Malinauskas, M. Farsari, A. Piskarskas, S. Juodkasis, *Phys. Rep.* **2013**, 533, 1-31; d) T. G. Leong, A. M. Zarafshar, D. H. Gracias, *Small* **2010**, 6, 792-806.
- [143] S. Juodkasis, V. Mizeikis, H. Misawa, *J. Appl. Phys.* **2009**, 106, 051101-051113.
- [144] a) M. Deubel, M. Wegener, S. Linden, G. von Freymann, S. John, *Opt. Lett.* **2006**, 31, 805-807; b) W. Haske, V. W. Chen, J. M. Hales, W. Dong, S. Barlow, S. R. Marder, J. W. Perry, *Opt. Express* **2007**, 15, 3426-3436; c) N. Tetreault, G. von Freymann, M. Deubel, M. Hermatschweiler, F. Perez-Willard, S. John, M. Wegener, G. A. Ozin, *Adv. Mater.* **2006**, 18, 457-460.
- [145] a) P. Galajda, P. Ormos, *J. Opt. B* **2002**, 4, S78-S81; b) C. Schizas, V. Melissinaki, A. Gaidukeviciute, C. Reinhardt, C. Ohrt, V. Dedoussis, B. N. Chichkov, C. Fotakis, M. Farsari, D. Karalekas, *Int. J. Adv. Manufact. Technol.* **2010**, 48, 435-441; c) L. Amato, Y. Gu, N. Bellini, S. M. Eaton, G. Cerullo, R. Osellame, *Lab Chip* **2012**, 12, 1135-1142; d) S. Maruo, H. Inoue, *Appl. Phys. Lett.* **2006**, 89; e) S. Maruo, A. Takaura, Y. Saito, *Opt. Express* **2009**, 17, 18525-18532.
- [146] a) R. Narayan, P. Goering, *Mrs Bull* **2011**, 36, 973-982; b) A. Waldbaur, H. Rapp, K. Lange, B. E. Rapp, *Anal. Methods* **2011**, 3, 2681-2716; c) S. G. Zhang, F. Gelain, X. J. Zhao, *Seminars in Cancer Biol.* **2005**, 15, 413-420; d) A. Abbott, *Nature* **2003**, 424, 870-872; e) E. Stratakis, A. Ranella, M. Farsari, C. Fotakis, *Prog. Quantum Electronics* **2009**, 33, 127-163.
- [147] V. Melissinaki, A. A. Gill, I. Ortega, M. Vamvakaki, A. Ranella, J. W. Haycock, C. Fotakis, M. Farsari, F. Claeysens, *Biofabrication* **2011**, 3, 045005-045017.
- [148] a) M. Kaupp, K. Hildebrandt, V. Trouillet, P. Mueller, A. S. Quick, M. Wegener, C. Barner-Kowollik, *Chem. Commun.* **2016**, 52, 1975-1978; b) M. Kaupp, A. S. Quick, C.

- Rodriguez-Emmenegger, A. Welle, V. Trouillet, O. Pop-Georgievski, M. Wegener, C. Barner-Kowollik, *Adv. Funct. Mater.* **2014**, *24*, 5649-5661.
- [149] L. Stolzer, A. S. Quick, D. Abt, A. Welle, D. Naumenko, M. Lazzarino, M. Wegener, C. Barner-Kowollik, L. Fruk, *Chem. Commun.* **2015**, *51*, 3363-3366.
- [150] K. K. Oehlenschlaeger, Diplomarbeit, Karlsruher Institut für Technologie (KIT) (Karlsruhe), **2011**.
- [151] a) Q. Q. Tang, Y. Wu, P. Sun, Y. M. Chen, K. Zhang, *Macromolecules* **2014**, *47*, 3775-3781; b) K. Hildebrandt, T. Pauloehrl, J. P. Blinco, K. Linkert, H. G. Börner, C. Barner-Kowollik, *Angew. Chem. Int. Ed.* **2015**, *54*, 2838-2843.
- [152] L. Stolzer, I. Ahmed, C. Rodriguez-Emmenegger, V. Trouillet, P. Bockstaller, C. Barner-Kowollik, L. Fruk, *Chem. Commun.* **2014**, *50*, 4430-4433.
- [153] a) B. Richter, T. Pauloehrl, J. Kaschke, D. Fichtner, J. Fischer, A. M. Greiner, D. Wedlich, M. Wegener, G. Delaitre, C. Barner-Kowollik, M. Bastmeyer, *Adv. Mater.* **2013**, *25*, 6117-6122; b) A. S. Quick, H. Rothfuss, A. Welle, B. Richter, J. Fischer, M. Wegener, C. Barner-Kowollik, *Adv. Funct. Mater.* **2014**, *24*, 3571-3580.
- [154] T. Tischer, T. K. Claus, M. Bruns, V. Trouillet, K. Linkert, C. Rodriguez-Emmenegger, A. S. Goldmann, S. Perrier, H. G. Börner, C. Barner-Kowollik, *Biomacromol.* **2013**, *14*, 4340-4350.
- [155] A. Paptchikhine, K. Itto, P. G. Andersson, *Chem. Commun.* **2011**, *47*, 3989-3991.
- [156] J. van Ameijde, R. M. Liskamp, *Org. Biomol. Chem.* **2003**, *1*, 2661-2669.
- [157] T. D. Schladt, K. Schneider, M. I. Shukoor, F. Natalio, H. Bauer, M. N. Tahir, S. Weber, L. M. Schreiber, H. C. Schroder, W. E. G. Muller, W. Tremel, *J. Mater. Chem.* **2010**, *20*, 8297-8304.
- [158] M. J. Palte, R. T. Raines, *J. Am. Chem. Soc.* **2012**, *134*, 6218-6223.
- [159] B. C. Froehler, P. G. Ng, M. D. Matteucci, *Nucl. Acids Res.* **1986**, *14*, 5399-5407.
- [160] a) A. A. Patchett, *J. Med. Chem.* **1993**, *36*, 2051-2058; b) M. de Gasparo, S. Whitebread, *Regul. Pept.* **1995**, *59*, 303-311; c) V. S. Ananthanarayanan, S. Tetreault, A. Saint-Jean, *J. Med. Chem.* **1993**, *36*, 1324-1332.
- [161] C. A. G. N. Montalbetti, V. Falque, *Tetrahedron* **2005**, *61*, 10827-10852.
- [162] B. S. Jursic, Z. Zdravkovski, *Synth. Commun.* **1993**, *23*, 2761-2770.
- [163] a) V. Gotor, *Bioorg. Med. Chem.* **1999**, *7*, 2189-2197; b) F. van Rantwijk, M. A. P. J. Hacking, R. A. Sheldon, *Monatsh. Chem.* **2000**, *131*, 549-569.
- [164] E. Valeur, M. Bradley, *Chem. Soc. Rev.* **2009**, *38*, 606-631.
- [165] G. W. Anderson, J. E. Zimmerman, F. M. Callahan, *J. Am. Chem. Soc.* **1963**, *85*, 3039-3039.
- [166] a) L. Fruk, C. M. Niemeyer, *Angew. Chem. Int. Ed.* **2005**, *44*, 2603-2606; b) J. Quinton, S. Kolodych, M. Chaumonet, V. Bevilacqua, M. C. Nevers, H. Volland, S. Gabillet, P. Thuery, C. Creminon, F. Taran, *Angew. Chem. Int. Ed.* **2012**, *51*, 6144-6148.
- [167] M. M. Madden, C. I. R. Vera, W. J. Song, Q. Lin, *Chem. Commun.* **2009**, 5588-5590.
- [168] W. Song, Y. Wang, J. Qu, M. M. Madden, Q. Lin, *Angew. Chem. Int. Ed.* **2008**, *47*, 2832-2835.
- [169] R. K. V. Lim, Q. Lin, *Acc. Chem. Res.* **2011**, *44*, 828-839.
- [170] S. Arndt, H. A. Wagenknecht, *Angew. Chem. Int. Ed.* **2014**, *53*, 14580-14582.
- [171] J. L. Ravanat, T. Douki, J. Cadet, *J. Photochem. Photobiol. B* **2001**, *63*, 88-102.
- [172] a) J. Cadet, T. Douki, J. P. Pouget, J. L. Ravanat, S. Sauvaigo, *Curr. Probl. Dermatol.* **2001**, *29*, 62-73; b) R. P. Rastogi, Richa, A. Kumar, M. B. Tyagi, R. P. Sinha, *J. Nucl. Acids* **2010**, *2010*, 592980.
- [173] T. Douki, *Photochem. Photobiol. Sci.* **2013**, *12*, 1286-1302.
- [174] C. Kielbassa, L. Roza, B. Epe, *Carcinogenesis* **1997**, *18*, 811-816.
- [175] W. J. Schreier, T. E. Schrader, F. O. Koller, P. Gilch, C. E. Crespo-Hernandez, V. N. Swaminathan, T. Carell, W. Zinth, B. Kohler, *Science* **2007**, *315*, 625-629.

- [176] a) M. Dizdaroglu, P. Jaruga, M. Birincioglu, H. Rodriguez, *Free Radic. Biol. Med.* **2002**, *32*, 1102-1115; b) J. Baier, T. Maisch, M. Maier, E. Engel, M. Landthaler, W. Baumler, *Biophys. J.* **2006**, *91*, 1452-1459.
- [177] P. Yates, A. C. Mackay, F. X. Garneau, *Tetrahedron Lett.* **1968**, 5389-5392.
- [178] A. Chang, M. Scheer, A. Grote, I. Schomburg, D. Schomburg, *Nucl. Acids Res.* **2009**, *37*, D588-D592.
- [179] L. Chang, S. H. Chiang, A. R. Saltiel, *Mol. Med.* **2004**, *10*, 65-71.
- [180] M. A. Meyers, P. Y. Chen, A. Y. M. Lin, Y. Seki, *Prog. Mater. Sci.* **2008**, *53*, 1-206.
- [181] F. W. Krainer, A. Glieder, *Appl. Microbiol. Biotechnol.* **2015**, *99*, 1611-1625.
- [182] a) M. J. Davies, *Biochem. Biophys. Res. Commun.* **2003**, *305*, 761-770; b) M. Correia, M. T. Neves-Petersen, A. Parracino, A. K. di Gennaro, S. B. Petersen, *J. Fluoresc.* **2012**, *22*, 323-337.
- [183] F. Kukulka, C. M. Niemeyer, *Org. Biomol. Chem.* **2004**, *2*, 2203-2206.
- [184] P. I. Ohlsson, K. G. Paul, *Acta Chem. Scand. B* **1976**, *30*, 373-375.
- [185] M. Barbatti, A. J. Aquino, H. Lischka, *Phys. Chem. Chem. Phys.* **2010**, *12*, 4959-4967.
- [186] W. Siti, A. K. Khan, H. P. M. de Hoog, B. Liedberg, M. Nallani, *Org. Biomol. Chem.* **2015**, *13*, 3202-3206.
- [187] a) A. V. Pinheiro, D. R. Han, W. M. Shih, H. Yan, *Nat. Nanotechnol.* **2011**, *6*, 763-772; b) C. Lin, Y. Liu, H. Yan, *Biochemistry* **2009**, *48*, 1663-1674; c) D. Y. Zhang, G. Seelig, *Nat. Chem.* **2011**, *3*, 103-113; d) P. K. Lo, K. L. Metera, H. F. Sleiman, *Curr. Opin. Chem. Biol.* **2010**, *14*, 597-607.
- [188] a) M. I. Stockman, *Phys. Today* **2011**, *64*, 39-44; b) M. Nirmal, L. Brus, *Acc. Chem. Res.* **1999**, *32*, 407-414; c) M. Pumera, *Chem. Soc. Rev.* **2010**, *39*, 4146-4157; d) T. W. Odom, J. L. Huang, P. Kim, C. M. Lieber, *Nature* **1998**, *391*, 62-64.
- [189] a) E. Boisselier, D. Astruc, *Chem. Soc. Rev.* **2009**, *38*, 1759-1782; b) M. De, P. S. Ghosh, V. M. Rotello, *Adv. Mater.* **2008**, *20*, 4225-4241; c) E. C. Dreaden, A. M. Alkilany, X. H. Huang, C. J. Murphy, M. A. El-Sayed, *Chem. Soc. Rev.* **2012**, *41*, 2740-2779.
- [190] a) Q. W. Song, Y. Shi, D. C. He, S. H. Xu, J. Ouyang, *Chem. Eur. J.* **2015**, *21*, 2417-2422; b) Y. Geng, A. C. Pearson, E. P. Gates, B. Uprety, R. C. Davis, J. N. Harb, A. T. Woolley, *Langmuir* **2013**, *29*, 3482-3490.
- [191] a) F. Alonso, Y. Moglie, G. Radivoy, M. Yus, *Tetrahedron Lett.* **2009**, *50*, 2358-2362; b) W. D. Yang, C. Y. Liu, Z. Y. Zhang, Y. Liu, S. D. Nie, *J. Mater. Sci. Mater. Electron.* **2013**, *24*, 5175-5182; c) R. M. Tilaki, A. I. Zad, S. M. Mahdavi, *Appl. Phys. A* **2007**, *88*, 415-419.
- [192] C. Chen, I. Ahmed, L. Fruk, *Nanoscale* **2013**, *5*, 11610-11614.
- [193] M. B. Gawande, A. Goswami, F. X. Felpin, T. Asefa, X. X. Huang, R. Silva, X. X. Zou, R. Zboril, R. S. Varma, *Chem. Rev.* **2016**, *116*, 3722-3811.
- [194] a) A. K. Chatterjee, R. Chakraborty, T. Basu, *Nanotechnol.* **2014**, *25*, 135101-135113; b) M. S. Usman, M. E. El Zowalaty, K. Shameli, N. Zainuddin, M. Salama, N. A. Ibrahim, *Int. J. Nanomed.* **2013**, *8*, 4467-4478.
- [195] Y. Lee, J. R. Choi, K. J. Lee, N. E. Stott, D. Kim, *Nanotechnol.* **2008**, *19*.
- [196] a) B. Thakur, E. Bernalte, J. P. Smith, C. W. Foster, P. E. Linton, S. N. Sawant, C. E. Banks, *Analyst* **2016**, *141*, 1233-1238; b) J. M. Zen, C. T. Hsu, A. S. Kumar, H. J. Lyuu, K. Y. Lin, *Analyst* **2004**, *129*, 841-845.
- [197] K. Susumu, H. T. Uyeda, I. L. Medintz, T. Pons, J. B. Delehanty, H. Mattoussi, *J. Am. Chem. Soc.* **2007**, *129*, 13987-13996.
- [198] a) J. Xiong, Y. Wang, Q. J. Xue, X. D. Wu, *Green Chem.* **2011**, *13*, 900-904; b) L. H. Liu, J. Lyu, T. H. Li, T. K. Zhao, *Dig. J. Nanomater. Biostruct.* **2015**, *10*, 1303-1310.
- [199] C. Kind, A. Weber, C. Feldmann, *J. Mater. Chem.* **2012**, *22*, 987-993.

- [200] P. Kanninen, C. Johans, J. Merta, K. Kontturi, *J. Colloid Interface Sci.* **2008**, *318*, 88-95.
- [201] D. Deng, Y. Jin, Y. Cheng, T. Qi, F. Xiao, *ACS Appl. Mater. Interf.* **2013**, *5*, 3839-3846.
- [202] G. G. Jang, C. B. Jacobs, R. G. Gresback, I. N. Ivanov, H. M. Meyer, M. Kidder, P. C. Joshi, G. E. Jellison, T. J. Phelps, D. E. Graham, J. W. Moon, *J. Mater. Chem. C* **2015**, *3*, 644-650.
- [203] C. H. Liu, R. H. E. Hudson, N. O. Petersen, *Synthesis* **2002**, 1398-1406.
- [204] G. H. Chan, J. Zhao, E. M. Hicks, G. C. Schatz, R. P. Van Duyne, *Nano Lett.* **2007**, *7*, 1947-1952.
- [205] A. Herrmann, G. Mihov, G. W. M. Vandermeulen, H. A. Klok, K. Mullen, *Tetrahedron* **2003**, *59*, 3925-3935.
- [206] B. F. Lundt, N. L. Johansen, A. Volund, J. Markussen, *Int.J. Pept. Protein Res.* **1978**, *12*, 258-268.
- [207] a) H. A. Behrendorf, M. Pignot, N. Windhab, A. Kappel, *Nucl. Acids Res.* **2002**, *30*, e64-69; b) L. Ma, M. Su, T. Li, Z. Wang, *Analyst* **2013**, *138*, 1048-1052.
- [208] a) K. M. Abu-Salah, M. M. Zourob, F. Mouffouk, S. A. Alrokayan, M. A. Alaamery, A. A. Ansari, *Sensors* **2015**, *15*, 14539-14568; b) E. Palecek, M. Bartosik, *Chem. Rev.* **2012**, *112*, 3427-3481.
- [209] S. M. H. T. Yazdi, Y. B. Yuan, J. Ma, H. M. Zhao, O. Milenkovic, *Sci. Rep.* **2015**, *5*, 14138-14148.
- [210] a) M. N. Khan, V. Tjong, A. Chilkoti, M. Zharnikov, *Angew. Chem. Int. Ed.* **2012**, *51*, 10303-10306; b) D. Samanta, A. Sarkar, *Chem. Soc. Rev.* **2011**, *40*, 2567-2592; c) S. Balamurugan, A. Obubuafo, S. A. Soper, D. A. Spivak, *Anal. Bioanal. Chem.* **2008**, *390*, 1009-1021.
- [211] a) A. C. Pease, D. Solas, E. J. Sullivan, M. T. Cronin, C. P. Holmes, S. P. Fodor, *Proc. Natl. Acad. Sci.* **1994**, *91*, 5022-5026; b) B. Y. Chow, C. J. Emig, J. M. Jacobson, *Proc. Natl. Acad. Sci.* **2009**, *106*, 15219-15224.
- [212] X. Z. Zhou, F. Boey, F. W. Huo, L. Huang, H. Zhang, *Small* **2011**, *7*, 2273-2289.
- [213] a) M. Mrksich, G. M. Whitesides, *Trends Biotechnol.* **1995**, *13*, 228-235; b) R. Singhvi, A. Kumar, G. P. Lopez, G. N. Stephanopoulos, D. I. C. Wang, G. M. Whitesides, D. E. Ingber, *Science* **1994**, *264*, 696-698.
- [214] J. Choithani, D. Sethi, P. Kumar, K. C. Gupta, *Surf. Sci.* **2008**, *602*, 2389-2394.
- [215] B. Yameen, C. Rodriguez-Emmenegger, C. M. Preuss, O. Pop-Georgievski, E. Verveniotis, V. Trouillet, B. Rezek, C. Barner-Kowollik, *Chem. Commun.* **2013**, *49*, 8623-8625.
- [216] A. Vigovskaya, D. Abt, I. Ahmed, C. M. Niemeyer, C. Barner-Kowollik, L. Fruk, *J. Mater. Chem. B* **2016**, *4*, 442-449.
- [217] G. Y. Liu, N. A. Amro, *Proc. Natl. Acad. Sci.* **2002**, *99*, 5165-51670.
- [218] A. Bruckbauer, D. Zhou, L. Ying, Y. E. Korchev, C. Abell, D. Klenerman, *J. Am. Chem. Soc.* **2003**, *125*, 9834-9839.
- [219] A. Ovsianikov, V. Mironov, J. Stampf, R. Liska, *Expert Rev. Med. Dev.* **2012**, *9*, 613-633.
- [220] a) M. P. Stevens, *Polymer Chemistry: An Introduction, third ed.*, Oxford University Press, New York **1999**; b) P. C. Hiemenz, T. P. Lodge, *Polymer Chemistry, second ed.*, CRC Press, New York, **2007**.
- [221] a) F. Claeysens, E. A. Hasan, A. Gaidukeviciute, D. S. Achilleos, A. Ranella, C. Reinhardt, A. Ovsianikov, S. Xiao, C. Fotakis, M. Vamvakaki, B. N. Chichkov, M. Farsari, *Langmuir* **2009**, *25*, 3219-3223; b) B. Bhuian, R. J. Winfield, S. O'Brien, G. M. Crean, *Appl. Surf. Sci.* **2006**, *252*, 4845-4849.
- [222] J. K. Gansel, M. Thiel, M. S. Rill, M. Decker, K. Bade, V. Saile, G. von Freymann, S. Linden, M. Wegener, *Science* **2009**, *325*, 1513-1515.

- [223] K. Busch, G. von Freymann, S. Linden, S. F. Mingaleev, L. Tkeshelashvili, M. Wegener, *Phys. Rep.* **2007**, *444*, 101-202.
- [224] M. Farsari, G. Filippidis, K. Sambani, T. S. Drakakis, C. Fotakis, *J. Photochem. Photobiol. A* **2006**, *181*, 132-135.
- [225] K. Terzaki, M. Kissamitaki, A. Skarmoutsou, C. Fotakis, C. A. Charitidis, M. Farsari, M. Vamvakaki, M. Chatzinikolaidou, *J. Biomed. Mater. Res. A* **2013**, *101*, 2283-2294.
- [226] a) W. D. Zhang, P. Soman, K. Meggs, X. Qu, S. C. Chen, *Adv. Funct. Mater.* **2013**, *23*, 3226-3232; b) S. K. Seidlits, C. E. Schmidt, J. B. Shear, *Adv. Funct. Mater.* **2009**, *19*, 3543-3551.
- [227] a) J. D. Pitts, A. R. Howell, R. Taboada, I. Banerjee, J. Wang, S. L. Goodman, P. J. Campagnola, *Photochem. Photobiol.* **2002**, *76*, 135-144; b) S. Basu, P. J. Campagnola, *J. Biomed. Mater. Res. A* **2004**, *71*, 359-368; c) P. J. Su, Q. A. Tran, J. J. Fong, K. W. Eliceiri, B. M. Ogle, P. J. Campagnola, *Biomacromolecules* **2012**, *13*, 2917-2925.
- [228] Y. L. Sun, W. F. Dong, L. G. Niu, T. Jiang, D. X. Liu, L. Zhang, Y. S. Wang, Q. D. Chen, D. P. Kim, H. B. Sun, *Light Sci. Appl.* **2014**, *3*, 129-136.
- [229] A. S. Quick, H. Rothfuss, A. Welle, B. Richter, J. Fischer, M. Wegener, C. Barner-Kowollik, *Adv. Funct. Mater.* **2014**, *24*, 3571-3580.
- [230] E. Blasco, B. Yameen, A. S. Quick, P. Krolla-Sidenstein, A. Welle, M. Wegener, C. Barner-Kowollik, *Macromolecules* **2015**, *48*, 8718-8728.
- [231] a) T. K. Claus, B. Richter, V. Hahn, A. Welle, S. Kayser, M. Wegener, M. Bastmeyer, G. Delaittre, C. Barner-Kowollik, *Angew. Chem. Int. Ed.* **2016**, *55*, 3817-3822; b) E. Blasco, J. Muller, P. Muller, V. Trouillet, M. Schon, T. Scherer, C. Barner-Kowollik, M. Wegener, *Adv. Mater.* **2016**, *28*, 3592-3595.
- [232] X. Q. Qian, B. X. Han, Y. Liu, H. K. Yan, R. L. Liu, *J. Sol. Chem.* **1995**, *24*, 1183-1189.
- [233] H. F. Arlinghaus, M. Ostrop, O. Friedrichs, J. Feldner, U. Gunst, D. Lipinsky, *Surf. Interf. Anal.* **2002**, *34*, 35-39.
- [234] F. Kukulka, M. Lovrinovic, R. Wacker, C. M. Niemeyer, *Methods Mol. Biol.* **2004**, *283*, 181-196.
- [235] M. Gonzalez, L. A. Bagatolli, I. Echabe, J. L. Arrondo, C. E. Argarana, C. R. Cantor, G. D. Fidelio, *J. Biol. Chem.* **1997**, *272*, 11288-11294.
- [236] C. Chen, I. Ahmed, L. Fruk, *Nanoscale* **2013**, *5*, 11610-11614.
- [237] S. Lata, A. Reichel, R. Brock, R. Tampe, J. Piehler, *J. Am. Chem. Soc.* **2005**, *127*, 10205-10215.
- [238] C. Ligeour, A. Meyer, J. J. Vasseur, F. Morvan, *Eur. J. Org. Chem.* **2012**, 1851-1856.

7 List of Figures

- Figure 1.1:** Space model of the DNA double helix (left), structure of the single DNA strand (middle) and the principle of the base pairing (right), R = phosphate-sugar backbone. 1
- Figure 1.2:** Common protecting groups (red) used in the oligonucleotide synthesis developed by Korana *et al.*^[30-31] 4
- Figure 1.3:** Physical adsorption of the negatively charged single stranded DNA onto the positively charged amino-functionalized glass substrate.^[79] 16
- Figure 1.4:** Most commonly used organosilane reagents for functionalization of glass and silicon surfaces. APTES = (3-aminopropyl)triethoxysilane, MPTS = (3-mercapto-propyl)trimethoxy silane, GOPTS = (3-glycidoxypropyl)triethoxysilane, TPICC = *N*-(3-triethoxysilylpropyl)-4-(isothiocyanato-methyl)cyclohexane-1-carboxamide..... 18
- Figure 1.5:** Schematic depiction of the Jablonski diagram including electronic excitation *via* absorption, radiative relaxation processes such as fluorescence and phosphorescence, and non-radiative processes such as internal conversion, intersystem crossing and vibration relaxation. 20
- Figure 1.6:** Scheme of the *in situ* photolithographic preparation of the oligonucleotides directly on the surface. Based on [79].^[79] 22
- Figure 1.7:** General experimental direct laser writing (DLW) setup. The inset shows the principle of drawing by a moving laser beam, which is focused onto the photoresist material. Adapted with permission from [143].^[143] 29
- Figure 3.1:** Overlay of HPLC chromatograms of PE1-DNA1 48 and photoreaction between PE1-DNA1 48 and Do-TEG-Mal 64. 47
- Figure 3.2:** Analysis of photoreaction between PE2-DNA2 54 and 64; a) HPLC chromatograms of PE2-DNA2 (P1) and photoreaction (P2); b) native PAGE analysis of photoreaction, DM: 10 bp DNA marker, I: DNA2, II: PE2-DNA2, III: cycloadduct 67; gel conditions: 21% polyacrylamide, 100 V, 2 h, running buffer: 1×TBE, SYBR Gold staining..... 49
- Figure 3.3:** HPLC chromatograms of control reactions; a) I: DNA2 only; II: DNA2 irradiated with Do-TEG-Mal 64 at 320 nm for 16 h; III: PE2-DNA2 54 only; IV: PE2-DNA2 54 incubated with Do-TEG-Mal for 16 h in the dark; b) I: PE2-DNA2 54 without irradiation, II: PE2-DNA2 54 after irradiation with 320 nm light for 16 h. 49
- Figure 3.4:** Analysis of photoreaction between PE2-DNA1 53 and 64; a) HPLC chromatograms of PE2-DNA1 (P1) and of photoreaction (P2); b) native PAGE analysis of photoreaction, DM: 10 bp DNA marker, I: cycloadduct 66, II: PE2-DNA1, III: DNA1; gel conditions: 21% polyacrylamide, 100 V, 1.5 h, running buffer: 1×TBE, SYBR Gold staining. 50
- Figure 3.5:** HPLC chromatograms of control reactions; a) I: DNA1 only; II: DNA1 and Do-TEG-Mal 64 irradiated at 320 nm for 16 h, III: PE2-DNA1 53 only, IV: PE2-DNA1 53 incubated with Do-TEG-Mal 64 for 16 h in the dark; b) I: PE2-DNA1 53 only, II: PE2-DNA1 53 irradiated at 320 nm for 16 h..... 51
- Figure 3.6:** HPLC chromatogram of Tz-DNA2 63 (1.00 eq.) and model reaction with maleimide 64 (1.00 eq.)..... 53

- Figure 3.7:** Photoreaction of PE2-DNA2 56 (a, c) and Tz-DNA2 63 (b, d) with 15.0 eq. of Do-TEG-Mal 64 under 320 nm irradiation for 3 h. HPLC chromatograms of PE2-DNA2 (a) and Tz-DNA2 (b) show I: PE2-DNA2 or Tz-DNA2 only; II: photoreaction; III: photoreaction after 3 h incubation in the dark; IV: irradiation of PE2-DNA2 and Tz-DNA2 without maleimide; c) and d) correspond to the gel electrophoretic analysis of the PE2-DNA2 and Tz-DNA2 photoreactions respectively. DM: 10 bp DNA marker, gel conditions: 21% polyacrylamide, 100 V, 2 h, running buffer: 1×TBE, SYBR Gold staining..... 54
- Figure 3.8:** Kinetic study of the photoreaction between PE2-DNA2 56 and Do-TEG-Mal 64. HPLC chromatograms and ESI-MS data for 5.00 eq. (a, c) and 15.0 eq. (b, d) Do-TEG-Mal 64. Irradiation was performed with a 320 nm light sources for 0 min, 15 min, 30 min, 1 h and 3 h. 56
- Figure 3.9:** HPLC chromatograms of PE2-DNA2 56 (P1) and photoreaction between 56 and 100 eq. Do-TEG-Mal 64 (P2)..... 56
- Figure 3.10:** ESI-MS spectra (top) and the kinetic plots derived from the integration of the corresponding mass spectra (bottom) for photoreaction of PE2-DNA2 56 with a) 5.00 eq. and b) 15.0 eq. of Do-TEG-Mal 64 at different irradiation times with 320 nm light. 57
- Figure 3.11:** Expansion of the ESI mass spectrum region (bottom) and comparison between experimental and simulated data (top) for a) reactant 56 (m/z range: 1221.9 - 1224.0) and b) photoadduct 68 (m/z range: 1301.50 - 1303.0)..... 58
- Figure 3.12:** Kinetic study of the photoreaction between Tz-DNA2 63 and 5.00 eq. (a, c) and 15.0 eq. (b, d) of Do-TEG-Mal 64 using HPLC (top) and ESI-MS mass spectrometry (bottom) at different irradiation time. 60
- Figure 3.13:** HPLC chromatograms of the reaction between Tz-DNA2 63 and 100 eq. dienophile 64 after 0 min, 5 h and 24 h irradiation. 61
- Figure 3.14:** ESI-MS spectra (top) and the kinetic plots derived from the integration of the corresponding mass spectra (bottom) for photoreaction of Tz-DNA2 63 with a) 5.00 eq. and b) 15.0 eq. of Do-TEG-Mal 64 at different irradiation times with 320 nm light. 62
- Figure 3.15:** Expansion of the ESI mass spectrum region (bottom) and comparison between experimental and simulated data (top) for a) Tz-DNA2 63 (m/z range: 1226.3 - 1228.3) and b) photoadduct 69 (m/z range: 1301.0 - 1303.0)..... 63
- Figure 3.16:** SDS-PAGE characterization of irradiated horseradish peroxidase HRP* in comparison to non-irradiated HRP. Conditions: 12% SDS-PAGE; Running buffer: 1×SDS-running buffer; Voltage: 30 min at 80 V, 1 h at 100 V; Staining: silver staining; Loading: 25.0 pmol; PM: protein marker (Precision Plus Protein Dual Xtra Standards, BioRad). 66
- Figure 3.17:** a) HRP structure with lysine moieties (black sticks); graphics was created using a software UCSF Chimera 1.11rc and 1W4W data from the protein data bank; b) modification of lysine moieties of HRP with sSMCC 70. 66
- Figure 3.18:** a) FPLC chromatogram of HRP-DNA2 conjugate purification; absorption detection at 260 nm (black curve) and 403 nm (red curve); b) native PAGE characterization of the FPLC fractions F1, F2 and F3 in comparison to PE2-DNA2 54, HRP and HRP-Mal; DM: 10 bp DNA marker; oligonucleotide and protein band visualization by SYBRGold® and silver staining respectively..... 68
- Figure 3.19:** FPLC chromatograms of control reactions: a) incubation of PE2-DNA2 54 and HRP-Mal for 16 h in the dark; b) irradiation of PE2-DNA2 54 and HRP for 16 h at 320 nm; c) irradiation of

- DNA2 and HRP-Mal for 16 h at 320 nm; d) irradiation of DNA2 and HRP for 16 h at 320 nm. The black curve represents the absorption at 260 nm (DNA) and the red curve the absorption at 403 nm (HRP)..... 69
- Figure 3.20:** FPLC chromatograms of HRP-DNA2 obtained in the photoreaction between PE2-DNA2 54 and HRP-Mal (black curve) and of the side product obtained after irradiation of PE2-DNA2 54 and HRP (red curve). 70
- Figure 3.21:** Native PAGE analysis of hybridization of HRP-DNA2 with complementary strands cDNA2 and 6-FAM-cDNA2, DM: 1kb DNA-marker, I: native HRP; II: control reaction (HRP+DNA2+cDNA2), III: HRP-DNA2 conjugate, IV: HRP-DNA2+cDNA2, V: control reaction (HRP+DNA2+6-FAM-cDNA2), VI: HRP-DNA2+6-FAM-cDNA2; Conditions: 12.5% PAGE; Running buffer: tris/glycine; Voltage: 30 min at 80 V, 90 min at 100 V; Loading: 25.0 pmol; DM: 1kb DNA marker; Visualization: UV irradiation, ethidium bromide and silver staining..... 70
- Figure 3.22:** a) Principle of the peroxidase activity assay using Amplex Red and HRP in the presence of H₂O₂; b) the average of fluorescence intensity as a function of time after 0 min, 30 min and 60 min reaction duration obtained by Amplex[®]Red assay using native HRP (blue bar) or HRP-DNA2 conjugate (red bar). 71
- Figure 3.23:** Agarose gel (0.8%) electrophoresis study of photoreaction between PE2-DNA2 54 and maleimide Cu NPs nanoparticles at 320 nm. Visualization of bands was afforded by use of the visible and UV light after SYBRGold[®] staining of DNA. Gels were exposed to 100 V for 15 min in 0.5xTBE buffer..... 75
- Figure 3.24:** Tested reactant ratios a) for the synthesis of Cu-NTA nanoparticles and b) UV-Vis characterization of the obtained Cu-NTA nanoparticles. 76
- Figure 3.25:** UV-Vis characterization of Cu-NTA-Mal immediately after the synthesis (black curve) and after 24 h of storage (red curve)..... 78
- Figure 3.26:** Photograph of the sample holder (1), silicon wafer (2) and shadow mask with a wave pattern (3), employed for the spatially controlled immobilization of PE2-DNA2 54. 80
- Figure 3.27:** Schematic illustration of the spatially controlled light-induced immobilization of PE2-DNA2 54 on maleimide functionalized silicon wafer. 81
- Figure 3.28:** ToF-SIMS imaging of photo-patterned PE2-DNA2 54 a) derived from the sum of the signals detected at 96.95 (H₂PO₄⁻), 150.01 (G⁻), 125.02 (T⁻), 134.03 (A⁻) and 110.01 (C⁻) and ToF-SIMS imaging of photo-patterned non-modified DNA2 b) derived from the sum of the signals detected at 96.97 (H₂PO₄⁻), 150.03 (G⁻), 125.04 (T⁻), 134.04 (A⁻) and 110.03 (C⁻) assigned to fragments of the corresponding oligonucleotides. Adapted with permission from [216].^[216] 82
- Figure 3.29:** a) Schematic illustration of the hybridization of the PE2-DNA2 54 modified silicon surface with a Cy[®]3 labeled complementary oligonucleotide Cy[®]3-cDNA2; b) fluorescence image of hybridized Cy[®]3-cDNA2; c) fluorescence image of the control hybridization with a non-complementary Cy[®]3 labeled oligonucleotide Cy[®]3-cDNA4. Adapted with permission from [216]. 83
- Figure 3.30:** The home-built DLW setup for multiphoton microfabrication..... 85
- Figure 3.31:** a) Principle of the light-induced PE2 DNA2 56 immobilization using direct laser writing (DLW); b) Photoenolization of 56, induced by laser light absorption, and subsequent [4+2] cycloaddition with maleimide moiety bound to the surface. 87

- Figure 3.32:** a) ToF-SIMS image of PO_2^- ion of PE2-DNA2 56 immobilized on maleimide functionalized glass surface *via* DLW; b) fluorescence image of hybridized $\text{Cy}^{\text{®}}3$ -cDNA2 squares, written by employing the laser power of 2 - 16 mW. 88
- Figure 3.33:** Fluorescence images of hybridized $\text{Cy}^{\text{®}}3$ -cDNA2 of 2D line fields constructed by 1-fold, 2-fold and 4-fold scanning repetition; z position change from left to the right, laser power increasing linearly from bottom to top from 0 to 20 mW. 89
- Figure 3.34:** Fluorescence images of $\text{Cy}^{\text{®}}3$ -cDNA2 hybridised to PE2-DNA2 immobilized onto the 2D line array written by DLW using 4-fold scanning repetition and the speed of $100 \mu\text{m s}^{-1}$. Laser power was increased from left to the right: 0.4 mW, 0.8 mW, 2 mW, 4 mW, 8 mW, 16 mW and 24 mW. Zoomed section is the column, written using 4mW laser power and different distances between the line segments (image on the right). 91
- Figure 3.35:** Microscopic of $100 \times 100 \mu\text{m}$ image of polymer frame written by DLW utilizing 83 and 84 as polymerization reagents. 92
- Figure 3.36:** Top: fluorescence images of the two DNA sequence patterns for $\text{Cy}^{\text{®}}3$ (left), $\text{Cy}^{\text{®}}5$ (right) and merged signals (middle). Bottom: magnification of the four lower line segments of the merged image image and fluorescence intensity profiles along the green line for $\text{Cy}^{\text{®}}3$ lines (left) and for $\text{Cy}^{\text{®}}5$ (right) lines to illustrate the regularity of the line pattern. $\text{Cy}^{\text{®}}3$ ($\lambda_{\text{ex}} = 550 \text{ nm}$, $\lambda_{\text{em}} = 570 \text{ nm}$; $\text{Cy}^{\text{®}}5$ ($\lambda_{\text{ex}} = 649 \text{ nm}$, $\lambda_{\text{em}} = 666 \text{ nm}$). 93
- Figure 3.37:** Fluorescence images of a) 3×3 ($10 \times 10 \mu\text{m}$) and b) 2×2 ($45 \times 45 \mu\text{m}$) checkerboard pattern containing two different sequences hybridized with corresponding $\text{Cy}^{\text{®}}5$ and $\text{Cy}^{\text{®}}3$ complementary DNA. Merged patterns are shown in the middle. Laser power : 6 mW, writing speed $50 \mu\text{m s}^{-1}$. 94
- Figure 3.38:** Fluorescence images of PE2-DNA2 56 containing surfaces incubated with $\text{Cy}^{\text{®}}3$ -cDNA2 of different concentrations (1.00 pM, 100 pM, 1.00 nM and 1.00 μM). 95
- Figure 3.39:** ToF-SIMS image of PO_3^- ion of 2×2 checkerboard pattern containing PE2-DNA2 (1) and PE2-DNA3 (2) after hybridization with HRP-cDNA2. 96
- Figure 3.40:** Fluorescence images of Atto550-biotin bound to a) two sequence pattern containing immobilized STV-cDNA2 (squares labeled 1) and b) STV free surface. (Atto550: $\lambda_{\text{ex}} = 554 \text{ nm}$, $\lambda_{\text{em}} = 576 \text{ nm}$). 97
- Figure 5.1:** Drawing of the cusom-built photoreactor employed in the current study. 108
- Figure 5.2:** Emission spectrum of the employed compact low-pressure fluorescent lamp (36 w, Arimed B6, $\lambda_{\text{max}} = 320 \pm 30 \text{ nm}$). 109

8 List of Tables

Table 1.1: Commonly employed linkages/reactions for in-the solution oligonucleotide conjugation. Adapted with permission from [56]. ^[56]	12
Table 1.2: Overview of different techniques used for surface structuring of oligonucleotides. Adapted with permission from [11d]. ^[11d]	27
Table 3.1: Overview of different reaction conditions for the coupling of H-phosphonate 51 to DNA1.	40
Table 3.2: Peak assignment of the ESI mass spectra of reactant 56 from $m/z = 1218.0$ to $m/z = 1263.0$ (a–e) and photoadduct 68 from $m/z = 1297.0$ to $m/z = 1328.0$ (a'–e'). Peak labels correspond to the spectra shown in Figure 3.11. Both experimental and theoretical m/z values and their differences ($\Delta m/z$) are shown.	58
Table 3.3: Peak assignment of the ESI mass spectra of reactant 63 from $m/z = 1222.5$ to $m/z = 1235.5$ (a - d) and photoadduct 69 from $m/z = 1296.0$ to $m/z = 1311.0$ (a' - d'). Peak labels correspond to the spectra shown in Figure 3.15. Both experimental and theoretical m/z values and their differences ($\Delta m/z$) are shown.	64
Table 5.1: Sequences and extinction coefficients of used oligonucleotides.	102
Table 5.2: Buffers and the corresponding recipes.	102
Table 5.3: Standard gradient for the purification of oligonucleotides by HPLC. Eluent A: 0.1 M ammonium acetate, eluent B: acetonitrile.	106
Table 5.4: Recipe for 21% PA gel.	106
Table 5.5: Recipe for SDS-PA gel.	107
Table 5.6: Recipe for non-denaturing PA gel.	107
Table 5.7: Standard coupling protocol for natural bases with thymine (T) as example.	126
Table 5.8: Coupling protocol for the photoenol phosphoramidite 46.	127
Table 5.9: MALDI-TOF MS results for the photoenol modified oligonucleotide PE1-DNA1 48, theoretical and found values in [g/mol].	128
Table 5.10: MALDI-TOF MS results for the photoenol modified oligonucleotides; theoretical and found values in [g/mol].	128
Table 5.11: MALDI-TOF MS results for the photoenol/tetrazole modified amino terminated oligonucleotides; theoretical and found values in [g/mol].	129
Table 5.12: MALDI-TOF MS results for the photo-cycloadducts 66 und 67; theoretical and found values in [g/mol].	130
Table 5.13: MALDI-TOF MS results for the photo-cycloadducts 68 and 69, theoretical and found values in [g/mol].	131

Table 5.14: Reactant amounts used for the synthesis of CuNPs..... 138

9 Abbreviations

AFM	Atomic Force Microscopy
APS	Ammonium Peroxydisulfate
APTES	(3-Aminopropyl)triethoxysilane
CPG	Controlled Pore Glass
CuAAC	Copper(I)-Catalyzed Azide Alkyne Cycloaddition
DCC	<i>N,N'</i> -Dicyclohexylcarbodiimide
DCM	Dichloromethane
DDI	DNA Directed Immobilization
DLW	Direct Laser Writing
DMAP	4-(Dimethylamino)pyridine
DMF	<i>N,N</i> -Dimethylmethanamid
DMSO	Dimethyl sulfoxide
DMT	4,4'-Dimethoxytrityl
DNA	Deoxyribonucleic Acid
EDC	1-Ethyl-3-(3-dimethylaminopropyl)carbodiimid
EDC	3-(Ethyliminomethyleneamino)- <i>N,N</i> -dimethylpropan-1-amine
eq.	Equivalent
ESI	Electrospray Ionization
HBTU	3-[Bis(dimethylamino)methylumyl]-3 <i>H</i> -benzotriazol-1-oxide hexafluorophosphate
HOBt	Benzotriazol-1-ol
HPLC	High Pressure Liquid Chromatography
HRP	Horseradish Peroxidase
L	Liter
MALDI	Matrix Assisted Laser Desorption Ionization
NHS	1-Hydroxy-2,5-pyrrolidinedione
nm	Nanometer
NP	Nanoparticles
PCR	Polymerase Chain Reaction
PE	Photoenol
PEG	Polyethylene Glycol
RNA	Ribonucleic Acid
RT	Room Temperature
SAM	Self-assembled Monolayer
SDS	Sodium Dodecyl Sulfate
SIMS	Secondary Ion Mass Spectrometry
SNP	Single Nucleotide Polymorphism
SPAAC	Strain-Promoted Alkyne-Azide
STV	Streptavidin
TEMED	<i>N,N,N',N'</i> -Tetramethylethane-1,2-diamine
THF	Tetrahydrofuran
TOF	Time of Flight
Tz	Tetrazole
UV-Vis	Ultraviolet-Visible Spectroscopy

10 Danksagung

An erster Stelle möchte ich mich bei der Frau PD Dr. Ljiljana Fruk herzlichst bedanken. Zuerst möchte ich für die Möglichkeit, diese Arbeit in ihrer Gruppe anfertigen zu können, danken. Ich bin vor allem für die Art und Weise ihrer Betreuung dankbar, die sich durch das mir entgegengebrachte Vertrauen in meine Person und meine Fähigkeiten auszeichnet und mir dadurch ermöglicht hat, Forschungsprojekte selbständig zu gestalten und durchzuführen. Weiterhin bedanke ich mich für die hohe fachliche Kompetenz, immer offene Tür und ein freies Ohr auch für die nicht wissenschaftliche Angelegenheiten. Danke für Deine immer positive Art und ansteckende Begeisterung für die Forschung. Außerdem, DANKE, dass Du in für Dich schwierigen Situationen, immer an mich gedacht hast und gesorgt hast, dass es mir gut geht.

Beim Herrn Prof. Bräse möchte ich mich für die Aufnahme als Doktorandin am Karlsruher Institut für Technologie bedanken.

Beim Herrn Prof. Barner-Kowollik möchte ich mich für die Übernahme des Korreferats sowie für die produktive Diskussionen bedanken.

Beim Herrn Prof. Niemeyer möchte ich mich für die Aufnahme in seiner Arbeitsgruppe im dritten Jahr meiner Promotion und die Möglichkeit meine Arbeit fortzusetzen und abzuschließen bedanken.

Beim Herrn Prof. Dr. Hans-Achim Wagenknecht möchte ich mich für die Möglichkeit zur Durchführung der Oligonukleotidsynthese bedanken. Besonders danke ich der Frau Dr. Claudia Stubinitzky für die Hilfe mit dem DNA-Synthesizer .

Beim Herrn Prof. Wegener möchte ich mich für die Möglichkeit, DLW Versuche in seinen Laboren durchzuführen, bedanken.

Bei allen ehemaligen Mitarbeiter der Fruk Group möchte ich mich für das stets familiäre Klima in unserer Arbeitsgruppe bedanken. Ganz besonders danke ich Dr. Ishtiaq Ahmed für die kompetente Ratschläge in der organischen Synthese, produktive wissenschaftliche

Diskussionen, aber auch für die unterhaltsame, nicht chemische Gespräche. Außerdem möchte ich Ishtiaq für die tolle gemeinsame Zeit am IBG-1 danken, DANKE, dass du immer ein offenes Ohr für meine Probleme hattest. Ein großes Dankeschön an Dr. Dennis Bauer, Dr. Dania Kendziora und Dr. Bianca Geiseler, die mir bei Fragen in der Biochemie stets weiterhelfen konnten. Dr. Lukas Stolzer danke ich für die Hilfe mit lichtinduzierten Reaktionen, Dr. Cheng Chen für die Cu-Nanopartikeln und Dr. Marko Miljevic für die gute Atmosphäre im Chemielabor.

Andreas Elkeries danke ich für die Behebung der großen und kleinen Laborgeräten- und Computerprobleme und für die Hilfe beim Laborumzug.

Patrick Müller möchte ich für die kompetente Durchführung zahlreicher DLW Versuche und LSM Messungen, aber auch für die netten Gespräche herzlich danken.

Bei den Mitarbeitern des AK Niemeyer möchte ich mich herzlich für die freundliche Aufnahme in die Gruppe und gute Zusammenarbeit in der Endphase meiner Promotion bedanken. Besonderer Dank gilt Dr. Tim Scharnweber für die Lösung aller organisatorischen Fragen, Dr. Kersten Rabe für die Behebung der Computerprobleme und das Korrekturlesen der Zusammenfassung, Simone Weigel für die Hilfe mit Oberflächen und sehr nette Gespräche, Arnold Leidner und Jens Bauer für die tolle Arbeitsatmosphäre im Labor, Alex Gerwald danke ich für die technische Unterstützung, Katja Koßmann für die netten Gespräche und das Korrekturlesen der Zusammenfassung, Frau Hermida-Hernandez und Frau Ivanitsch für die Unterstützung in administrativen Fragen.

Den Mitarbeitern der Analytikabteilung des Instituts für Organische Chemie, Angelika Mösle, Pia Lang, Tanja Ohmer und Ingrid Rossnagel möchte ich für die schnelle und kompetente Messung der NMR, MS, HR-MS und IR-Spektren danken. Annette Hochgesand, möchte ich herzlich für die zahlreiche MALDI-Messungen danken.

Den Sekretärinnen am CFN, Ursula Mösle und Renate Bender, danke ich für ihre stets freundliche und unkomplizierte Hilfsbereitschaft bei allen Formalitäten.

Dr. Alexander Welle und Doris Abt danke ich für die TOF-SIMS Messungen.

Dr. Michael Kaupp danke ich für die schnelle und kompetente Messung der ESI-MS Spektren.

Der größte Dank gilt meiner Familie, insbesondere meinen Eltern. DANKE, dass ihr immer an mich geglaubt habt. Ohne eure Unterstützung wäre mein Studium nicht möglich gewesen. Meinem Bruder danke ich für die Lösung aller Softwareprobleme. Meinem Ehemann danke ich, dass er in schwierigen Zeiten an meiner Seite stand und mir Kraft gegeben hat.